WILEY-VCH

Reactive Distillation

Status and Future Directions

Edited by
Kai Sundmacher and Achim Kienle

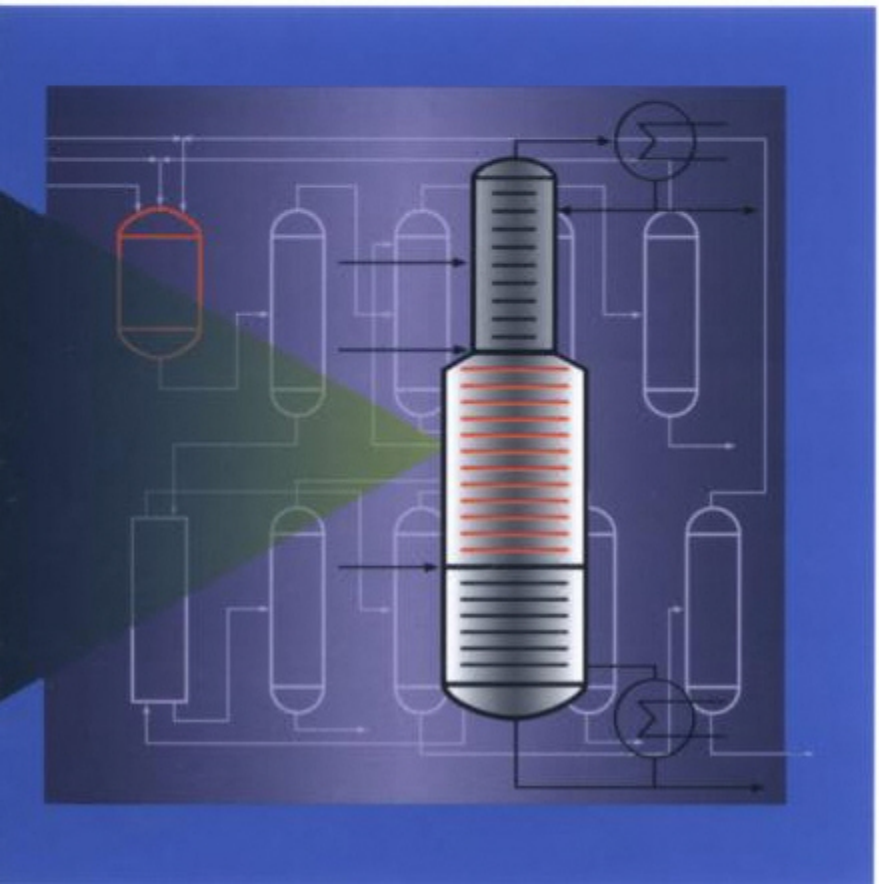

Reactive Distillation. Edited by Kai Sundmacher, Achim Kienle

ISBNs: 3-527-30579-3 (Hardback); 3-527-60052-3 (Electronic)

Kai Sundmacher and Achim Kienle (Eds.)

Reactive Distillation

Status and Future Directions

Reactive Distillation. Edited by Kai Sundmacher, Achim Kienle

ISBNs: 3-527-30579-3 (Hardback); 3-527-60052-3 (Electronic)

Also of Interest

W. Ehrfeld, V. Hessel, H. Löwe

Microreactors – New Technology for Modern Chemistry (2000)

ISBN 3-527-29590-9

S. P. Nunes and K.-V. Peinemann (Eds.)

Membrane Technology in the Chemical Industry (2001)

SBN 3-527-28485-0

J. G. Sanchez Marcano and Th. T. Tsotsis

Catalytic Membranes and Membrane Reactors (2002)

ISBN 3-527-30277-8

H. Schmidt-Traub (Ed.)

Preparative Chromatography of Fine Chemicals and Pharmaceutical Agents (planned 2003)

ISBN 3-527-30643-9

Reactive Distillation. Edited by Kai Sundmacher, Achim Kienle

ISBNs: 3-527-30579-3 (Hardback); 3-527-60052-3 (Electronic)

Kai Sundmacher and Achim Kienle (Eds.)

Reactive Distillation

Status and Future Directions

WILEY-VCH

Reactive Distillation. Edited by Kai Sundmacher, Achim Kienle

ISBNs: 3-527-30579-3 (Hardback); 3-527-60052-3 (Electronic)

Prof. Dr.-Ing. Kai Sundmacher,
Prof. Dr.-Ing. Achim Kienle
Max Planck Institute for Dynamics
of Complex Technical Systems
Sandtorstraße 1
39106 Magdeburg
Germany

Library of Congress Card No.: applied for
A catalogue record for this book is available from the British Library.
Bibliographic information puplished by Deutsche Bibliothek
Die Deutsche Bibliothek lists this publication in the Deutsche Nationalbibliografie; detailed bibliographic data is available in the Internet a http://dnb. ddb.de.

Printed in the Federal Republic of Germany.

Printed on acid-free paper.

Typesetting Hagedorn Kommunikation, Viernheim
Printing Strauss Offsetdruck GmbH, Mörlenbach
Bookbinding Litges & Dopf Buchbinderei GmbH, Heppenheim

ISBN 3-527-30579-3

Reactive Distillation. Edited by Kai Sundmacher, Achim Kienle
Copyright © 2002 Wiley-VCH Verlag GmbH & Co. KGaA
ISBNs: 3-527-30579-3 (Hardback); 3-527-60052-3 (Electronic)

Contents

Reactive Distillation. Edited by Kai Sundmacher, Achim Kienle

ISBNs: 3-527-30579-3 (Hardback); 3-527-60052-3 (Electronic)

Preface

In the chemical process industries, chemical reaction and the purification of the desired products by distillation are usually carried out sequentially. In many cases, the performance of this classic chemical process structure can be significantly improved by integration of reaction and distillation in a single multifunctional process unit. This integration concept is called 'reactive distillation' (RD); when heterogeneous catalysts are applied the term 'catalytic distillation' is often used.

As advantages of this integration, chemical equilibrium limitations can be overcome, higher selectivities can be achieved, the heat of reaction can be used in situ for distillation, auxiliary solvents can be avoided, and azeotropic or closely boiling mixtures can be more easily separated than in non-RD. Increased process efficiency and reduction of investment and operational costs are the direct results of this approach. Some of these advantages are realized by using reaction to improve separation; others are realized by using separation to improve reaction.

Most important industrial applications of RD are in the field of esterification processes such as the famous Eastman Chemical Co.'s process for the synthesis of methyl acetate [1]. This process combines reactive and non-reactive sections in a single hybrid RD column and thereby replaces a complex conventional flowsheet with 11 process units. With this RD technology investment and energy costs were reduced by factor five [2]. Another success story of RD was started in the 1980s by using this technology for the preparation of the ethers MTBE, TAME, and ETBE, which are produced in large amounts as fuel components because of their excellent antiknock properties [3].

Nowadays, many research and development activities are under way to introduce RD into other chemical processes. But despite the convincing success of RD in esterification and etherification applications, it is important to note that RD is not always advantageous. In some cases it is not even feasible. Therefore, the development of reliable tools for the conceptual design of RD processes is one of the most important fields of current research activities.

Due to the interaction of reaction and distillation in one single apparatus, the steady-state and dynamic operational behavior of RD can be very complex. Therefore, suitable process control strategies have to be developed and applied, ensuring

optimal and safe operation. This is another very important area of current and future research and development.

Today, RD is discussed as one part of the broader area of reactive separation, which comprises any combination of chemical reaction with separation such as distillation, stripping, absorption, extraction, adsorption, crystallization, and membrane separation. In the next decade, unifying approaches to reactive separators should be developed allowing the rigorous selection of the most suitable type of separation to be integrated into a chemical reactor.

Despite the fact that the basic idea of combining reaction and distillation is old, there has been an enormously growing interest in the design and operation of RD processes in recent years. Fig. 1 shows the number of journal papers that have appeared on the subject during the last 30 years. It is worth noting that the total number of publications including the papers in conference proceedings and so on is a multiple of the number of publications in scientific journals. In an analogous manner, the industrial interest in applying this attractive process technology has increased continuously. This is reflected by the steadily growing number of patents applied since 1970.

Despite the large number of publications only a few review papers have been written on this topic so far. Podrebarac et al. [4] highlighted the advantages of RD and gave an overview on potential uses of catalytic distillation. The review by Taylor and Krishna [5] focused mainly on the modeling aspects of RD. Doherty and Malone [6] gave valuable commentaries on future trends and challenges in this field of research. Gorak and co-workers [7] summarized rate-based modeling techniques for RD and also for reactive absorption. Book chapters on RD are available in volumes on distillation technology by Stichlmair and Fair [8], and by Doherty and Malone [9], and also in a recent book on reactive separations [10].

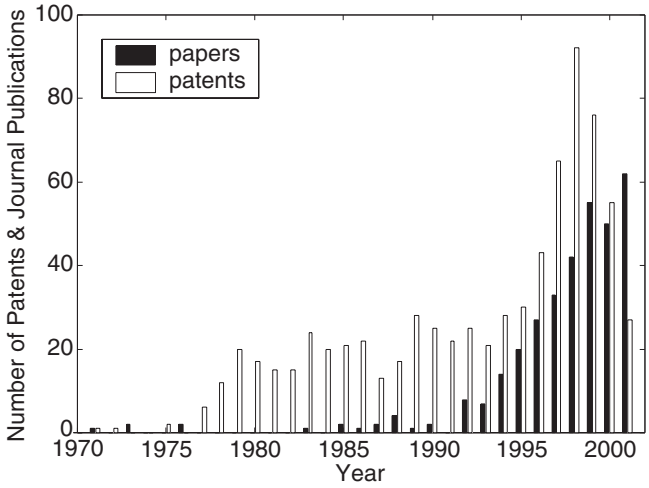

Fig. 1. Journal publications on reactive and catalytic distillation over the last three decades according to the Science Citation Index and patents in these fields according to the Deutsches Patent- und Markenamt (www.depatis.net)

Moreover, since RD is going to become a more established technology, it has found its way into classic chemical engineering encyclopedias [11, 12].

However, a comprehensive volume covering all aspects of application, design, analysis, and control of RD processes is still missing. To fill this gap, the present book was prepared. Its chapters are written by leading international experts from both academic institutions and industrial companies. They summarize the present state of knowledge and give an outlook on challenging issues in the future.

The book is divided into four parts: Part I surveys various industrial applications and covers both established large-scale processes as well as new chemical reaction schemes with high future potential. Part II provides the vital details for analysis of reactive phase equilibria, and discusses the importance of chemical reaction kinetics, while Part III focuses on identifying feasible column configurations and the design of their internal structure. Analysis and control of the complex dynamic and steady-state behavior of RD processes are described in Part IV.

Part I Industrial Applications

Chapters 1–3 give a survey of chemical reaction schemes that are performed successfully in RD columns and present ideas for new applications. Sharma and Mahajani (Chapter 1) point out that RD has acquired its new status only recently in spite of the fact that the concept has been used in various processes since 1860s. Over the last two decades, especially after the commissioning of large-scale plants for MTBE and methyl acetate production, RD has been seen as a promising reactor/separator that can fulfill multiple objectives simultaneously. With respect to applications, engineers and chemists have started looking beyond the classic esterification and etherification reactions. Hydrogenation, hydrodesulfurization, isomerization, and oligomerization are some of the unconventional examples to which RD has been successfully applied on a commercial scale. Moreover, hydrolysis, alkylation, acetalization, hydration, and transesterification have also been identified as potential candidates for RD. Another important area of application is the removal of small amounts of impurities to obtain high quality product (e. g., phenol). RD can also be used for the recovery of valuable products like acetic acid, glycols, lactic acid, and so on from waste streams.

Schoenmakers and Bessling (Chapter 2) give an overview of the tools that are available today and the methods that are now introduced in the industrial practice of chemical companies. A process synthesis procedure gives good qualitative reference points. Simulation tools have been developed that are mainly based on equilibrium models. But there are further steps to go on the way to the realization of an industrial plant. The scale-up from the miniplant scale used for the experimental validation of a new process is well known for conventional distillation, but complicated by several facts for RD especially in the case of heterogeneous catalysis. To overcome these problems either reference plant experience on an industrial scale or (if not available) further research is required. Other options both for homogeneous and heterogeneous catalysis are possible and are discussed

in the contribution. The authors emphasize that the combination of reaction and distillation not necessarily has to be operated in a counter-current column. For slower reactions a broad variety of equipment not necessarily containing columns can be used.

In Chapter 3, Tuchlenski and colleagues illustrate a procedure for process design on an industrial scale using the decomposition of the fuel ether MTBE into methanol and isobutene as an important example. Based solely on thermodynamic considerations, a plausible column configuration is derived. In order to study the scale-up of structured packing, experiments were performed on the lab scale as well as on the pilot scale. While lab scale experiments could be described satisfactorily with a simple equilibrium stage model, the same approach failed in the case of pilot plant experiments. Hydrodynamics, maldistribution and/or mass-transfer limitations might be a reasonable explanation and are worth more thorough investigation. The authors conclude that pilot plant operation is indispensable to establish a heterogeneously catalyzed RD process.

Part II Physicochemical Fundamentals

Chapters 4 and 5 are dedicated to the thermodynamic and kinetic fundamentals of RD processes. In Chapter 4, Hasse reviews the fundamentals of thermodynamic modeling of simultaneous phase and reaction equilibria. The author emphasizes the importance of consistency of phase equilibrium models. Thermodynamic consistency provides a sound basis for developing predictive reaction models for RDs, which are valid over a wide range of concentrations. To develop phase equilibrium models, reliable experimental data of phase equilibria in reactive systems have to be available. For successful measurements, suitable experimental techniques are needed, which are briefly summarized in this chapter. Criteria for their selection are also given.

Sundmacher and Qi (Chapter 5) discuss the role of chemical reaction kinetics on steady-state process behavior. First, they illustrate the importance of reaction kinetics for RD design considering ideal binary reactive mixtures. Then the feasible products of kinetically controlled catalytic distillation processes are analyzed based on residue curve maps. Ideal ternary as well as non-ideal systems are investigated including recent results on reaction systems that exhibit liquid-phase splitting. Recent results on the role of interfacial mass-transfer resistances on the attainable top and bottom products of RD processes are discussed. The third section of this contribution is dedicated to the determination and analysis of chemical reaction rates obtained with heterogeneous catalysts used in RD processes. The use of activity-based rate expressions is recommended for adequate and consistent description of reaction microkinetics. Since particles on the millimeter scale are used as catalysts, internal mass-transport resistances can play an important role in catalytic distillation processes. This is illustrated using the syntheses of the fuel ethers MTBE, TAME, and ETBE as important industrial examples.

Part III Process Design

Chapters 6–8 focus on process design, i. e. determining suitable column configurations, suitable operating conditions, and suitable column internals. Chapter 6 by Doherty and co-workers is concerned with conceptual process design. Geometrical methods are provided, which allow at the initial stages of process development to decide quickly whether RD is likely to be a good process concept. The attainable region approach for reaction-mixing systems is applied to systems with simultaneous reaction and separation in order to assess the possible selectivity-yield-conversion benefits of this technology. Feasible direct and indirect sharp splits are predicted with a model in which each column section is represented by a series of cocurrent isobaric flashes. In the limits of no reaction, or of chemical equilibrium, the model reduces to conventional models for distillation lines, and each column section can be represented by the same equations. However, at intermediate rates of reaction the models for the column sections are different, and new results are obtained. A bifurcation study shows the limits of feasibility including the influence of flow rate, catalyst level and holdup. Unlike distillation without reaction, limited ranges of feasibility in all of these variables are found.

Chapter 7 by Krishna is concerned with hardware selection and design for RD columns. An overview on available hardware for homogeneously as well as heterogeneously catalyzed RD processes is given. Criteria for suitable hardware selection are discussed and illustrated by different case studies. It is shown that the requirements for hardware selection are different from conventional non-RD. The author concludes that especially for heterogeneously catalyzed RD processes it is almost impossible to reconcile the conflicting requirements and introduces the side reactor concept as a promising alternative to overcome many of these conflicting hardware issues.

Chapter 8 by Kunz and Hoffmann introduces a special catalyst technology developed by the authors. State of the art in industrial catalyst technology is to use catalyst particles with a size in the millimeter range and to sew these particles into a wire mesh or glass-fiber clothing to form structured packing. The manufacturing process makes this type of packing expensive. In contrast to this, unstructured packing materials like Raschig rings are much cheaper. However, so far, Raschig rings with comparable catalytic activity are not commercially available. In the present contribution the authors introduce various methods for the preparation of catalytically active rings by polymerization of ion-exchange resin into the pores of a carrier material. Application is tested for MTBE synthesis. Based on this technology monolithic polymer/carrier materials were developed, which can be used for other reactive separation processes like reactive chromatography and polymer-assisted solution-phase organic synthesis.

Part IV Modeling and Process Control

Chapters 9 and 10 are on modeling, dynamics, and control of RD processes. The contribution by Taylor and Krishna (Chapter 9) deals with the modeling of homogeneously and heterogeneously catalyzed RD processes. The focus of this contribution is on steady-state behavior. First, the equilibrium stage model is introduced, which is readily obtained from the non-reactive case by adding reaction terms. Afterwards, non-equilibrium stage models are introduced as a more rigorous approach. It is shown that different types of non-equilibrium models apply to homogeneously and heterogeneously catalyzed processes. In the homogeneous case, further distinction has to be made between slow and fast liquid-phase reactions. In the heterogeneous case distinction between negligible and finite intraparticle diffusion inside the catalyst is essential. Finite intraparticle diffusion can be modeled with the dusty fluid model, which is an extension by the authors of the well-known dusty gas model. Finally, cell models are introduced to account for non-ideal flow patterns on distillation trays and maldistribution in packed columns. Equilibrium and non-equilibrium models are compared for different process applications including MTBE, TAME, and ethylene glycol synthesis and a perspective on the use of non-equilibrium models in RD process design is given.

The final contribution by Kienle and Marquardt (Chapter 10) gives an overview of the present knowledge of non-linear dynamics and control of RD columns. First, focus is on open-loop dynamics. It is shown that RD processes can sometimes show an intricate non-linear dynamic behavior, a profound understanding of which is not only of scientific interest but also very important for improved process design and operation. Basic terminology, methods, and tools are introduced for analyzing and understanding non-linear dynamics. Three different types of reaction systems are introduced including esterification, etherification, and the ethylene glycol system. Different patterns of behavior are identified depending on the reaction systems and the operating conditions. In the equilibrium regime of the chemical reaction the dynamic behavior of a RD column is qualitatively similar to a non-RD column, whereas in the kinetic regime the chemical reaction rate is dominating. For closely boiling mixtures, like in many etherification processes, the behavior in the kinetic regime is very similar to a single phase isothermal reactor. Additional effects arise for mixtures of components with completely different boiling points as for the ethylene glycol system, for example. In the second part, available guidelines for control structure selection and control system design are summarized. Emphasis is on the equilibrium regime. Here, similar methods as in non-RD apply. Additional complexity is introduced in inferential control schemes, where temperature is used as a cheap, fast, and reliable measurement instead of concentration. The authors conclude that control studies for kinetically controlled processes are missing to a large extent.

Book History and Acknowledgments

The present book is the outcome of the *1st International Workshop on Reactive Distillation* held at the Max Planck Institute for Dynamics of Complex Technical Systems in Magdeburg, Germany, on 2–3 July 2001. The goal of this workshop was to bring together world-renowned pioneering scientists and leading industrial experts in the field of RD on a common platform. The workshop was organized by the editors and their colleagues with financial support from the Kompetenznetz Verfahrenstechnik Pro3 e. V., Germany, which is gratefully acknowledged.

The editors would like to thank their colleagues Nancy Eckstein, Erik Stein, and Frank Steyer for their support in organizing the Max Planck workshop. We are also very grateful to Erik Stein, Martin Häfele, Henning Schramm, and Zhiwen Qi for their support in collecting the manuscripts and in standardizing formats. Last but not least, we are very thankful to Karin Sora of Wiley-VCH for her helpful assistance during the preparation of the book.

Max-Planck-Institut für Dynamik
komplexer technischer Systeme
Magdeburg, Germany
April 2002

Kai Sundmacher
and Achim Kienle

References

1 V. H. Agreda, L. R. Partin, W. H. Heise, *Chem. Eng. Progr.* **1990**, *86*, 40–46.
2 J. J. Siirola, *AIChE Symp. Ser.* **1995**, *91*, 222–233.
3 L. A. Smith, *Method for the Preparation of Methyl Tertiary Butyl Ether*, US Patent No. 4.978.807, **1990**.
4 G. G. Podrebarac, F. T. Ng, G. L. Rempel, *Chemtech* **1997**, *May*, 37–45.
5 R. Taylor and R. Krishna, *Chem. Eng. Sci.* **2000**, *55*, 5183–5229.
6 M. F. Doherty, M. F. Malone, *Ind. Eng. Chem. Res.* **2000**, *39*, 3953–3957.
7 C. Noeres, E. Y. Kenig, A. Gorak, *Chem. Eng. Proc.* **2002**, in press.
8 J. G. Stichlmair, J. R. Fair, *Distillation: Principles and Practices*, Wiley-VCH, New York, **1998**, 252–283.
9 M. F. Doherty, M. F. Malone, *Conceptual Design of Distillation Systems*, McGraw-Hill, New York, **2001**, 427–505.
10 G. P. Towler, S. T. Frey, in *Reactive Separation Processes* (Ed. S. Kulprathipanja), Taylor & Francis, New York, **2002**.
11 M. Sakuth, D. Reusch, R. Janowsky, in *Ullmann's Encyclopedia of Industrial Chemistry* (Eds. B. Elvers, S. Hawkins, G. Schulz), 6th edn, Wiley-VCH, Weinheim, **1999**.
12 M. Doherty, in *Chemical Engineers Handbook* (Eds: Perry, Green), Vol 13, McGraw Hill, New York, **1998**, 81–85.

Reactive Distillation. Edited by Kai Sundmacher, Achim Kienle

ISBNs: 3-527-30579-3 (Hardback); 3-527-60052-3 (Electronic)

List of Contributors

B. Bessling
BASF Corporation
Wyandotte, MI, USA

N. Chadda
Department of Chemical Engineering
University of Massachusetts
Amherst, MA 01003-3110, USA

M. F. Doherty
Department of Chemical Engineering
University of California
Santa Barbara, CA 93106, USA
mfd@engineering.ucsb.edu

T. Frey
Lehrstuhl für Fluidverfahrenstechnik
Technische Universität München
85747 Garching, Germany

S. B. Gadewar
Department of Chemical Engineering
University of Massachusetts
Amherst, MA 01003-3110, USA

H. Hasse
Institute of Thermodynamics
and Thermal Process Engineering
University of Stuttgart
70550 Stuttgart, Germany
hasse@itt.uni-stuttgart.de

U. Hoffmann
Institut für Chemische Verfahrens-
technik
Technische Universität Clausthal
Leibnitzstr. 17
38678 Clausthal-Zellerfeld, Germany

A. Kienle
Max Planck Institute for Dynamics
of Complex Technical Systems
Sandtorstr. 1
39106 Magdeburg, Germany
kienle@mpi-magdeburg.mpg.de

R. Krishna
Department of Chemical Engineering
University of Amsterdam
Nieuwe Achtergracht 166
1018 WV Amsterdam, The Netherlands
krishna@science.uva.nl

U. Kunz
Institut für Chemische Verfahrens-
technik
Technische Universität Clausthal
Leibnitzstr. 17
38678 Clausthal-Zellerfeld, Germany

S. M. Mahajani
Department of Chemical Engineering
Indian Institute of Technology
Bombay, Powai, Mumbai, India 400 076

M. F. Malone
Department of Chemical Engineering
University of Massachusetts
Amherst, MA 01003-3110, USA

W. Marquardt
Lehrstuhl für Prozesstechnik
RWTH Aachen
Turmstrasse 46
52064 Aachen, Germany
secretary@lfpt.rwth-aachen.de

F. Nierlich
Oxeno Olefinchemie GmbH
45764 Marl, Germany

T. Pöpken
Process Technology & Engineering
Degussa AG
45764 Marl, Germany

Z. Qi
Max Planck Institute for Dynamics
of Complex Technical Systems
Sandtorstr. 1
39106 Magdeburg, Germany
qi@mpi-magdeburg.mpg.de

D. Reusch
Process Technology & Engineering
Degussa AG
45764 Marl, Germany

H. G. Schoenmakers
Process Engineering
BASF AG
67056 Ludwigshafen, Germany

M. M. Sharma
Jawaharlal Nehru Centre
for Advanced Research
502 Saurabh
Plot No. 39
Kunger Marg, Swastik Park
Chembur, Mumbai, India 400 071
mmsharma@bom3.vsnl.net.in

J. Stichlmair
Lehrstuhl für Fluidverfahrenstechnik
Technische Universität München
85747 Garching, Germany

K. Sundmacher
Max Planck Institute for Dynamics
of Complex Technical Systems
Sandtorstr. 1
39106 Magdeburg, Germany
sundmacher@mpi-magdeburg.mpg.de

R. Taylor
Department of Chemical Engineering
Clarkson University
Potsdam, NY, 13699–5705 USA
taylor@clarkson.edu

A. Tuchlenski
Process Technology & Engineering
Degussa AG
45764 Marl, Germany
axel.tuchlenski@degussa.com

Reactive Distillation. Edited by Kai Sundmacher, Achim Kienle

ISBNs: 3-527-30579-3 (Hardback); 3-527-60052-3 (Electronic)

Part I
Industrial Applications

Reactive Distillation. Edited by Kai Sundmacher, Achim Kienle

ISBNs: 3-527-30579-3 (Hardback); 3-527-60052-3 (Electronic)

1
Industrial Applications of Reactive Distillation

M. M. Sharma and S. M. Mahajani

1.1
Introduction

Reactive distillation (RD) is a combination of separation and reaction in a single vessel. The concept of combining these two important functions for enhancement of overall performance is not new to the chemical engineering world. The recovery of ammonia in the classic Solvay process for soda ash of the 1860s may be cited as probably the first commercial application of RD, as shown in Fig. 1.1. Many old processes have made use of this concept. The production of propylene oxide, ethylene dichloride, sodium methoxide, and various esters of carboxylic acids are some examples of processes in which RD has found a place in some form or the other, without attracting attention as a different class of operation. It was not until the 1980s, thanks to the enormous demand for MTBE (methyl *tert*-butyl ether), that the process gained separate status as a promising multifunctional reactor and separator.

The commercial success of RD for the production of MTBE was immediately followed by another remarkable achievement with the Eastman Kodak process that condensed the whole chemical plant for methyl acetate in a single RD unit that accepts reactants and delivers pure products. Since this demonstration of its ability to render cost-effectiveness and compactness to the chemical plant, RD has been explored as a potentially important process for several other chemicals and reactions. Along with esterifications and etherification, other reactions such as acetalization, hydrogenation, alkylation, and hydration have been explored. This chapter gives an overview of the efforts being made in this direction and suggests some potentially important processes for RD. The objectives of existing and potential applications of RD are to: surpass equilibrium limitation, achieve high selectivity towards a desired product, achieve energy integration, perform difficult separations, and so on. One or more of these benefits are offered by the processes in which RD

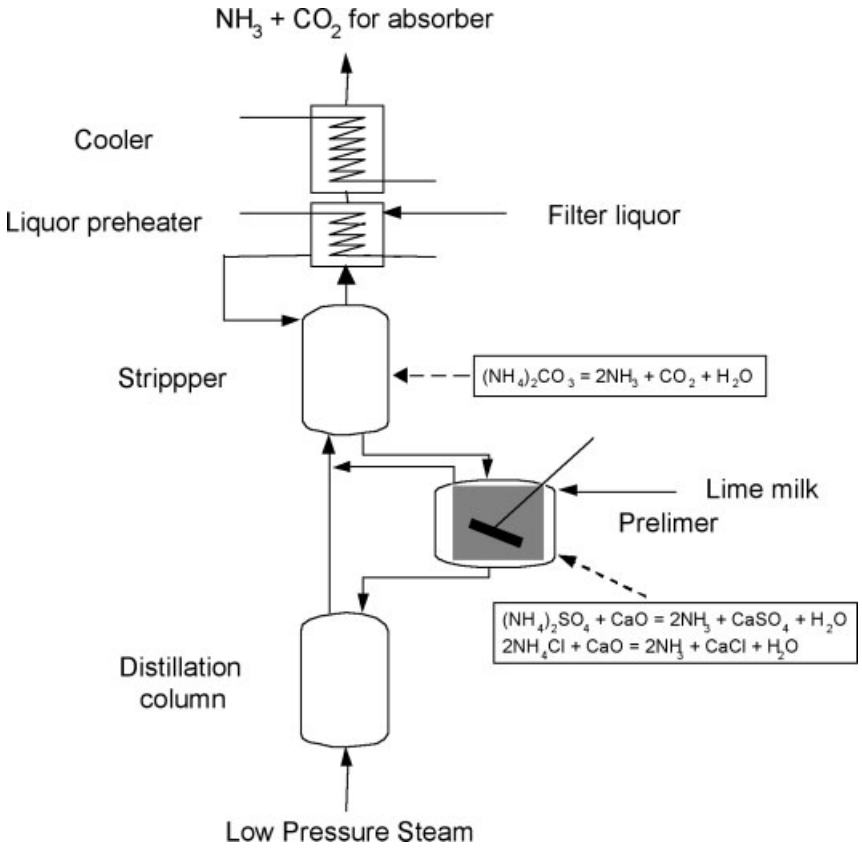

Fig. 1.1 Ammonia recovery in Solvay process

is used. Tab. 1 gives a comprehensive list of the reactions that have been investigated as candidates for RD. Tab. 2 suggests some potentially important reactions that should be investigated. Because of the large number of such reactions, it is not possible to describe each reacting system in detail here. The application of RD to the most important reactions is described here to give an overview of the issues related to industrial use of RD.

Table 1.1 Industrially important reactions, either implemented on a commercial scale or have been investigated on laboratory scale, using RD.

Reaction	*Catalyst/column internals etc.*	*Remarks on motives and achievements*	*Reference*
Etherification			
methanol + isobutene = methyl *tert* butyl ether (MTBE)	Amberlyst-15	to enhance the conversion of isobutene and achieve separation if isobutene from C_4 stream	[1, 2]
methanol + isoamylene = *tert* amyl methyl ether (TAME)	ion-exchange resin	to enhance the conversion of isoamylene	[1, 3]
ethanol/bioethanol + *tert* butyl alcohol = ethyl *tert* butyl ether (ETBE) + water	Amberlyst-15 pellet structured Amberlyst-15	to effectively utilize bioethanol and surpass equilibrium conversion	[4]
isopropanol + propylene = diisopropyl ether (DIPE)	ZSM 12, Amberlyst-36 Zeolite	a two-stage process that uses water and propylene as feed	[5]
Esterification with alcohols/olefins			
acetic acid + methanol = methyl acetate + water	Dowex 50 W X-8	recovery of acetic acid from dilute streams (30–60 % w/w)	[6]
	Amberlyst-15 (baskets on trays)	recovery of acetic acid from dilute streams (2.5–10 % w/w)	[7]
	Katamax packing		[8]
	sulfuric acid	recovery of dilute acetic acid in carbonylation process	[9]
		manufacture of methyl acetate; overcomes azeotrope formation; enhances conversion (> 99 %)	[12]
butanol + acetic acid = butyl acetate + water	cation exchange resin	for recovery of acetic acid from dilute aqueous solutions	[13, 14]
2-methyl propanol + acetic acid = 2-methyl propyl acetate	Katapak-S	manufacture of 2-methyl propyl acetate	[15]
lactic acid + methanol = methyl lactate + water	Dowex 50-W	for recovery of lactic acid from fermentation broth	[16]
myristic acid + isopropanol = isopropyl myristate + water		for recovery of myristic acid	[17]

Table 1.1 (continued)

Reaction	*Catalyst/column internals etc.*	*Remarks on motives and achievements*	*Reference*
Esterification with alcohols/olefins			
silylated compounds + sulfuric acid = silylated sulfuric acid ester	non-reactive packings	for recovery of silylated compounds from pharmaceutical wastes	[18]
propane diol monoalkyl ether + carboxylic acid = propylene glycol monoalkyl ether carboxylate	acidic catalyst; toluene as an entrainer		[19]
acetic acid/acrylic acid/formic acid + cyclohexene = cyclohexyl carboxylate	ion-exchange resin bags		[20]
Synthesis of vinyl acetate			
acetaldehyde + acetic anhydride = vinyl acetate		improved safe process with high yields	[21]
Transesterification			
polytetramethylene glycol diacetate + methanol = polytetramethylene glycol + methyl acetate			[22]
dialkyl carbonate + phenol/ethanol = diaryl carbonate + alcohol	lead compound/zeolites; phenol as entrainer	alternative to the conventional process that uses phosgene; effective removal of alcohol to improve yields	[23, 24]
acetic acid + vinyl stearate = stearic acid + vinyl acetate			[25]
Hydrolysis			
methyl acetate + water = methanol + acetic acid	ion-exchange resin bags	recovery of acetic acid and methanol in polyvinyl alcohol (PVA) and terephthalic acid (PTA) manufacture	[26, 27]
	fluidized RD		[28]
	cation exchanger on inert	recovery of acetic acid in PVA manufacture	[29]
acrylonitrile to acrylamide	copper oxide catalyst	less side product formation	[30]

Table 1.1 (continued)

Reaction	*Catalyst/column internals etc.*	*Remarks on motives and achievements*	*Reference*
Acetalization			
methanol + aqueous formaldehyde = methylal + water	ion-exchange resins zeolites, ion-exchange resins	to surpass equilibrium conversion; to remove formaldehyde as an impurity (e. g., from 1,2-butyne diol)	[31, 32, 33]
ethanol + aqueous formaldehyde = ethylal + water	ion-exchange resins	recovery of formaldehyde and synthesis of ethylal	[34]
ethylene glycol + formaldehyde	ion-exchange resins	recovery of formaldehyde and synthesis of acetal	[35]
propylene glycol + acetaldehyde/formaldehyde	ion-exchange resin	recovery of propylene glycol	[36]
MeCOCHO + methanol = methyl glyoxal dimethyl acetal + water	acid catalyst, preferably ion exchanger; azeotropic separation of water	to enhance rate and conversion	[37]
Aldol condensation followed by dehydration			
acetone to diacetone alcohol (DAA) and mesityl oxide	anion exchange resin	high selectivity towards DAA; enhanced conversion level	[38]
n-butaraldehyde to 2-ethyl hexenal	aqueous alkaline solution	formation of trimers/tetramers of aldehyde is avoided	[39]
Hydration/dehydration			
ethylene oxide + water = ethylene glycol	cationic/anionic exchange resins	to enhance selectivity towards MEG and avoid formation of diethylene glycol (DEG); attain better temperature control over the exothermic reaction	[40, 41, 42]
isobutene + water = *tert* butyl alcohol	cationic exchange resin	to overcome equilibrium limitation	[43, 44]
hydration of propylene to isopropanol	cationic exchange resin	to overcome equilibrium limitation	[45]
hydration of isoamylene to *tert*-amyl alcohol	Amberlyst-15 (catalytic-bales)	enhanced yield and selectivity	[5]
hydration of cyclohexene to cyclohexanol	SiO_2/Ga_2O_3	surpass equilibrium conversion	[46]

Table 1.1 (continued)

Reaction	*Catalyst/column internals etc.*	*Remarks on motives and achievements*	*Reference*
Alkylation/trans-alkylation/dealkylation			
benzene + propylene = cumene	Union Carbide- LZY-82 molecular sieves	use of exotherm of reaction; high purity cumene	[48, 44]
	suspended catalyst process	suitable for dilute benzene and dilute olefin	[49]
m-xylene (MX) + di-*tert*-butyl benzene (TBB) = *tert* butyl *m*-xylene (TBMX) + *tert*-butyl benzene and TBB + MX = TBMX + benzene		separation of *m*-xylene and *p*-xylene	[50]
benzene + ethylene/propylene = alkyl benzene	zeolite-β	suitable for dilute benzene and dilute olefin	[51, 52]
benzene (from refinery stream) + ethylene/propylene = alkyl benzene		to reduce amount of benzene from gasoline	[53]
alkylation of aromatics with C_4 to C_{15} olefins and dealkylation of the alkylated product	molecular sieves	the product is considered to be the best motor octane component of gasoline; indirect skeletal isomerization of olefins	[54]
isobutane + propylene/butylene = highly branched paraffins	Lewis acid promoted inorganic oxide catalyst	selectivity for C_7/C_8 branched alkanes	[55]
Isomerization			
α-isophorone = β-isophorone	adipic acid, ZSM-5, alumina	to surpass the equilibrium conversion	[56]
butene-2 = butene-1	alumina-supported palladium oxide	to upgrade C_4 stream and get high conversion	[57]
butene-1 = butene-2	standard hydrogenation catalyst	for separation of isobutylene from C_4 stream	[58]
n-paraffin to *iso*-paraffins	Chlorinated alumina catalyst, presence of hydrogen (< 8 bar)	To increase the octane value of paraffin stock	[59]
Chlorination			
dichlorobenzene to trichlorobenzene		to increase selectivity towards trichlorobenzene	[60]
dichlorodimethyl silane to dichloro (chloromethyl) silane	photochlorination	increased yields towards monochlorinated product	[61]

Table 1.1 (continued)

Reaction	*Catalyst/column internals etc.*	*Remarks on motives and achievements*	*Reference*
Hydrogenation/hydrodesulfurization/dehydrogenation			
hydrogenation of alkyl anthraquinone		in manufacture of hydrogen peroxide	[62]
hydrogenation of benzene to cyclohexane	alumina supported Ni catalyst	avoids formation of methyl cyclopentane and cracking products; used for removal of benzene from light reformate	[63, 64]
hydrogenation of AMS to cumene	palladium oxide supported on alumina, carbon, or silica	removal of impurities of AMS in cumene based phenol plant; side chain hydrogenation is prominent in reactive distillation than ring hydrogenation	[65]
hydrogenation of mesityl oxide to methyl isobutyl ketone (MIBK)	bifunctional catalyst: cation exchange resin with palladium/nickel	to surpass equilibrium limitations; column uses acetone and hydrogen as feed; acetone is dimerised and dehydrated in the same column to give mesityl oxide.	[66]
hydrodesulfurization of vacuum gas oil	hydrogenation catalyst with acidic support	mild conditions compared to trickle bed reactor	[67, 68, 69]
hydrogenation of butadiene	alumina supported palladium oxide	selectivity for butene-1	[57]
hydrogenation of isophorone to trimethylcyclohexanol (TMP)		simultaneous separation of TMP; in-situ catalyst washing	[70]
dehydrogenation of isopropanol to acetone		in chemical reaction heat pump system	[71]
hydrogenation of acytelene		for removal of butadiene from crude C_4 stream	[72]
hydrogenation of aniline to cyclohexylamine		high conversion and less formation of dicyclohexyl amine	[73]
methanol from synthesis gas	copper/zinc/alumina in the presence of an inert solvent (C_7–C_{12})	better temperature control and improved yields	[74]

Table 1.1 (continued)

Reaction	*Catalyst/column internals etc.*	*Remarks on motives and achievements*	*Reference*
Metathesis/disproportionation			
butene-1 = propylene + pentene or butene-1 = ethylene + trans hexene-2	activated metal oxide	to surpass equilibrium limitation, increase in selectivity and operation under mild conditions	[75]
Condensation of aldehydes			
formaldehyde to trioxane	strong acid catalyst hydrophobic shape selective (modified ZSM-5)	to enhance conversion	[76, 77]
Dimerization/Oligomerization			
Oligomerization of C_4 iso-olefins	solid phosphoric acid, cation exchange resins	to produce octane boosting oligomers; alternative to HF alkylation process	[78]
oligomerization of linear butenes	acid catalyst; Ni-based catalyst	to avoid formation of C_{16} oligomers	[79]
oligomerization of dienes in C_4 to C_5 from FCC	Al-silicates or ion exchangers	removal of diene impurity, an alternative to hydrogenation of etherified C_4–C_5 stream	[80]
Production of diethanol amine			
monoethanolamine + ethylene oxide = diethanolamine (DEA)	no catalyst or ion exchange resins	high selectivity towards DEA	[81]
Carbonylation			
methanol/dimethyl ether + CO = acetic acid	homogeneous system	production of high purity acetic acid	[82]
Addition of amines to aldehydes/ketones			
primary amine + mesityl oxide = acetone + imine		separation of primary amine from secondary amines as the later has no reactivity for mesityl oxide imine can be hydrolysed back to primary amine	[83]
acroelin + substituted anilines = Schiff's base	mineral acid	to facilitate the separation aldehyde impurity from desired product (e. g., acrylonitrile)	[84]

Table 1.1 (continued)

Reaction	*Catalyst/column internals etc.*	*Remarks on motives and achievements*	*Reference*
Amination			
alcohols + ammonia = amine + water	in the presence of hydrogen and hydrogenation catalyst	better selectivity towards the desired amine	[85]
Alcoholysis			
diacetate ester of polytetramethylene ether + alkanol = polytetramethylene ether glycol (PTMEG) + alkanol acetate ester	alkali metal oxide or alkaline earth metal oxide; in the presence of hot methanol	PTMEG is used to make polyesters, polyurethanes etc.; complete conversion of diester.	[86]
Neutralization (protonation of organic bases)			
pyridines + carboxylic acids = salt		for the separation of close-boiling pyridine mixture	[87]
propylene oxide from propylene chlorohydrin	alkali catalyst (NaOH)	better selectivity toward oxide; less formation of glycol	[88]
Amidation			
hexamethylene diamine + adipic acid = nylon 6, 6 prepolymer	a fine control over water removal is necessary	enhanced conversion and good quality polymer	[89]
Nitration			
chlorobenzene + nitric acid = nitrochlorobenzene	azeotropic removal of water	removal of water increases acidity and enhances conversion to facilitate nitration with nitric acid alone	[90]

Table 1.2 Potentially important reactions as candidates for RD.

Reaction details	*Relevant reference*
Etherification/acetalization	
wet ethanol (80 % w/w) to ETBE at high temperature to minimise *tert*-butanol formation	[91]
reaction of 1,4 butene-2-diol with acetone and 2-methyl propanal	
reaction of *cis* and *trans*- cyclohexane diol with formaldehyde	[92]
Esterification with alcohols/olefins	
ethyl formate from ethanol and formic acid	[93]
isopropyl acetate from isopropanol and acetic acid	[94]
recovery of glycolic acid, glyoxylic acid from aqueous solutions as esters	
recovery of acetic acid/acrylic acid through formation of *n*-butyl acetate, isoamyl acetate (V-L-L system)	
reaction of propylene (butylenes) with acetic acid to give isopropyl (*sec* butyl) acetate.	
esterification of succinic, glutaric, and adipic acid	[95]
esterification of petanoic acid with ethanol for better selectivity	[96]
Hydration	
propylene glycol from propylene oxide	
Transesterification	
production of dimethyl carbonate (DMC) through the reaction of methanol and ethylene (propylene) carbonate	[97]
methyl phenyl carbonate and diphenyl carbonate from phenol and dimethyl carbonate	
Condensation	
acetone to isophorone	[70]
acetaldehyde to paradehyde	
Amination	
reaction of acetone with ammonia to give 2,2,6,6 tetramethyl-4-piperidone	
Alkylation/Dimerization	
removal of AMS from cumene through dimerization/alkylation	
removal of styrene from ethyl benzene	
ethylene to 1-butene and 1-hexene	
C_5 fraction: cyclopentadiene and further to dicyclopentadiene; C_5 olefins to diolefins	[98]

Table 1.2 (continued)

Reaction details	*Relevant reference*
Hydrogenation/hydrodesulphurisation/hydrodenitrogenation	
hydrogenation of dimethyl maleate	
hydrogenation of Methyl acetylene and butyne (in C_3 and C_4 fractions from naphtha cracker)	
hydrodenitrogenation of petroleum fraction as feed to hydrocracking	[99]
Acetalization/ketalization	
reaction of acetaldehyde, acetone with methanol, ethanol	
(Photochemical) chlorination	
chlorination of toluene: selectivity for benzyl chloride	[100]
Separation of close boiling compounds	
m/p- cresol and 2,6 xylenol: preferential reaction with amine: reactive extractive distillation	
mixture of cyclohexene and cyclohexane: through hydration/esterification of cyclohexene	[101]
Isomerization	
1,4 dichloro 2-butene to 1,2 dichloro 3-butene	[102]
cyclohexanone oxime to epsilon-caprolactum	[102]
epichlorohydrin from glycerol dichlorohydrin	
aniline production (V-L-L)	[103]
Cracking	
dicyclopentadiene to cyclopentadiene	
Impurities removal	
carbonyl compounds removal from phenol	[104]
removal of minute amount of ethyl acetate in aqueous solution of ethanol	[105]
removal formaldehyde, acetaldehyde impurities from crude acetone by reaction with diamine	[106]

1.2 Etherification: MTBE, ETBE, and TAME

Gasoline reformulation using ethers such as MTBE, ethyl *tert*-butyl ether (ETBE), and *tert*-amyl methyl ether (TAME) as octane boosters and oxygenates has been driven by the Clean Air Act in USA in late seventies, which boosted MTBE production to a new level in the early 1980s; TAME and ETBE also emerged as promising fuel additives. In addition to its antiknock property, enhancing the octane number of the fuel, MTBE improves the water tolerance limit of the fuel and has a higher calorific value than other additives such as methanol. The RD process can exceed the equilibrium limitation and offer more than 99 % conversion. The process is shown in Fig. 1.2. Another important aspect of carrying out the etherification to near complete conversion, is its efficient use in separating the *iso*-olefins from the refinery stream containing both normal and secondary butenes (C_4 or C_5), which otherwise are very difficult to isolate. The RD column can handle the mixed olefins quite effectively and exploits the presence of inert butenes to improve its own performance. This separation is necessary because *n*-butenes are required in the pure form for producing pure butene-1, as a co-monomer for polymerization of ethylene, feed for acrylates, and for the oxidative production of butadiene.

The decision to ban MTBE in California from 2003 will force refiners to look for a new fuel additive and will probably have adverse implications for the existing and proposed production units for MTBE and other fuel ethers. Nevertheless, MTBE has been mainly responsible for the initiation of research and development in RD and its high status today. In the last two decades, especially in the 80s, the patents and published literature on RD have been mainly focussed on its application for MTBE and other ethers.

The conventional processes for the manufacture of MTBE uses a catalytic reactor with a slight excess of methanol (methanol/isobutylene = 1.05 to 2). The products correspond to the near-equilibrium conversion of 90–95 %. The reaction mixture is separated using distillation, but this is complicated by the formation of the binary azeotropes methanol–MTBE and isobutylene–methanol. The unreacted isobutylene is difficult to separate from other volatile C_4 products. In the RD process,

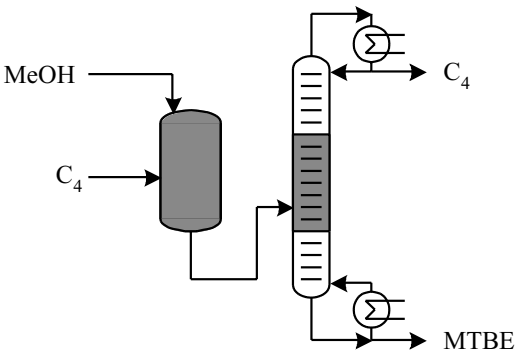

Fig. 1.2 Process for MTBE production: an adiabatic reactor and an RD column

on the other hand, almost complete conversion of isobutylene is obtained, thereby eliminating the separation and recycling problems. The RD column consists of three sections, of which the middle section is the reactive zone packed with a solid catalyst. The top non-reactive rectifying section performs the separation of inert gases and excess methanol, and the bottom section separates out MTBE in almost pure form. The boiling point of MTBE is 328 K and that of methanol is 337.5 K. Surprisingly, MTBE is the bottom product while unreacted high-boiling methanol is collected through distillate. This behavior is caused by the formation of the isobutylene–methanol low-boiling azeotrope, which lifts methanol from the stripping section of the column.

The pioneering work to commercialize this technology was performed by Smith from the Chemical Research and Licensing Company (CR&L), who has been awarded several patents for different catalyst structures, internal column design, and flow schemes [1]. Some patents have been assigned to the researchers from Elf who describe using alternating catalytic and non-catalytic zones to carry out the etherification. The efforts in these studies were directed towards minimizing the pressure drop in the catalyst bed and providing maximum residence time for the liquid in the catalytic zone. This was achieved by providing separate free passage to the upflowing vapor stream either by packing the catalyst in the downcoming stream or by providing annular space in the catalyst bed, thereby isolating reaction and distillation zones in a single column. UOP, Koch Engineering, and Hüls AG have jointly developed the Ethermax process for producing ethers by RD. The process uses Koch Engineering's Katamax packing where a solid acid catalyst is confined in screen envelopes.

The existence of multiple steady states has attracted the attention of several researchers [2]. Simulation studies indicated that the same column configuration operating under similar conditions can give rise to different steady-state conversions. Bravo and co-workers reported the only experimental evidence of multiple steady states in the synthesis of TAME in the pilot plant of Neste Oy [3]. The MTBE system also shows oscillatory behavior, as reported by Sundmacher and Hoffmann [2].

The use of RD in the manufacture of other ethers such as ETBE, TAME, and so on, has been demonstrated to be beneficial and several patents and investigations have emerged [3, 4]. UOP describes a process for the manufacture of DIPE (di-isopropyl ether), which uses propylene and water feedstock. It is a two-stage RD process associated with simultaneous hydration and etherification [5]. The ethers, being the heaviest components, are collected in the bottom stream.

1.3 Dimerization, Oligomerization, and Condensation

Owing to the uncertainty in the MTBE market, many new projects are being placed on hold. Some of the existing plants are being modified to produce an alternate product such as alkylate (typically the mixture of branched octanes). Alkylate can be an ideal gasoline blendstock as it has high octane and paraffinic nature. A re-

cent patent from UOP describes a process based on indirect alkylation, which uses RD in the production of isobutylene dimer, disobutylene, which on hydrogenation gives the alkylate [78]. This process uses the same feedstock, that is, the C_4 stream along with methanol. The advantage of conducting dimerization in the presence of methanol or MTBE is to protect the catalyst from coking and avoid formation of the undesired oligomers. The motive behind using RD is to increase the catalyst life, achieve better selectivity, avoid formation of C_{12} oligomers and reduce C_4 recycle. Oligomerization of linear butenes and removal of butadiene through dimerization in RD unit, as an alternative to selective hydrogenation, has also been described [79, 80].

The condensation reactions of aldehydes, for example acetaldehyde to paraldehyde or formaldehyde to trioxane, also exhibit similar features and can become important candidate reactions for RD [76, 77]. An RD column with total reflux and removal of condensed product through the bottom stream is a recommended configuration for such systems. Aldol condensation of acetone to diacetone alcohol has been widely studied as a reaction that may give better conversion and higher selectivity to diacetone alcohol in the RD column, by suppressing the further formation of mesityl oxide. The reaction takes place in the presence of anion-exchange resins [38]. Similarly condensation of butaraldehyde to 2-ethyl hexanal has also been investigated in RD, with a view to increasing selectivity [39]. In all these reactions the condensation product is normally heavier than the rest of the components and can be conveniently separated out during the course of the reaction.

1.4
Esterification: Methyl Acetate and Other Esters

Methyl acetate is another high-volume commodity chemical that is manufactured commercially using RD. It is used as an intermediate in the manufacture of variety of polyesters such as photographic film base, cellulose acetate, Tenite cellulosic plastics, and Estron acetate. The conventional processes used multiple reactors with a large excess of one of the reactants to achieve high conversion of the other. The product was difficult to purify because of the formation of methyl acetate–methanol and methyl acetate–water azeotropes. Different means of dissociating the methyl acetate–methanol azeotrope were employed, such as the use of several atmospheric and vacuum distillation columns or extractive distillation. A typical process contained two reactors and eight distillation columns, making it complex and capital intensive.

Eastman Kodak developed an RD process for the manufacture of high-purity and ultra-high-purity methyl acetate [12]: the traditional process and the RD process are shown in Fig. 1.3. The remarkable fact is that, in spite of the reaction having an unfavorable equilibrium limitation, a high-purity product is obtained using a near-stoichiometric ratio of methanol and acetic acid in the RD column. The whole process is integrated in a single column eliminating the need for a complex distillation column system and recycling of the methanol–methyl acetate azeo-

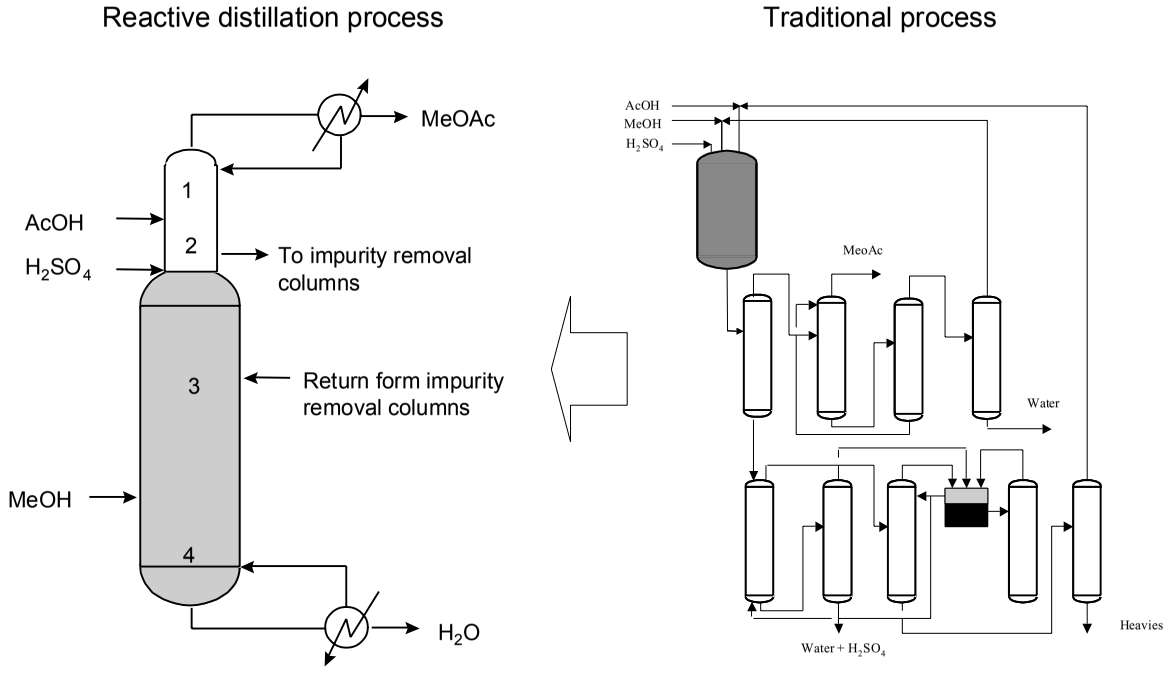

Fig. 1.3 RD and traditional process for methyl acetate

trope. A single RD column at Eastman Kodak's Tennessee plant produces 180 000 tons/year of high-purity methyl acetate.

Methyl acetate production with a heterogeneous catalyst such as ion-exchange resins is also feasible and an excellent review of various investigations into this subject has been published [10]. This gives a rigorous analysis of the reacting system in the RD column with the help of experiments and modeling. For all practical purposes, chemical and phase equilibria can be assumed to explain the experimental findings; at high reflux ratios the system may deviate slightly from this assumption. The role of reflux ratio is quite crucial. It not only dictates the capital cost and energy requirements but also influences the extent of reaction taking place in the column. At low reflux ratio, separation is poor whereas at high reflux ratio the reactant methanol tends to get separated through enrichment of the azeotrope of methanol and methyl acetate. Sufficient conversion is possible only through a double-feed strategy. This has also been demonstrated, in a different context, by Doherty and co-workers for the same system [11].

Apart from methyl acetate, RD may be used for the production of other esters such as ethyl acetate, isopropyl acetate, and butyl acetate [13, 15]. The reaction may also be used as tool for recovery of acetic acid and other carboxylic acids from aqueous solutions, detailed discussion of which is in the section on recovery of chemicals with RD.

1.5 Hydrolysis of Esters

A methyl acetate–water mixture is produced in large quantities by the purification of terephthalic acid (PTA). The manufacture of poly vinyl alcohol (PVA) also produces large quantities of methyl acetate (1.68 kg/kg PVA). Methyl acetate is a comparatively low-value solvent, hence it has to be sold at a lower price. Alternatively, it can be hydrolyzed efficiently to recover methanol and acetic acid for reuse in the process [26–28].

The conventional process for the hydrolysis of methyl acetate uses a fixed-bed reactor followed by a complex arrangement of several distillation/extraction columns. The conversion is limited by unfavorable equilibrium (equilibrium constant 0.14–0.2) and a large amount of unconverted methyl acetate needs to be separated and recycled. The reaction is carried out in a fixed-bed reactor and the product stream contains all four components. It needs four additional columns to separate the methanol and acetic acid streams and recycle unconverted methyl acetate along with methanol to the reactor.

Fuchigami developed an RD process at laboratory level for the hydrolysis of methyl acetate using an ion-exchange resin catalyst in a special form [26] (Fig. 1.4). Converting the process from conventional to RD can eliminate many complicated steps. The use of solid acid catalysts obviates the need for spent acid recovery and exotic construction materials. The resin was molded into 7 mm $\times$ 7 mm pellets using polyethylene powder. The distillation column was

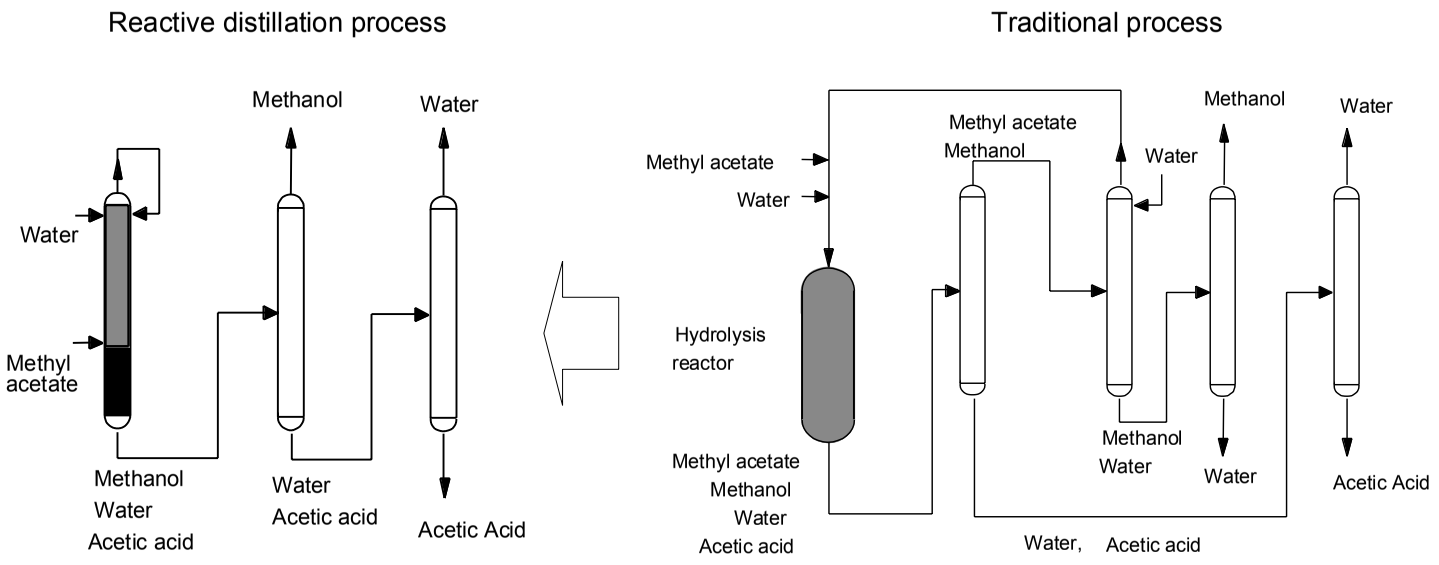

Fig. 1.4 RD and traditional process for hydrolysis of ethyl acetate

directly packed with these pellets, which played the role of both catalyst and packing.

Water is fed at the top of the reactive section and methyl acetate is introduced at the bottom of the reactive section. The column is operated under total reflux of methyl acetate–methanol azeotrope. The stripping section strips all the methyl acetate and the bottom product is essentially free of methyl acetate. The bottom product, which now contains only methanol, water, and acetic acid, can be easily separated using two distillation columns in series giving methanol and acetic acid as products. Thus, this process eliminates two main pieces of equipment from the conventional process: first the water wash column for the separation of methanol from methyl acetate and second the methanol enriching column for recovery of water-diluted methanol. Conversions of about 99 % are achieved in this process. The estimated energy savings for this process are 50 % of that of the conventional process. The reaction also has been investigated using a fluidized bed RD column in which catalyst particles are kept suspended over a distillation tray [28].

1.6 Hydration

Hydration of ethylene oxide to ethylene glycol has also received considerable attention because of the potential benefits that RD can offer for this reaction [40–42]. The reaction is exothermic and the heat can be utilized effectively in the RD; moreover, the control over temperature that is desired for avoiding diethylene glycol formation, can easily be achieved in RD. It is a multi-feed operation in which ethylene oxide is fed at the bottom of the column and water feeds can be introduced at several locations in the upper section. The column is operated under total reflux.

The possibility of hydrating various olefins such as isobutylene, propylene, isoamylene, and cyclohexene has also been successfully explored in separate studies [5, 43–47]. In most cases, alcohol, being a higher-boiling component, is collected at the bottom of the column operated under total reflux. Hydration of cyclohexene represents a peculiar example of vapor–liquid–liquid equilibrium in an RD column: a subject that has not been studied in depth.

1.7 Hydrogenation/Hydrodesulfurization/Hydrocracking

Hydrogenation in RD is a typical class of reacting system in which one of the components is non-condensable under the operating conditions. Hydrogenative distillation for conversion of isophorone to trimethyl cyclohexanone has been practiced since the 1960s. Recently many hydrogenation or hydrodesulfurization reactions have been investigated and commercialized successfully using RD. The following are few important examples.

1.7.1 Benzene to Cyclohexane

Benzene is an undesirable carcinogenic impurity in gasoline. The RD process developed by CR&L, shown in Fig. 1.5, uses a supported nickel catalyst at high temperature (260–280 °C) and high pressure (6 atm) and offers several advantages apart from highly selective separation. RD facilitates efficient contact of hydrogen with benzene, substantial removal of heat of reaction, good temperature control, and in-situ catalyst washing to increase its life [63, 64].

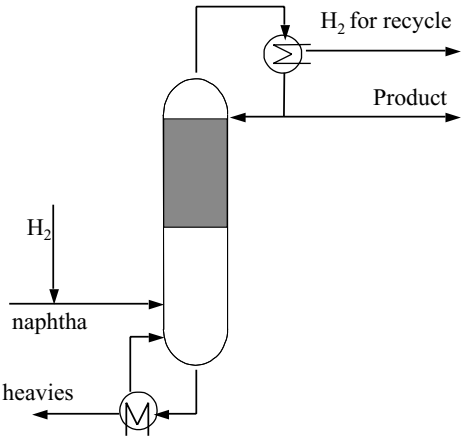

Fig. 1.5 RD process for hydrogenation of aromatics (removal of benzene from light reformate)

1.7.2 Selective Hydrogenation of C_4 Stream

The selective hydrogenation of butadiene from the C_4 stream is essential for its conversion to normal butenes to avoid the increased consumption and regeneration cost of acid in alkylation units. RD technology offered by CR&L for the C_4 stream selectively hydrogenates butadiene in the same column that is used for MTBE. The existing MTBE columns can be conveniently modified to suit this purpose. The butadiene content can be brought down to less than 100 ppm [57, 64].

1.7.3 Hydrogenation of Pentadiene

For C_5 alkylation, or for TAME production, removal of petandiene is required as it increases the acid consumption in alkylation and fouling in the TAME unit. The simple hydrogenation catalyst is quite sensitive to the presence of mercaptans present in this stream from cat crackers and cokers, and mercaptan removal also becomes necessary for effective hydrogenation. However, the technology of CR&L for pentadiene removal achieves both goals: hydrogenation of pentadiene and removal of mercaptans in the same unit. The mercaptans react with olefins in the

presence of catalyst to form olefinic sulfides and, being high-boiling components, can be easily fractionated as the bottom product. Hence RD eliminates the mercaptan removal step effectively. The product from the RD unit is an ideal feedstock for the TAME or alkylation unit [64].

1.7.4
C_4 Acetylene Conversion

The acetylene purge from the butadiene extraction unit contains a significant amount of butadiene. The loss is typically 2.5 % of the total butadiene. Though hydrogenation and recycling of this stream looks like an attractive option, it is not practiced because of the very short life of the catalyst owing to the presence of acetylene. In such a case the conventional debutanizer can be packed with hydrogenation catalyst and the acetylene purge is fed to this column. The components such as butadiene and ethyl acetylene get concentrated in the reaction zone and significant conversion can be realized [64].

1.7.5
Hydrodesulfurization, Hydrodenitrogenation, and Hydrocracking

Like hydrogenation, hydrodesulferization (HDS) of various fractions of crude oil distillation, vacuum gas oil, and even the effluent from an FCC (Fluid Catalytic Cracker) unit can be performed effectively in an RD column. Mercaptans and thiopenes can be converted to non-sulfur compounds and H_2S in the presence of a hydrogenation catalyst on an acid support that facilitates hydrocracking. HDS in RD requires relatively mild conditions such as low partial pressure of hydrogen. Along with HDS, hydrodehidrogenation (HDN) also takes place in this unit. The overhead gases may be recycled back to a crude distillation unit to facilitate efficient stripping [67–69]. RD has also been found useful in hydrocracking of heavy petroleum feedstock to lighter components and subsequent hydrogenation of the unsaturated light products, the products being lower boiling and easily separated out in the distillation column [69].

1.7.6
Miscellaneous Hydrogenations

Apart from refining, RD also finds application in hydrogenation to synthesize various fine and other petrochemicals. As mentioned earlier, hydrogenation of isophorone to trimethyl cyclohexanone has been conducted in an RD column, as the later has a lower boiling point. The advantage is the better control over temperature of this exothermic reaction [70]. Hydrogenation of anthraquinone, as a key step to produce hydrogen peroxide is also an interesting application of RD [62]. CDTech has developed a technology for production of methyl isobutyl ketone by hydrogenation of mesityl oxide in RD column. The process uses acetone and hydrogen as feedstock [66].

1.8 Chlorination

Many hydrocarbon chlorinations that follow free a radical mechanism are associated with the problems of poor selectivity towards the intermediate products. Since most of the time there happens to be a distinct difference between the volatilities of the various chlorinated products, RD can be an appropriate choice of reactor for obtaining better selectivity towards the particular chlorinated product. The important example of commercial relevance is the photochlorination of aromatics such as benzene or toluene [60, 100]. Like hydrogenation, this process is also associated with the use of a non-condensing gas (chlorine) and hence its flow rate would make a significant impact on design considerations.

1.9 Acetalization/Ketalization

Acetalization and ketalization, like esterification, are also important candidate reactions for RD. It is a reversible reaction between aldehyde/ketone and alcohol that generates one molecule of water with one molecule of acetal/ketal. Various acetals, such as methylal and dioxalane, are useful solvents in the chemical industry. Masamuto and Matsuzaki (1994) first prepared methylal from formaldehyde and methanol in the presence of cation-exchange resins using a laboratory scale RD column conveniently packed in the form of tea-bag structures [31]. Kolah et al. studied this reaction in both batch and continuous RD column, as shown in Fig. 1.6, with a theoretical analysis of multiple reactions in the RD column [32]. Along with the acetal, formation of dimers and hemiacetals also takes place with substantial con-

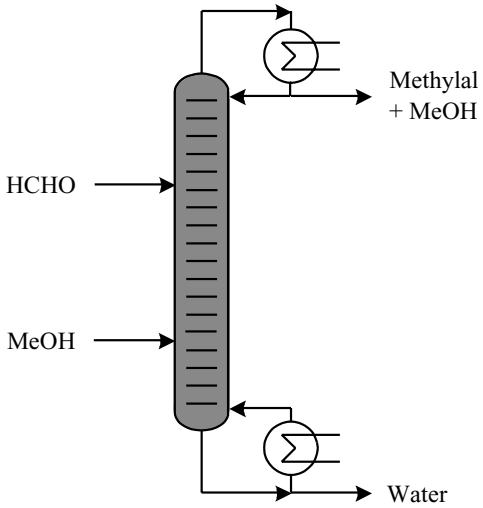

Fig. 1.6 RD process for methylal from methanol and formaldehyde

version. It was found that in a closed system, the conversion is 85 % with 6:1 mole ratio of methanol to formaldehyde, whereas, in an RD column conversion close to 99 % can be realized with even 3:1 mole ratio. Apart from the synthesis of useful acetals, this reaction is potentially an important tool for recovering certain valuable aldehydes, ketones, and alcohols. As the product acetal/ketal has relatively lower boiling point it can be separated easily during the course of the reaction and then can be conveniently hydrolyzed back to the parent alcohol or aldehyde/ketone. The investigations in this direction have been performed and the details are given in the next section on recovery of chemicals.

1.10 Recovery and Purification of Chemicals

Apart from its application as a multifuctional reactor, RD can be looked upon as an efficient separator for the recovery or purification of chemicals. The reversible reactions such as esterification and acetalization can be exploited for this purpose. The component to be removed is allowed to react in the distillation column and the resultant product can be separated simultaneously. The esters or acetals formed can be easily hydrolyzed back to the original component under different conditions.

Dilute acetic acid is produced in large quantities in many processes such as manufacture of cellulose esters, terephthalic acid, and dimethyl terephthalate; and in reactions such as acetylation and nitration. The recovery of acetic acid from these streams is a daunting problem. The conventional methods of recovery are azeotropic distillation, simple distillation, and liquid–liquid extraction. With the advent of RD processes, esterification of acetic acid with methanol seems to be an attractive alternative. Neumann and Sasson [6] carried out laboratory experiments to recover acetic acid in an RD column through esterification with methanol. Commercially available ion-exchange resin particles were used along with Raschig rings in the column. The use of a solid acid catalyst offers non-corrosive conditions so that a less expensive material of construction can be used. Up to 84 % recovery of acetic acid as methyl acetate was achieved. Xu et al. [8] have recently performed detailed experimental and simulation work on recovery of acetic acid from about 10 % (w/w) aqueous solutions using the same reaction with Amberlyst-15 in the form of catalyst baskets. More than 50 % recovery was obtained in a 1.5 m high column. They also explained their experimental results with the help of a steady state simulator. Hoechst Celanese Corporation have described an RD process for the recovery of acetic acid from aqueous solutions as methyl acetate. With the use of acidic ion-exchange resin as catalyst, more than 90 % recovery from 5–30 % aqueous acetic acid is described. They also suggest the use of Koch Engineering's Katamax packing as the catalyst for this reaction [9]. Apart from esterification with methanol, esterification with other alcohols may also be used for recovery. Saha et al. [14] have explored the possibility of esterifying acetic acid from aqueous solution with *n*-butanol in an RD column. In this case one gets an over-

head product of composition close to the ternary heterogeneous azeotrope of butanol, butyl acetate, and water. The high-molecular weight acids such as lactic acid and myristic acid can be successfully recovered through esterification with alcohols such as methanol and isopropanol respectively [16, 17]. The same logic may work for the other acids such as adipic acid, succinic acid, chloroacetic acid, trifluoroacetic acid, and glycolic acid.

RD can be applied for recovery of many other chemicals from their dilute streams. The polymer industry is often faced with the challenge of treatment of aqueous formaldehyde solutions, which are environmentally damaging but difficult to remove. RD with methanol, ethanol, or ethylene glycol not only brings down the formaldehyde concentration to ppm level but also yields useful acetal products [34, 35]. On the other hand, the high-boiling alcohols such as ethylene and propylene glycol from fermentation streams can possibly be recovered through acetalization with either formaldehyde or acetaldehyde in an RD column [36]. Similarly, non-boiling chemicals such as glyoxal and glyoxylic acid can be recovered from their aqueous solutions through the formation of their corresponding acetals or esters, which can be separated by distillation [107, 108].

RD is reported to have been employed for purification of phenol as the raw material for the manufacture of bisphenol A of polycarbonate grade. The impurities, in the form of carbonyl compounds such as acetone, mesityl oxide, and hydrotropaldehyde, are required to be reduced from about 3000 ppm to vanishing levels ($<$ 10 ppm). A continuous RD column has been described as a versatile method to achieve this objective [109]. Hydrogenative distillation has been demonstrated to be an attractive choice for the removal of the impurities of carcinogenic benzene from light reformate and α-methyl styrene from cumene [64, 65]. The acrylonitrile product stream has been successfully purified by facilitating the reaction of aldehyde (e. g., acrolein) impurities with suitable amine in RD [84]. Similarly crude acetone may be purified by removing aldehyde (formaldehyde or acetaldehyde) impurities through the reaction with diamines in RD [105].

1.11 Difficult Separations

As mentioned before, RD can be used as an efficient separator to achieve difficult quantitative separations. The difference in the reactivity of the components can be exploited advantageously. A comprehensive review of separations through selective reactions has been published, which covers several systems that fall under this category [110]. The use of reversible chemical reactions to enhance isomer distillation can be traced back to the 1970s. The separation of a mixture of isomers such as *m*-xylene and *p*-xylene through selective transalkylation of *m*-xylene has been reported and is still under investigation. Gau suggested transmetallization with organometallic compounds for this purpose [50]. RD of pyridine mixtures with organic acids [87] and cresol isomers with amines [101] has also been explored. Similarly, the separation of cyclohexene and cyclohexane through either esterification or hydration

may be conveniently performed in an RD column. This separation is of prime importance in a new route for manufacturing cyclohexene by partial hydrogenation of benzene.

1.12 Chemical Heat Pumps

The chemical heat pump system involves the combination of an endothermic reaction at low temperature and an exothermic reaction high temperature. It essentially absorbs heat at low temperature and liberates the same at high temperature. Normally a reversible reaction such as dehydrogenation of 2-propanol to acetone at low temperature and hydrogenation of acetone at high temperature is chosen for this purpose. The reactions can be performed in RD units in order to achieve good conversion, in-situ separation, and high energy-efficiency [71].

1.13 RD with Supercritical Fluids

Supercritical fluids are known to posses several useful characteristics required to achieve efficient separation and enhanced reaction rates. It is also quite likely that the introduction of the additional supercritical phase can be beneficial in certain cases (Tab. 1.3). Suitable candidates are the reactions that involve components having their critical properties close to the reaction conditions. The reaction pressure may be manipulated to fine-tune the required conditions. Hydration of ethylene, propylene, *n*-butenes and isobutylene, esterifications of carboxylic acids with these olefins, and even alkylations (e. g., cumene production, C_8 alkylates from C_4 streams) may be explored as potentially important reactions in this category.

Table 1.3 Potentially important candidates for RD with supercritical fluids.

Esterfication of acetic acid with ethylene, propylene, butenes and isobutylene
Hydration of ethylene, propylene, butenes and isobutylene
Alkylation of benzene with propylene
Alkylation of *n*-butenes with isobutane
Metathesis/disproportionation of olefins (C_2 to C_6)

1.14 Conclusions

RD is based on the concept of combining reaction and distillation to enhance the performance of either of them. Though it is an old concept and has been successfully used in some traditional processes, its application area has widened signifi-

cantly in recent years. Many more reactions and separations are yet to be evaluated for their use in RD. We have tried to suggest a few such potential applications. Nevertheless, with the remarkable progress that has been seen on several other fronts, such as in the development of column hardware, modeling for design and simulation, control strategies and so on, and considering the pace at which new applications are being explored, RD is destined to become one of the most important tools for process integration and intensification.

References

1 Quang D. V., Amigues P., Gaillard J., Leonard J., Nocca J., **1989**, US Pat. 4,847,430; US Pat 4,847,431; Smith Jr. L. A., **1980**, US Pat. 4,215,011; **1981**, US Pat. 4,307,254; **1990**, US Pat. 4,978,807; Marker T. L., **1993**, US Pat. 5,258,560.

2 Jacobs R. and Krishna R. S. R., *Ind. Eng. Chem. Res.*, **1993**, *32*, 1706–1709; Nijhuis S. A., Kerkhof F. P. J. M., and Mak A. N. S., *Ind. Eng. Chem. Res.*, **1993**, *32*, 2767–2774; Hauan S., Hertzberg T., and Lein K. M., *Ind. Eng. Chem. Res.*, **1995**, *34*, 987–991; Mohl K. D., Kienle A., Gilles E. D., Rapmund P., Sundmacher K., and Hoffmann U., *Comp. Chem. Eng.*, **1997**, *21*, S989–S994; Sundmacher K. and Hoffmann U., *Chem. Eng. J.*, **1995**, *57*, 219–228.

3 Bravo J. L., Pyhalahti A., and Jarvelin H., *Ind. Eng. Chem. Res.*, **1993**, *32*, 2220–2226; Brockwell R., Sarathy P. R., and Trotta R., *Hydro. Process.*, **1991**, *70* (9), 133–136.

4 Quitain A., Itoh H., and Goto S., *J. Chem. Eng. Japan*, **1999**, *32*, 280–287; Oudshoorn O. L., Janissen M., van Kooten W. E. J., Jansen J. C., van Bekkum H., van den Bleek C. M., and Calis H. P. A., *Chem Eng. Sci.*, **1999**, *54*, 1413–1418.

5 Marker T. L., Funck G. A., Barger T., and Hammershaimb U., **1996** US Pat. 5,504,258.

6 Neumann R. and Sasson Y., *Ind. Eng. Chem., Pro. Des. Dev.*, **1984**, *23*, 654–659.

7 Jones S. and Fallon D. G., **1997**, US Pat 56,485,29.

8 Xu Z., Afacan A., and Chuang K., *Can. J. Chem. Eng.*, **1999**, *77* (8), 676–681; *ibid*, Part 2, 682–687.

9 Scates M. O., Parker S. E, Lacy J. B., and Gibbs R. K., **1997**, US Pat 5,599,976.

10 Bessling B.; Löning J. M.; Ohligschläger A.; Schembecker G., and Sundmacher K., *Chem. Eng, Technol.*, **1998**, *21*, 393–400.

11 Barbosa D. and Doherty M. F., *Chem. Eng. Sci.*, **1988**, *43*, 1523–1537; *ibid.*, 2377–2389.

12 Agreda V. H., Partin L. R., and Heise W. H., *Chem. Eng. Progress*, **1990**, *86*, 40–46.

13 Zhicai Y., Xianbao C., and Jing G., *Chem. Eng. Sci.*, **1998**, *53*, 2081–2088; Leyes C. E. and Othmer D. F., *Trans AIChE*, **1945**, *41*, 157–196.

14 Saha B., Chopade S. P., and Mahajani S. M., *Catal. Today*, **2000**, *60*, 147–157.

15 Hanika J., Smejkal Q., and Kolena J., *Int. Symp. Catal. Multiphase Reactors*, **2000**, 343–349.

16 Choi J. and Hong W. H., *J. Chem. Eng. Japan*, **1999**, *32* (2), 184–189.

17 Bock H., Wozny G., and Gutsche B., *Chem. Eng. Process*, **1997**, *36*, 101–109.

18 Lopez R., **2000**, US Pat. 6,013,821.

19 Fang Y., Jiang G., Gu J., Dai D., and Han C., Faming Zhuanli Sheqing Gongkai Shuomingshu, **1998**.

20 Saha, B. and Sharma, M. M., *React. Funct. Polymers*, **1996**, *28* (3), 263–278.

21 Zoeller J. R., Lane D. W. C.; Eleanor H., Fuller, Jr. D. W., and Barnicki S. D., 1998, US Pat. 58,21,384.

22 Anonymous, ECN, March **1999**, 29.

23 Oyevaar M. H., To B. W., Doherty M. F., and Malone M. F., **2000**, WO Pat. 018,720A.

24 Luo H. and Xiao W., *Chem. Eng. Sci.*, **2001**, *56*, 403–410.

25 Geelen H. and Wijffels J. B., *3rd Int. Symp. Chemical Reaction Engineering*, 125–133, Pergamon Press. Oxford, UK, 1965

26 Fuchigami Y., *J. Chem. Eng. Japan*, **1990**, *23*, 354–360.

27 Kim K. and Roh H. D., **1995**, US Pat 57,70,770; Palmor D. A., Larson K. D., and Fjare K. A., **1992**, US Pat. 51,13,01.

28 Han S. J., Jin Y., and Yu Z. Q., *Chem. Eng. J.*, **1997**, *66*, 227–230.

29 Wang C. and Shen Q., *Huaxue Fanying Gongcheng*, **2000**, 136–141.

30 Anonymous, (edited by Parkinson G.) *Chem. Eng.*, Jan **2001**, p.15.

31 Masamoto J. and Matsuzaki K., *J. Chem. Eng. Japan*, **1994**, *27*, 1–5.

32 Kolah A. K., Mahajani S. M., and Sharma M. M., *Ind. Eng. Chem. MasamotoRes.*, **1996**, *35*, 3707–3720.

33 Smith L. A. and Arganbright R. P., **2000**, US Pat 60,15,875.

34 Chopade S. P. and Sharma M. M., *React. Funct. Polym.*, **1997**, *32*, 53–64.

35 Chopade S. P. and Sharma M. M., *React. Funct. Polym.*, **1997**, *34*, 37–45.

36 Broekhuis R. R., Lynn S., and King C. J., *Ind. Eng. Chem. Res.*, **1994**, *33*, 3230–3237.

37 Groening C., Ebel K., Kaibel G., Therre J., Koopmann J., Menig H., Fritz G., and Broekhuisd Dretz R., **1996**, EP 7,04,422.

38 Podrebarac G., Ng F. T. T., and Rempel G. L., *Chem. Eng. Sci.*, **1998**, *53*, 1067–1075; *ibid*, 1077–1088.

39 Mori T., Fujita K., Kajita Y., and Takai M., 1996, US Pat 56,67,644.

40 Ciric A. R. and Miao P., *Ind. Eng. Chem. Res.*, **1994**, *33*, 2738–2748.

41 Ciric A. R. and Gu D., *AIChE J.*, **1994**, *40*, 1479–1487.

42 Monroy-Loperena R. and Alvarez-Ramirez J., *Ind Eng. Chem. Res.*, **1999**, *38*, 451–455.

43 Smith L. A., **1980**, US Pat 43,07,254.

44 Smith L. A., **1993**, US Pat 52,21,441.

45 Knifton J. F., Sanderson J. Ronald S., Melvin E., 1998, US Pat 58,11,620; US Pat 58,49,971.

46 Gonzalez J. C., Subawalla H., and Fair J. R., *Ind. Eng. Chem. Res.*, **1997**, *36*, 3833–3844; *ibid*, Part 2, 3845–3853.

47 Watanbe R., Nakanishi A., **1997**, Jap Pat. 2,87,600.

48 Shoemaker J. D. and Jones E. M., *Hydro. Process.*, **1987**, *66* (6), 57–60.

49 Wen l., Min E., Peng G., and Yu W., *Huagong XueBao*, **2000**, *51* (1), 115–119.

50 Venkataraman, Chan, W. K., and Boston J. F., *Chem. Eng. Prog.*, **1990**, 45–55; Saito S., Michishita T., and Maeda S., *J. Chem. Eng. Japan*, **1971**, *4*, 37–43; Gau G., **1974**, US Pat., 3,849,261.

51 Hendriksen D. E., Lattner J. R., and Janssen M. J. G., 1999, US Pat. 60,02,057.

52 Hearn D,. Arganbright R. P, Smith L., and Adams J., **1999**, US Pat 60,02,058; Chen J., **1999**, US Pat. 58,66,736.

53 Hsieh C. R. and Robinson; R. 1993, US Pat 52,10,348.

54 Ryu J. Y. and Groten W. A., 1998, US Pat. 58,11,623.

55 Huss A. and Kennedy C. R., **1990**, US Pat. 49,35,577.

56 Krill S., Giray G., Hiibner F., Hahn R., Huthmacher K., and Tanner H., **1999**, US Pat. 59,07,065.

57 Arganbright R. P., **1991**, US Pat. 50,87,780; Dorbon M., Lyons, F., Chodorge J., Cosyns; J., Viltard J., and Didillon B., 1999, US Pat. 59,69,203.

58 Anonymous, (edited by Parkinson G.) *Chem. Eng.*, Jan **2001**, p.15.

59 Lebas E., Jullian S., Travers C., Capron P., Joly J., and Thery M., **1999**, US Pat. 59,48,948.

60 Feathers R. E. and Mansell J. D, 1992, US Pat. 51,49,892.

61 Barnum C. S. and Blaisdell C. T., **1995**, US Pat. 54,49,801.

62 Gotze L. and Bailer O., *Sulzer Tech. Review*, **1999**, *4*, 29–31.

63 Gildert G. R., Hearn D.and Putman H. M., **1998**, US Pat. 57,73,670.

64 Rock K., Gildert G. H., and Meguirk T., *Chem. Engng. New York.*, **1997**, July, 78–82; E & CN News, 20–26 July, **1998**, p.20.

65 Hildreth J., **1999**, US Pat. 59,05,178.
66 Lowson K. and Nkosi B., **1999**, US Pat. 60,08,416.
67 Clifford S. C., **1998**, US Pat 58,37,130.
68 Hearn D. and Putman H. M., **1998** US Pat 57,79,883.
69 Hicky T. P., Hearn D., and Putman H. M., **1999**, US Pat. 59,61,815.
70 Schmitt K., New acetone chemistry in Germany, Scholven report, A reprint from *Chemische Industrie Int.*, **1966.**
71 Chung Y., Jeong H, Song H. K., and Park W. H., *Comp. Chem. Eng.*, **1997**, *21,* S1007–S1012.
72 Imai T., **2000**, US Pat. 60,40,489.
73 Hearn D. and Nemphos S., **1997**, US Pat. 55,99,997.
74 Nemphos S. P., Groten W. A., and Adams J. R., **1999**, US Pat. 58,86,055.
75 Jung C. W., Garrou P. E., and Strickler G. R., **1987**, US Pat. 47,09,115.
76 Hu M., Zhou X., and Yuan W. K., *Chem. Eng. Sci.*, **1999**, *54*, 1353–1358.
77 Anonymous, *Chemical Weekly* (India), **1996**, 91.
78 Vora B. V. and Hammershaimb H. U., **2000**, US Pat. 60,25,533.
79 Podrebarac G. G., Ng F. T. T., and Rempel G. L., *CHEMTECH*, **1997**, May, 37–45.
80 Zao Y., Qin S., Yu Z., and Xue F., **2000**, CN Pat 1,230,583.
81 DiGuilio; R. M. and McKinney M. W., 2000, US Pat 60,75,168.
82 Voss B., **2000**, EP 978,501.
83 Smith L. A., **1982**, US Pat. 4,332,968.
84 Patel N. R., Lewis V. E., and Enderson M. D., **2000**, EP 9,99,207.
85 Nemphos S. P. and Hearn D., 1997, US Pat 56,79,862.
86 Dorai S., **1998**, US Pat 58,52,218.
87 Duprat F. and Gau G., *Can. J. Chem. Eng.*, **1991**, *69,* 1321–1326; *ibid*, 1327–1335.
88 Carra S., Santacesaria E., Morbidelli M., and Cavalli L., *Chem. Eng. Sci.*, **1979**, *34,* 1123–1132.
89 Doherty M. F. and Buzad G., *Trans IChemE*, **1992**, *70* (A), 448–458; Grosser J. H., Doherty M. F., and Malone M. F., *Ind Eng. Chem.Res.*, **1987**, *26,* 983–989; Jaswal I. and Pungi K., **1975**, US Pat. 39,00,450.
90 Belson D. J., *Ind Eng. Chem. Res.*, **1990**, *29,* 1562–1565.
91 Jaydeokar S. S. and Sharma M. M., *React. Polym.*, **1993**, *19,* 169–175.
92 Matkar N., PhD Thesis, University of Bombay, **1996.**
93 Rhim J. K., Bae S. Y., and Lee H. T., Hwahak Konghak, **1983**, *21* (1), 35–45.
94 Lee L. and Kuo M., *Fluid Phase Equilibria*, **1996**, *123*, 147–165.
95 Tang Q., Qingrong X., and Lanyue H. X., **1999**, CN pat 1,225,911.
96 Bollyn M. P. and Wright A. R., *Comp. Chem. Eng.*, **1998**, *22,* S87–S94.
97 Duranleau R. G., Nieh E. C. Y., and Knifton J. F., **1987**, US Pat. 46,91,041.
98 Robinson C. S. and Gilliland E. R., *Elements of Fractional Distillation*, McGraw-Hill, New York, **1950.**
99 Sie S. T. and Lebens P. J. M., Monolithic reactor for countercurrent gas–liquid operation, In *Structured Catalyst and Reactors* (edited by Cybulski A. and Moulijn J. A.), Marcel Dekker, New York, **1998**, 305–321.
100 Xu Z. and Dudukovic M, *Chem. Eng. Sci.*, **1999**, *54*, 1397–1403.
101 Gaikar V. G. and Sau G. K., *Sep. Technol*, **1996**, *31*, 1979–1988; Ningoo S. R. and Gaikar V. G., *ibid.*, **1994**, *4,* 249–251.
102 Lee J. W., Hauan S., and Westerberg A. W., *AIChE J.*, **2000**, *46,* 1218–1233.
103 Gumus Z. H. and Ciric A. C., *Comp. Chem.Eng.*, **1997**, *21,* S983–S988.
104 Imamura T., *Jpn Kokai Tokkoyo Koho*, **1992**, JP 04,234,334.
105 Ikari A., Harate Y., and Akio R., *Kagaku Kogaku Ronbun*, **1998**, *24* (4), 638–641.
106 Fraini E. A., Tepera G. W., **1995**, US Pat. 53,99,776.
107 Mahajani S. M., *React. Funct. Polym.*, **2000**, *43* (3), 253–268.
108 Mahajani S. M. and Sharma M. M., *Org. Proc. Res. Dev.*, **1997**, *1,* 97–105.
109 Sharma, M. M., *React. Funct. Polym.*, **1995**, *26,* 3–23.
110 Gaikar V. G. and Sharma M. M., *Sep. Pur. Methods*, **1989**, *18,* 111–176.

Reactive Distillation. Edited by Kai Sundmacher, Achim Kienle

ISBNs: 3-527-30579-3 (Hardback); 3-527-60052-3 (Electronic)

2
Reactive Distillation Process Development in the Chemical Process Industries

H. G. Schoenmakers and B. Bessling

2.1
Introduction

Reactive distillation (RD) is a key opportunity for improving the structure of a process [1, 2]. The combination of distillation and reaction is possible, of course, only if the conditions of both operations can be combined. This means that the reactions have to show data for reasonable conversions at pressure and temperature levels that are compatible with distillation conditions. The type of catalysis is also important. Homogeneous catalysis is possible in most cases but needs a separation step to recycle the catalyst. This can be avoided in heterogeneous catalysis, but here special constructions are necessary to fix the catalyst in the reaction zone. If everything harmonizes, considerable advantages arise: for the production of methyl acetate via RD , for example, only one column is needed instead of nine and a reactor (Fig. 2.1).

Is this an exception or does it represent a type of process with a considerable potential for improvement?

The question is:

- how processes can be identified that exhibit potential for RD,
- how such a process can be developed, and
- how the equipment can be designed.

Some answers to this question will be offered from the viewpoint of an industrial user. The first question refers to the phase of the process synthesis, the second to process development by simulation and experimental validation, and the third to the choice and design of suitable equipment.

The results presented here are not only internal research results but also from joint research in Europe.

In view of the fact that, unlike conventional distillation, there was no integrated development strategy for progressing from the idea to a working process for RD, several European companies and universities joined forces in 1996 to work on a development strategy for RD processes under the umbrella of a Brite-Euram pro-

Production of methyl acetate at Eastman Kodak: without / with reactive distillation

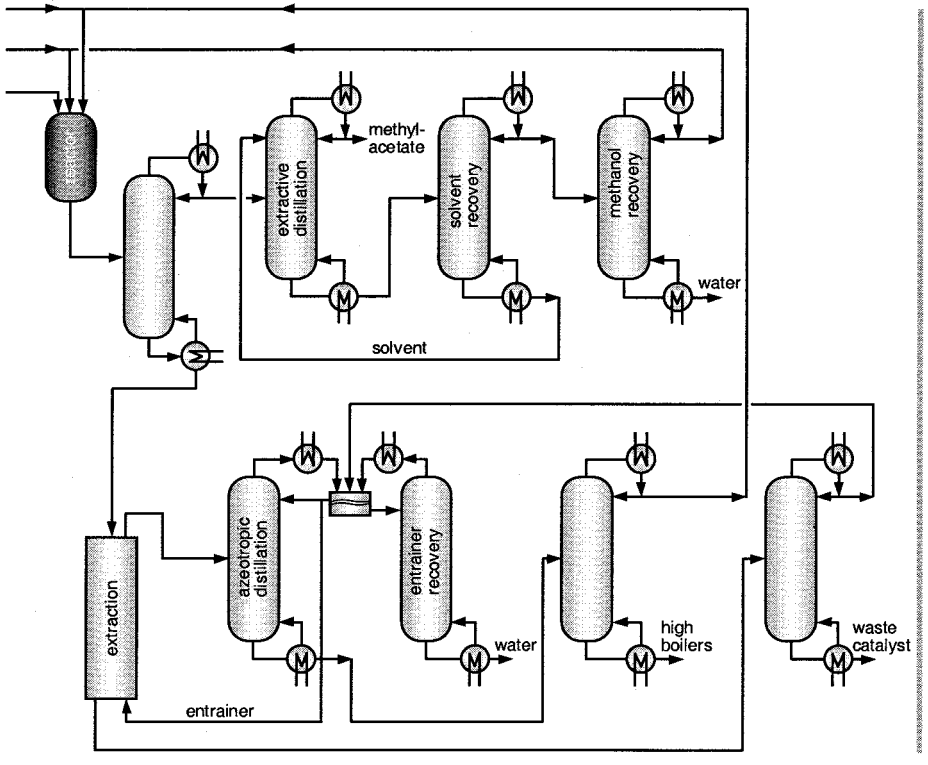

Fig. 2.1 Eastman Kodak process for methyl acetate

ject. The partners from industry were BASF, BP, Hoechst, Neste Oy, and Snamprogetti. The academic partners were the Universities of Aston, Bath, Clausthal, Dortmund, Helsinki, and Moscow [3].

This first Brite-Euram Project had a duration of 3 years and a budget of about 3.8 million dollars. The task of the Universities was to develop methods and software; the task of the industrial partners was to run the experiments. The key subject areas for this project were process synthesis, process design, and experiments using industrially relevant reaction systems and catalyst systems. In the areas of process synthesis and design, computational tools were developed in accordance with the CAPE programming guidelines.

Now a second European project has started. It is called *Intelligent column internals for reactive distillation* (INTINT) and deals specifically with the design of suitable column internals adapted to the requirements of reaction and distillation, not only of distillation, as is the case with normal packing. Again, experimental results and simulation tools are the key subjects. The project duration is 3 years, up to 2003, and the budget is comparable with that of the first EU project.

In addition, results of internal research at BASF will be reported in connection with questions about suitable equipment.

2.2 Process Synthesis

In RD, the reaction is superimposed on distillative separation. On the one hand, this results in synergistic effects, such as a shift in the chemical equilibrium as a result of products being removed and distillation limits being exceeded owing to the reaction, while, on the other hand, it is precisely these synergies which make RD so extraordinarily complex. It should be borne in mind that today's Eastman Kodak process was not patented until 60 years after the first MeAc patent.

A vital aim of process synthesis is therefore to reduce the complexity of RD in order to enable simple solutions of this sort to be recognized quickly. To analyze processes involving reversible reactions systematically, a comprehensive process synthesis strategy has been developed. One element of this strategy is the analysis of RD lines. RD lines enable the feasibility of RD processes to be examined simply. The simplification is based on the fact that, according to the Gibbs phase rule (Fig. 2.2), the number of degrees of freedom of a system in physical and chemical equilibrium is reduced by the number of independent equilibrium reactions. Thus, in the case of a liquid-boiling system composed of three components A, B, C, which react according to $A + B \leftrightarrow C$, only one concentration has to be defined in order to fix the composition, unlike the case of a system without a reaction where two concentrations have to be defined.

In order to be able to handle these concentration parameters appropriately, various authors have developed transformation methods [4]. These transformation methods enable RD to be described by a system of equations that is known from conventional distillation. The transformation converts the concentration para-

Transformation of the system A + B ↔ C

- **Gibbs phase rule: F = C – Ph – R + 2**

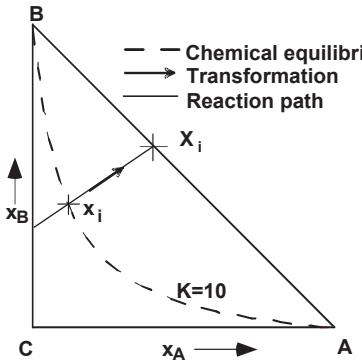

$$\sum_{i=1}^{nc} \nu_i A_i = 0$$

$$X_i = \frac{x_i - \frac{\nu_i x_P}{\nu_P}}{1 - \frac{\nu_T x_P}{\nu_P}}$$

$$Y_i = \frac{y_i - \frac{\nu_i y_P}{\nu_P}}{1 - \frac{\nu_T y_P}{\nu_P}}$$

Fig. 2.2 Gibbs rule

meters *x* and *y* for the liquid- and gas-phase concentrations into the concentration parameters *X* and *Y*, Fig. 2.3.

At the same time, the transformation eliminates the reaction term in the balance equation. The operating line for the rectifying section of a reaction column is formally identical to the operating line of a non-reactive column. An infinite reflux ratio gives an expression that is formally identical to the one for calculating conventional distillation lines [5, 6]. Accordingly, we will refer to lines that have been calculated by this procedure as RD lines. These analogies are found for all the relationships that are important in distillation [7, 8].

These analogies become particularly clear if we look at the synthesis of methyl acetate (MeAc) from methanol (MeOH) and acetic acid (HAC) as an example. Essentially, we see diagrams that are similar to the distillation line diagrams of non-reactive systems. As a result of the transformation, the four pure substances lie at the corners of a square and the non-reactive binary systems lie along the edges.

Balance: Rectifying operating line of a RD column

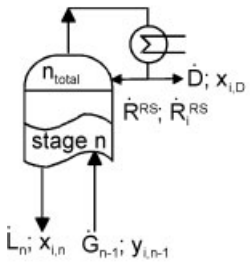

$$\dot{G}_{n-1} = \dot{D} + \dot{L}_n - \dot{R}^{RS}$$

$$\dot{G}_{n-1} y_{i,n-1} = \dot{D} x_{i,D} + \dot{L}_n x_{i,n} - \dot{R}_i^{RS}$$

$$\overline{G_{n-1}} = \overline{L_n} + \overline{D}$$

$$\overline{G_{n-1}} Y_{i,n-1} = \overline{L_n} X_{i,n} + \overline{D} X_{i,D}$$

$$Y_{i,n-1} = \frac{\nu_n}{\nu_n + 1} X_{i,n} + \frac{1}{\nu_n + 1} X_{i,D}$$

$$\nu \to \infty \; ; \; Y_{i,n-1} = X_{i,n}$$

Fig. 2.3 Transformation of variables

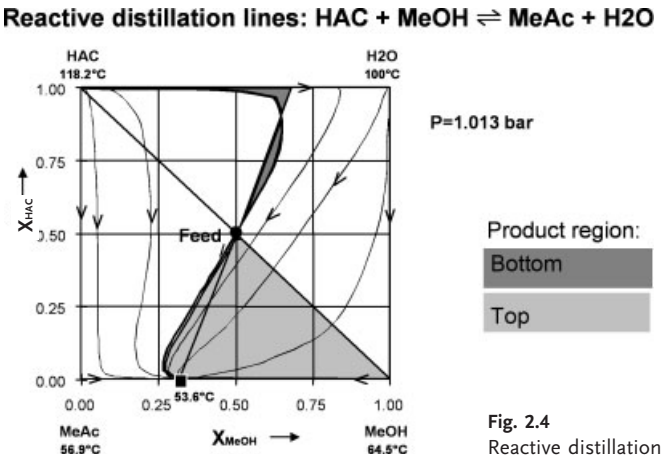

Fig. 2.4
Reactive distillation lines with one feed

The highest boiling point in the system is that of acetic acid, while the lowest boiling point is displayed by the MeOH–MeAc azeotrope (Fig. 2.4). The RD line diagram makes it possible to determine the product regions of RD for infinite reflux. Analogously to conventional distillation, the top and bottom products have to lie on an RD line and on the balance line. It can be seen that the desired products, namely MeAc and water, do not lie in the product region.

But by analogy with extractive distillation, it can be expected that a second feed point would drastically widen the product region at a finite reflux ratio and thus also increase the conversion. Between the two feed points, the column profile is perpendicular to the distillation lines (Fig. 2.5). Since this effect is based on the finite nature of the reflux ratio employed, we can expect product purity and conversion to first increase with an increase in the reflux ratio and then slowly decrease again. The limiting value that is established for an infinite reflux ratio is determined by the azeotrope concentration in the methyl acetate/methanol system.

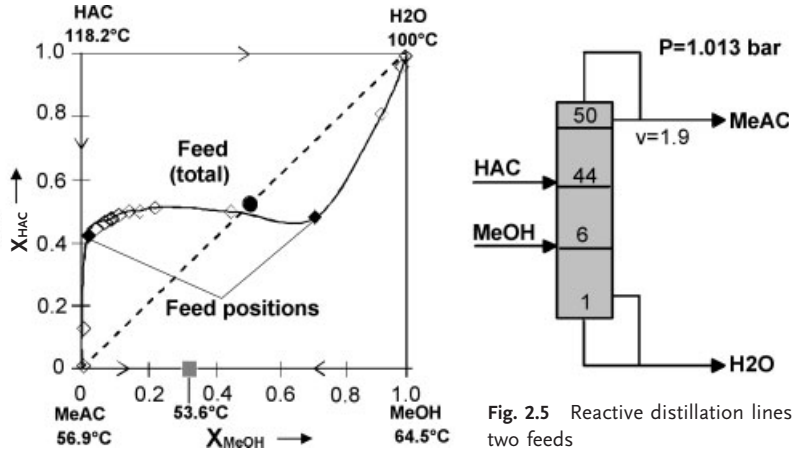

Fig. 2.5 Reactive distillation lines with two feeds

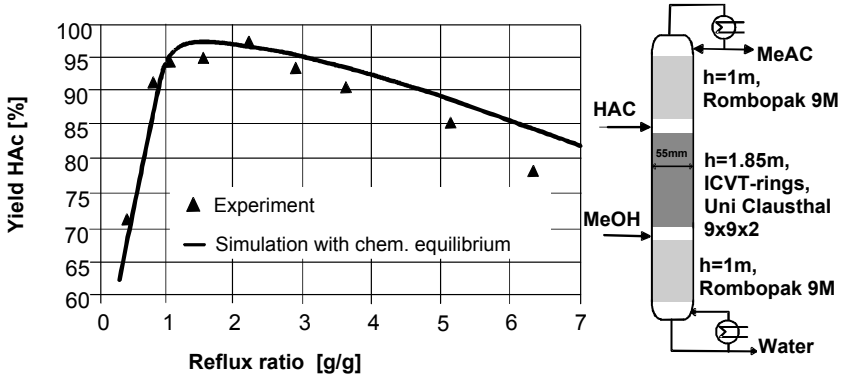

Fig. 2.6 Comparison simulation: experiment for an equilibrium stage model

Our calculations using an equilibrium stage model agreed well with the experiments based on separation performance measurements using catalytic rings as internals (Fig. 2.6). On the basis of these results, we have to contradict various publications that attribute the decrease to reaction-kinetic effects. The primary effect is the saddle-point character of the products and the associated choice of a second feed point. The options for calculation and especially interpretation of RD lines, which have merely been outlined here are implemented in the program SYNTHESISER, a software product from the first EU-project.

2.3 Process Design and Optimization

While process synthesis gives good qualitative reference points, for industrial implementation we need quantitative results, which are as exact as possible. The development of a program called Designer to simulate reactive rectification was therefore a further major focus of the first EU project.

Firstly, process synthesis is used to determine whether RD is feasible and, if so, the configuration required (second feed point, combination of reactive and non-reactive zones). This provides first initial values and thus a good starting point for deriving a zero-design using the stage model. The results from the stage model in turn give usable initial values for refinement using the mass-transfer model. Apart from the stepwise change in the level of detail in the model, it is also possible to systematically match the solution tools to one another:

After the introductory estimate, a first profile can be determined by the relaxation method that gives initial values sufficiently good for the subsequent use of a rigorous method of solution (Fig. 2.7).

Fig. 2.8 shows an example of process simulation using the mass-transfer model and kinetic starting points for the reaction. The simulation and experiment results are shown for the preparation of MTBE from isobutene and methanol. This is an

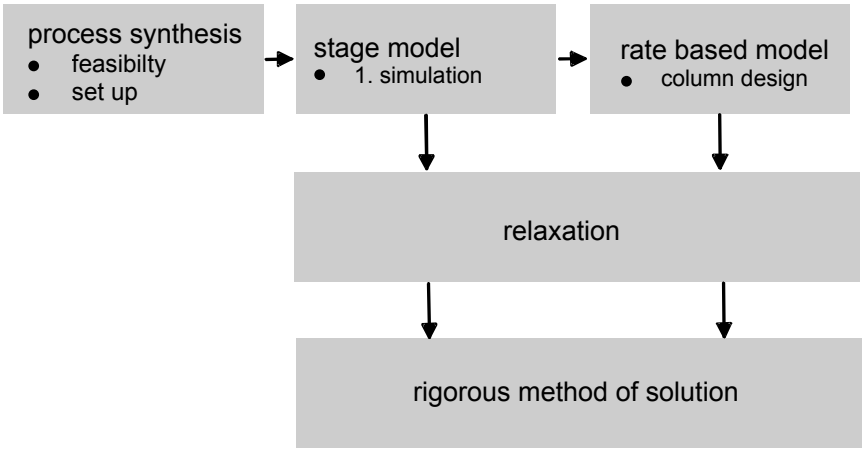

Fig. 2.7 Convergence with Designer

- simulation of the university Helsinki/Finnland
- experiments with cat. rings of the university Clausthal/Germany

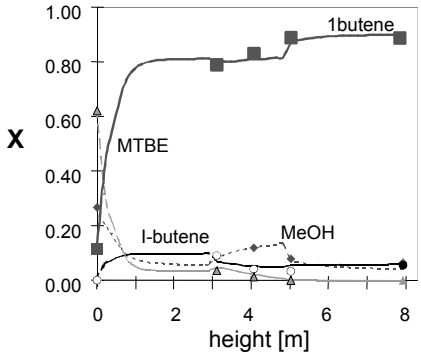

IB+MeOH⇆MTBE
Δh_R=-35kJ/mol

Fig. 2.8 Comparison of experiment with simulation

example of a reaction in which the number of moles of products is different from the number of moles of reactants. The heat of reaction is of the same order of magnitude as the molar heat of vaporization of the participating components. It can be seen that computational results and the experimental points fit well.

This program is a result of the first European project and has not (yet) been commercialized. However there are programs on the market that do the job at least partly. In many cases the results of these programs and the results cited above will agree. Some of the major companies have in-house tools suitable for RD. It is an open question if a rate-based approach as in Designer is really necessary. There are many examples where RD can be simulated adequately with an equilibrium model for thermodynamics.

2.4
Limitations of the Methods for Synthesis and Design: the Scale-Up Problem

It has been shown what can be achieved using the tools and methods developed in the last few years and especially in the first EU project. A question that is at least as interesting is what can, and cannot yet be achieved. In this context, attention should be focused on the main and secondary reactions of a simple esterification, see Fig. 2.9. For such a reaction system it is frequently the case, for time and cost reasons, that a complete kinetic model cannot be developed.

It may be of little consequence whether the process development chemist or engineer lacks an understanding of the secondary reactions on the basis of customary kinetic studies, since they frequently play hardly any role, as long as the distillation does not continuously shift the equilibrium. However, the careful process engineer will carry out experiments in a reaction column to verify the achievable purities and yields. And with the results of these experiments a scale-up problem exists. The reason is that in these experiments, reaction and mass transfer interact with one another. This interaction can be explained with reference to the main reaction, Fig. 2.10. If a separation process is superimposed on this reaction, the products water and ester (as an example, not valid for every ester) are separated off as low- and high-boilers respectively. However, the removal of the product accelerates the forward reaction. If the forward reaction is accelerated by raising the tempera-

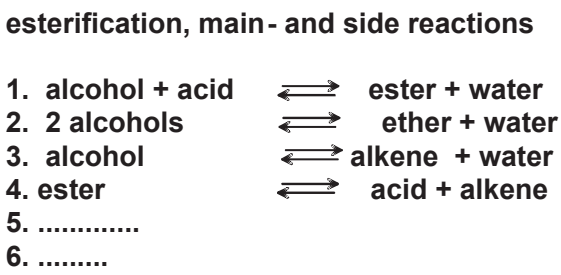

Fig. 2.9 Main and side reactions for esterification

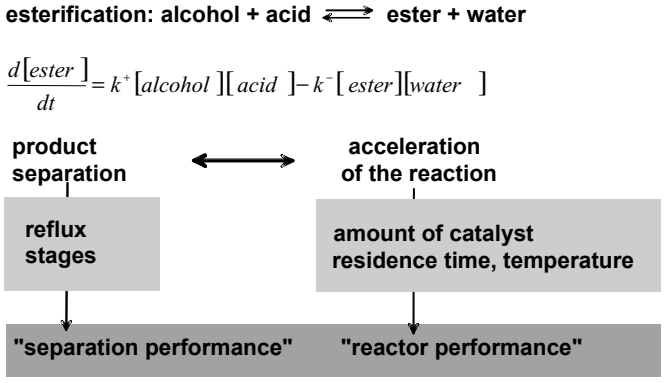

Fig. 2.10 Interaction of reaction and separation

ture or by an increase in the amount of catalyst, the products have to be removed more rapidly in order to avoid a change in concentration.

We would like to refer to the intensity of product removal in a reaction column using the term separation performance and the property of converting the starting materials using the term reactor performance.

If a development engineer has to design an industrial column purely on the basis of miniplant experiments, he has to maintain not only the separation performance but also the ratio of separation performance/reactor performance so that main and secondary reactions proceed to a comparable extent in the industrial-scale reaction column. One way in which this can be achieved is in terms of construction by separating reaction and product separation from one another both in miniplant tests and on an industrial scale. This is possible, for example, when the reaction is carried out in the presence of a heterogeneous catalyst in the downcoming stream or with side reactors at the column. An alternative is to use structured packing with well-defined paths for the liquid flow. This problem has not yet been solved, the main reason being the lack of reference columns on an industrial scale.

As we see it, the way forward is either:

– to develop scale-up methods or
– to carry out RD experiments on an industrial scale.

The latter possibility, which represents a step back to the process-engineering stone-age design of columns, will in many cases mean the end of the line for RD, since a company will rarely be prepared, for time and cost reasons, to build integrated experimental plants on an industrial or semi-industrial scale. So developing an appropriate scale-up procedure for reactive column internals is a key task. The second European project (INTINT) will hopefully provide some contributions.

2.5 Choice of Equipment

Up to now it was assumed that reaction and distillation can favorably be combined in a column: in a normal distillation column in the case of homogeneous catalysis and in a column with special internals or an additional exterior volume in the case of heterogeneous catalysis. This was discussed in the previous chapter under the aspect of scale-up in connection with separation and reaction performance. However columns are an appropriate solution only for reactions that are so fast as to achieve considerable conversions in the residence time range of such columns. The question is whether the full potential for combining reaction and distillation can be found and industrially implemented using columns only.

At BASF, there has been some research on this point in the last couple of years, and the results will be included in the following chapters [9]. For reasons of simplicity the focus will be on equilibrium reactions where the advantages of combining reactions and distillation are obvious. The aspects influencing the choice of the equipment will become particularly clear.

In simple equilibrium reactions, the reaction equation can be described like this

$$A_1 + A_2 \underset{k_{min1}}{\overset{k_1}{\rightleftharpoons}} A_3 + A_4 \tag{2.1}$$

The rate constants for the forward and the reverse reaction may be different. The equilibrium state (when the reaction velocity goes to zero) is described by the law of mass action

$$\frac{c_3^* c_4^*}{c_1^* c_2^*} = \frac{k_1}{k_{min1}} = K_c \tag{2.2}$$

The conversion of the stoichiometrically limiting reactant, for example component 1, in the equilibrium state is

$$U_1^* = 1 - \frac{\dot{V}\, c_3^* c_4^*}{\dot{V}_0\, c_1^* c_2^* K_c} \tag{2.3}$$

The indices 0 indicate the initial state, the indices * the final state (i. e., the equilibrium state). This last equation was developed using some additional simple balance equations.

The equation shows that, the most efficient way of enhancing the conversion is to reduce the concentration of one of the reaction products. That is the principle of superimposing a distillation on a reaction: the theme of this contribution. In the equation the volume effect of a superimposed distillation has been taken into account.

Fig. 2.11 (equilibrium lines) is a graphical representation of the equation above that shows more clearly the possibilities of such a combination: The fractional conversion of component 1 approaches 1 only if the concentration of one reaction product is significantly reduced. This holds true even for extremely unfavorable equilibrium constants. If, for example, the equilibrium constant is 0.01, in the equilibrium state only 1 % of component 1 has been converted. However if component 3 is removed to $x = 0.0001$ mole/mole, conversions of more than 90 % are possible for component 1.

The real conversion may be defined in analogy to an equilibrium conversion but without the equilibrium values:

$$U1 = \frac{n_1^0 - n_1}{n_1^0} \tag{2.4}$$

The reaction velocity of reactant 1 can, in most cases, be described by the simple equation:

$$\tau = k_1 c_1 c_2 - k_{min1} c_3 c_4 \tag{2.5}$$

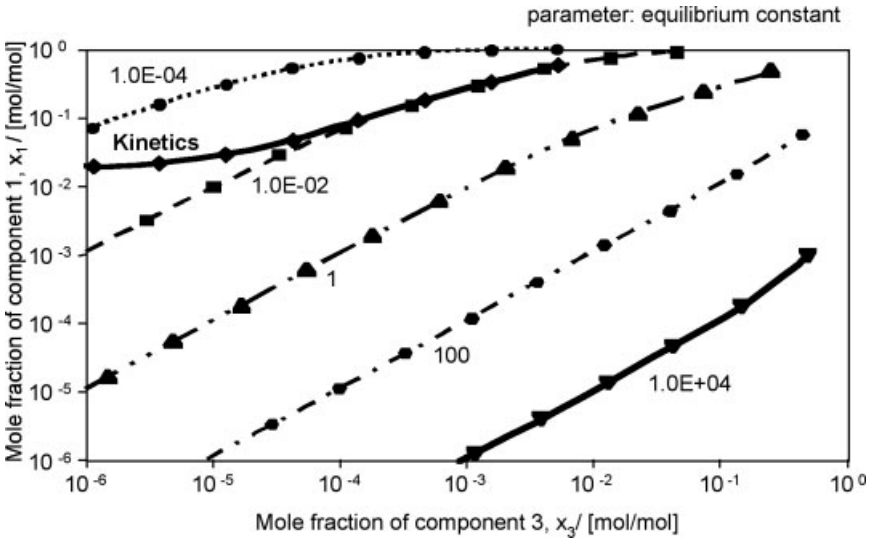

Fig. 2.11 Equilibrium lines and kinetic line

Assuming stoichiometric input, with the volume correction term taking into account the distillation and with some simple balance equations, the equations above can be rearranged in the following way:

$$U_1 = \tau \frac{k_1 c_1 c_2 - k_{\min 1} c_3 c_4}{c_1^0} \tag{2.6}$$

Hence the real conversion is increased if the reverse reaction is suppressed by removing one of the reaction products, for example by decreasing the concentration of component 3. The real conversion is also influenced by the residence time τ or by the product τk . This can be seen in Fig. 2.11, kinetic line. It is obvious that the suppression of the reverse reaction influences conversion only up to a certain limit. A further drop in the concentration of the reaction product does not increase the conversion. The contribution of the reverse reaction has become so low that the conversion depends on the forward reaction rate only, which is a function of the residence time τ and of the reaction constant k.

Thus two operating conditions can be distinguished.

- The range in which the conversion is influenced mainly by the concentration of the component to be separated; this range is called 'controlled by distillation'.
- The range in which the conversion is influenced mainly by the residence time and the reaction constant; this range is called 'controlled by kinetics'.

Industrial process design should aim at operating conditions within these two ranges: just the sufficient residence time and only the necessary expenditure for the distillation.

So we have a second scale-up problem: what is the suitable equipment for complying with these demands? That means more precisely: How can the reactor performance be reached over a broad range of reaction velocities? As preparation for discussion on this question, an alternative configuration is considered (Fig. 2.12): A reaction can be run within a column, that normally is understood as RD, but can also be run in an outside reactor with a pump recycle. Such a sequential arrangement exhibits the same conversion as the simultaneity of reaction and separation as can be seen from Fig. 2.13, where a reactor with pump recycle system and a RD configuration are compared.

So different equipment may be chosen to combine reaction and distillation within the limiting conditions of reaction velocity, relative volatility, and catalytic mechanism as is indicated in Fig. 2.14.

The equipment in question includes:

- stirred vessels,
- cascades of stirred vessels, both with or without columns, and
- reaction columns.

Additional volume can be provided for all of them, examples are listed in Fig. 2.15.

The next considerations concentrate on homogeneous catalysis. Similar considerations apply to heterogeneous catalysis, and this will be commented on later.

At first, a *slow reaction* is considered. 'Slow' means, that the reaction time is slow, compared with the residence times typical for separation equipment such as distillation trays. For residence time reasons a stirred vessel or, better, a cascade of stirred vessels is needed. Each vessel is supplied with energy to evaporate the component to be separated. If the relative volatility of this component is very high, a one stage evaporation is sufficient. At a lower relative volatility the separation requires more stages, so a column has to be put on top of the vessel. If the separation is even more difficult, a stripping section must be added to the column and a reboiler is necessary. In the limiting case of a very low relative volatility, each stage of the cascade can be operated as a countercurrent stage. The first stage is additionally provided with a fractionating column to enrich the component to be separated. Such a setup is equivalent to a reaction column with a large holdup on each reaction stage.

Fast reactions do not demand long residence times, 'fast' meaning that the reaction reaches equilibrium in the residence time range that is typical for column internals. The equipment therefore may be selected under the aspect of separation efficiency . If the relative volatility of the component to be removed is low, a considerable number of stages is necessary. The only appropriate equipment is a column. Depending on the required residence time it may be a packed or a tray column. A relative volatility in the medium range allows the number of stages to be reduced, though the total hold up has to be kept constant. A tray column, perhaps with special bubble cap trays is possible. At a certain (low) relative volatility the

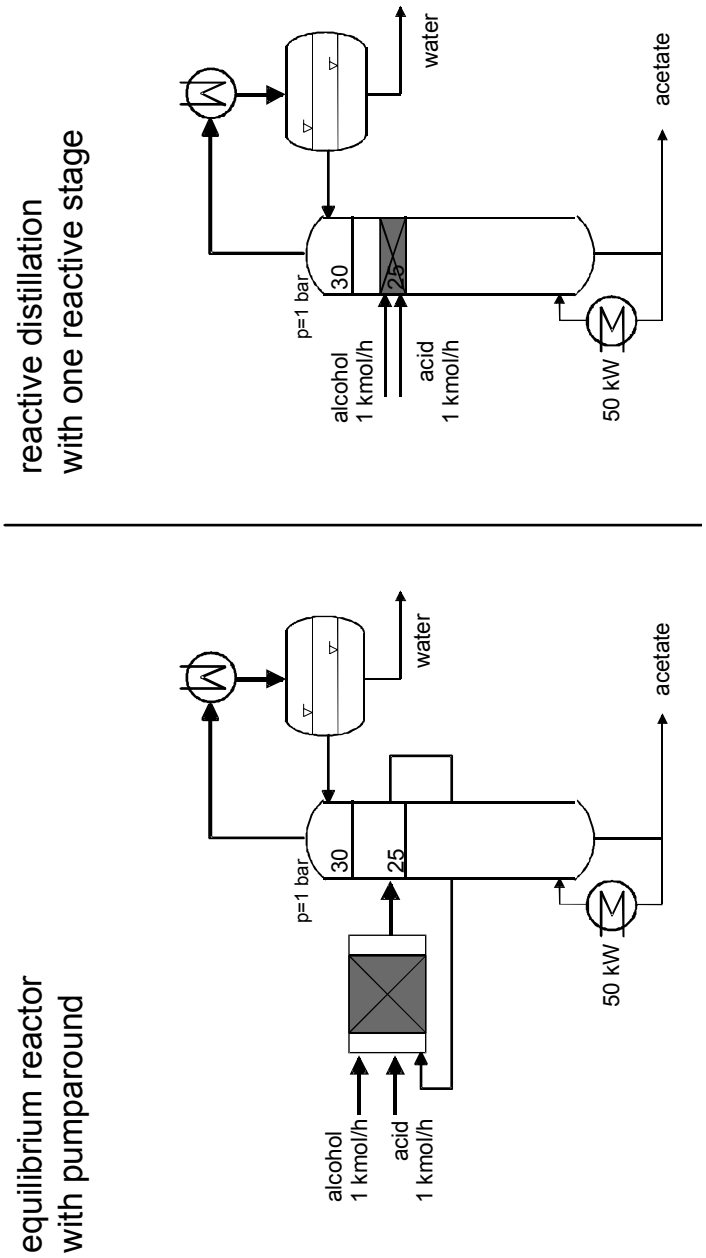

Fig. 2.12 Alternative configurations

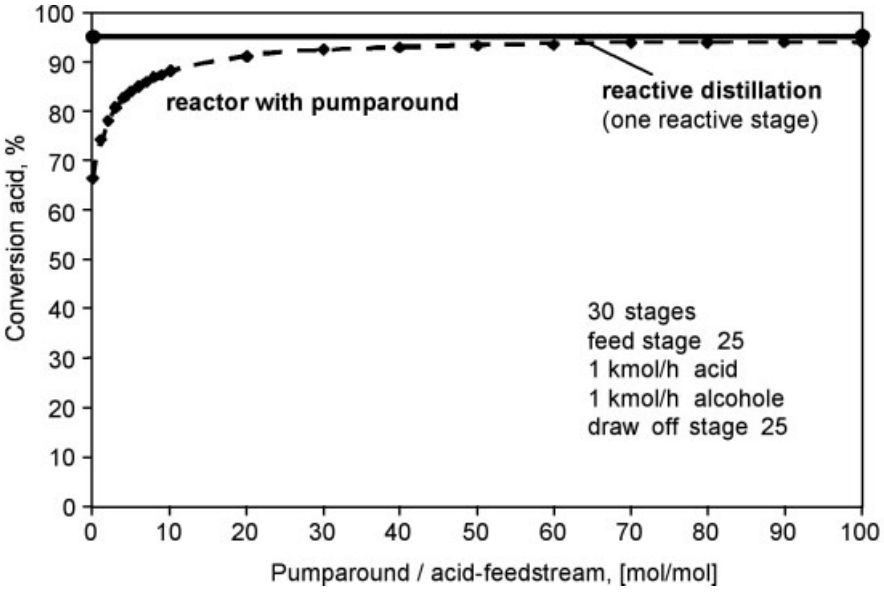

Fig. 2.13 Comparison of reactor with pumparound with RD

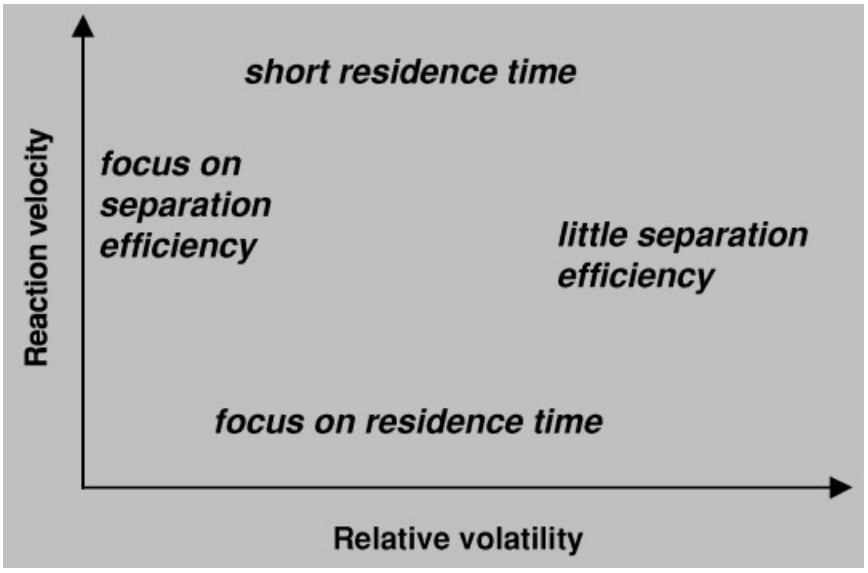

Fig. 2.14 Design with respect to residence time and relative volatility

homogeneous catalysis

- rectification column
- column with larger volume in the bottom
- stirred vessel with rectifying column
- strirred vessel with full column
- vessel cascade with column
- strirred vessel with evaporator
- evaporator
- .....

Fig. 2.15 Equipment suitable for combining reaction and distillation (homogeneous catalysis)

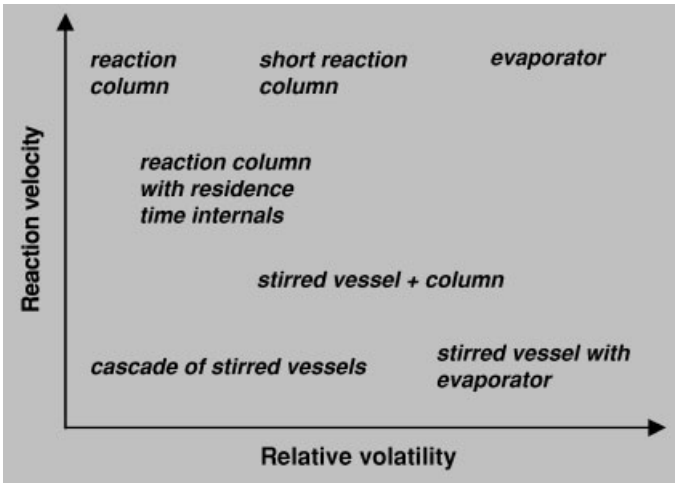

Fig. 2.16 Principles of the choice of equipment (homogeneous catalysis)

number of stages necessary to influence the reaction in a desired way becomes so small and consequently the volume per stage becomes so large that a small reactor with a superimposed column or even a reactor with an evaporator can be used.

In the range of *medium reaction velocities*, mixed constructions are the ideal solution, for example special column trays with large holdup or reactor cascades with a column on the first stage only.

The resulting principles for the choice of equipment for homogeneous catalysis are presented in Fig. 2.16.

As mentioned earlier, heterogeneous catalysis can be treated in a similar manner: Additional, separate reaction volumes are necessary to retain the catalyst. These volumes can be arranged either within the equipment or in a side position [10], coupled by recycle systems. Fig. 2.17 lists the equipment alternatives for heterogeneous catalysis [11]. As in the case of homogeneous catalysis, principles for

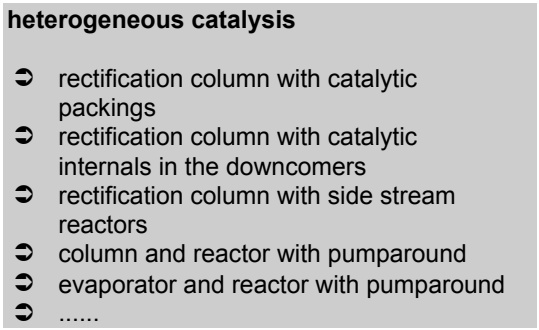

Fig. 2.17 Equipment suitable for combining reaction and distillation (heterogeneous catalysis)

the choice of equipment may be formulated. Some, not all of the possibilities are shown in Fig. 2.18 [12–15].

After the choice of the equipment, which is in principle determined by the reaction velocity and the relative volatility the next step follows: the proper design of the chosen equipment under the special conditions of the process. Only if this step is done with care will the advantage of the proper choice of equipment, the optimum in energy consumption, be realized.

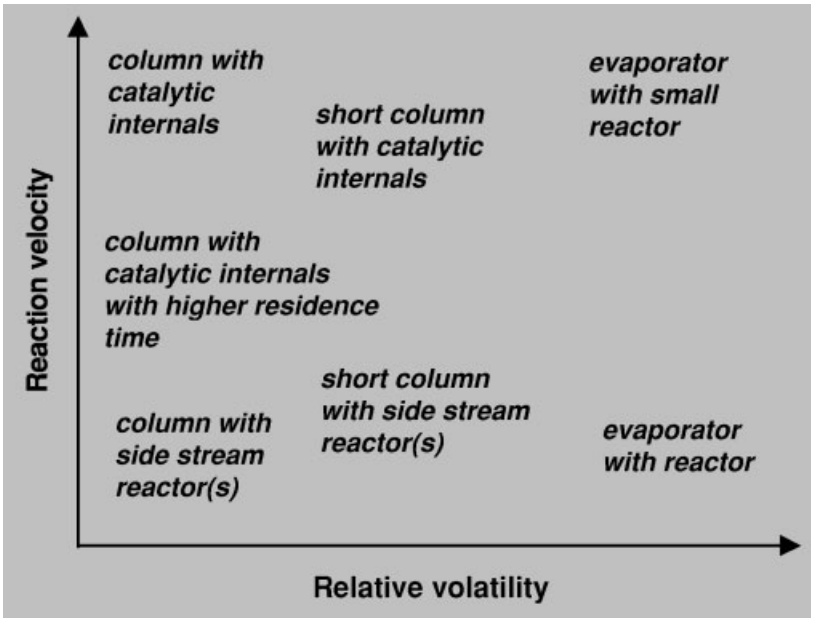

Fig. 2.18 Principles of the choice of equipment (heterogeneous catalysis)

2.6 Some Remarks on the Role of Catalysis

Catalysis can be autocatalytic, homogeneous, or heterogeneous. This is of course also true for RD.

In the case of autocatalytic reactions the reaction velocity can only be influenced by the reaction temperature, in other words for RD by the pressure of the equipment.

Homogeneous catalysis allows the reaction velocity to be influenced by changing the catalyst concentration. Thus the reaction velocity can be adapted over a wide range to the needs of the distillation equipment.

Heterogeneous catalysis requires a structure to fix the catalytic particles in the reaction zone. This may cause construction and operation problems and is also factor that limits the catalyst concentration that can be achieved. The reaction velocity can be enhanced only to the limit set by the attainable concentration range. Furthermore, the possibility of enhancing the reaction velocity by higher temperature or pressure is limited, because in general the catalyst consists of ion-exchange particles, whose temperature range is limited.

So, homogeneous catalysis is much more flexible but has its price in an additional separation step necessary for catalyst recycling and by demands for expensive materials in the case of mineral acids. Heterogeneous catalysis is simpler in principle, but technical problems have to be solved. In general the equipment will need more volume, for example the columns must have a bigger diameter. It should be clear from these considerations that decisions have to be made in each case.

2.7 Conclusions

In the case of conventional distillation, a sufficient body of knowledge has been acquired to enable the tasks in process synthesis, design, and scale-up to be solved quickly in many cases, thanks to intensive development. For RD, the methods of design and synthesis have been developed to a considerable extent, partly with the aid of the many analogies to distillation. A major focus of research and development in future years should be the scale-up of reaction columns. This is where great deficiencies still lie (Fig. 2.19). Also, the methods of choosing the best equipment will have to be improved. In the expert community, columns are often seen as the only possible choice. Work will have to be done to ensure that the benefit of combining reaction and distillation can be enjoyed to the full by employing the most suitable equipment.

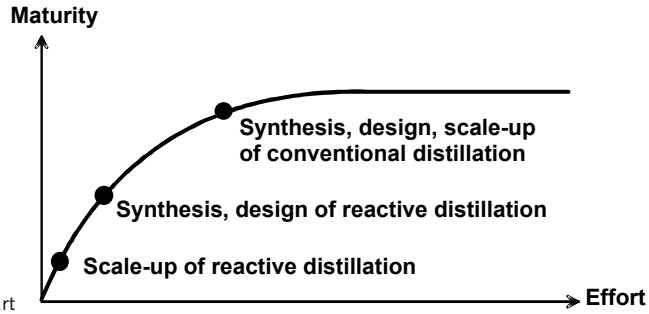

Fig. 2.19 State of the art

2.8 Acknowledgments

We would like to thank to the project teams of the EU projects. This report would not have been possible without the joint work on these projects, some of which are still running. Further, we thank Dr. Ulrich Block, former BASF colleague, with whom the question of the choice of suitable equipment was worked out.

2.9 Notation

A_i component i
c_i component concentration, kmol/m^3
k_1 rate constant of the forward reaction, m^3/kmol h
k_{-1} rate constant of the backward reaction, m^3/kmol h
K_c equilibrium constant
U_i fractional conversion of component i
V volume, m^3
$\dot{V}$ volumetric flow rate, m^3/h
τ residence time, h

References

1 M. Doherty, F. Michael, G. Buzad, *Trans. I. Chem. E.*, **1992**, *70*, 448.
2 J. L. DeGarmo, V. N. Parulekar, V. Pinjala, *Chem. Eng. Progr.*, **1992**, *March*, 43.
3 B. Bessling, J. M. Löhning, A. Ohligschläger, G. Schembecker, K. Sundmacher, *Chem. Eng. Technol.*, **1998**, *21*, 393–400.
4 D. Barbosa, M. Doherty, *Proc. R. Soc. Lond.*, **1987**, *A413*, 459.
5 J. Stichlmair, *Chem. Ing. Tech.*, **1988**, *60*, 747.
6 J. Stichlmair, H. Offers, R. W. Potthoff, *Ind. Eng. Chem. Res.*, **1993**, *32*, 2438.
7 B. Bessling, PhD Thesis, Universität Dortmund, **1998.**
8 D. Barbosa, PhDThesis, University of Massachusetts, **1988.**
9 U. Block, *Chem. Ing. Tech.*, **1977**, *49*, 444.
10 H. Schoenmakers, W. Buehler, *Ger. Chem. Eng.*, **1982**, 292.
11 E. M. Jones, **1991**, EP 461855.
12 L. A. Smith, M. N. Huddleston, *Hydrocarbon Processing*, **1982,** *3*, 121.
13 J. Krafczyk, J. Gmehling, *Chem. Ing. Tech.*, **1994**, *66*, 1372.
14 U. Hoffmann, K. Sundmacher, *Chem. Ing. Tech.*, **1997**, *69*, 613.
15 A. Gorak, L. Kreul, **1997**, DE 197 01 045 A1.

Reactive Distillation. Edited by Kai Sundmacher, Achim Kienle

ISBNs: 3-527-30579-3 (Hardback); 3-527-60052-3 (Electronic)

3
Application of Reactive Distillation and Strategies in Process Design

T. Frey, F. Nierlich, T. Pöpken, D. Reusch, J. Stichlmair, and A. Tuchlenski

3.1
Introduction

Mixed C_4 streams, containing butadiene, butenes, and butanes, are co-produced in steam-cracking processes. These streams contain valuable components, which can be either processed in situ or extracted purely. A typical composition of a steam-cracker C_4 cut is shown in Fig. 3.1. Maximizing its value is a major objective for most petrochemical companies. Therefore, a variety of techniques exists for upgrading the C_4 streams by removal of pure C_4 components and conversion of low-value streams to higher-value products.

Over the last decade reactive distillation (RD) has become a key technology for meeting increased productivity demands. The best-known example in C_4 chemistry is given by MTBE (methyl *tert* butyl ether) synthesis. Both the CD Tech process and the Ethermax process by UOP consist of fixed-bed reactors followed by an RD col-

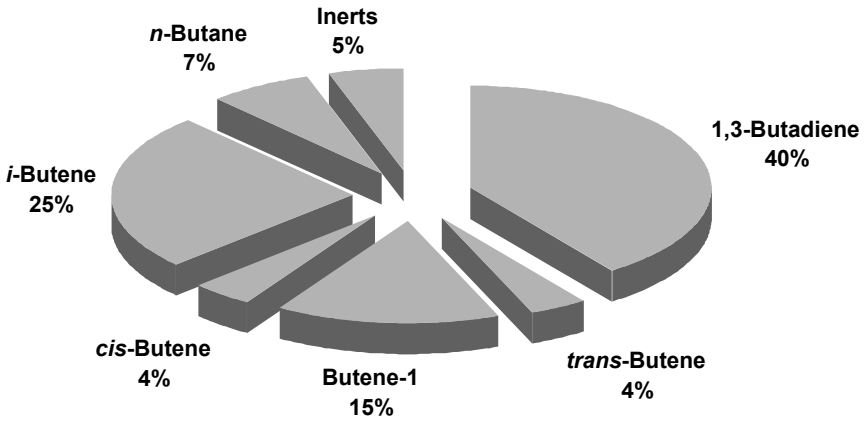

Fig. 3.1. Typical composition of steam-cracker based C_4 cut ([18], reprinted from *Chem. Eng. Sci.*, Vol 57, Beckmann et al., Pages 1525–1530, Copyright 2002, with permission from Elsevier Science)

umn to reach high conversions. More than 90 % conversion, limited by chemical equilibrium, occurs in the fixed-bed reactors, the rest in the RD column.

Besides MTBE synthesis, other attractive applications of RD can be found in C_4 processing, for example in the production of isobutene. Pure isobutene demand is forecast to reach 0.8 million metric tons in Europe by 2010. Production of polybutenes will probably dominate the demand for isobutene, with an average annual growth rate of 3.9 %.

Pure isobutene can be obtained from a number of sources: raffinate I, pseudo-raffinate (the product stream from selectively hydrogenated mixed C_4s), FCC (Fluid Catalytic Cracking) C_4 raffinate, isobutane dehydrogenation, etc. In general, conventional distillation fails because of the very close boiling points of C_4 components. In the case of streams like raffinate I or hydroraffinate, isobutene can be extracted either by cold acid extraction with sulfuric acid or by conversion to an oxygenated intermediate, for example MTBE, and subsequent back-cracking of this stream. The production cost of pure isobutene depends mainly on the C_4 source. However, MTBE decomposition is becoming the preferred way of producing isobutene since it can be integrated easily into refinery processes.

Fig. 3.2 shows the flow diagram of such a reactive-separation process [1]. An isobutene-containing stream, for example raffinate I, is fed to a standard MTBE synthesis plant, where the reactive component isobutene is converted to the intermediate MTBE while the inert C_4 components are separated as distillate. Pure MTBE enters a second RD column and is decomposed. Isobutene, as the low-boiling component, is recovered at the top, while the bottom product methanol, acting as a reactive entrainer, is recycled to MTBE synthesis.

This promising way of producing isobutene will be discussed below. A further objective is to illustrate our understanding of process design for RD from the industrial point of view.

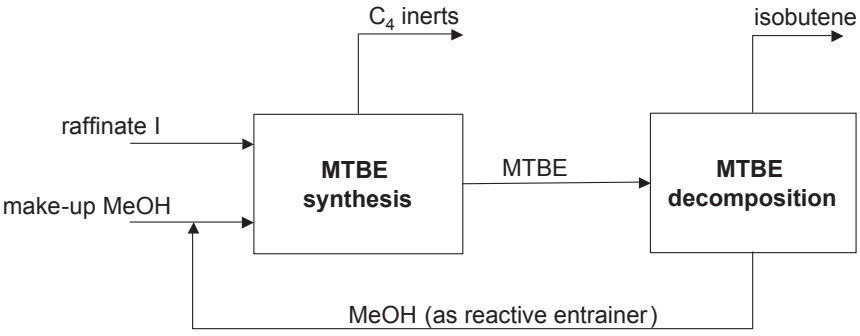

Fig. 3.2. Process scheme of reactive separation for the production of isobutene by MTBE synthesis and subsequent decomposition of MTBE ([18], reprinted from *Chem. Eng. Sci.*, Vol 57, Beckmann et al., Pages 1525–1530, Copyright 2002, with permission from Elsevier Science)

3.2
Challenges in Process Design for Reactive Distillation

A strategy for designing and developing reactive distillation processes involves three stages: feasibility analysis, catalyst and hardware selection, and column scale-up.

3.2.1
Feasibility Analysis

Knowledge of the equilibrium is a fundamental prerequisite for the design of non-reactive as well as reactive distillation processes. However, the equilibrium in reactive distillation systems is more complex since the chemical equilibrium is superimposed on the vapor–liquid equilibrium. Surprisingly, the combination of reaction and distillation might lead to the formation of reactive azeotropes. This phenomenon has been described theoretically [2] and experimentally [3] and adds new considerations to feasibility analysis in RD [4]. Such reactive azeotropes cause the same difficulties and limitations in reactive distillation as azeotropes do in conventional distillation. On the basis of thermodynamic methods it is well known that feasibility should be assessed at the limit of established physical and chemical equilibrium. Unfortunately, we mostly deal with systems in the kinetic regime caused by finite reaction rates, mass transfer limitations and/or slow side-reactions. This might lead to different column structures depending on the severity of the kinetic limitations [5]. However, feasibility studies should identify new column sequences, for example fully reactive columns, non-reactive columns, and/or hybrid columns, that deserve more detailed evaluation.

3.2.2
Catalyst and Hardware Selection

Within the scope of conventional distillation, the optimum choice of internals is sometimes difficult, even in the area of packing because of the large variety that exists. For reactive distillation with catalytic packing, there are only a couple of alternatives. The major task of catalytic packing structures is to ensure an adequate contact between catalyst surface and liquid phase. Alternative catalyst carriers are given by catalyst coated/impregnated random packing materials, catalysts wrapped in fabric, and various methods of placing the catalyst in tray columns. An evident requirement in catalyst selection is a fairly long lifetime since the entire catalytic structure has to be removed during catalyst replacement. For some processes, external reactors may be a promising alternative.

3.2.3
Column Scale-Up

When scaling up a reactive distillation process, the optimum column diameter and height must be chosen. Similarly to conventional distillation, the determination of

the required column height is one of the most difficult tasks in process design. In general, it is based on the packing separation efficiency, which is obtained from non-reactive experiments with well-known test mixtures and chemically inert packing. Care must be taken because data from lab scale packing may differ appreciably from the packing applied on the industrial scale. According to Moritz and Hasse [6], the Sulzer Katapak-S has about three theoretical stages per meter on the lab scale, while on the industrial scale, the same packing provides only one to one-and-a-half theoretical stages per meter.

Besides these essential questions various criteria such as location of the reactive zone and catalyst mass must be taken into account. In the case of reactive distillation, the column height is influenced not only by the separation efficiency but also by the required residence time. Further difficulties in scale-up calculations arise from complex mass-transfer phenomena and hydrodynamic effects.

Simulation might be a decisive basis for process design when all major data are present. However, with the current state of the art it is unlikely that any company would build a new reactive distillation without any pilot plant tests or reliable references.

3.3
MTBE Decomposition via Reactive Distillation

3.3.1
Conceptual Design

In Fig. 3.3 the vapor–liquid equilibrium and the chemical equilibrium of the ternary system isobutene–MTBE–methanol are illustrated. There are two minimum azeotropes in the non-reactive mixture, the first one between the high-boiling MTBE and the intermediate-boiling methanol, and the second one between methanol and the low-boiling isobutene. A border distillation line between the two azeotropes divides the entire concentration space into two distillation regions. The curve of the chemical equilibrium extends between the two products isobutene and methanol. It approaches the MTBE/methanol binary edge in the methanol corner and the MTBE/isobutene binary edge in the isobutene corner. According to Frey and Stichlmair [7], reactive azeotropes can arise wherever the concentration change due to distillation is co-linear to the concentration change due to reaction. In the present system, this consideration gives rise to two curves on which reactive azeotropes may exist. The first locus curve of reactive azeotropes passes between MTBE and the minimum azeotrope of MTBE/methanol and the second one between isobutene and the minimum azeotrope of isobutene/methanol. At a pressure of 500 kPa, the equilibrium curve does not intersect either of the two locus curves of reactive azeotropes anywhere in the entire concentration space. Accordingly, no reactive azeotrope exists in the system under these conditions.

A feasible column design can be devised from thermodynamic principles, as illustrated in Fig. 3.4. The reactive section is located in the center between the

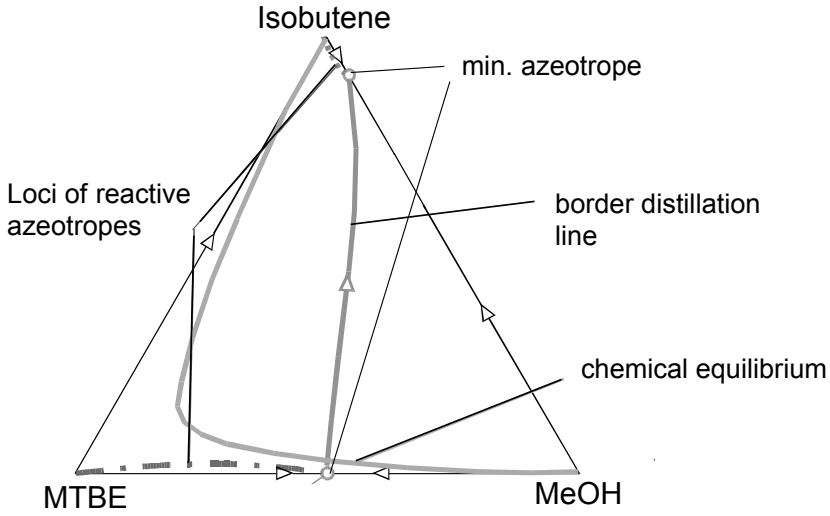

Fig. 3.3. Azeotropes, distillation border, and chemical equilibrium of the ternary system isobutene–MTBE–methanol at a pressure of 500 kPa ([18], reprinted from *Chem. Eng. Sci.*, Vol 57, Beckmann et al., Pages 1525–1530, Copyright 2002, with permission from Elsevier Science)

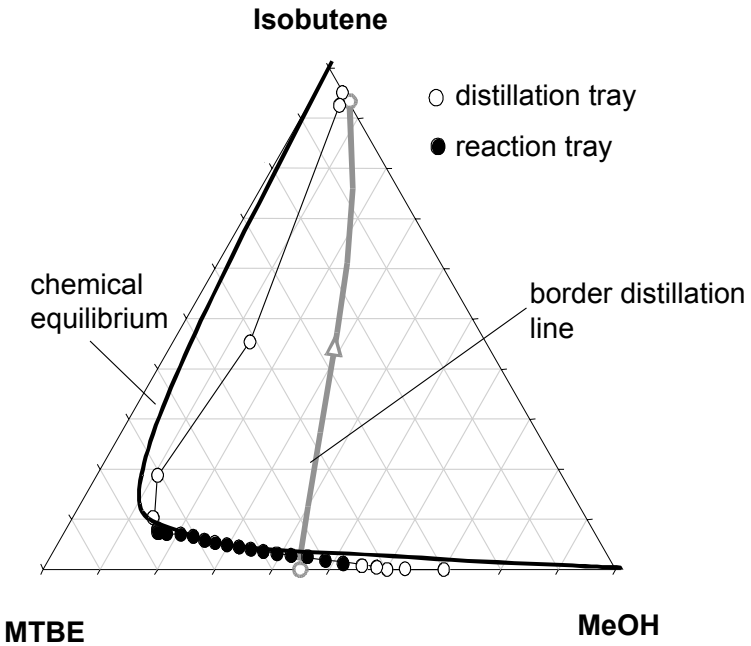

Fig. 3.4. Conceptual design of an RD column for the decomposition of MTBE and the corresponding concentration profile calculated from thermodynamic considerations ([18], reprinted from *Chem. Eng. Sci.*, Vol 57, Beckmann et al., Pages 1525–1530, Copyright 2002, with permission from Elsevier Science)

non-reactive stripping and rectifying sections. The corresponding ternary plot shows the concentration profile as a sequence of phase- or phase-and-chemical equilibrium stages. In the rectifying section, conventional distillation takes place leading to an azeotropic concentration of isobutene and methanol in the distillate. The concentration change in the reactive section coincides with the chemical equilibrium lines. Therefore, the composition of the ternary mixture crosses the border distillation line from the left to the right in downward direction. In the stripping section, isobutene is removed and a binary mixture of methanol/MTBE can be collected as the bottom product.

As discussed above, thermodynamic simplifications allow an easy description and, in turn, a good understanding of the fundamental mechanisms effective in RD.

3.3.2 Model Development

Depending on the complexity, various combinations of models including reaction and mass transfer can be used to simulate reactive distillation (Fig. 3.5). The mass transfer can be described by either assuming an equilibrium or applying a kinetic model. By analogy, the reaction can be expressed as an established chemical equilibrium or with reaction kinetics. However, the complexity of the modeling is greatly increased if mass transfer and/or reaction kinetics are taken into account [8].

In the majority of cases the so-called equilibrium stage model is used for simulation of distillation without chemical reaction. This has also been shown to be useful in reactive distillation. The equilibrium stage model is a pragmatic approach suitable not only in the early stage of process development. In general, it is implemented in all current process simulators [9]. The mass-transfer stage model is recommended (e. g., RATEFRAC in AspenPlus) in the advanced stage of process development. Unfortunately, there are only few data available on suitable mass-transfer kinetics. Furthermore, Higler et al. [10] have shown that small deviations (about ±10 %) in the mass transfer coefficients cawed deviations in computed conversion of the same magnitude. This makes the application of these models fairly difficult. For this reason, the equilibrium stage model was used in this study.

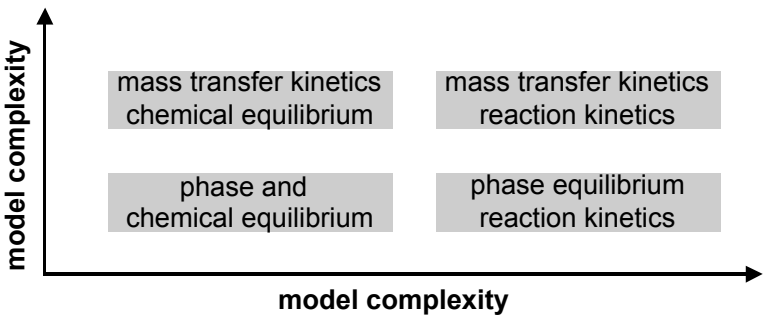

Fig. 3.5. Model complexity in simulation of reactive distillation

3.3.2.1 Catalyst Selection and Reaction Kinetics

By analogy with MTBE synthesis, the decomposition of MTBE is also an acid-catalyzed and equilibrium-limited reaction. Ion-exchange resins were found to be suitable for this reaction. Besides catalyst activity and selectivity, a major requirement is to provide a catalyst lifetime of the same scale of time as the period of plant turnaround. Otherwise, catalyst replacement would require a shutdown of the entire unit. However, the results of run-time testing experiments have shown that the ion-exchange catalyst used provides high stability for more than 8000 h. Only slight decreases in catalyst activity have been observed.

To determine reaction kinetics, batch experiments were performed in the temperature range 90–120 °C. Beginning with pure MTBE, or different mixtures of MTBE and methanol or isobutene, all experiments were started in the kinetic regime and were continued until chemical equilibrium was reached. Fitting the experimental data to the well-known kinetic approach suggested by Rehfinger and Hoffmann [11], good agreement was found between model prediction and experimental data (Fig. 3.6). This holds for both the description of the kinetic regime and the approach to chemical equilibrium. A consideration of the reaction medium influence on the chemical reaction as suggested by Fité et al. [12] gave no further improvement in the fit. All relevant side reactions have been included in the model, for example, diisobutene formation [12, 13], dimethyl ether formation, and hydration of isobutene.

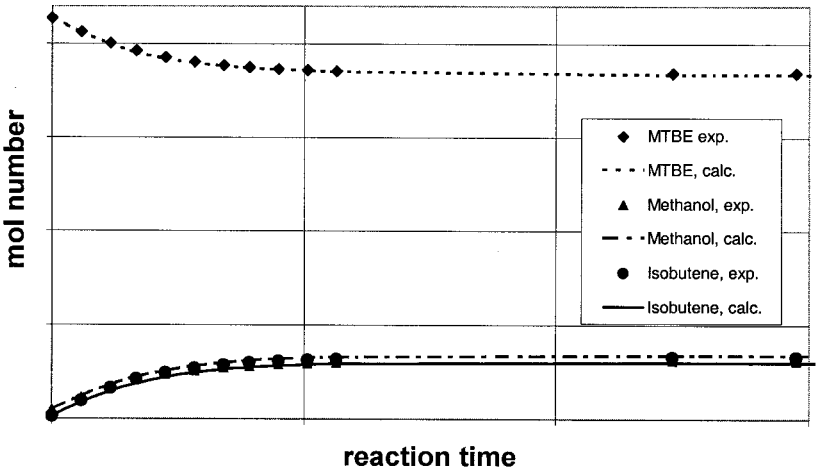

Fig. 3.6. Results of a kinetic experiment performed in batch mode and comparison with model predictions based on the kinetic approach suggested by Rehfinger and Hoffmann [11] ([18], reprinted from *Chem. Eng. Sci.*, Vol 57, Beckmann et al., Pages 1525–1530, Copyright 2002, with permission from Elsevier Science)

3.3.2.2 Phase Equilibrium Model

The UNIQUAC model [14] was used to account for liquid phase non-idealities. The vapor phase was modeled using the Redlich–Kwong EOS [15]. The combination of both is implemented in Aspen Plus as the UNIQ-RK property model. UNIQUAC

parameters were fitted to experimental vapor–liquid equilibrium data from the literature and our own measurements. Special attention was paid to the exact description of the azeotropes (including the temperature dependence), as they were found to have a strong influence on the calculated conversion.

3.3.2.3 **Steady-State Simulation**

After the feasibility analysis had shown that the process for the decomposition of MTBE can be carried out using reactive distillation equipment, this conclusion had to be verified using a rigorous model. Since no information on mass-transfer limitations is available, the equilibrium stage approach is the model of choice. Therefore, such a simulation was set up in Aspen Plus (Version 10.2) with a column configuration containing a reactive section and non-reactive stripping and rectifying sections. The chemical reaction was implemented as a user subroutine. The amount of catalyst per theoretical stage was adjusted to match the properties of Katapak-S by Sulzer. The feed position was set to the top of the reactive section, since the reactant MTBE is high-boiling. The feed was pure MTBE. Its amount was varied in order to assess the influence on column performance. The distillate-to-feed ratio was adjusted to collect the isobutene–methanol azeotrope as top product. Two calculated concentration profiles are depicted in Fig. 3.7. It can be seen that both profiles are fairly similar, although MTBE conversion is very differ-

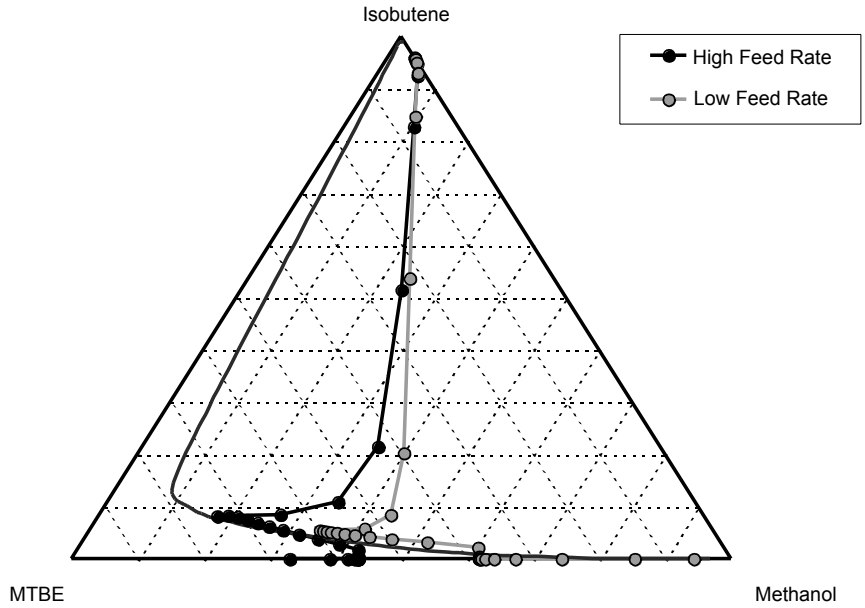

Fig. 3.7. Composition profiles of a reactive distillation column equipped with 10 reactive trays, and 10 non-reactive trays in the stripping and rectifying section each for high and low feed-rates. The feed position was located above the reactive section ([18], reprinted from *Chem. Eng. Sci.*, Vol 57, Beckmann et al., Pages 1525–1530, Copyright 2002, with permission from Elsevier Science)

ent in both. For the low conversion case, MTBE is enriched in the stripping section while for the high conversion case, the desired product methanol is enriched.

In conclusion, MTBE decomposition may be performed using reactive distillation equipment. The top product is fairly pure isobutene and will contain some methanol, which has to be separated downstream using conventional technology.

3.3.3 Lab-Scale Experiments

In order to evaluate the developed model and to its limitations, laboratory experiments and accompanying simulations were carried out. The laboratory runs were performed using a pressure column having a diameter of 80 mm and up to 25 bubble cap trays. The reactive zone was equipped with Sulzer Katapak-S in heights of 20–40 cm. The column set-up is shown in Fig. 3.8. The catalyst pockets of the packing were filled with the ion-exchange resin described above. The column was operated at a pressure of 500 kPa. Feed rates were set between 2 and 5 kg/h and the reflux ratio was varied in the range 5–10. The feed was introduced above the reactive section. Further experiments were performed with the feed position below the reactive section.

In a set of various experiments stable operation was observed. The bottom product was free of isobutene. Besides the expected mixture of isobutene and methanol, the distillate contained also small amounts of MTBE. This is due to the insufficient separation performance in the rectifying section. However, this can be alleviated easily by placing more trays or conventional packing in this section. The maximum conversion achieved by using this laboratory column set-up was 78 %.

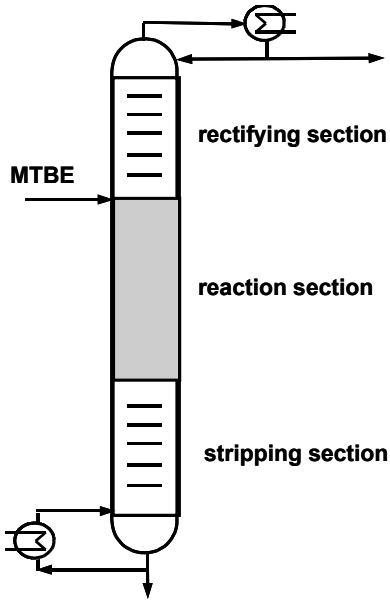

Fig. 3.8. Configuration of the lab-scale reactive distillation column. The distillation section is equipped with bubble cap trays, the reactive section with Sulzer Katapak-S ([18], reprinted from *Chem. Eng. Sci.*, Vol 57, Beckmann et al., Pages 1525–1530, Copyright 2002, with permission from Elsevier Science)

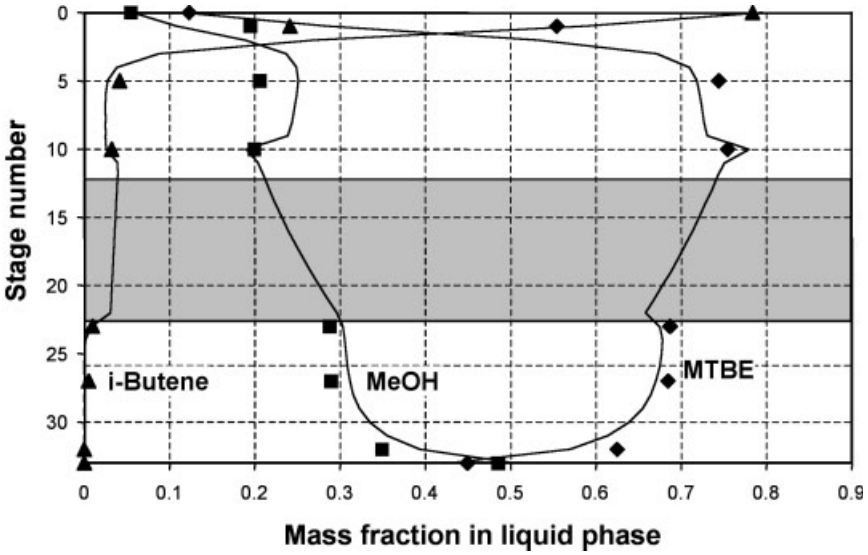

Fig. 3.9. Comparison of experimental data and model prediction for the concentration profiles of the lab scale column ([18], reprinted from *Chem. Eng. Sci.,* Vol 57, Beckmann et al., Pages 1525–1530, Copyright 2002, with permission from Elsevier Science)

In order to model lab-scale experiments the separation performance of the bubble cap trays was derived from our own measurements, while data concerning the reactive packing were provided by Sulzer Chemtech.

Fig. 3.9 shows a comparison between experimental and calculated concentration profiles in the laboratory column. A good agreement between model prediction and experiment can be observed. The simulation was able to describe all experimental data sets with the same accuracy as shown in Fig. 3.9. From these results, it was concluded that the equilibrium stage model is capable of describing the lab-scale experiments based solely on information on phase equilibrium, reaction kinetics and hardware set-up, giving the simulation a predictive character.

3.3.4
Pilot-Plant Experiments

The scale-up of reactive distillation processes from the laboratory scale to full commercial scale is still an unsolved problem. One of the most important questions is whether the performance of large scale equipment can be predicted with the same approach as applied in the lab-scale. For future developments, this would allow us to dispense with costly and time-consuming experiments on the pilot scale.

The experimental data on the pilot scale were obtained using a column 316 mm in diameter. The non-reactive stripping and rectifying sections contained wire gauze packing, while the reactive section of the column was equipped with Katapak SP-12 from Sulzer. The elements contained the same catalyst as already used in the

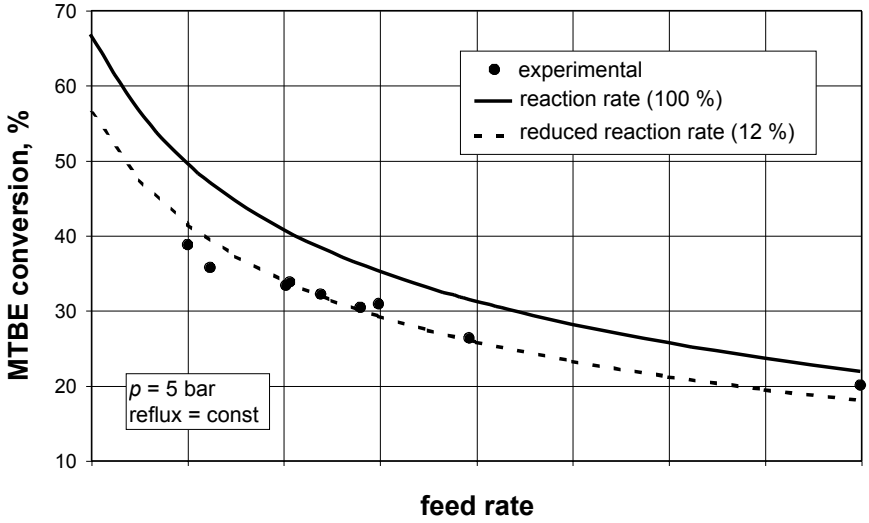

Fig. 3.10. Comparison of experimental conversion values with the simulation using a reaction rate constant of 100 % (solid line) and 12 % (dotted line) ([18], reprinted from *Chem. Eng. Sci.*, Vol 57, Beckmann et al., Pages 1525–1530, Copyright 2002, with permission from Elsevier Science)

kinetic and laboratory scale experiments. This column was applied to perform a set of experiments by varying the feed rate, the feed position (below, within and above the reactive section), the reflux ratio (2–15) and the pressure (500–650 kPa). The temperature in the rectifying section was controlled by varying the reboiler load. As a result, the overhead product was always the isobutene–methanol azeotrope containing small amounts of dimethyl ether formed in a side reaction.

Simulating the pilot column with the same model that was successfully used for the 80 mm column, the computed conversion was systematically too high (Fig. 3.10). Reaction kinetics (reduced reaction rates due to incomplete catalyst wetting, mass-transfer limitations, or maldistribution) and separation efficiency of the reactive packing were considered as possible reasons for these deviations. It was found that the sensitivity of the computed conversion against in these factors was small compared with the experimentally observed trends. The best agreement was attained by significant reduction of the reaction rate constant. Assuming a reduced reaction rate of 12 %, the performance of the pilot column could be described satisfactorily as depicted in Fig. 3.10. This implies that pilot-scale experiments provide the only basis for scale-up. This conclusion is supported by the data shown in Fig. 3.11. In this figure, experimental conversion data is plotted against the feed location and compared with the model prediction using the reduced reaction rate of 12 %. For the upper feed positions, the agreement is good, the trend in the conversion for the lower feed positions is qualitatively correct.

However, the observed reduction in reaction rate still remains unexplained. The pilot-scale RD column was operated at similar space velocity and hydrodynamic

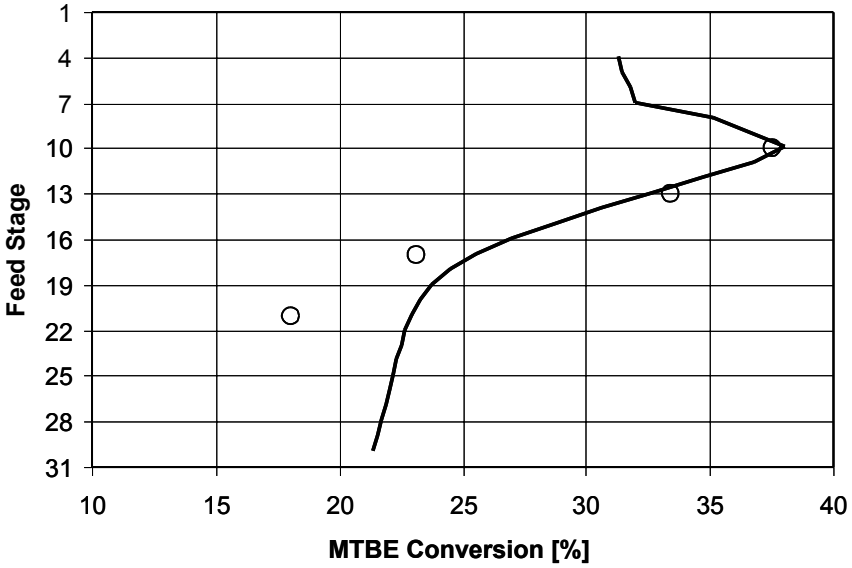

Fig. 3.11. Experimental conversion as a function of feed position (symbols). The line shows the model prediction for a reaction rate constant of 12 %

loading compared with the lab-scale column. The concentrations in the reactive sections were likewise similar in both cases. Nonetheless, the simulation showed that the model was able to describe observed concentration and temperature profiles of the laboratory column very well but failed in the simulation of the pilot column.

A similar observation was made by other authors in the investigation of the synthesis of methyl acetate. Whereas a 50 mm laboratory column could be described very well [16] with the equilibrium stage model, this held no longer in the case of a pilot column [17].

It is known that the geometry of the reactive packing types for lab- and pilot-scale applications differs. This is accounted for in the present model by using the appropriate values for NTSM (Number of Theoretical Stages per Meter) and catalyst mass per stage. A more detailed description of the hydrodynamics has hitherto not been included and remains necessary for future work. Possible explanations for the lower conversion compared to the lab column may be incomplete catalyst wetting due to maldistribution effects, mass-transfer phenomena, or the formation of temperature gradients in the reactive packing. As long as this puzzle remains unsolved, a reliable scale-up of RD processes is not possible without expensive pilot testing.

3.4 Conclusions

In order to design a reactive distillation for the decomposition of MTBE a feasibility analysis was performed on the basis of thermodynamic considerations. The results led to a reasonable column configuration. A confirmation of the thermodynamic suggestions was derived by simple steady-state simulations of the suggested column set-up. In the next stage of process design a suitable catalyst and column internals were selected. The final task was to develop a scale-up procedure based on experimental data in the lab and pilot scale. While the lab-scale experiments could be described satisfactorily with a simple equilibrium stage model, the same approach failed in the case of pilot-plant experiments. Hydrodynamics, maldistribution, and/or mass transfer limitations might be a reasonable explanation and are worthy of deeper investigation. In order to fit the pilot-plant data to the equilibrium-stage model, a reduced catalyst activity was introduced. As a result we obtained good agreement between model prediction and experimental data in a broad range of operating conditions.

However, with the present state of the art it has to be concluded that experiments at the pilot-plant scale are indispensable for establishing any heterogeneously catalyzed reactive distillation process. Reliable scale-up solely on the basis of laboratory scale experiments does not appear to be possible yet.

References

1 E. Stein, A. Kienle, K. Sundmacher, *Chem. Eng.*, **2000**, *Dec.*, 68–72.
2 S. Ung, M. F. Doherty, *AIChE J.*, **1995**, *41*, 2383–2392.
3 W. Song, R. S. Huss, M. F. Doherty, M. F. Malone, *Nature*, **1997**, *32* 561–563.
4 M. F. Malone, M. F. Doherty, *Ind. Eng. Chem. Res.*, **2000**, *39*, 3953–3957.
5 R. Taylor, R. Krishna, *Chem. Eng. Sci.*, **2000**, *55*, 5183–5229.
6 P. Moritz, H. Hasse, *Chem. Eng. Sci.*, **1999**, *54*, 1367–1374.
7 T. Frey, J. Stichlmair, *Chem. Ing. Tech.*, **1998**, *70*, 1373–1381.
8 D. Reusch, *Entwicklung und Überprüfung eines pragmatischen Modells für die Reaktivrektifikation*, PhD Dissertation, Universität zu Köln, **1997**.
9 Aspen Technologies Inc., *Aspen Plus*, Cambridge, MA, **2000**.
10 A. P. Higler, R. Taylor, R. Krishna, *Chem. Eng. Sci.*, **1999**, *54*, 1389–1395.
11 A. Rehfinger, U. Hoffmann, *Chem. Eng. Sci.*, **1990**, *45*, 1605–1617.
12 C. Fité, J. Tejero, M. Iborra, F. Cunill, J. F. Izquirdo, *AIChE J.*, **1998**, *44*, 2273–2279.
13 M. Gravekarstens, U. Hoffmann, *Chem. Ing. Tech.*, **1999**, *71*, 500–503.
14 D. S. Abrams, J. M. Prausnitz, *AIChE J.*, **1975**, *21*, 116–128.
15 O. Redlich, J. N. S. Kwong, *Chem. Rev.*, **1979**, *44*, 223–244.
16 T. Pöpken, S. Steinigeweg, J. Gmehling, *Ind. Eng. Chem. Res.*, **2001**, *40*, 1566–1574.
17 P. Moritz, *Scale-up der Reaktivdestillation mit Sulzer Katapak-S*, PhD Dissertation, Universität Stuttgart, **2001**.
18 A. Beckmann, F. Nierlich, T. Pöpken, D. Reusch, C. von Scala, A. Tuchlenski, *Chem. Eng. Sci.*, **2002**, *57*, 1525–1530.

Reactive Distillation. Edited by Kai Sundmacher, Achim Kienle

ISBNs: 3-527-30579-3 (Hardback); 3-527-60052-3 (Electronic)

Part II
Physicochemical Fundamentals

Reactive Distillation. Edited by Kai Sundmacher, Achim Kienle

ISBNs: 3-527-30579-3 (Hardback); 3-527-60052-3 (Electronic)

4
Thermodynamics of Reactive Separations

H. Hasse

4.1
Introduction

Reactive separations are widespread operations. In typical reactive separation processes such as reactive absorption or distillation the superposition of reaction and separation is deliberately used. In other cases, simultaneous reaction and separation simply cannot be avoided. This is, for instance, the case when side reactions occur in separation equipment or when intrinsically chemically reactive mixtures, such as solutions of weak electrolytes or formaldehyde solutions, have to be separated. Furthermore, in many reactors products are directly removed, which is basically a reactive separation.

Thermodynamics plays a key role in understanding and designing all these processes. The fact that reaction and separation occur simultaneously gives rise to special challenges both in experimental investigations and modeling the processes. It is these challenges that we will focus on in the present chapter. This will be done using case studies, which illustrate general facts, rather than by trying to cover the subject comprehensively.

There are several contributions of thermodynamics to the field of reactive separations. Thermodynamics provides the basic relations, such as energy balances of equilibrium conditions, used in the process models, which again are the key to reactive separation design. Furthermore, thermodynamics provides models and experimental methods for the investigations of the properties of the reacting fluid that have to be known for any successful process design. We will focus on equilibrium thermodynamics here but discuss relations to kinetic models.

The present chapter is aimed at readers interested in reactive distillation (RD). The basic ideas can, however, easily be applied to other reactive separation processes.

4.2 Process Models for Reactive Distillation

4.2.1 Outline

Process models for RD have to take into account both the chemical and the physical side of the process. Two basic types of model are used: stage models, which are based on the idea of the equilibrium stage with phase equilibrium between the outlet streams, and rate-based models, which explicitly take into account heat and mass transfer. Similarly to the physical side of RD, the chemical reaction is either modeled using the assumption of chemical equilibrium or reaction kinetics are taken into account. Note that a kinetic model, either for physical transport processes or for chemical reactions, always includes an equilibrium model. The equilibrium model is the stationary solution of the kinetic model, for which all derivatives with respect to time become zero. Hence, whatever model type is used, it has to be based on a sound knowledge of the chemical and phase equilibrium, which is supplied by thermodynamic methods. Starting from there, kinetic effects can be included.

Only a limited amount of data is needed to develop models for RD processes if the assumption of both phase and chemical equilibrium is used. Nevertheless, even the development of a reliable equilibrium model alone is a challenging task, which is often underestimated. The amount of information needed to develop reliable kinetic models greatly exceeds that for the equilibrium models. Finding reliable model parameters is often the bottleneck in model development.

An excellent comprehensive survey on the fundamentals of different types of model for RD processes has recently been given by Taylor and Krishna [1]. In that paper the focus is on modeling concepts, we focus here on the application of such models, especially the comparison of model predictions with experimental data and the background of the complexity of the model and the effort needed for its parameterization. We do account for the fact that the results of any such comparison will depend on the chosen example, but emphasize that comparison with experimental data, especially in predictions, is the final test for any modeling strategy. Unfortunately, there is only a very limited amount of data on RD experiments available in the open literature for such comparisons.

4.2.2 Case Study: Methyl Acetate

Here we briefly discuss results from a case study on methyl acetate RD, in which, based on detailed investigations of thermodynamics [2] and fluid dynamics [3], different process models were not only compared with each other but also with experimental data. Full details are reported by Moritz [4].

Methyl acetate production is often used as an example to demonstrate the advantages of RD processes [5]. The basic set-up of the heterogeneously catalyzed methyl

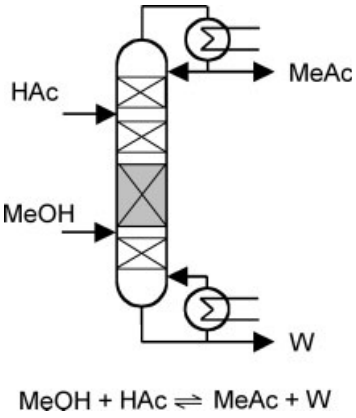

Fig. 4.1 Heterogeneously catalyzed methyl acetate RD (MeOH = methanol, Hac = acetic acid, MeAc = methyl acetate, W = water; shaded = reaction zone)

acetate RD process is shown in Fig. 4.1. The catalytic packing used in the present study was Katapak-S with an Amberlyst ion-exchange catalyst. Experiments were carried out both at the laboratory scale [6] and the semi-industrial scale [4].

Two major classes of modeling concepts, the equilibrium stage and the rate-based approach, were tested. The chemical reaction is assumed to occur only in the liquid phase. A survey of the four models used is given in Fig. 4.2. Three variants of the equilibrium stage model were considered. In the simplest model (Model 1) the RD column is modeled as a countercurrent multistage process with physical and chemical equilibrium on each stage. In Model 2 the assumption of chemical equilibrium is dropped and the reaction on each stage is described by second-order bulk reaction kinetics. Model 3 was developed to take into account the residence time behavior of the liquid flow in the packing. For this goal the reaction zone is described by a relatively large number of stages, or, in terms of reaction modeling, stirred tank reactors. Neither phase nor chemical equilibrium is reached

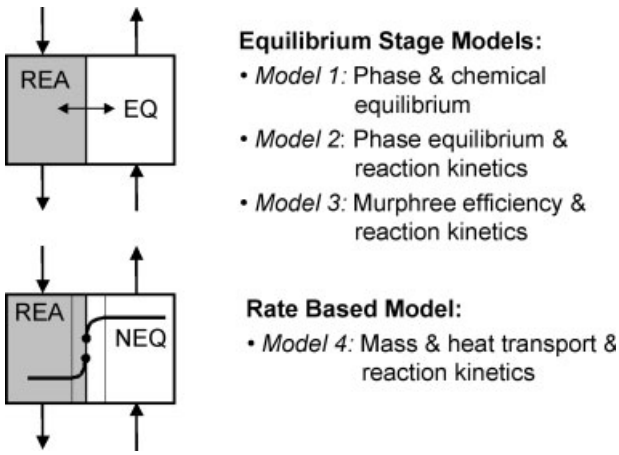

Fig. 4.2 RD process model types used in the methyl acetate case study

at these stages. Reaction kinetics are the same as in Model 2, Murphree efficiencies are used to give the desired separation capacity. In the rate-based approach (Model 4) heat and mass transfer are directly taken into account using two-film theory. Multicomponent diffusion is modeled with the Maxwell–Stefan equations. Bulk reaction kinetics are included as in Models 2 and 3.

Obviously, parameterizing these models meaningfully requires a very different amount of experimental data, increasing from Model 1 to Model 4. The minimum requirement is reliable information on vapor–liquid and chemical equilibrium (Model 1). The phase equilibrium model and the chemical equilibrium model should be consistent, as discussed in more detail below. Extending the equilibrium model to Model 2, which accounts for reaction kinetic effects, is not straightforward. In the case of methyl acetate, the reaction kinetic model obtained from stirred-tank experiments is not in agreement with the results obtained from trickle-bed experiments, so that empirical factors have to be introduced [4, 7]. Furthermore, the macrokinetic model requires information on the liquid flow velocity, so that the thermodynamic design and the fluid dynamic design, which can be done sequentially when using Model 1, are now directly coupled. The reaction kinetic model should be consistent with the chemical equilibrium model.

Going from Model 2 to Model 3, the only additional information needed is the residence time distribution of the packing, which is available for Katapak-S [3]. The residence time distribution of a packing segment of length L is modeled using a cascade of N_{rea} stirred tank reactors. The same packing segment has a known number of theoretical stages N_{sep}. As N_{rea} is always larger than N_{sep}, the differences in separation and reaction capacity of one stage (stirred tank) can easily be accounted for by introducing a Murphree efficiency.

$$\eta = \frac{N_{sep}}{N_{rea}} \tag{4.1}$$

In the fluid dynamic design with Models 1–3, information on the density and viscosity of the mixtures is needed, which usually has to be estimated as no experimental data is available. This can, however, be done with an accuracy sufficient for most cases using standard methods [8].

The amount of additional information needed to be able directly to take into account heat and mass transfer in Model 4 is high. Using the two-film theory, information on the film thickness is needed, which is usually condensed into correlations for the Sherwood number. That information was not available for Katapak-S so that correlations for similar non-reactive packing had to be adopted for that purpose. Furthermore, information on diffusion coefficients is usually a bottleneck. Experimental data is lacking in most cases. Whereas diffusion coefficients can generally be estimated for gas phases with acceptable accuracy, this does unfortunately not hold for liquid multicomponent systems. For a discussion, see Reid et al. [8] and Taylor and Krishna [9]. These drawbacks, which are commonly encountered in applications of rate-based models to reactive separations, limit our ability to judge their value as deviations between model predictions and experimen-

tal results may stem either from an inadequate model itself or from bad parameters.

Fig. 4.3 shows a comparison of Models 1–4 with data from an RD experiment, which is typical of the results from the study discussed here; other examples can be found elsewhere [4]. All model results are predictions in the sense that no adjustments to RD data were made. The predictions from the stage models, which take into account reaction kinetics (Models 2 and 3), are good and do not differ largely.

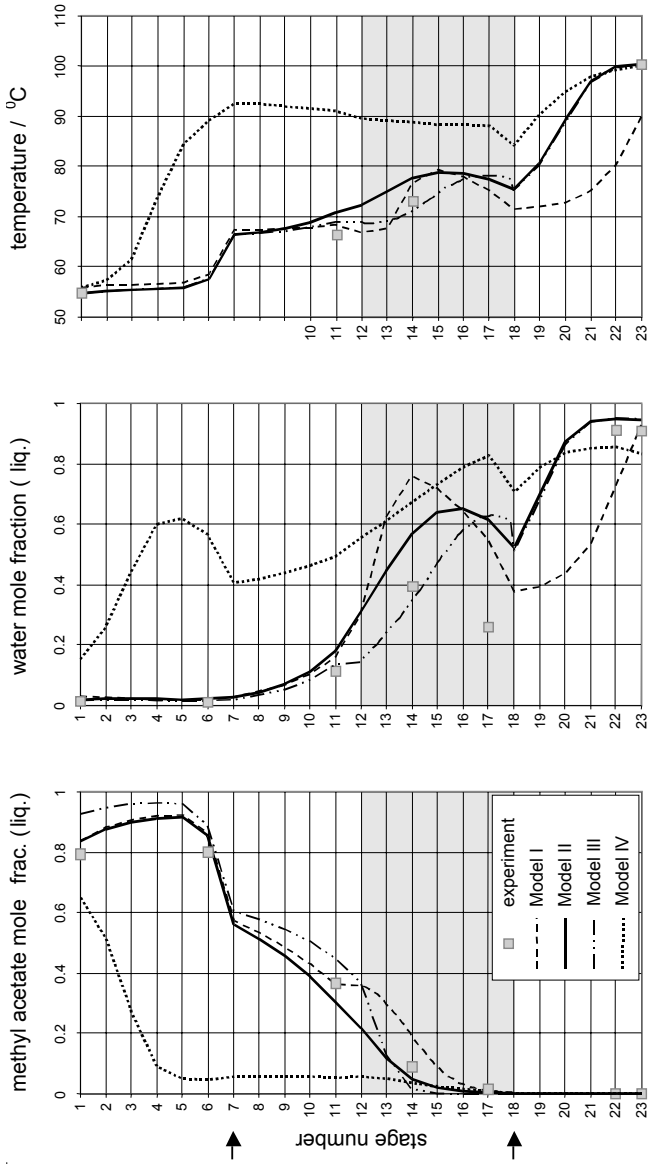

Fig. 4.3 Comparison of different process models with experimental data on the heterogeneously catalyzed methyl acetate RD (p = 1 bar, arrows = feed location, shaded = reaction zone, models cf. Fig. 4.2)

Differences between Model 2 and Model 3 would only have been expected for residence time sensitive reaction systems, such as, for instance, ethylene glycol production from ethylene oxide and water, but not for the esterification studied here. The very simple Model 1 still gives reasonable predictions, which would, for instance, be sufficient for conceptual design studies. The fact that the rate-based Model 4 gives entirely wrong predictions in the present case should not be overemphasized and may be due to the very limited amount of available thermophysical and fluid dynamic input data.

Obviously, the choice of an appropriate modeling level for RD processes strongly depends on the input available to parameterize the different models. Thermodynamics plays a key role in providing that input.

4.3 Equilibrium Thermodynamics of Reacting Multiphase Mixtures

In any reactive separation process the mixtures involved undergo changes driving them towards chemical and phase equilibrium. As stated in the previous section, stage models with the simple assumption of chemical equilibrium in the streams leaving the stage and phase equilibrium between these streams often already provide a process model with reasonable predictive power. Any more detailed model will include an equilibrium model as a limiting case and will therefore have to be based on reliable information about the equilibrium. We will give a brief outline of the basic concepts of thermodynamic modeling of simultaneous chemical and phase equilibrium here. The focus is on the options provided by classical thermodynamics. A discussion of different G^E models or equations of state is not within the scope of the present chapter. The reader is referred to standard textbooks for that purpose (for instance, Walas [10] and Prausnitz et al. [11]).

It is expected that entirely new options for thermodynamic modeling of simultaneous chemical and phase equilibrium will become available from molecular simulations techniques. Such methods are beginning to become available [12, 13], but can not be covered in the scope of the present chapter.

The conditions for simultaneous phase and chemical equilibrium at constant temperature T and pressure p derived from the second law of thermodynamics are well known and are given here for a system of N components i, P phases j, in which R chemical reactions r occur.

Phase equilibrium

$$\mu_i^j = \mu_i^{j+1} \qquad i = 1...N; j = 1...(P-1) \tag{4.2}$$

Chemical equilibrium

$$\sum_{i=1}^{N} \nu_i^{r,j} \mu_i^j = 0 \quad j = 1...P; r = 1...R \tag{4.3}$$

where μ_i^j is the chemical potential of component i in phase j, $\nu_i^{r,j}$ is the stoichiometric coefficient of component i in reaction r in phase j. $\nu_i^{r,j}$ is positive for products, negative for educts, and zero if the component i does not take part in reaction r in phase j.

For practical purposes, working equations have to be derived from the fundamental relations (4.2) and (4.3) by using appropriate normalizations of the chemical potential. Which working equation is appropriate will depend on the application. Some popular choices for the normalization of the chemical potential are as follows.

For components in vapor, liquid, and supercritical phases

$$\mu_i^j = \mu_i^{\text{pure id.gas}}(T,p^\circ) + \mathrm{R}\,T\,\ln\left(\frac{p\,x_i^j\,\varphi_i^j}{p^\circ}\right) \tag{4.4}$$

for condensable components in liquid phases (normalization according to Raoult)

$$\mu_i^j = \mu_i^{\text{pure liq.}}(T,p) + \mathrm{R}\,T\,\ln\left(x_i^j\,\gamma_i^j\right) \tag{4.5}$$

for non-condensable components in liquid phases (normalization according to Henry)

$$\mu_i^j = \mu_i^*(T,p_{\text{solv}}^{\text{s}},\mathbf{x}^{j,i*}) + \int_{p_{\text{solv}}^{\text{s}}}^{p} v_i^\infty\,\mathrm{d}p + \mathrm{R}\,T\,\ln\left(x_i^j\,\gamma_i^{j*}\right) \tag{4.6}$$

where the reference chemical potential is a function of the composition of phase j, in the case of infinitely diluted component i, denoted as $\mathbf{x}^{j,i*}$ here. The vapor pressure of that mixture at temperature T is $p_{\text{solv}}^{\text{s}}$.

Relations similar to equation (4.6) are used for electrolytes $(A^+)_{\nu+}$ $(B^-)_{\nu-}$ in solution

$$\mu_i^j = \mu_i^{\text{c}*}(T,p,\mathbf{x}^{j,i*}) + \mathrm{R}\,T\,\ln\left(\frac{c_{A^+}^j}{c^\circ}\right)^{\nu_+}\left(\frac{c_{B^-}^j}{c^\circ}\right)^{\nu_-} + \mathrm{R}\,T\,\ln\left(\gamma_i^{j\text{c}*}\right)^{(\nu_+ + \nu_-)} \tag{4.7}$$

$$\mu_i^j = \mu_i^{\text{m}*}(T,p,\mathbf{x}_i^{j*}) + \mathrm{R}\,T\,\ln\left(\frac{m_{A^+}^j}{m^\circ}\right)^{\nu_+}\left(\frac{m_{B^-}^j}{m^\circ}\right)^{\nu_-} + \mathrm{R}\,T\,\ln\left(\gamma_i^{j\text{m}*}\right)^{(\nu_+ + \nu_-)} \tag{4.8}$$

Note that, in principle, there is a free choice to apply any of the equations (4.4)−(4.8) to any component in any phase. The only condition that has to be fulfilled is the Gibbs–Duhem equation for each phase, which reads at constant temperature and pressure

$$\sum_{i=1}^{N} n_i^j\,\mathrm{d}\mu_i^j = 0 \quad j = 1\ldots P \tag{4.9}$$

In most cases in RD equations (4.4) and (4.5) are applied to all components of the gas and the liquid phase respectively. This leads to the well-known extended form of Raoult's law for the phase equilibrium between a liquid phase ′ and a gas phase ″

$$p_i^s \, \varphi_i^s \exp\left(\int_{p_i^s}^{p} v_i \, \mathrm{d}p \right) x_i' \, \gamma_i' = p \, x_i'' \, \varphi_i'' \qquad i = 1...N \tag{4.10}$$

or, neglecting gas-phase non-idealities and the pressure dependence of the liquid-phase chemical potential

$$p_i^s \, x_i' \, \gamma_i' = p \, x_i'' \qquad i = 1...N \tag{4.11}$$

Once the choice regarding the description of the chemical potential is made, not only the working equations for the phase equilibrium, such as equation (4.11), are fixed but also those for the chemical equilibrium. For instance, insertion of equation (4.5) into equation (4.3) leads after some rearrangement to the following, thermodynamically consistent form for the chemical equilibrium constant of reaction r

$$K_r^{\text{pure liq.}}(T,p) = \prod_{i=1}^{N} (x_i)^{\nu_i^r} \prod_{i=1}^{N} (\gamma_i)^{\nu_i^r} \tag{4.12}$$

with

$$K_r^{\text{pure liq.}}(T,p) = \exp\left(- \frac{\sum_{i=1}^{N} \nu_i^r \, \mu_i^{\text{pure liq.}}(T,p)}{\mathrm{R}\,T} \right) \tag{4.13}$$

In equations (4.12) and (4.13), the superscript 'pure liq.' refers to the state chosen for the normalization of the chemical potentials of the reacting components.

If the normalization according to equation (4.4) is applied, as usual for the gas phase, equation (4.3) leads to another thermodynamically consistent chemical equilibrium constant of reaction r

$$K_r^{\text{pure id. gas}}(T,p^\circ) = \left(\frac{p}{p^\circ} \right)^{\left(\sum_{i=1}^{N} \nu_i^r \right)} \prod_{i=1}^{N} (x_i)^{\nu_i^r} \prod_{i=1}^{N} (\varphi_i)^{\nu_i^r} \tag{4.14}$$

with

$$K_r^{\text{pure id. gas}}(T,p^\circ) = \exp\left(- \frac{\sum_{i=1}^{N} \nu_i^r \, \mu_i^{\text{pure id. gas}}(T,p^\circ)}{\mathrm{R}\,T} \right) \tag{4.15}$$

The different forms of the chemical equilibrium constant are not independent. For instance, the chemical equilibrium constants $K_r^{\text{pure liq.}}(T,p)$ and $K_r^{\text{pure id. gas}}(T,p^0)$ as given by equations (4.12)–(4.15) are related by equation (4.16), as can, for instance, be shown by applying equation (4.10)

$$\frac{K_r^{\text{pure id. gas}}(T,p^o)}{K_r^{\text{pure liq.}}(T,p)} = \prod_{i=1}^{N}\left(\frac{p_i^s}{p^o}\right)^{\nu_i^r}\left(\prod_{i=1}^{N}\left(\varphi_i^s\right)^{\nu_i^r}\right)\exp\left(\sum_{i=1}^{N}\nu_i^r\int_{p_i^s}^{p}v_i\,\mathrm{d}p\right) \tag{4.16}$$

Equation (4.16) allows us to calculate liquid-phase reaction equilibria from gas-phase equilibrium constants and vice versa.

Equations such as equation (4.13) or (4.15) make it possible to calculate chemical equilibrium constants from the chemical potentials of the pure components μ_i^{pure}, which again can be obtained from data on pure component enthalpies h_i^{pure} and entropies s_i^{pure}

$$\mu_i^{\text{pure}} = h_i^{\text{pure}} - T\,s_i^{\text{pure}} \tag{4.17}$$

Numbers for h_i^{pure} and s_i^{pure} in the standard state are available for many substances (for instance Stull et al. [14], Reid et al. [8], Frenkel et al. [15, 16]). Numbers for h_i^{pure} and s_i^{pure} at other conditions can be obtained from the standard state data using information on heat capacities and enthalpies of vaporization, which are also available in many cases, for instance in the sources cited above. It should be noted that the accuracy of chemical equilibrium constants obtained by this way is limited and may not be sufficient for a given application. This is mainly caused by the fact that due to the summation of the chemical potentials in equations such as equation (4.13) or (4.15), even small errors in the numbers for the pure component chemical potentials μ_i^{pure} may become very important in the calculation of the equilibrium constant from equations such as equations (4.13) and (4.15). Therefore, the chemical equilibrium constants generally have to be determined from direct experimental investigations. A comparison of some chemical equilibrium constants of esterifications and transesterifications as obtained from direct measurements and from estimated numbers for μ_i^{pure} is given in Table 4.1, underlining the need for accurate experimental data on chemical equilibrium constants.

For any application, it is particularly important to consider on which variables the chemical equilibrium constant depends. For gas-phase reactions, equations (4.14) and (4.15) are generally applied, where $K_r^{\text{pure id. gas}}(T,p^0)$ is a function of the temperature alone. For liquid-phase reactions, equations (4.12) and (4.13) are used in most cases. As the influence of pressure on $K_r^{\text{pure liq.}}(T,p)$ can generally be neglected, again only a function of temperature has to be known.

It should be remembered that that situation is more complicated when chemical equilibrium constants based on normalizations of the type shown in equations (4.6)–(4.8) are used. Even though those chemical equilibrium constants are thermodynamically consistent, they are functions of the composition of the reacting liquid phase. For example, if a dissolved gas k normalized according to equation

Table 4.1 Comparison of chemical equilibrium constants of some esterifications and transesterifications as obtained from experimental data and from numbers for μ_i^{pure}

Second reactant	*T/°C*	$K_{fit}^{pure\ liq.}$	$K_{predict}^{pure\ liq.}$
esterifications with acetic acid			
methanol	45	31.8	23.5
1-butanol	85	16.9	39
esterifications with formic acid			
methanol	20	28.4	59.3
ethanol	50	12.9	42
transesterifications with 1-butanol			
methyl acetate	50	0.91	2.6
ethyl acetate	35	1.1	2.3

(4.6) takes part in a reaction r and all other components are normalized according to Raoult's law, then the following expression is obtained for the thermodynamically consistent chemical equilibrium constant from equations (4.3), (4.5), and (4.6)

$$K_r^{\text{pure liq.}}(T,p,\mathbf{x}_k^*) = \prod_{i=1}^{N} (x_i)^{\nu_i^r} \prod_{\substack{i=1,\\ i\neq k}}^{N} (\gamma_i)^{\nu_i^r} (\gamma_k^*)^{\nu_k^r} \tag{4.18}$$

with

$$K_r^{\text{pure liq.}}(T,p,\mathbf{x}^{k*}) = \exp\left(- \frac{\sum_{\substack{i=1\\ i\neq k}}^{N} \nu_i^r \mu_i^{\text{pure liq.}}(T,p) + \nu_k^r \mu_k^*(T,p,\mathbf{x}^{k*})}{\mathrm{R}\,T} \right) \tag{4.19}$$

where $\mathbf{x}^{k*}$ refers to the composition of the solution when the concentration of the dissolved gas k approaches 0 that is, the solvent concentration. Hence, the equilibrium constant $K_r^{\text{pure liq.}}(T,p,\mathbf{x}^{k*})$ is a function of the composition of the solvent in that case.

4.4 Fluid Property Models for Reactive Distillation

4.4.1 Outline

For using the basic thermodynamic conditions for chemical and physical equilibrium presented in the previous section, models for the activity coefficients γ_i and/or the fugacity coefficients φ_i have to be applied. They are based either on

G^E models or equations of state and usually contain binary adjustable parameters, which have to be determined from experimental data. It is beyond the scope of the present chapter to discuss details of these models, which are presented in many standard textbooks [10, 11]. We will instead focus here on some questions related to applying these models to RD processes, especially to the questions of sensitivity to inaccurate input data, predictions of properties of multicomponent mixtures from binary data, benefits from thermodynamically consistent models and consequences of inconsistent models. These topics will be addressed using some typical examples of RDs, mainly on esterifications. Furthermore, an example from a technically important intrinsically chemically reactive mixture (formaldehyde + water + methanol) is included.

4.4.2 Examples

4.4.2.1 Hexyl Acetate: Sensitivity Analysis

Let us first consider the esterification

1-hexanol + acetic acid ⇌ hexyl acetate + water.

A scheme of an RD process to produce hexyl acetate is shown in Fig. 4.4. There are two feeds below and above the reactive section of the column for acetic acid and 1-hexanol respectively. Owing to a low-boiling heterogeneous azeotrope, two liquid phases form upon condensation, so that a phase separator is used.

For process simulation, the thermodynamic properties of the quaternary mixture 1-hexanol + acetic acid + hexyl acetate + water have to be known. The vapor–liquid equilibrium model of that quaternary mixture is, as usual, parameterized based on information from the binary systems alone. There are six binary mixtures for a quaternary mixture, two of which are reactive in our example. The special challenges in the experimental determination of phase equilibria in reactive systems will be discussed later. Using typical G^E models, at least 12 parameters have to be adjusted to experimental binary data or estimated. Additionally, at least the

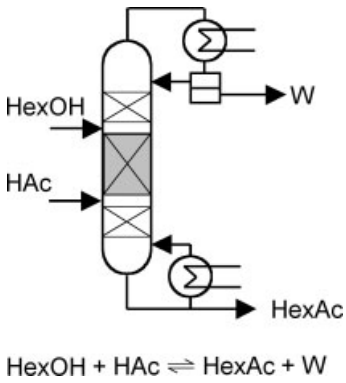

Fig. 4.4 Set-up for the production of hexyl acetate by RD (HexOH = 1-hexanol, HAc = acetic acid, HexAc = hexyl acetate, W = water; shaded = reaction zone)

chemical equilibrium constant of the esterification has to be known for the simulation of the RD process.

In principle, it would be desirable to have information on vapor–liquid equilibria of all binary systems in the temperature range in which the RD is carried out, which is about 100–150 °C in the case studied here. Furthermore, it would be desirable to have at least some data points for ternary systems (all of which are reactive) and for the quaternary system to be able to check the predictive power of the phase equilibrium model. That ideal situation is almost never encountered in reality. In many cases, even reliable experimental data on the binary systems is missing. In the present study, no data was available for the binary systems acetic acid + hexyl acetate and 1-hexanol + hexyl acetate. Estimations of missing data using group contribution methods such as UNIFAC are possible, but their quality is often hard to assess.

Furthermore, in the present case not only vapor–liquid equilibria have to be known, but also liquid–liquid equilibria. It is well known that the simultaneous description of both vapor–liquid and liquid–liquid equilibria often fails with standard models, if quantitative agreement is needed. Therefore, in practice, often different sets of model parameters are used for the distillation columns and the decanters.

The information on phase equilibria in the different binary systems need not have the same quality for all binary systems. For instance, in distillation of zeotropic mixtures, the information on the binary system of the lowest and the highest boiling component will often only be of minor importance, due to the high relative volatility, so that predictions from UNIFAC or even the assumption of ideality will be sufficient.

A helpful but rarely used tool for deciding whether accurate information on a given binary system is needed for the design of a certain separation is provided by sensitivity analysis. An example for such an analysis of the hexyl acetate RD process shown in Fig. 4.4 is given in Fig. 4.5. The basis of the sensitivity analysis is a given operating point of the RD column and a fully parameterized process model. In our case the NRTL model with two adjustable parameters per binary system was used to describe liquid-phase non-idealities in that model. Parameters for systems, for which no experimental data was available were estimated with UNIFAC in a first step.

The strategy for the sensitivity analysis is based on the variation of the limiting activity coefficients of the binary systems. The binary NRTL parameters can be determined from the knowledge of the two limiting activity coefficients. Therefore, a given variation in the limiting activity coefficients of the binary systems produces a certain variation of the phase equilibrium model and, hence, a certain variation of the model predictions. In the case study shown in Fig. 4.5, both limiting activity coefficients were increased by 30 %, which is about three times the typical experimental uncertainty for that property. The results presented in Fig. 4.5 show that in the case studied here, obviously the parameters for the three water-free binary systems I, II, and IV have the strongest influence on the simulation results, whereas the quality of the data for the water-containing systems is much less important. It should be noted that in the sensitivity study shown in Fig. 4.5 the decanter model

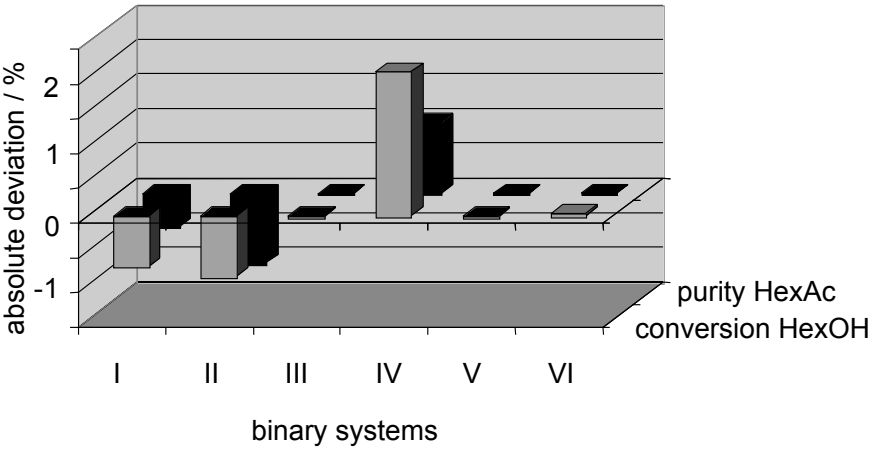

I: HAc - HexOH
II: HAc - HexAc
III: W - HAc
IV: HexOH -HexAc
V: W - HexOH
VI: W - HexAc

Fig. 4.5 Sensitivity analysis: Influence of errors in binary data on predictions of hexyl acetate RD (example for a given operating point)

was not changed, so that it reflects only the influence of the data on the different binary systems on the RD column itself. For the decanter, a different picture is obtained: a similar sensitivity analysis for that apparatus shows the influence of the aqueous systems data, as could be expected.

Such sensitivity analysis is a valuable tool for planning the experimental program for the phase equilibrium measurements, which are often needed to complement the literature data. Another field of application of such sensitivity analysis is the assessment of possible errors in process simulation results due to uncertainties of the thermophysical data. In the case studied here, the sensitivity analysis showed that the two binary systems, where data was missing (acetic acid + hexyl acetate and 1-hexanol + hexyl acetate) have an important influence on the process model predictions.

Presently, the type of sensitivity analysis proposed here is not supported by any commercial process simulator. It would be desirable and fairly easy to implement such a tool.

4.4.2.2 **Methyl Acetate: Prediction of Polynary Vapor–Liquid Equilibria**

In the previous section, the influence of the quality of binary data on simulation results of RDs was discussed. We will now focus on the fact that even very similar descriptions of binary data may lead to distinctly differing predictions for processes with multicomponent mixtures, such as RD. The example used here is the methyl acetate RD already discussed above. In modeling that process, two variants of the UNIQUAC model were used: one with two adjustable binary parameters and one

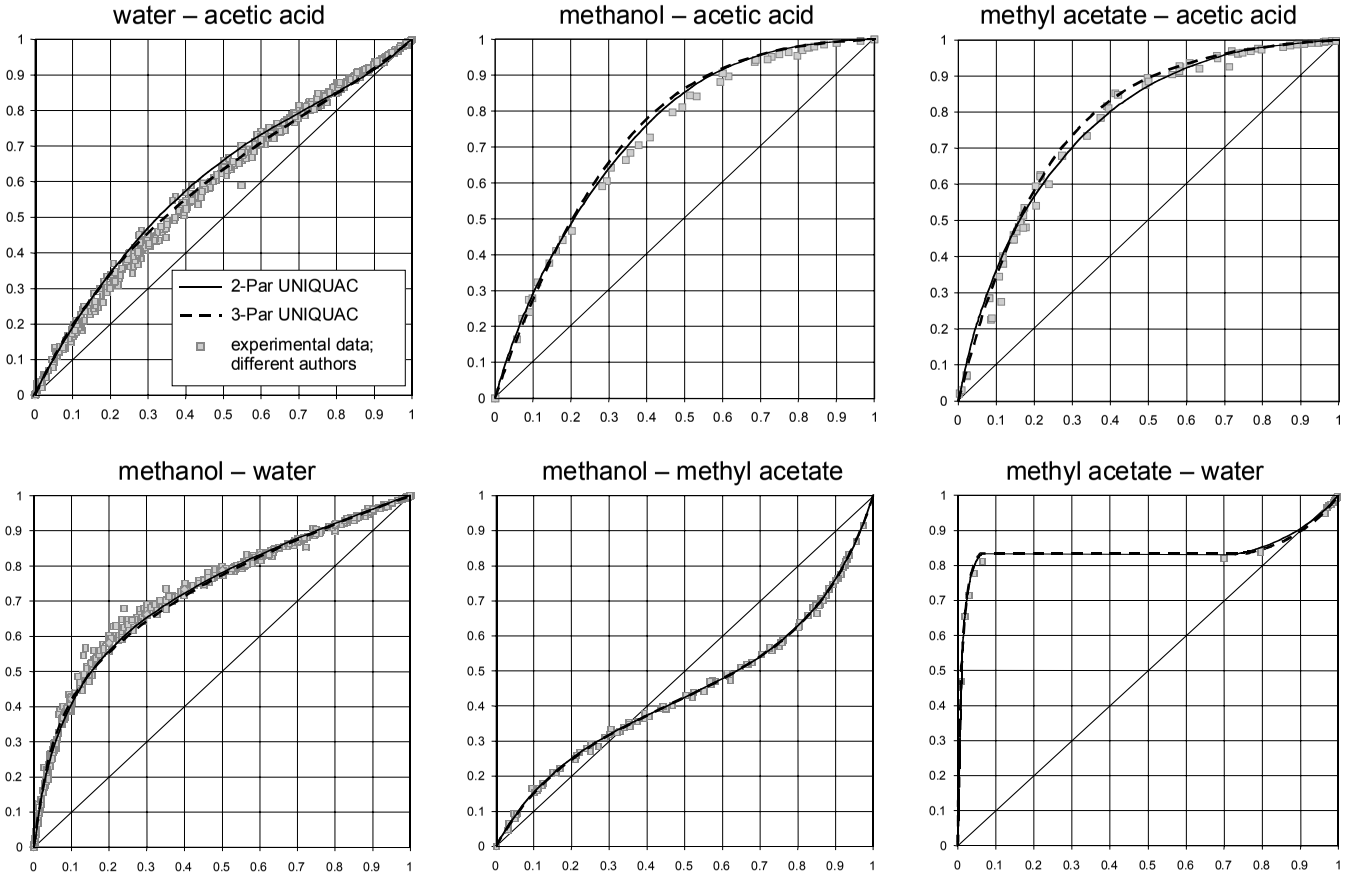

Fig. 4.6 Binary data fit for the six binary subsystems of the system methanol + acetic acid + methyl acetate + water at 1 bar with two variants of the UNIQUAC model. (McCabe Thiele Diagrams for $p = 1$ bar in mole fractions of the component appearing first in the system title)

with three binary parameters allowing to take into account more flexibly influences of the temperature. From Fig. 4.6 it can be seen that these two variants of UNIQUAC yield comparable correlations of the available experimental data for all six binary subsystems of the quaternary mixture methanol + acetic acid + methyl acetate + water. The predictions of ternary systems, however, appreciably differ. This can be seen from Fig. 4.7, in which distillation lines for the four ternary subsystems of the studied quaternary mixture are shown. Whereas for the three water-containing ternary systems, very similar predictions of the distillation lines are obtained with both models, the predictions for the system methanol + methyl acetate + acetic acid differ unexpectedly strong. These differences also lead to differing predictions of the RD process itself, as can be seen from Fig. 4.8. From Fig. 4.6 alone, one would not have expected such differences. Taking into account that in the example discussed here the data base for the binary data fit was identical for both models and that only different variants of the same thermodynamic model were used, clearly highlights the high sensitivity of RD process models to the thermodynamic fluid-properties models they rely on.

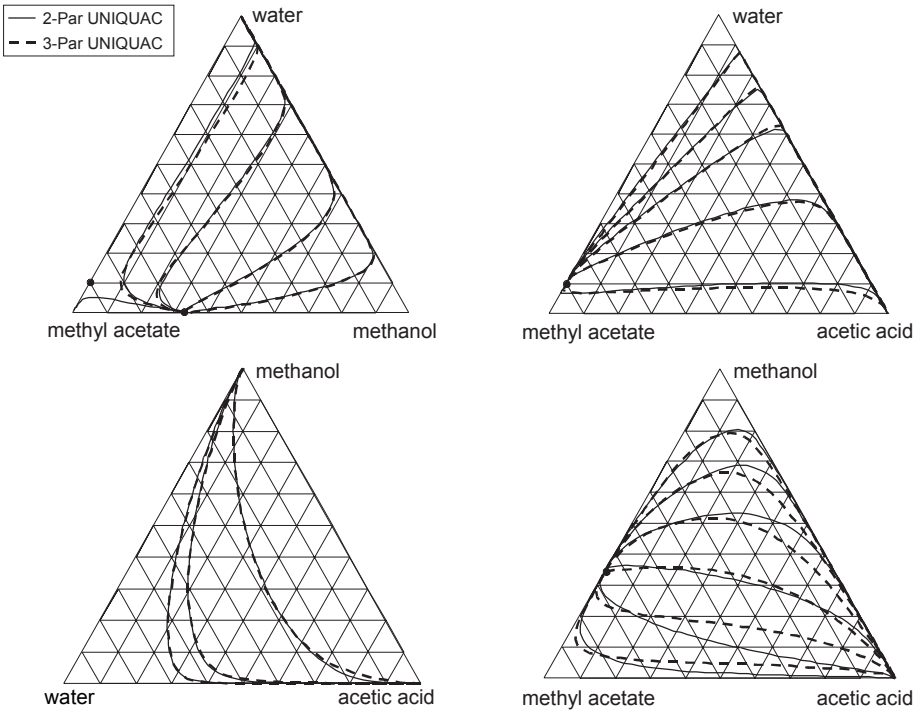

Fig. 4.7 Predictions of ternary distillation lines at $p = 1$ bar based on the binary data fit shown in Fig. 4.6. (Gibbs triangular diagrams in mole fractions)

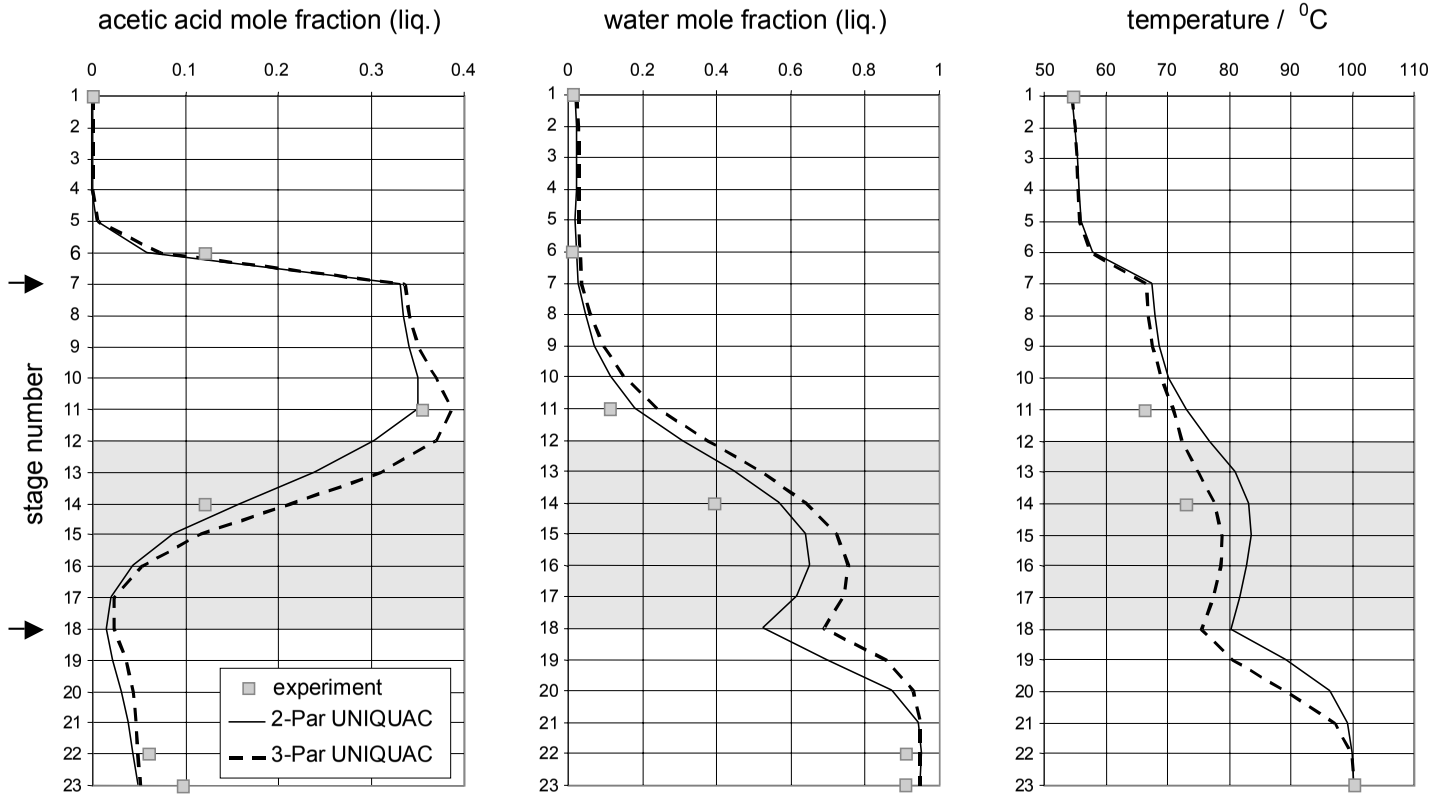

Fig. 4.8 Predictions of RD column profiles based on the binary data fit shown in Fig. 4.6 (set-up in Fig. 4.1, $p = 1$ bar, arrows = feed location, shaded = reaction zone)

4.4.2.3 Butyl Acetate: Thermodynamic Consistency

From a theoretical standpoint, it is obvious that only thermodynamic consistent models of chemical and phase equilibria should be applied in RD modeling. We will discuss the subject from a more practical standpoint here, using typical liquid-phase reactions as examples, for which the thermodynamic consistent chemical equilibrium constant is given by equations (4.12) and (4.13).

The following abbreviations are used here

$$K_x(T,p,\mathbf{x}) = \prod_{i=1}^{N} (x_i)^{\nu_i} \tag{4.20}$$

$$K_\gamma(T,p,\mathbf{x}) = \prod_{i=1}^{N} (\gamma_i)^{\nu_i} \tag{4.21}$$

where K_x is the (inconsistent) mass action law equilibrium constant of the reaction of interest, which depends on the composition of the mixture, K_γ is the corresponding term from the activity coefficients, which again is a function of the composition. The thermodynamically consistent equilibrium constant defined according to equation (4.12), which is *in*dependent of the composition of the mixture, is denoted simply by K here.

From equation (4.12) in the rearranged form

$$K_x(T,p,\mathbf{x}) = \frac{K(T,p)}{K_\gamma(T,p,\mathbf{x})} \tag{4.22}$$

it can be seen that it should principally be possible to predict the concentration dependence of K_x from activity coefficient data condensed into K_γ. Experimental data on K_x is unfortunately often subject to considerable uncertainties, especially in those regions, where one ore more components are dilute. However, it is just in those regions where the strongest influence of the composition on K_x is observed, due to the large numbers of the activity coefficients in the diluted regions.

The question of whether it is possible to predict the concentration dependence of K_x from information on K_γ via equation (4.22) is discussed here using the esterification of 1-butanol with acetic acid at 80 °C as an example. The experimental data given in Fig. 4.9 show that K_x is a strong function of the composition for that liquid-phase reaction. The numbers for K_x are in the range 2–8 and systematically vary with composition. In the studied system, there is a liquid–liquid miscibility gap intersecting with the chemical equilibrium surface. No measurements with liquid–liquid phase split were carried out in the present work.

Fig. 4.9 also contains results from a thermodynamic consistent model of the studied esterification. The activity coefficients were modeled on the basis of phase equilibrium data alone using the NRTL equation. With that model the number for the thermodynamic equilibrium constant K of the studied esterification at 80 °C was determined from a fit to the experimental data shown in Fig. 4.9 to be

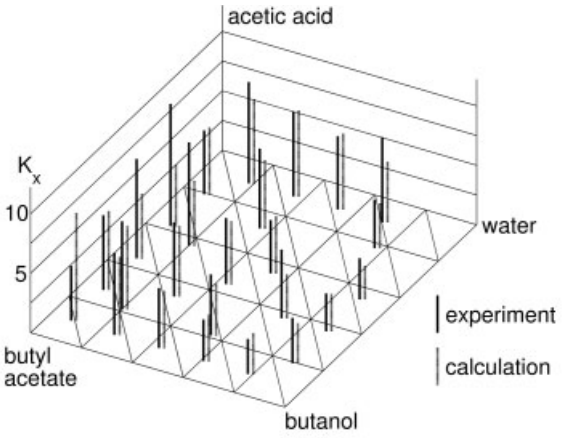

Fig. 4.9 Concentration dependence of the mass action law equilibrium constant K_x of the reaction 1-butanol + acetic acid ⇌ butyl acetate + water at 80 °C: comparison of experimental data (this work) with predictions from a thermodynamic consistent model using activity coefficients from a NRTL model with parameters from phase equilibrium data ($K = 22.7$)

$K = 22.7$. Based on that single number, the activity coefficient model predicts the influence of concentration on K_x via equation (4.22). It can be seen from Fig. 4.9 that the comparison of that prediction to the experimental data generally shows good agreement. Larger deviations are only observed for a few diluted samples and may partially be due to experimental errors. Results such as those shown in Fig. 4.9 are typical also for other esterifications.

4.4.2.4 **Ethyl Acetate: Consequences of Inconsistency**

Besides the benefits of thermodynamic consistent models of chemical reactions, also the problems that can arise, when inconsistent models are used should be considered. Two examples will be discussed here, one in the present and the other in the following subsection. The example discussed first relates to ethyl acetate production by RD.

For designing RD processes, RD lines have become a widely used tool. RD line diagrams (at constant pressure) usually do not contain information on the temperature. In many systems, reactive azeotrope are observed in these diagrams. Users generally assume that the reactive azeotrope coincides with an extremum in the temperature. It can be shown, using the Gibbs-Konovalev theorems applied to reactive mixtures [17] that this is always true, as long as a thermodynamic consistent description of the chemical and the phase equilibrium is used [18, 19]. If, however, an inconsistent model is applied, there is no reason, why the reactive azeotrope and the temperature extremum should coincide. An example is given in Fig. 4.10. It shows RD lines in the system acetic acid + ethanol + ethyl acetate + water at 1 bar. The RD lines were obtained using $K_x = 3.7$. The phase equilibrium model takes into account liquid-phase non-idealities and, hence, the description of the chemical and the phase equilibrium is inconsistent. As a result, the reactive azeotrope and the temperature minimum no longer coincide (compare Fig. 4.10).

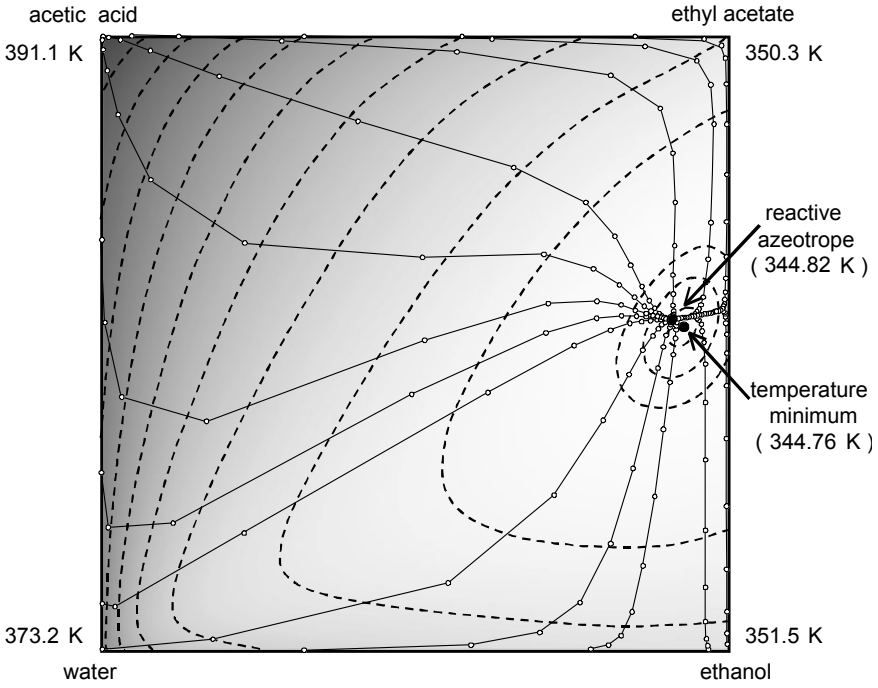

Fig. 4.10 RD lines (full lines) and isotherms (dashed lines) in the system ethanol + acetic acid + ethyl acetate + water at 1 bar. The reactive azeotrope and the temperature minimum do not coincide as a result of thermodynamic inconsistency

4.4.2.5 **Formaldehyde + Water + Methanol: Intrinsically Reactive Complex Mixture**

Formaldehyde is one of the most important C1 building blocks in the chemical industry and is the basis for a large variety of products. It is usually handled in aqueous solutions, which generally also contain methanol. In those solutions, formaldehyde (CH_2O) and water react to methylene glycol ($HOCH_2OH$) and a series of oligomer poly(oxymethylene) glycols ($HO[CH_2O]_nH$, $n > 1$). Similar reactions occur in methanolic formaldehyde solutions, yielding hemiformal (H_3COCH_2OH) and poly (oxymethylene) hemiformals ($H_3CO[CH_2O]_nH$, $n > 1$).

Analysis of formaldehyde solutions by conventional methods such as titration only gives the overall formaldehyde concentration that results from the sum of the free formaldehyde (usually a very small amount) and that bound in its various reaction products. The true concentrations in the solution can only be measured with NMR-spectroscopy.

It should be kept in mind that while formaldehyde + water + methanol mixtures are ternary from an overall standpoint, they are polynary mixtures with more than 20 components in appreciable concentrations if the true species are taken into account.

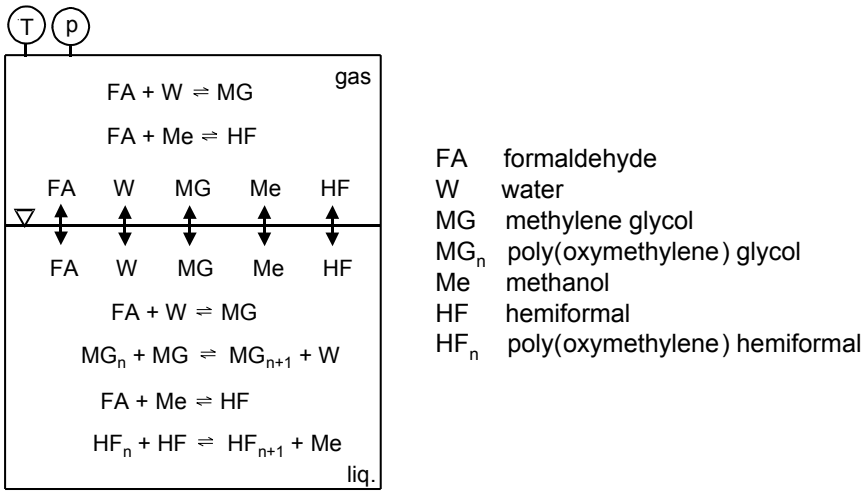

Fig. 4.11 Scheme of a physicochemical vapor–liquid equilibrium model of the system formaldehyde + water + methanol

A predictive thermodynamic model for thermodynamic properties of formaldehyde solutions, has been developed by Maurer and coworkers [20–23]. It explicitly takes into account the chemical reactions in these complex systems. Fig. 4.11 shows a scheme of the vapor–liquid equilibrium model. The methylene glycol and hemiformal formation take place both in the gas and the liquid phase. The oligomers are present only in the liquid phase and do not have to be considered in the gas phase due to their low vapor-pressures. The gas phase is a mixture of ideal gases, non-idealities in the liquid phase are taken into account by the UNIFAC group contribution method. Some of the UNIFAC parameters are adjusted to experimental vapor–liquid equilibrium data of systems containing formaldehyde. The chemical equilibrium model is based on NMR spectroscopic data of the liquid phase reactions and gas density measurements [24]. The results obtained with that model are usually given in overall concentrations to allow direct comparison with results from standard analysis. The agreement with experimental data on vapor–liquid equilibria is excellent in binary, ternary, and multicomponent formaldehyde containing mixtures over a wide range of compositions and temperatures [22, 23].

Fig. 4.12 gives an example of results of the application of that model. RD lines are shown for the system formaldehyde + water + methanol at 1 bar in overall concentrations. The distillation boundary between the low-boiling azeotrope in the formaldehyde + water system and methanol, the global low boiler, can clearly be seen.

One advantage of such physicochemical models is that they can easily be extended to include effects of reaction kinetics. This is shown in Fig. 4.13 where results from a case study on reactions kinetic effects on separations of mixtures of formaldehyde + water + methanol are shown. Whereas the equilibrium model

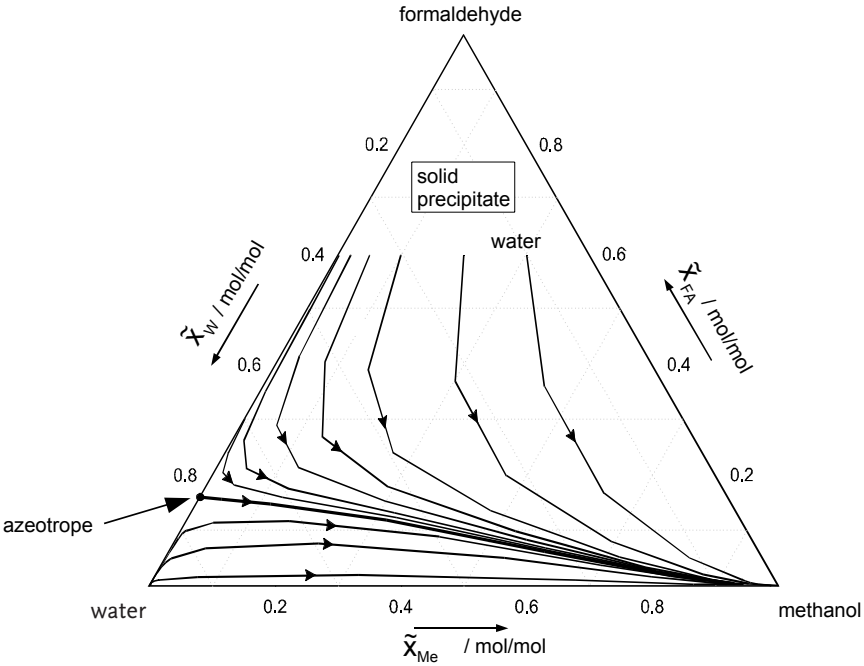

Fig. 4.12 RD lines in the system formaldehyde + water + methanol at 1 bar

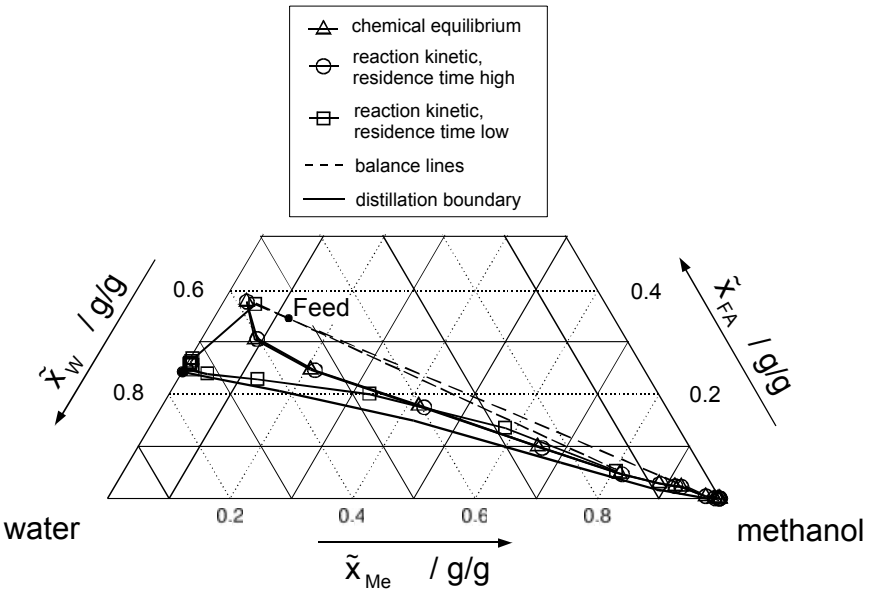

Fig. 4.13 Case study on the effect of reaction kinetics on distillation of formaldehyde + water + methanol mixtures at 1 bar

predicts a top product that is almost pure methanol for the investigated distillation process, the result from the model, which takes into account reaction kinetics, shows that the top product contains considerable amounts of formaldehyde and water, which is in agreement with the findings from technical distillations.

The formaldehyde + water + methanol system is just one example for many technically important systems, which are intrinsically chemically reactive. Other examples include aqueous solutions of weak electrolytes, such as amine solutions used to scrub carbon dioxide and other sour gases from gaseous streams, or the solutions containing bases used for chemical extraction of acids from aqueous streams. In many of these cases, the key to the development of predictive thermodynamic models is a quantitative model of the often complex chemical reactions in those mixtures. The necessary information often only can be obtained using spectroscopic methods [25].

In all these cases, it is essential to use thermodynamic consistent models. As an example, modeling results for the azeotrope in the formaldehyde + water system are discussed in more detail here using Fig. 4.14. Note that this azeotrope is in fact one of the technically most important examples for a reactive azeotrope. The left side of Fig. 4.14 shows results from a thermodynamic consistent model of the system formaldehyde + water [22]. At 140 °C the pressure is plotted as a function of the overall formaldehyde concentration $\tilde{x}_{FA}$. There is a low boiling azeotrope at about $\tilde{x}_{FA} = 0.5$ mol/mol. The right side of Fig. 4.14 shows the result that is obtained, when in that model arbitrarily K_γ is set to unity, while the activity coefficients are still used in the phase equilibrium calculation. Hence, the resulting model is inconsistent. It is not important here that the vapor–liquid equilibrium calculated with that modified model is strongly shifted, which only underlines the influence of liquid-phase non-idealities in that system. The important message from the plot on the right side of Fig. 4.14 is that applying the inconsistent model leads to a completely erroneous shape of the dew and bubble line. The dew and the bubble line do not touch with a horizontal tangent as in the picture of the left hand side of Fig. 4.14 (which is a result of the Gibbs–Konovalev theorem applied to reactive solutions in equilibrium) but intersect twice. Formally, there are two concentrations at which the condition for the reactive azeotrope $\tilde{x}_{FA} = \tilde{y}_{FA}$ is fulfilled and two other concentrations at which the dew and the bubble line pressures are maximal. Obviously, it is not even worth to try to interpret this and a use of such an inconsistent model can not be recommended.

The examples given in this and the previous sections underline the necessity for using thermodynamic consistent models of chemical equilibria and phase equilibria. It should be kept in mind that this also applies to reaction kinetic models, which always contain information on the chemical equilibrium. It should, however, be taken into account that there is also a price to pay for the advantages of thermodynamic consistency: the evaluation of phase equilibrium data and chemical equilibrium data can no longer be carried out separately and any change either in the chemical reaction model or in the phase equilibrium model will affect the other model too.

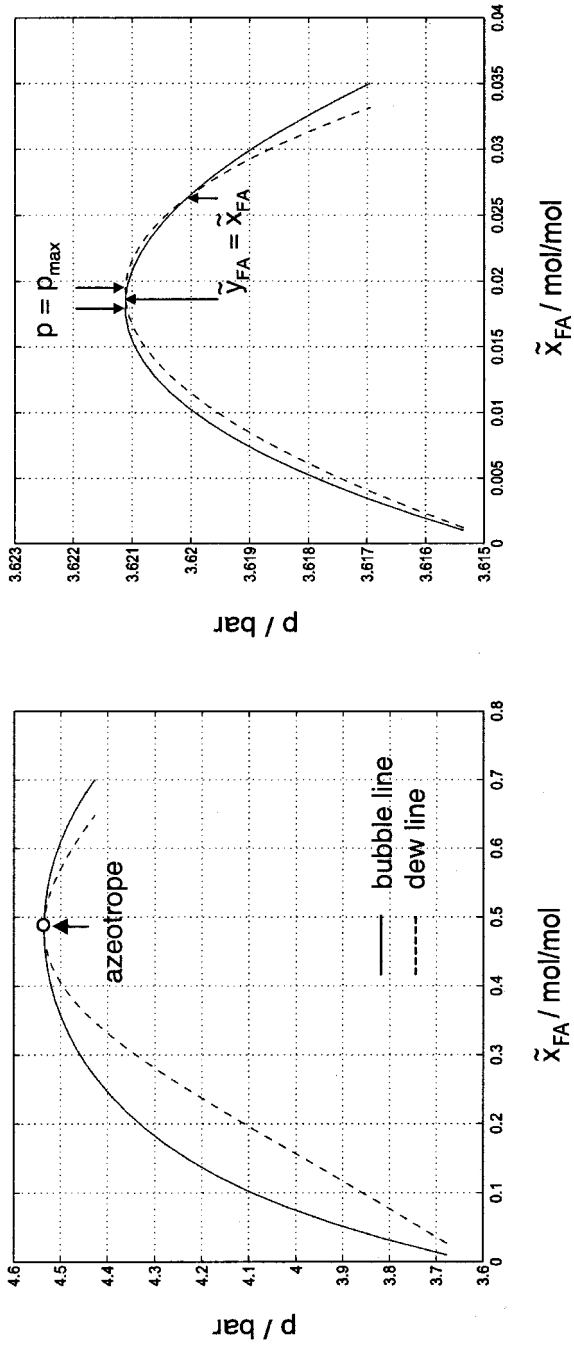

Fig. 4.14 Vapor–liquid equilibrium in the system formaldehyde + water at 140 °C. Left side: model with consistent description of chemical and phase equilibrium. Right side: inconsistent model

4.5
Experimental Studies of Phase Equilibria in Reacting Systems

4.5.1
Outline

For the design of RD processes, besides information on the reaction, information on phase equilibria is of prime importance, especially on vapor–liquid equilibria and in some cases also on liquid–liquid equilibria (see above). The systematic investigation of phase equilibria for the design of RD processes will generally involve also studies of reactive systems (see examples above). Studies of phase equilibria in reactive systems generally pose no problem if the reaction is either very fast or very slow as compared with the time constant of the phase equilibrium experiment (high or low Damköhler number *Da*). In the first case, the solution will always be in chemical equilibrium, in the second case, no reaction will take place. The definition of the time constant of the phase equilibrium experiment will depend on the type of apparatus used. If the RD process is catalyzed and the catalyst does not substantially influence the phase equilibrium, the phase equilibrium experiments can often be performed without catalyst and again no or only little conversion will take place.

Problems with phase equilibrium experiments in reactive systems arise mainly if the reaction time constant is of the same order magnitude as the time constants of phase equilibrium experiments (intermediate Damköhler number *Da*). For typical fluid phase equilibrium experiments, time constants are of the order of 10–1000 s, depending on the choice of the apparatus (and the definition of the time constant). These are however also typical time constants for many reactions, which are of interest for RD. It is therefore worthwhile to discuss measurements of reactive phase equilibria in more detail.

Measurements of reactive phase equilibria in the non-trivial case of intermediate Damköhler numbers *Da* can be classified into two groups: in the first, only the fully established equilibrium is investigated, whereas in the second the attempt is made to measure phase equilibrium without having reached chemical equilibrium. In experiments of the second type, reproducible results can only be expected, if their time constant is distinctly smaller than that of the chemical reaction.

Phase equilibrium experiments are usually classified into synthetic methods and analytical methods. In synthetic methods, the analysis of the coexisting phases is avoided by using information on the feed composition. The value of synthetic methods for measuring phase equilibria in reactive systems is obviously limited, even though they can in principle be applied to studies of fully equilibrated reacting mixtures, and are sometimes used together with extrapolation techniques to eliminate the influence of the reaction (see examples below).

Analytical methods for phase equilibrium measurements can be classified into methods that need sampling, such as gas chromatography or titration, and methods that do not need sampling, such as spectroscopic methods. Sampling is often a problem in chemically reactive systems. It may, for instance, shift the concentra-

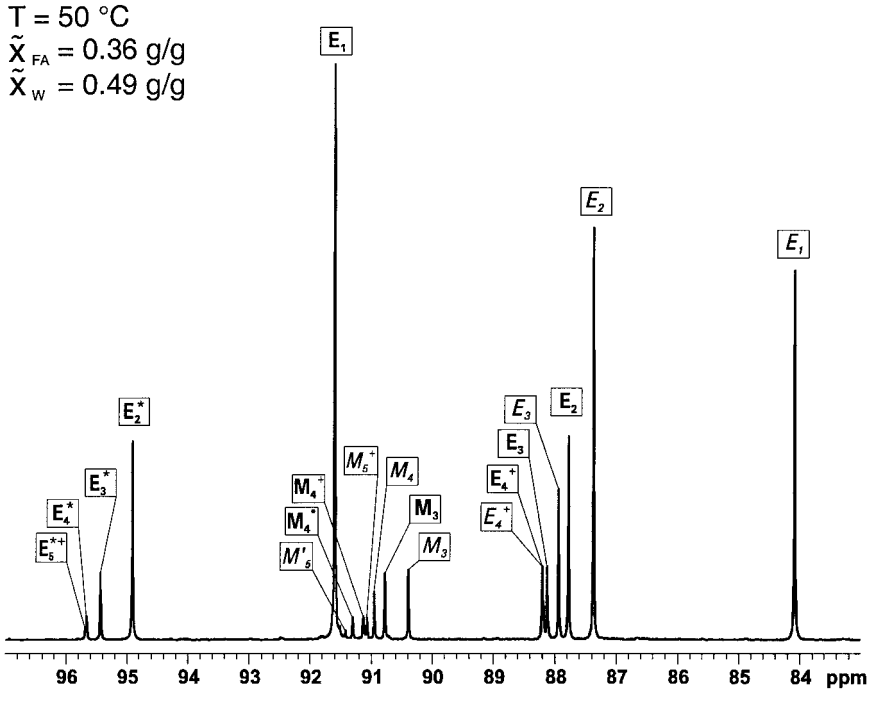

Fig. 4.15 ^{13}C NMR-spectrum of a formaldehyde + water + methanol mixture

MG$_1$ HO-CH$_2$-OH
E_1

MG$_2$ HO-CH$_2$-O-CH$_2$-OH
E_2 E_2

MG$_3$ HO-CH$_2$-O-CH$_2$-O-CH$_2$-OH
E_3 M_3 E_3

MG$_4$ HO-CH$_2$-O-CH$_2$-O-CH$_2$-O-CH$_2$-OH
E_4 M_4 M_4 E_4

MG$_5$ HO-CH$_2$-O-CH$_2$-O-CH$_2$-O-CH$_2$-O-CH$_2$-OH
E_5 M_5 M'_5 M_5 E_5

HF$_1$ HO-CH$_2$-O-CH$_3$
E_1

HF$_2$ HO-CH$_2$-O-CH$_2$-O-CH$_3$
E_2 $E_2^{\cdot}$

HF$_3$ HO-CH$_2$-O-CH$_2$-O-CH$_2$-O-CH$_3$
E_3 M_3 $E_3^{\cdot}$

HF$_4$ HO-CH$_2$-O-CH$_2$-O-CH$_2$-O-CH$_2$-O-CH$_3$
E_4 M_4 $M_4^{\cdot}$ $E_4^{\cdot}$

HF$_5$ HO-CH$_2$-O-CH$_2$-O-CH$_2$-O-CH$_2$-O-CH$_2$-O-CH$_3$
E_5 M_5 M'_5 $M_5^{\cdot}$ $E_5^{\cdot}$

tion away from an established chemical equilibrium or probes may react further after the sampling step. Therefore, spectroscopic methods, which allow a feedback free analysis of different components of the mixture, are of special interest for investigations of reacting systems.

It is beyond the scope of the present work to discuss the different options for the analytical methods. We only present one example here, showing what can be achieved with modern instrumental analysis. Fig. 4.15 shows a ^{13}C NMR-spectrum of a formaldehyde + water + methanol mixture taken with an online technique with a 400 MHz NMR spectrometer. Signals from a large number of different species can be resolved. Obviously, the band assignment is non-trivial for such complex mixtures and special techniques, such as two dimensional NMR, have to be applied. One of the most attractive features of NMR spectroscopy compared with other spectroscopic methods is that the quantitative evaluation of spectra such as that shown in Fig. 4.15 can be achieved without calibration, as the area below the peaks is directly proportional to the number of the different nuclei in the solution if the NMR experiment is carried out properly.

In the following discussion, we will focus on reactive vapor–liquid equilibria. Measurements of reactive liquid–liquid equilibria can be done in standard batch cells operated as mixer-settlers using appropriate analytical methods, as long as only data on the fully established equilibrium is needed. Practically no data seems to be available in the literature on liquid–liquid equilibria in mixtures that have not reached chemical equilibrium.

4.5.2
Reactive Vapor–Liquid Equilibria

Methods for measuring reacting vapor–liquid equilibria can roughly be classified into three groups: *static* or *batch experiments*, *flow experiments* and, as an intermediate between the first and the second type, *recirculation experiments* (Fig. 4.16).

4.5.2.1 Batch Experiments

For measuring vapor–liquid equilibria in reactive systems, analysis is needed in most cases. Most analytical techniques require sampling. This, however, often is non-trivial in batch cells. Special care has to be taken in sampling the gas phase, as this tends to alter the pressure. Batch cells are, therefore, especially attractive for measurements of reactive phase equilibria, when combined to feedback free analytical techniques such as spectroscopy. As time constants to establish equilibrium are rather high in batch cells, their application for studies of reacting systems is limited either to investigations of the fully established vapor–liquid and chemical equilibrium or to studies of slow reactions. Batch cells are often combined with sampling loops, which is a step in the direction of a recirculating still.

Batch cells have been used to study reactive phase equilibria, for instance by Patel and Young [26] and Arlt [27]. These authors employ extrapolation techniques to gain information on the state, where no reaction has occurred. This allows them

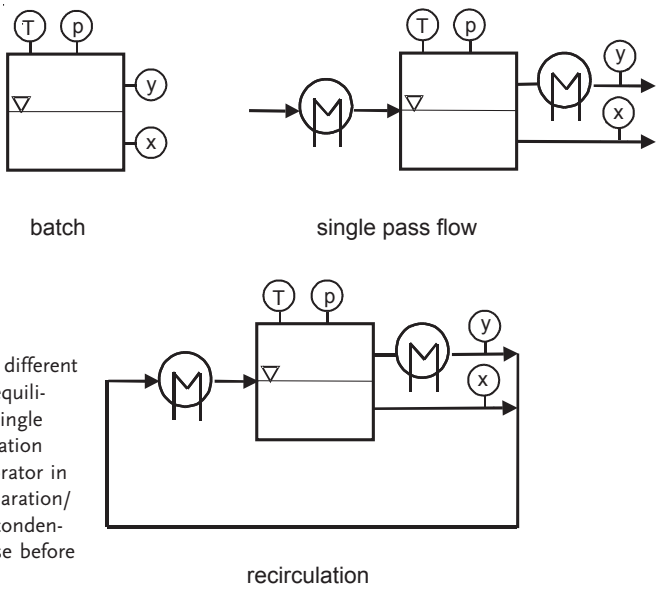

Fig. 4.16 Schemes of different basic types of phase equilibrium experiments. (Single pass flow and recirculation techniques with evaporator in front of the phase separation/equilibrium unit and condensation of the gas phase before sampling)

to use the information on the amounts of the different reactants charged into the batch cell and avoid problems with analysis. Interesting designs, in which batch cells have been coupled with spectroscopic analytics are described by Krissmann et al. [28] and Rogers et al. [29]. Krissmann et al. [28] used UV spectroscopy for their studies of aqueous, sulfur dioxide containing systems. The liquid phase was analyzed in situ in the batch cell whereas for the gas phase a special optical cell was connected to the batch cell by a probe loop. Rogers et al. [29] studied aqueous amine solutions containing carbon dioxide using IR-spectroscopic analysis, employing probe loops both for the liquid and the gas phase. Roederer [30] describes a versatile cell with in situ IR-spectroscopic analysis of both phases, in which both vapor–liquid equilibria and reaction kinetics were studied.

4.5.2.2 **Flow Experiments**

The basic advantage of flow cells compared to batch cells is that sampling generally poses less a problem, especially for the gas phase. Furthermore, the time to establish phase equilibrium after evaporation in the phase separator-equilibrium unit (Fig. 4.16) can be kept low using suitable designs. For instance, in Cottrell-type units, such as the one described by Rafflenbeul and Hartmann [31] that time is of the order of 10–20 s. For reactions with time constants of the order of some minutes, flow techniques can therefore be used for measuring phase equilibrium without having reached chemical equilibrium. The disadvantage of the technique is the high amount of substance needed due to the single pass mode.

Single pass flow techniques have been used for studies of vapor–liquid equilibria of reacting systems by various authors. Maurer and coworkers describe a special

type of thin film evaporator with a residence time of about 1–2 min, which they have extensively used for studies of vapor–liquid equilibria in formaldehyde containing systems in chemical equilibrium [20, 32]. In those studies, low evaporation ratios were used in order to only slightly shift the liquid-phase equilibrium upon evaporation. That idea has been extended by Hasse and Maurer [21] by using a gas saturation technique. More recently, a single pass Cottrell type flow cell was developed especially for phase equilibrium measurements in reacting systems by Reichl et al. [33]. Residence times are about 30–90 s in that cell.

4.5.2.3 **Recirculation Experiments**

The problem of high amounts of substance needed in flow cells in a single pass mode can be circumvented using recirculation techniques. However, the recirculation can cause problems in studies of chemically reactive systems if an ongoing chemical reaction in the recirculating stream leads to shifting compositions of the evaporator feed, so that no steady state is reached.

Nevertheless, recirculation techniques have been employed for studies of reactive phase equilibria by several groups. In an early paper, Hirata and Komatsu [34] suggest an extrapolation technique, similar to the one discussed above, to eliminate problems with the ongoing chemical reaction. Applications of recirculating stills for measurements of phase equilibria in esterification systems are described, for instance, by Kang et al. [35], Lee and Kuo [36], Lee and Liang [37], and Lee and Lin [38]. In these experiments enough time is given to reach a steady state. The question, how the comparatively quick evaporation with non-zero evaporation ratio affects the measurements, is, however, not discussed.

This brief survey shows that there are many options for measuring phase equilibria in reacting systems, which allow to carry out such studies for a wide range of systems and conditions. The main limitation for experimental investigations of reactive vapor–liquid equilibria is related to the velocity of the reaction itself: if phase equilibrium measurements of solutions are needed, which are not in chemical equilibrium, the reaction must be considerably slower than the characteristic time constant of the phase equilibrium experiment. Apparatus are available, where that time constant is distinctly below one minute. For systems with reactions too fast to be studied in such apparatuses, it should in many cases be possible to treat the reaction as an equilibrium reaction, so that the information on the phase equilibrium in mixtures, which are not chemically equilibrated is not needed.

4.6 Conclusions

Thermodynamics plays a key role in understanding, modeling, and designing reactive separation processes. The basic concepts of thermodynamic modeling of simultaneous chemical and phase equilibrium are summarized here with emphasis on the different options provided by classical thermodynamics. Several types of

RD process models are compared with each other and with experimental data on the background of the model complexity and the amount of information needed to parameterize the models.

Reliable models of reactive separation processes have to be based on a sound knowledge of the properties of the reacting fluid. Thermodynamics provides both the experimental methods and models to study and describe these properties. Different aspects of their use in RD process design are discussed, namely the question of sensitivity to inaccurate input data, predictions of properties of multicomponent mixtures from binary data, benefits of thermodynamically consistent models, and consequences of inconsistent models. These topics are addressed using examples from different esterifications and intrinsically chemically reactive systems. The examples given throughout the paper show the prime importance of reliable experimental data for the development of predictive process models of RDs. Therefore, also a brief survey on experimental techniques for studies of reactive phase equilibria is included.

Applying thermodynamics to RD processes is a fascinating subject, which covers all aspects, from experimental laboratory studies over modeling and simulation up to the industrial application of these complex processes.

4.7 Acknowledgments

I gratefully acknowledge the contributions of Sergei Blagov, Sascha Grob, Michael Ott, and Markus Schmitt of ITT, University of Stuttgart, Germany, who have provided examples used in the present work. Special thanks to Peter Moritz, Sulzer Chemtech, Winterthur, Switzerland, for our fruitful discussions on RD and the input to Section 4.2. Also the contribution of Tim Pöpken, formerly University of Oldenburg, Germany, to that section is acknowledged. Finally, I would like to thank Mr. Roos, formerly Hoechst AG, Frankfurt, Germany, who first found the effect shown in Fig. 4.14.

4.8 Notation

A^+	cation
B^{min}	anion
c	molarity
c^0	1 mol/liter
Da	Damköhler number (characteristic residence time/characteristic reaction time)
E	end group
EQ	phase equilibrium
FA	formaldehyde

G^{E}	excess Gibbs energy
h_i^{pure}	molar enthalpy of pure component i
HAc	acetic acid
HexOH	1-hexanol
HexAc	hexyl acetate
HF	hemiformal
HF_n	poly(oxymethylene) hemiformal with n CH_2O segments
i	component index
j	phase index
K	chemical equilibrium constant (thermodynamically consistent)
K_x	mass action law chemical equilibrium constant
K_γ	chemical equilibrium constant like term in activity coefficients
m	molality
m^0	1 mol/kg solvent
M	middle group
Me	methanol
MeAc	methyl acetate
MG	methylene glycol
MG_n	poly(oxymethylene) glycol with n CH_2O segments
MeOH	methanol
n	mole number
n	number of CH_2O segments
N	number of components
N_{sep}	number of theoretical stages
N_{rea}	number of stirred tank reactors
NEQ	not in phase equilibrium
NMR	nuclear magnetic resonance
p	pressure
p^0	normalization pressure
p^s	vapor pressure
P	number of phases
r	reaction index
R	universal gas constant (8.314 J/(mol K))
R	number of reactions
REA	reaction
s_i^{pure}	molar entropy of pure component i
T	temperature
v_i	molar volume of pure component i
v_i^∞	partial molar volume of component i at infinite dilution
W	water
$\mathbf{x}$	composition of phase
$\mathbf{x}^{i*}$	solvent composition (composition for infinite dilution of component i)
x_i	mole fraction of component i
$\tilde{x}_{FA}$	overall formaldehyde mole fraction (especially: liquid phase)
$\tilde{x}_{Me}$	overall methanol mole fraction

$\tilde{x}_W$	overall water mole fraction
$\boldsymbol{y}$	gas-phase composition
$\tilde{y}_{FA}$	overall formaldehyde mole fraction in vapor phase

Greeks

φ_i	fugacity coefficient of component i
γ_i	activity coefficient of component i
η	Murphree efficiency
μ_i	chemical potential of component i
ν_i^r	stoichiometric coefficient of component i in reaction r
ν_+	cation stoichiometric coefficient
ν_-	anion stoichiometric coefficient

Superscripts

c	referring to normalization using molarity
j	phase
m	referring to normalization using molality
pure liq.	referring to normalization according to Raoult's law
pure id. gas	referring to normalization according to pure ideal gas at T, p°
r	reaction
s	saturation (pure component)
0	referring to normalization
*	referring to normalization with $\gamma_i \rightarrow 1$ at infinite dilution
∞	referring to infinite dilution
$'$	liquid phase
$''$	gas phase

Subscripts

i	component
r	reaction
k	dissolved gas
solv	solvent

References

1 R. Taylor, R. Krishna, *Chem. Eng. Sci.*, **2000**, *55*, 5183–5229.
2 L. Götze, PhD Dissertation, Universität Oldenburg, **1998**.
3 P. Moritz, H. Hasse, *Chem. Eng. Sci.*, **1999**, *54*, 1367–1374.
4 P. Moritz, PhD Dissertation, Universität Stuttgart, **2001**.
5 B. Bessling, J. L. Löning, A. Ohligschläger, G. Schembecker, K. Sundmacher, *Chem. Eng. Technol.*, **1998**, *21*, 393–400.
6 T. Pöpken, S. Steinigeweg, J. Gmehling, *Ind. Eng. Chem. Res.*, **2001**, *40*, 1566–1574.

7 T. Pöpken, R. Geisler, L. Götze, A. Brehm, P. Moritz, J. Gmehling, *Chem. Eng. Technol.*, **1999**, *21*, 401–404.

8 R. C. Reid, J. M. Prausnitz, B. E. Poling, *The Properties of Gases and Liquids*, 4th edn. McGraw-Hill, New York, **1987**.

9 R. Taylor, R. Krishna, *Multicomponent Mass Transfer*, Wiley, New York, **1993**.

10 S. M. Walas, *Phase Equilibria in Chemical Engineering*, Butterworth-Heinemann, Boston, **1985**.

11 J. M. Prausnitz, R. N. Lichtenthaler, E. G. de Azevedo, *Molecular Thermodynamics of Fluid-Phase Equilibria*, 2nd edn, Prentice-Hall, Englewood Cliffs, **1986**.

12 M. Lisal, I. Nezbeda, W. R. Smith, *J. Chem. Phys.*, **1999**, *110*, 8597–8604.

13 M. Lisal, W. R. Smith, I. Nezbeda, *AIChE J.*, **2000**, *46*, 866-875.

14 D. R. Stull, F. W. Edgar, G. C. Sinke, *The Chemical Thermodynamics of Organic Compounds*, Wiley, New York, **1969**.

15 M. Frenkel, X. Hong, R. C. Wilhoit (eds.), *TRC Thermodynamic Tables – Non-Hydrocarbons, National Standard Reference Data Series*, National Institute of Standards and Technology (NIST), ISBN 1-886843-19-8, **2000**.

16 M. Frenkel, X. Hong, R. C. Wilhoit (eds.), *TRC Thermodynamic Tables – Hydrocarbons, National Standard Reference Data Series*, National Institute of Standards and Technology (NIST), ISBN 1-883400-06-6, **2000**.

17 I. Prigogine, R. Defay, *Chemical Thermodynamics*, Longmans, Green & Co., London, **1954**.

18 S. Ung, M. Doherty, *Chem. Eng. Sci.*, **1995**, *50*, 23–48.

19 S. Ung, M. Doherty, *AIChE J.*, **1995**, *41*, 2382–2392.

20 G. Maurer, *AIChE J.*, **1986**, *32*, 932–948.

21 H. Hasse, G. Maurer, *Fluid Phase Equilibria* **1991**, *64*, 185–199.

22 M. Albert, PhD Dissertation, Universität Kaiserslautern, **1998**.

23 M. Albert, B. C. Coto Garcia, C. Kuhnert, R. Peschla, G. Maurer, *AIChE J.*, **2000**, *46*, 1676–1687.

24 I. Hahnenstein, M. Albert, H. Hasse, C. G. Kreiter, G. Maurer, *Ind. Eng. Chem. Res.*, **1995**, *34*, 440–450.

25 H. Hasse, *Anwendungen der Spektroskopie in thermodynamischen Untersuchungen fluider Mischungen*, Fortschritt-Berichte VDI, Reihe 3: Verfahrenstechnik, Nr. 458, VDI Verlag, Düsseldorf, **1996**.

26 N. C. Patel, M. A. Young, *Fluid Phase Equilibria*, **1993**, *82*, 79–92.

27 W. Arlt, *Fluid Phase Equilibria*, **1999**, *158-160*, 973–977.

28 J. Krissmann, M. A. Siddiqi, K. Lucas, *Chem. Ing. Tech.*, **1996**, *68*, 1598–1602.

29 W. J. Rogers, J. A. Bullin, R. R. Davison, R. E. Frazier, K. N. Marsh, *AIChE J.*, **1997**, *43*, 3223–3231.

30 D. Roederer, *Untersuchungen zum Dampf-Flüssig-Gleichgewicht und zur Reaktionskinetik zweier Isomere für die Auslegung einer Reaktivrektifikationsanlage*, Ph. Dissertation, ETH Zürich, **1999**.

31 L. Rafflenbeul, H. Hartmann, *Chemie Technik*, **1978**, *7*, 145–148.

32 H. Hasse, I. Hahnenstein, G. Maurer, *AIChE J.*, **1990**, *36*, 1807–1814.

33 A. Reichl, U. Daiminger, A. Schmidt, M. Davies, U. Hoffmann, C. Brinkmeier, C. Reder, W. Marquardt, *Fluid Phase Equilibria*, **1998**, *153*, 113–134.

34 M. Hirata, H. Komatsu, *Kagaku Kogaku*, **1966**, *4*, 242–245.

35 Y. W. Kang,, Y. Y. Lee, W. K. Lee, *J. Chem. Eng. Japan*, **1992**, *25*, 649–655.

36 L. S. Lee, M. Z. Kuo, *Fluid Phase Equilibria*, **1996**, *123*, 147–165.

37 L. S. Lee, S. J. Liang, *Fluid Phase Equilibria*, **1998**, *149*, 57–74.

38 L. S. Lee, R. G. Lin, *Fluid Phase Equilibria*, **1999**, *165*, 261–278.

Reactive Distillation. Edited by Kai Sundmacher, Achim Kienle

ISBNs: 3-527-30579-3 (Hardback); 3-527-60052-3 (Electronic)

5
Importance of Reaction Kinetics for Catalytic Distillation Processes

K. Sundmacher and Z. Qi

5.1
Introduction

Reactive distillation (RD) processes are often designed from equilibrium assumptions for chemical reactions and interphase phenomena. Equilibrium-based design leads to important implications for the feasibility of RD. However, most of the chemical reactions carried out in RD columns are kinetically controlled and they can be strongly affected by the limitations of inter- or intraphase mass- and energy-transport resistances.

In the first part of this chapter, the general influence of reaction kinetics is discussed using isomerization in an ideal binary mixture as a simple model reaction. For this system, first design principles and important parametric dependencies are discussed.

In the second part, the possible products of kinetically controlled catalytic distillation processes are analyzed using residue curve maps. Ideal, as well as non-ideal, ternary mixtures are considered. Current research activities are presented that are focussed on reaction systems exhibiting liquid-phase splitting phenomena such as the hydration of cyclohexene to cyclohexanol at strongly acidic catalyst particles.

In the third part of this chapter, the experimental determination and the detailed theoretical analysis of reaction kinetics obtained at catalysts used in RD processes are discussed. For reliable column design, activity based microkinetic rate expressions are applied successfully to heterogeneously catalyzed processes. By increasing the particle size of heterogeneous catalysts to be used in RD processes, mass-transport resistances can become relevant and have to be considered for reliable column simulations. This is exemplified by the industrially relevant syntheses of the fuel ethers MTBE and ETBE.

5.2
Reactive Ideal Binary Mixtures

First, the role of reaction kinetics is analyzed considering RD processes for the simple reversible reaction $A_1 \leftrightarrow A_2$ in an ideal binary mixture. The educt A_1 is assumed to be the reaction component with the higher boiling point, so the product A_2 is obtained in the distillate. The reaction can be carried out in an RD column sequence with an external recycling loop (Fig. 5.1), a non-RD column on top of a reactive reboiler (Fig. 5.2), or a full RD column (Fig. 5.3). More possible configurations are analyzed elsewhere [1].

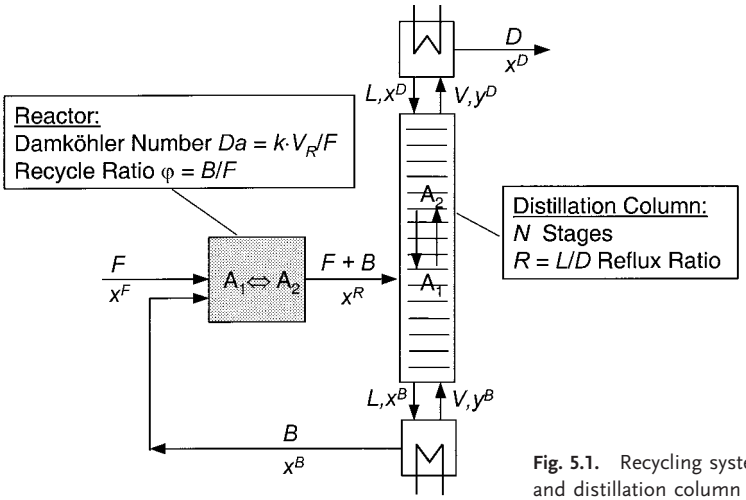

Fig. 5.1. Recycling system of reactor and distillation column

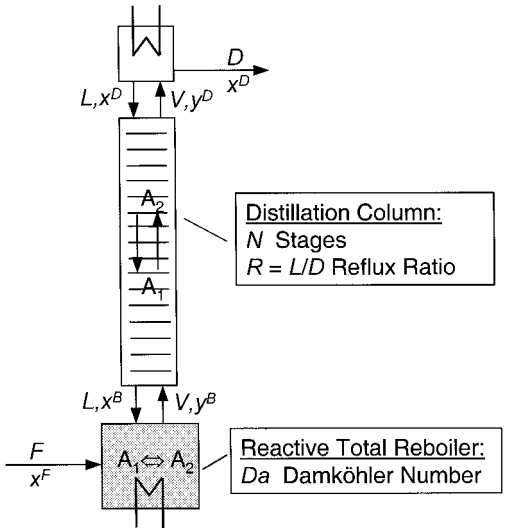

Fig. 5.2. Distillation column with reactive total reboiler

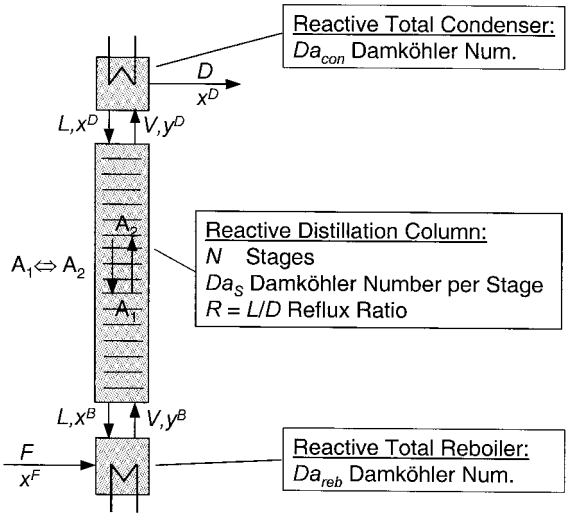

Fig. 5.3. RD column with reactive total condenser and reactive total reboiler

In the very early stage of conceptual process design, very little is known about the reaction kinetics, so a macrokinetic power-law expression in terms of liquid-phase mole fractions should be used

$$r = kx_1^n\left(1-\frac{1}{K}\frac{x_2}{x_1}\right) \tag{5.1}$$

with n as apparent reaction order with respect to A_1, K as chemical equilibrium constant, and k as the effective rate constant of forward reaction. K and k are dependent on the temperature T, but in a first step, they can be taken as constant parameters. K can be estimated from thermodynamic relations at a typical boiling temperature of the reaction mixture.

For the sake of a simplified nomenclature, the component indices are dropped by setting $x_2 = x$ and $x_1 = 1 - x$. In addition, a dimensionless reaction rate r^* is introduced

$$r^* \equiv \frac{r}{k} = (1-x)^n\left(1-\frac{1}{K}\frac{x}{(1-x)}\right) \tag{5.2}$$

As a special case of (5.2), the rate of a first-order reaction ($n = 1$) is given by

$$r^* = 1-\frac{x}{x_{ce}} \text{ with } x_{ce} = \frac{K}{K+1} \tag{5.3}$$

where x_{ce} is the mole fraction of A_2 at chemical equilibrium. The vapor–liquid equilibrium is described assuming a constant relative volatility $\alpha = p_2^S/p_1^S > 1$, which is

assumed to be constant. Then, the equilibrium mole fraction of component A_2 in the vapor phase, y^e, is given by

$$y^e = \frac{\alpha\, x}{1+(\alpha-1)x} \tag{5.4}$$

5.2.1 Reaction-Distillation Process with External Recycling

The simplest flow-sheet for the reaction $A_1 \leftrightarrow A_2$ is the RD column sequence with an external recycling loop shown in Fig. 5.1. The system as a whole is fed with pure A_1. According to the assumed relative volatility of the two components $\alpha > 1$, the reaction product A_2 is enriched in the column distillate product whereas the bottom product contains non-converted reactant A_1, which is recycled back to the reactor (continuous stirred tank reactor, CSTR, or plug flow tube reactor, PFTR). The process has two important operational variables: the recycling ratio $\varphi \equiv B/F$, that is the ratio of recycling flow B to feed flow rate F, and the reflux ratio of the distillation column $R \equiv L/D$. At steady-state conditions, $D = F$ since the total number of moles is assumed to be constant for the reaction $A_1 \leftrightarrow A_2$. As principal design variables, the Damköhler number,

$$Da \equiv \frac{kV_R}{F} \tag{5.5}$$

which characterizes the size of the reactor, and the number of theoretical stages N of the distillation column are considered. The relations between the operational and design variables are governed by the steady-state mass balances for the reactor and the column

$$0 = x^F + \varphi x^B - (1+\varphi)x^R + Da \cdot r^*(x^R) \tag{5.6}$$

$$0 = (1+\varphi)x^R - \varphi x^B - x^D \tag{5.7}$$

In (5.6), a CSTR is considered as reactor, and therefore the reaction rate r^* is calculated at the reactor outlet concentration, x^R. At infinite reflux ratio, $R = \infty$, the distillate (x^D) and bottom concentrations (x^B) are related to each other by the Fenske equation [2]

$$\frac{x^D}{1-x^D} \cdot \frac{1-x^B}{x^B} = \alpha^{N_{\min}+1} \tag{5.8}$$

with $N_{\min}$ as minimum number of theoretical column stages; (5.6)–(5.8) are used to determine the three unknown mole fractions x^R, x^B, and x^D.

5.2.1.1 (∞,∞)-Analysis

As the first step of conceptual process design, the distillation column is considered at infinite reflux ratio, $R = \infty$, with an infinite number of stages, $N = \infty$. Under these perfect separation conditions, the distillation column will yield a bottom product that contains pure A_2: $x^B = 0$. Then the distillate mole fraction x^D only depends on the size of the reactor (Da), the recycling ratio (φ), and the chemical equilibrium concentration x_{ce}. Combining (5.6) and (5.7) yields

$$x^D = \frac{Da}{r^*(x^R)} \text{ with } x^R = \frac{x^D}{(1+\varphi)} \tag{5.9}$$

For a first-order reaction, the distillate mole fraction is given by

$$x^D = \frac{Da}{1+\frac{Da}{(1+\varphi)x_{ce}}} \text{ for } n = 1 \tag{5.10}$$

In Fig. 5.4, the distillate quality is plotted versus the Damköhler number at different recycling ratios for fixed thermodynamic parameters $K = 2$ and $\alpha = 1.5$. As expected, by increasing the recycling flow rate the product quality is improved. At infinite Damköhler number, one obtains a maximum attainable composition level $x^D = (1 + \varphi)x_{ce}$. Obviously, there is a critical recycling ratio, φ_{crit}, that has to be attained in order to reach a specified product quality x^D

$$\varphi_{crit}(Da = \infty) = \frac{x^D}{x_{ce}} - 1 \tag{5.11}$$

In an analogous manner, at $\varphi = \infty$, there is a critical Damköhler number, Da_{crit}, (minimum reactor size) that has to be realized in order to attain a specified product quality x^D. This is given by

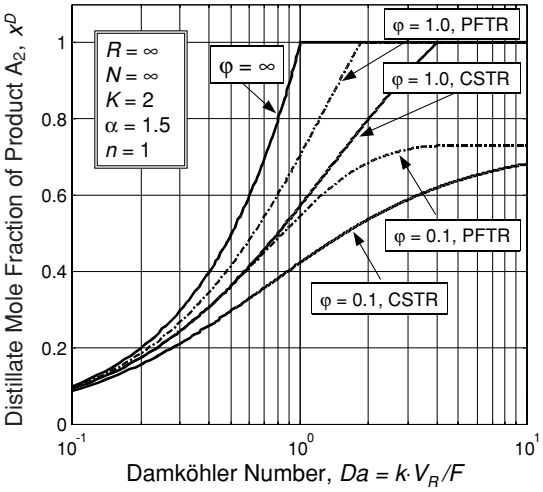

Fig. 5.4. Mole fraction of product A_2 against Damköhler number at different recycling ratios for configuration in Fig. 5.1 (CSTR or PFTR as reactor)

$$Da_{\mathrm{crit}}(\varphi = \infty) = x^{\mathrm{D}} \tag{5.12}$$

Note that (5.11) and (5.12) are only valid for perfect separation of the CSTR effluent, that is for $R = \infty$ and $N = \infty$.

Now, the question arises whether the use of a PFTR will result in a higher productivity of the recycling system than the use of a CSTR. For comparison, the attainable product compositions x^{D} are plotted in Fig. 5.4 for both types of reactor for various *Da* and φ. As expected, at finite recycling ratio $\varphi < \infty$, the application of a PFTR yields higher product content in the distillate than a CSTR. But at infinite recycling ratio, the operational curves of the PFTR and the CSTR coincide, since both reactors are fully backmixed in this situation. Therefore, an infinite external recycling ratio always yields the highest mole fraction of the desired product A_2, no matter whether a CSTR or a PFTR is used as reactor. The distillation column ensures that the product concentration in the recycling flux (x^{B}) is minimized, and as a consequence, the reaction rate at $\varphi = \infty$ is higher ($r^* = 1$) than the average reaction rate in a PFTR at $\varphi < \infty$ ($r^* < 1$).

5.2.1.2 (∞, N_{min})-Analysis

For conceptual process design it is essential to predict the design variables; these are the size of the reactor (*Da*) and the minimum number of distillation stages (N_{min}), for a specified distillate composition x^{D}. As before, the column is considered at infinite reflux ratio ($R = \infty$).

In Fig. 5.5, the minimum number of stages required to meet the product specification (here, $x^{\mathrm{D}} = 0.99$) is depicted against the Damköhler number. At a given φ value the number of stages decreases with increasing Damköhler number. At constant *Da* number, the necessary number of distillation decreases with increasing recycling ratio. One can also see that the smallest investment plant costs (a linearly

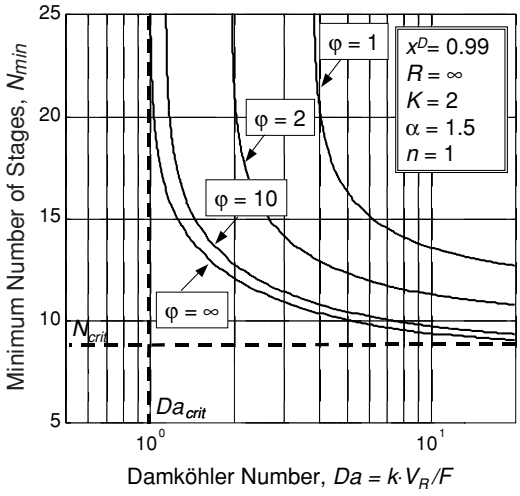

Fig. 5.5. Minimum number of distillation stages versus Damköhler number for specified distillate mole fraction of product A_2, $x^{\mathrm{D}} = 0.99$, for configuration in Fig. 5.1 (CSTR as reactor)

weighted sum of N_{min} and Da) will be obtained at infinite recycling ratio. For $\varphi < \infty$, the size of the plant needed to meet the specification will be larger. In conclusion, low costs for plant investment correlate with high operational costs caused by recycling pumping. The operational costs for recycling pumping can be avoided by internalization of the external loop, that is by application of an integrated RD process.

At $\varphi = \infty$ and $Da = \infty$, the smallest possible column size is reached ($N_{min} = N_{crit}$). The same is true for the Da number, the minimum value of which ($Da = Da_{crit}$) is obtained at $\varphi = \infty$, $N_{min} = \infty$. According to (5.12), this critical value is $Da_{crit} = x^D = 0.99$. Also at $\varphi < \infty$, a certain minimum Da number is required to meet the product specification.

5.2.2
Distillation Column with Reactive Reboiler

The integration of the recycling reactor directly into the distillation column leads to the process configuration shown in Fig. 5.2, in which the reaction takes place within the column total reboiler. On top of the reboiler a fully non-RD section is installed. This process can be seen as a simple hybrid RD column with only one reactive tray. Comparing the curves in Fig. 5.4 and Fig. 5.6, the operational characteristics of the two processes, recycling system and distillation column with reactive reboiler, are identical at $\varphi = \infty$ and $R = \infty$.

For conceptual design it is reasonable to represent the process operation in a classical McCabe–Thiele diagram (Fig. 5.7). A relative volatility of $\alpha = 10$ was assumed for the sake of better visualization. The specified distillate composition (assume $x^D = 0.95$) fixes the operating point of the condenser. The reboiler oper-

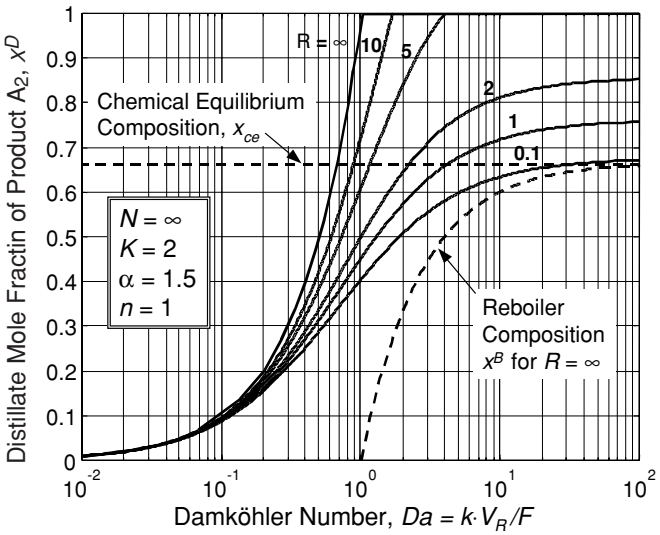

Fig. 5.6. Mole fraction of product A_2 against Damköhler number at different reflux ratios R for configuration in Fig. 5.2

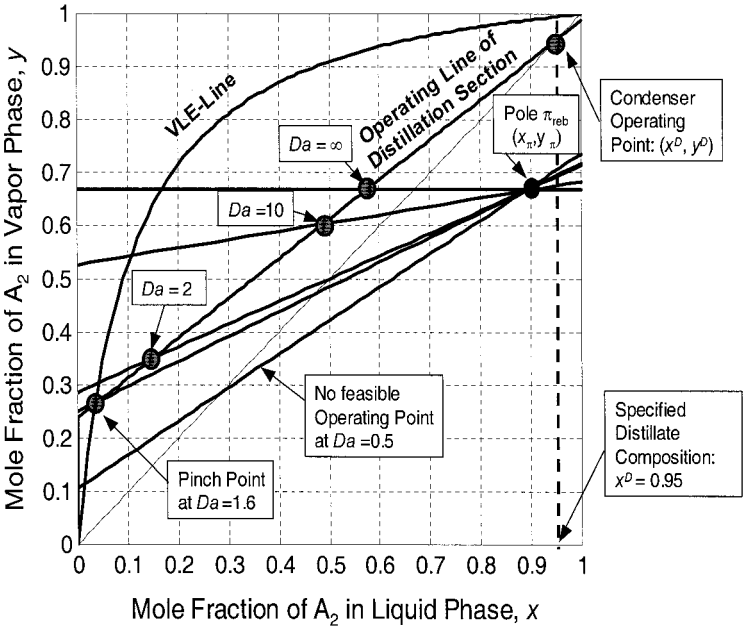

Fig. 5.7. Illustration of operation of process configuration in Fig. 5.2 in a McCabe–Thiele diagram at different Damköhler numbers

ating point is obtained from the intersection of the operating lines of the distillation section and of the reactive total reboiler. The latter is only a straight line for a first-order reaction ($n = 1$). The two operating lines are given by the corresponding mass balances

$$0 = -Rx^{\mathrm{B}} + (1+R)y^{\mathrm{B}} - x^{\mathrm{D}} \tag{5.13}$$

$$0 = Rx^{\mathrm{B}} - (1+R)y^{\mathrm{B}} + Da\left(1 - \frac{y^{\mathrm{B}}}{x_{\mathrm{ce}}}\right) \tag{5.14}$$

The resulting reboiler operating point has the coordinates

$$x^{\mathrm{B}} = \frac{1}{R}((1+R)y^{\mathrm{B}} - x^{\mathrm{D}}),\ y^{\mathrm{B}} = x_{\mathrm{ce}}\left(1 - \frac{x^{\mathrm{D}}}{Da}\right) \tag{5.15}$$

Fig. 5.7 shows how the reboiler operating point is shifted by changing the Damköhler number. All reboiler operating lines for the different *Da* numbers meet in the pole point π_{reb} whose coordinates are given by

$$x_\pi = \frac{1+R}{R}x_{ce} - \frac{x^D}{R},\ y_\pi = x_{ce} \tag{5.16}$$

At $Da = \infty$, chemical equilibrium is established in the reboiler, $y^B = x_{ce} = K/(K+1) = 2/3$, and the smallest number of stages N is required to attain $x^D = 0.95$ as top product concentration. At $Da < \infty$, the A_2 concentration in the reboiler is lower than at equilibrium and consequently more distillation trays are needed. At $Da = 1.6$, the intersection of the reboiler operating line and the distillation operating line is exactly located on the vapor–liquid equilibrium (VLE) line, so $x^B = x^e(y^B)$. At this pinch point the corresponding reflux ratio reaches a minimum value R_{min} and the number of stages is infinite. For $Da < 1.6$, no feasible operating point exists. The minimum reflux ratio is calculated as follows

$$R_{min} = \frac{y^B - x^D}{x^e(y^B) - y^B} \tag{5.17}$$

For $n = 1$, y^B can be calculated from (5.15). R_{min} depends on the kinetic parameters (Da, n) as well as on thermodynamic parameters (K, α) of the system. Fig. 5.8 illustrates how the minimum reflux ratio varies with the Damköhler number for different reaction orders n. Qualitatively, R_{min} decreases hyperbolically with increasing Da number. Multiple pinch points are possible for negative reaction orders within a certain Da window due to multiple intersections of the reboiler operating line with the VLE line. At $R_{min} = \infty$, the critical Damköhler number, $Da_{crit} = x^D$ (5.12) is recovered. At $Da = \infty$ the smallest possible reflux ratio R_{crit} is obtained, which only depends on thermodynamic parameters besides the product specification x^D

$$R_{crit} = \frac{x_{ce} - x^D}{x^e(x_{ce}) - x_{ce}} \tag{5.18}$$

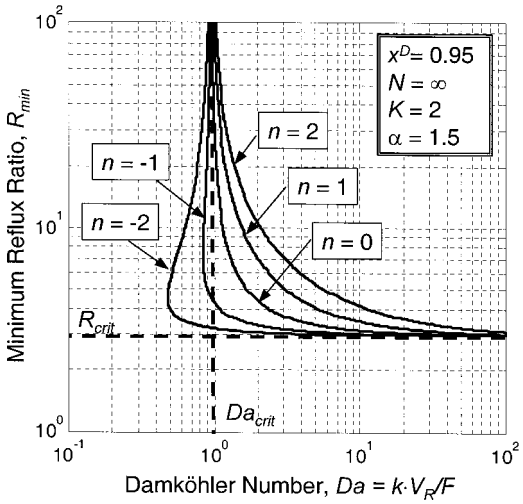

Fig. 5.8. Minimum reflux ratio versus Damköhler number at different reaction orders n for configuration in Fig. 5.2

The Fenske equation yields the minimum number of stages at $Da = \infty$ and $R = \infty$

$$N_{\min} = \frac{\log\left(\frac{x^{\mathrm{D}}}{1-x^{\mathrm{D}}} \cdot \frac{1-x_{\mathrm{ce}}}{x_{\mathrm{ce}}}\right)}{\log\alpha} - 1 \tag{5.19}$$

5.2.3 Fully Reactive Distillation Column

In Fig. 5.3, a fully RD column is depicted in which the chemical reaction $A_1 \leftrightarrow A_2$ takes place. The educt A_1 is fed at the point of its highest concentration within the column, that is the reboiler. In general, the Damköhler numbers of the reboiler, Da_{reb}, of the condenser, Da_{con}, and of the reactive stages, Da_{s}, can be chosen independently. Their corresponding mass balances are given by

$$\text{total condenser } (i = 1)\ 0 = (R+1)(y^{\mathrm{D}} - x^{\mathrm{D}}) + Da_{\mathrm{con}} r^*(x^{\mathrm{D}}) \tag{5.20}$$

$$\text{stages } (i = 2,..,\ NC)\ 0 = R(x^{i-1} - x^i) + (R+1)(y^e(x^i) - y^e(x^{i+1})) + Da_s r^*(x^i) \tag{5.21}$$

$$\text{total reboiler } (i = N)\ 0 = Rx^{\mathrm{B}} - (R+1)y^{\mathrm{B}} + Da_{\mathrm{reb}} r^*(y^{\mathrm{B}}) \tag{5.22}$$

Fig. 5.9 shows the geometric representation of these balances in the McCabe–Thiele diagram. The distillate composition x^{D} is located at the intersection of the condenser operating line and the operating line of the RD section. By specifying x^{D}, the number of reactive trays can be estimated from the classical staircase construction. From the intersection of the operating line of the column section with that of the reboiler line, the bottom composition is determined.

For design purposes, it is desirable to know the maximum attainable distillate concentration of the reaction product A_2. This composition can be found from the intersection of the reactive condenser operating line with the VLE line. At the intersection point, the following equation is valid

$$0 = (R+1)\left(y^e(x^{\mathrm{D}}_{\max}) - x^{\mathrm{D}}_{\max}\right) + Da_{\mathrm{con}} r^*\left(x^{\mathrm{D}}_{\max}\right) \tag{5.23}$$

In a similar manner, the minimum attainable bottom concentration is determined from

$$0 = Rx^e(x^{\mathrm{B}}_{\min}) - (R+1)x^{\mathrm{B}}_{\min} + Da_{\mathrm{reb}} r^*\left(x^{\mathrm{B}}_{\min}\right) \tag{5.24}$$

For $R \gg 1$, (5.23) and (5.24) correspond to the feasibility relations proposed first by Chadda et al. [3], which were derived from a cascadic flash calculation. From Fig. 5.10, one can see that the attainable top concentration for $n = 1$ is continuously decreasing with increasing Damköhler number Da_{con} due to the increased intensity of the backward reaction of A_2 to A_1 in the upper column section. For $Da_{\mathrm{con}} = \infty$, x^{D} approaches the chemical equilibrium composition x_{ce}. Similar trends

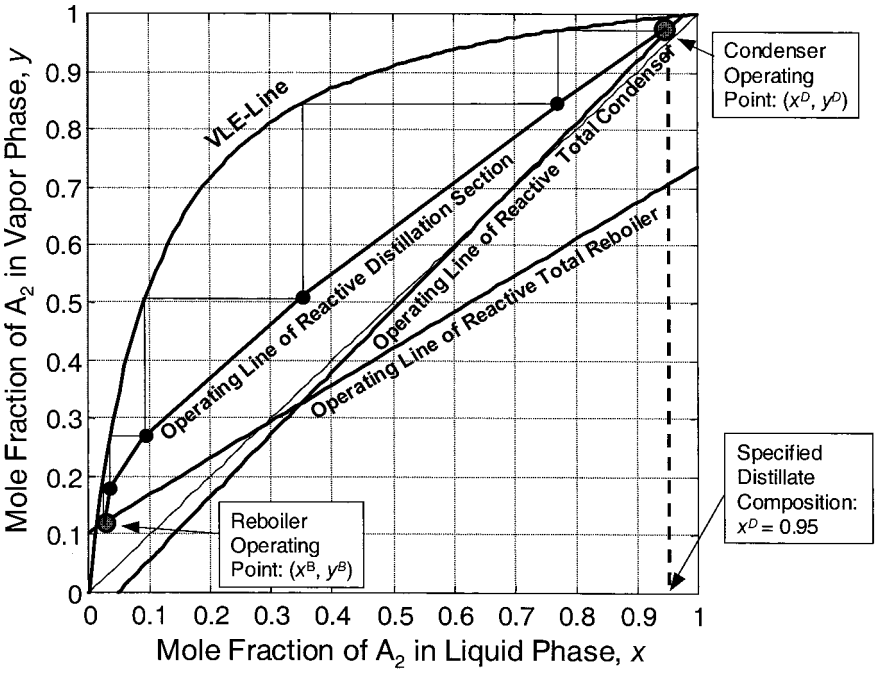

Fig. 5.9. McCabe–Thiele diagram for configuration in Fig. 5.3 ($R = 3$, $Da_{reb} = 0.5$, $Da_s = 0.2$, $Da_{con} = 0.2$, $\alpha = 10$, $K = 2$, $n = 1$)

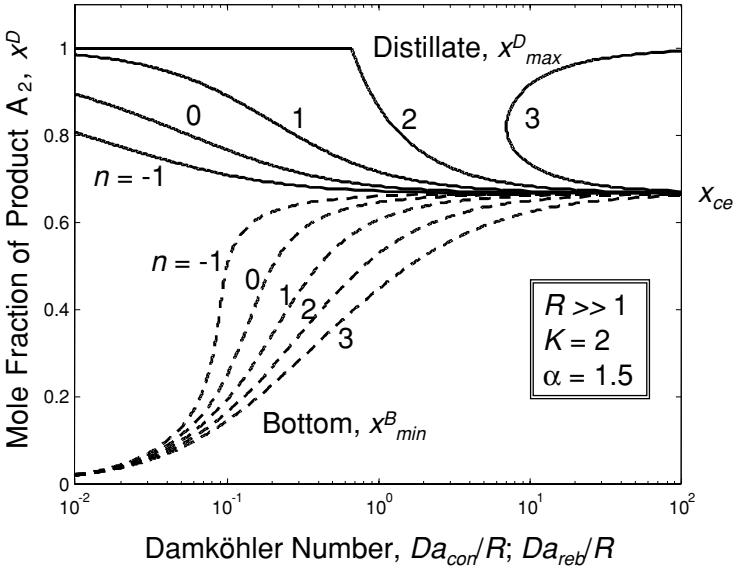

Fig. 5.10. Attainable product compositions (solid lines = distillate; dashed lines = bottom product) for process configuration in Fig. 5.3

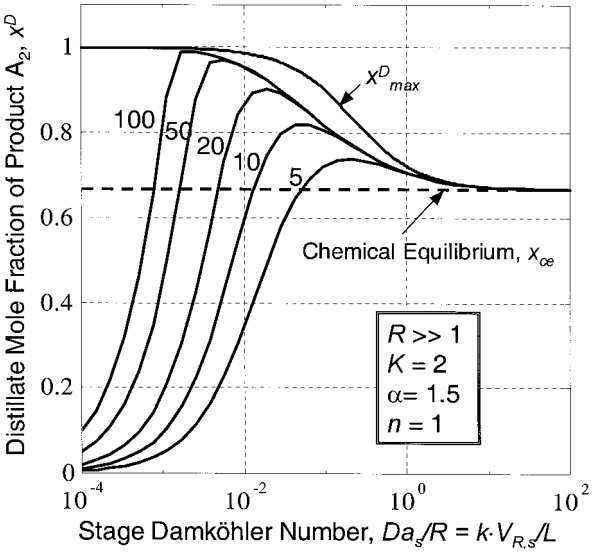

Fig. 5.11. Mole fraction of product A_2 in distillate versus stage Damköhler number at different number of stages N for process configuration in Fig. 5.3

are obtained for other reaction orders. At $n = 3$ multiple attainable compositions are possible.

Fig. 5.11 illustrates how the attainable distillate composition x^{D}_{max}, predicted from (5.23), compares with the distillate concentration x^D obtained from column simulations. At a finite number of trays N, above a certain Da_s/R ratio the chemical equilibrium x_{ce} is overcome and a maximum distillate mole fraction is obtained. Any further increase of the Damköhler number leads to a continuous decrease of the distillate concentration down to the chemical equilibrium level. Depending on the number of column stages N, the simulated maximum value of x^D can be significantly lower than the maximum attainable distillate composition x^{D}_{max}. As an example, for a 20-stage column with $Da_{con}/R = 0.1$, the compositions are $x^D = 0.82$ from simulation and $x^{D}_{max} = 0.89$ from (5.23). The McCabe–Thiele diagram in Fig. 5.12 reveals that the corresponding operating line of the RD section and the VLE line are in a tangent pinch situation at the given parameters.

Comparing the performance of the three different RD processes considered, one can conclude that a non-RD section on top of reactive total reboiler seems to be the best configuration for both productivity and reliability of design. The minimum reflux ratio R_{min} of this configuration can be estimated from (5.17) and (5.15). This R_{min} value can be significantly reduced by installation of a pre-reactor [1]. A fully RD column often suffers from splitting of the product in the upper column section owing to backward reaction.

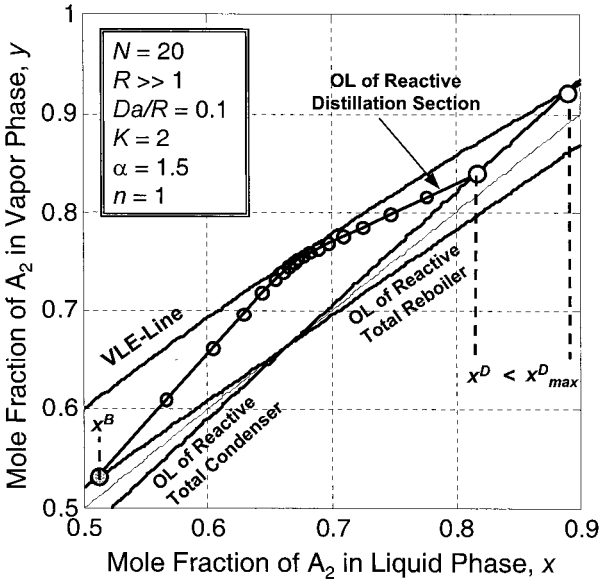

Fig. 5.12. Real and attainable distillate product composition illustrated in McCabe–Thiele diagram for configuration in Fig. 5.3 (OL = operating line)

5.3 Kinetic Effects on Attainable Products

As shown above, reaction kinetics have a significant influence on RD process performance in binary mixtures and the same is true for multicomponent mixtures. In the following, the attainable products of kinetically controlled RD processes are analyzed, first for ideal ternary mixtures, then for non-ideal ternary mixtures occurring in industrially important fuel ether synthesis, and finally for an extremely non-ideal system with potential liquid-phase splitting. In all cases, reversible reactions of type A + B ↔ C are considered.

As a common analysis tool, residue curve mapping (RCM) is well established. Fien and Liu [4] published a comprehensive review of the synthesis and shortcut design of non-reactive separation processes based on RCMs. Barbosa and Doherty [5] developed RCMs for RD processes with single chemical equilibrium reaction. Ung and Doherty [6] extended this method to systems with multiple equilibrium reactions.

The determination of the singular points appearing in these maps yields important information about the attainable bottom product compositions in real countercurrent columns. However, as shown by Chadda et al. [3], both the distillate and the bottom product compositions can be better obtained as singular points of a reactive enriching flash cascade or a stripping flash cascade, respectively. As will be shown, singular point analysis can also provide valuable information about the role of interfacial mass-transfer resistances in RD processes.

5.3.1 Singular Point Analysis

For counter-current RD columns with a single chemical reaction taking place, the attainable bottom compositions x^B can be interpreted as singular points of the mass balances of the reactive reboiler depicted in Fig. 5.13a

$$\frac{dx_i^B}{d\tau} = -\left(y_i^e(x^B) - x_i^B\right) + \left(v_i - x_i^B v_T\right) \cdot Da \cdot r^*(x^B); \quad i = 1, \ldots, NC-1 \tag{5.25}$$

where the Damköhler number is defined as $Da \equiv kV_{cat}/V$ with V as the vapor flow rate at the bottom of the column. The corresponding attainable distillate compositions x^D can be interpreted as singular points of the mass balances of the reactive condenser depicted in Fig. 5.13b

$$\frac{dy_i^e}{d\tau} = \left(y_i^e - x_i^D\ (y_i^e)\right) + \left(v_i - y_i^e v_T\right) \cdot Da \cdot r^*(x^D); \quad i = 1, \ldots, NC-1 \tag{5.26}$$

with the Damköhler number $Da \equiv kV_{cat}/V$ where V stands for the vapor flow rate at the top of the column. (5.25) and (5.26) are valid for an infinitely extended column operated at infinite reflux ratio (∞,∞-analysis). They correspond to (5.24), which was derived for the binary case. For $Da = 0$, the non-reactive singular points (pure components and non-reactive azeotropes) will be recovered. For $Da = \infty$, the singular points fulfill the chemical equilibrium condition. Then we get the relation

$$0 = \left(v_i - x_i^B v_T\right) \cdot r^*(x^B); \quad i = 1, \ldots, NC-1 \tag{5.27a}$$

$$0 = \left(v_i - y_i^e v_T\right) \cdot r^*(x^D); \quad i = 1, \ldots, NC-1 \tag{5.27b}$$

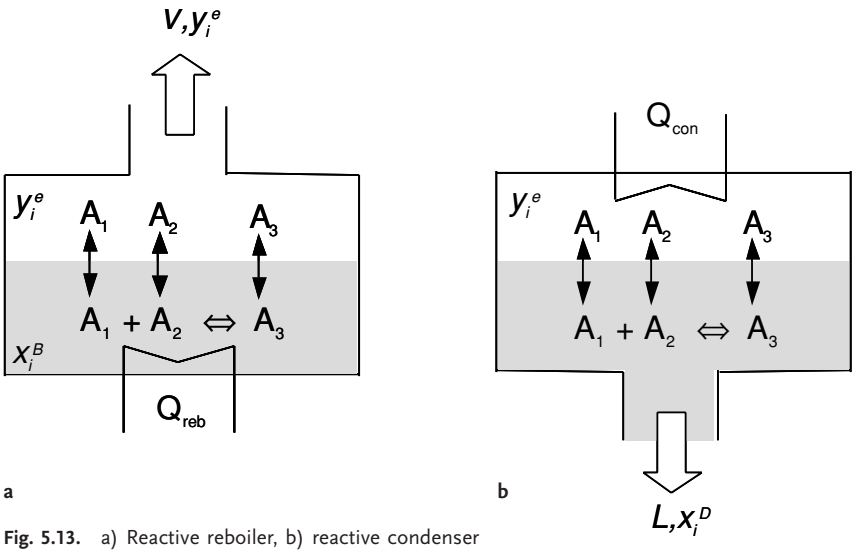

Fig. 5.13. a) Reactive reboiler, b) reactive condenser

There are three possible kinds of singular points from (5.27)

- reactive azeotropes,
- pure components, both in case of $r^* = 0$, and
- the pole π of stoichiometric lines, determined from $(\nu_i - x_i\nu_T) = 0$.

For a given single reaction, the pole π is single and is always outside the valid composition space since there should be at least one ν_i with a sign opposite to ν_T. For the special case with $\nu_T = 0$, the stoichiometric lines become parallel and the pole π approaches infinity.

From (5.25) and (5.26), the locations of the singular points in the composition space can be determined as follows. At the bottom, the condition for singular points for a component i from (5.25) is

$$0 = -\left(y_i^e(x^B) - x_i^B\right) + \left(\nu_i - x_i^B\nu_T\right) \cdot Da \cdot r^*(x^B) \tag{5.28}$$

For an arbitrary reference component k, the condition for singular points is given by

$$0 = -\left(y_k^e(x^B) - x_k^B\right) + \left(\nu_k - x_k^B\nu_T\right) \cdot Da \cdot r^*(x^B) \tag{5.29}$$

Using (5.29) to substitute the term $Da{\cdot}r^*$ in (5.28) yields

$$x_i^B - y_i^e = (\nu_i - \nu_T x_i^B)\ \frac{x_k^B - y_k^e}{\nu_k - \nu_T x_k} \tag{5.30}$$

(5.30) can be rearranged to obtain finally

$$X_i^B - Y_i^B = 0 \quad (i = 1, \cdots, NC-2) \tag{5.31}$$

where X_i^B and Y_i^B stand for the transformed liquid and vapor phase mole fractions

$$X_i^B \equiv \frac{\nu_k x_i^B - \nu_i x_k^B}{\nu_k - \nu_T x_k^B} \text{ and } Y_i^B \equiv \frac{\nu_k y_i^e - \nu_i y_k^e}{\nu_k - \nu_T y_k^e} \quad (i = 1, \cdots, NC-1) \tag{5.32}$$

For all singular points with and without chemical reaction, (5.31) gives the necessary conditions. They only depend on the vapor–liquid equilibria and on the reaction stiochiometry, and are completed by (5.29), which reflects the influence of the chemical reaction kinetics. For the distillate composition, one ends up with the corresponding singular point condition

$$X_i^D - Y_i^D = 0 \quad (i = 1, \cdots, NC-2) \tag{5.33}$$

The completing kinetic relation for the reference component k is given by

$$0 = \left(y_k^e(x^D) - x_k^D\right) + \left(\nu_k - y_k^e\nu_T\right) \cdot Da \cdot r^*(x^D) \tag{5.34}$$

5.3.2 Ideal Ternary Mixtures

For the purpose of illustration of the relations developed above, RD of an ideal mixture of three components being subject to the reversible liquid-phase reaction A + B ↔ C is considered. The rate of reaction is given by the power law expression

$$r = k\left(x_A x_B - \frac{x_C}{K}\right) \tag{5.35}$$

The chemical equilibrium constant is assumed to be constant, $K = 5$, and k is taken as independent of temperature. The vapor–liquid equilibrium is described by means of constant relative volatilities with $\alpha_{AC} \neq 1$, $\alpha_{BC} \neq 1$, and $\alpha_{AC} \neq \alpha_{BC}$.

5.3.2.1 Case a: $\alpha_{AC} = 0.2$, $\alpha_{BC} = 3.0$

In this case the reaction product C is the intermediate boiler. All potential singular points are located on an ellipse, which is the dashed curve given in Fig. 5.14. There, for better illustration, the behavior outside the physically relevant composition space is also depicted for the four Damköhler numbers considered. The solid curves represent the location of points fulfilling the kinetic relation of bottom products (5.29). The attainable bottom products at a given Damköhler number are obtained as intersection points of the potential singular point curve and the kinetic curve.

At $Da = 0$, there are three intersections, which are the three pure component vertices with different stabilities. At $Da = 0.5$, there are also three intersections, two of which are the pure A vertex (stable node) and the pure B vertex (unstable node). The third one with $\boldsymbol{x} = (-0.1560, 0.0785)$ is a saddle point. At $Da = 0.7$, five intersections exist. The point with $\boldsymbol{x} = (-0.4322, 0.4723)$ is a stable spiral while the points with $\boldsymbol{x} = (-0.2736, 0.1674)$ and $\boldsymbol{x} = (-0.0575, 0.9750)$ are saddle points. The pure A and B vertices remain their stabilities. At $Da = 2.33$, there are three intersections. The pure A vertex remains stable node but the pure B vertex is now a saddle point. The point with $\boldsymbol{x} = (0.6959, 1.0785)$ is an unstable node. In conclusion for this reaction system, only pure A will be a stable bottom product of a real counter-current RD column.

5.3.2.2 Case b: $\alpha_{AC} = 5.0$, $\alpha_{BC} = 3.0$

In this case the reaction product C is the highest boiler and all potential singular points are located on the two dashed hyperbola branches shown in Fig. 5.15. At $Da = 0$, only the three pure reaction components are attainable singular points (Fig. 5.15a). At $Da = 0.3$, besides the pure A vertex (unstable node) and the

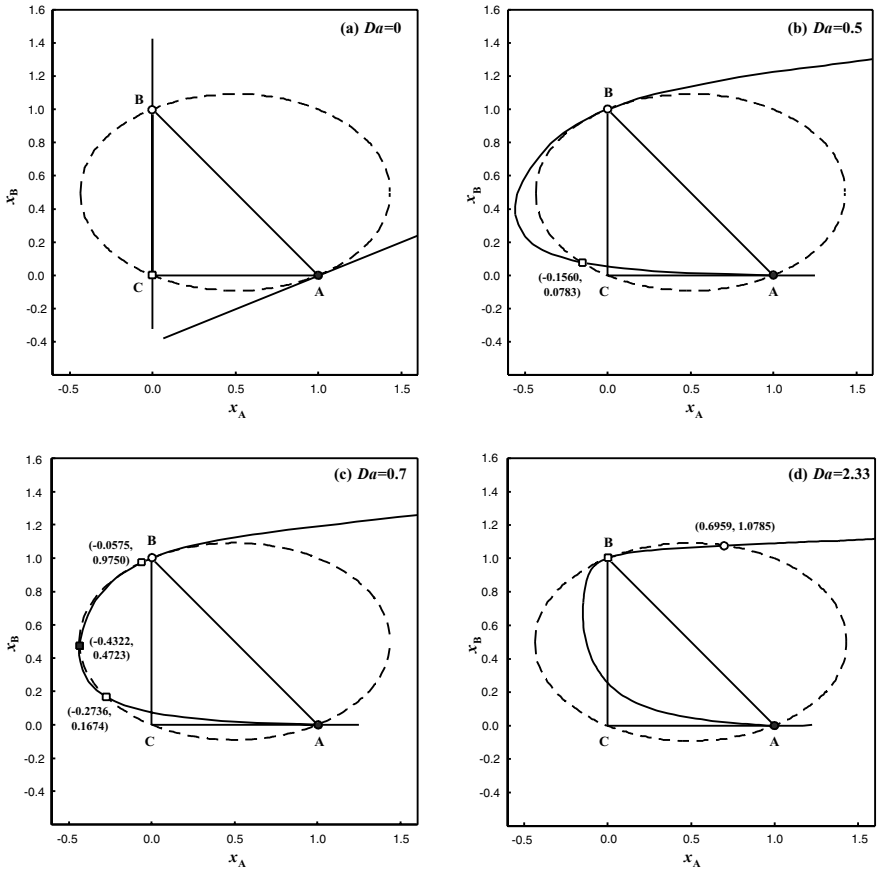

Fig. 5.14. Singular points for ideal ternary system A + B ↔ C, chemical equilibrium constant $K =$ 5.0, relative volatilities $\alpha_{AC} = 0.2$, $\alpha_{BC} = 3.0$ at different Damköhler numbers: ● = stable node, ○ = unstable node, □ = saddle point, dashed line = singular poin curve, solid line = kinetic curve

pure B vertex (saddle point), there exists one more attainable singular point inside the physically relevant composition space (Fig. 5.15b) and one additional point outside this space. At $Da = 1.5$, the pure A vertex is now a saddle point as the pure B vertex (Fig. 5.15c). The intersection point inside the valid composition space remains a stable node while the outside point is an unstable node. The stable node represents the attainable bottom composition of a infinitely high counter-current RD column operated at infinite reflux ratio. For the boiling sequence considered here, evidently low Damköhler numbers have to be applied in order to achieve pure C in the column bottom product.

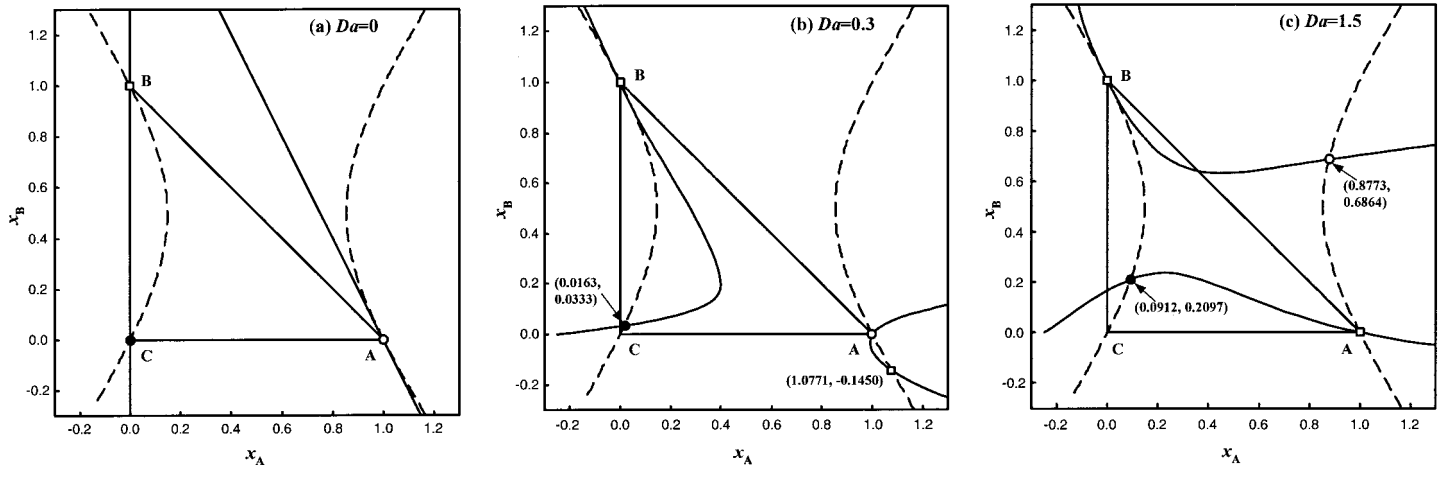

Fig. 5.15. Singular points for ideal ternary system A + B ↔ C, chemical equilibrium constant $K = 5.0$, relative volatilities $\alpha_{AC} = 5.0$, $\alpha_{BC} = 3.0$ at different Damköhler numbers: ● = stable node, ○ = unstable node, □ = saddle point

5.3.3 Non-Ideal Mixtures

After the above discussion on RD of ideal ternary mixtures, in this section two non-ideal ternary systems are considered. These are the heterogeneously catalyzed syntheses of the fuel ethers MTBE (methyl *tert*-butyl ether) and TAME (*tert*-amyl methyl ether) by etherification of methanol with isobutene or isoamlyenes respectively. Both reaction systems have enormous industrial importance because of the outstanding antiknock properties of MTBE and TAME as gasoline components.

5.3.3.1 Synthesis of MTBE

The fuel ether MTBE is synthesized by the liquid-phase reaction of isobutene (IB) and methanol (MeOH) using macroreticular sulfonic acid ion-exchange resins as catalysts. The stoichiometric equation is given by

$$\mathrm{MeOH} + \mathrm{IB} \overset{+\mathrm{H}^+}{\rightleftharpoons} \mathrm{MTBE} \tag{5.36}$$

The microkinetics of this reaction were investigated in detail by Rehfinger and Hoffmann [7]. These authors proposed the following rate expression in terms of liquid-phase activities: the derivation is described in Section 5.4.3

$$r = c_{\mathrm{L}} k(T) \left(\frac{a_{\mathrm{IB}}}{a_{\mathrm{MeOH}}} - \frac{1}{K(T)} \frac{a_{\mathrm{MTBE}}}{a_{\mathrm{MeOH}}^2} \right) \tag{5.37}$$

In (5.37), r stands for the volumetric reaction rate, c_{L} represents the concentration of acid groups per unit volume of catalyst, and a_i is the liquid-phase activity of component i. The temperature dependence of the reaction rate constant k can be expressed by the Arrhenius equation. All kinetic and thermodynamic parameters can be found elsewhere [7].

Fig. 5.16 shows residue curve maps for four selected values of the Damköhler number Da at an operating pressure of $p = 0.8$ MPa. The residue curve map for distillation without reaction ($Da = 0$, Fig. 5.16a) shows one saddle point, which is the binary azeotropic point between MeOH and MTBE. The second binary azeotropic mixture of MeOH and IB represents an unstable node. These two points are linked by a separatrix, which acts as a distillation boundary. Consequently, two stable nodes exist in the system: one stable node at pure MTBE for initial compositions below the distillation boundary and another stable node at pure MeOH fo mixtures having an initial composition above the distillation boundary.

By increasing the Damköhler number, the influence of the chemical reaction is fortified. For $Da = 10^{-4}$ (Fig. 5.16b) the shape of trajectories starting with a relatively high mole fraction of MeOH is still similar to those of distillation without reaction, so that pure MeOH remains a stable node in the system. Near the MTBE vertex, the conditions change remarkably. The reaction vector is pointed towards the chemical equilibrium line (dashed curve). As a consequence, the stable node moves from

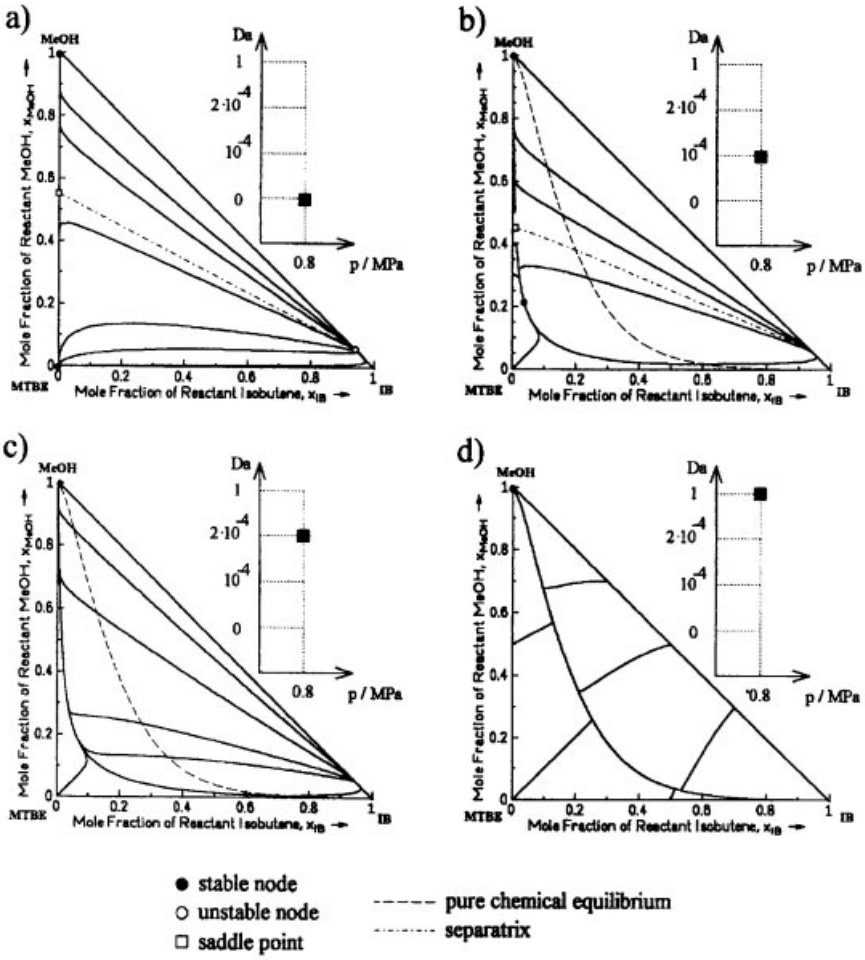

Fig. 5.16. Residue curve maps for heterogeneously catalyzed MTBE synthesis at operating pressure $p = 0.8$ MPa for different Damköhler numbers ([8], reprinted from *Chem. Eng. Sci.*, Vol 52, Thiel, Sundmacher and Hoffmann, Pages 993–1005, Copyright 1997, with permission from Elsevier Science)

pure MTBE to a point that has the composition $\boldsymbol{x} = (0.035, 0.2)$, while the unstable node has moved out of the physically relevant composition space.

Further enhancement of Damköhler number to $Da = 2 \times 10^{-4}$ (Fig. 5.16c) leads to the situation in which the lower stable node coincides with the saddle point so that they extinguish each other. Hence the trajectories run into pure MeOH. At $Da = 1$ (Fig. 5.16d) the reaction vector is dominant in relation to the separation vector. Thus every residue curve is dominated by the stiochiometric restriction when moving towards the curve of chemical equilibrium. Because of the dominance of chemical reaction, the trajectories do not pass this line, but remain on it until they reach the pure MeOH vertex.

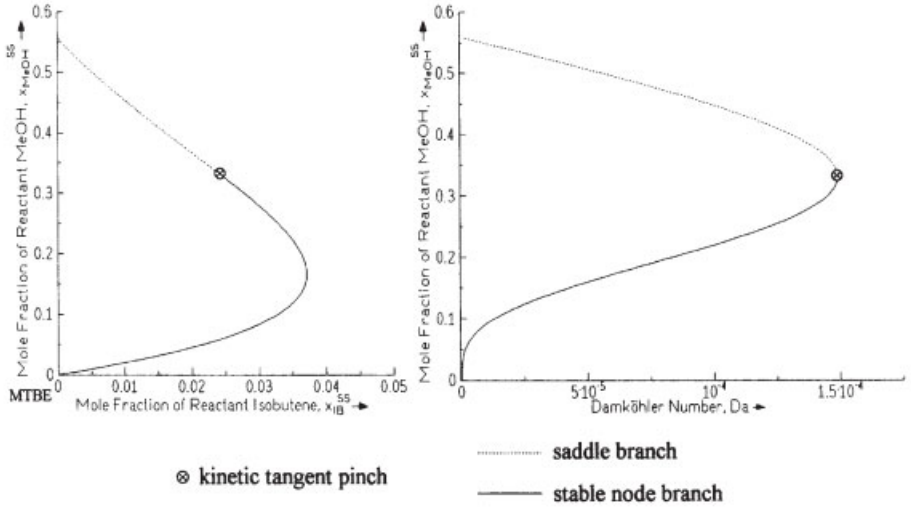

Fig. 5.17. Singular point curve starting from the MTBE vertex (left) and related Damköhler numbers (right) at $p = 0.8$ MPa ([8], reprinted from *Chem. Eng. Sci.*, Vol 52, Thiel, Sundmacher and Hoffmann, Pages 993–1005, Copyright 1997, with permission from Elsevier Science)

The results of the simulation shown in Fig. 5.16 can be summarized as follows. At a given operating pressure, p, it is possible to pass the distillation boundary by determining an adequately high Damköhler number Da. Hence, one stable point in the region of MTBE vertex disappears and every trajectory ends at pure MeOH. The second effect of raising Da is that the collecting line, which is also a separatrix, approaches the curve of chemical equilibrium. These findings were reported by Thiel et al. [8] for heterogeneously catalyzed MTBE synthesis, and, with some quantitative differences, also by Venimadhavan et al. [9] for the homogeneously catalyzed case.

To study the behavior of the singular points in the vicinity of the MTBE vertex, Thiel et al. [8] used a continuation method with the Damköhler number as continuation parameter. The results computed at $p = 0.8$ MPa are shown in Fig. 5.17. It can be observed that a stable node branch beginning from pure MTBE in the absence of chemical reaction moves away from MTBE vertex with rising Da. As the Damköhler number $Da = 1.49 \times 10^{-4}$ is reached, the stable node branch turns into a saddle branch. This point is called the kinetic tangent pinch [9]. The saddle branch arrives at $Da = 0.0$ in the binary azeotropic point between MeOH and MTBE.

5.3.3.2 **Synthesis of TAME**

TAME is produced by liquid-phase synthesis from methanol and isoamylenes. Among the three isoamylenes only 2-methyl-1-butene (2MB1) and 2-methyl-2-butene (2MB2) are reactive in etherification; 3-methyl-1-butene (3MB1) is non-reactive. Besides the two synthesis reactions, the isomerization of the reactive isoamylenes takes place simultaneously [10]

$$\mathrm{MeOH} + \mathrm{2MB1} \overset{r_1}{\rightleftharpoons} \mathrm{TAME} \tag{5.38a}$$

$$\mathrm{MeOH} + \mathrm{2MB2} \overset{r_2}{\rightleftharpoons} \mathrm{TAME} \tag{5.38b}$$

$$\mathrm{2MB1} \overset{r_3}{\rightleftharpoons} \mathrm{2MB2} \tag{5.38c}$$

To calculate residue curve maps for the synthesis of TAME one has to proceed in the same manner as the MTBE example and calculate phase equilibria between liquid and vapor phases, chemical equilibrium constants in the liquid phase, and kinetics of the chemical reactions.

Because there are three reactions taking place, three coupled chemical equilibria have to be considered. Rihko et al. [11] proposed the following expressions, which are based on their experiments (T in K)

$$\text{TAME synthesis from 2MB1} \quad K_1 = 1.057\times10^{-4}\exp(4273.5/T) \tag{5.39a}$$

$$\text{TAME synthesis from 2MB2} \quad K_2 = 1.629\times10^{-4}\exp(3374.4/T) \tag{5.39b}$$

$$\text{Isomerization reaction} \quad K_3 = K_1/K_2 \tag{5.39c}$$

Oost and Hoffmann [10] have developed a kinetic expression for the TAME synthesis of the lumped C5-reactants 2MB1 and 2MB2 in terms of liquid-phase activities

$$r_{1,2} = r_1 + r_2 = c_\mathrm{L} k_{1,2}(T)\left(\frac{a_\mathrm{2MB1}}{a_\mathrm{MeOH}} - \frac{1}{K_1(T)}\frac{a_\mathrm{TAME}}{a_\mathrm{MeOH}^2}\right) \tag{5.40}$$

where the reaction rate constant for the lumped TAME synthesis $k_{1,2}$ obeys the Arrhenius equation. For the isomerization reaction, the following rate expression was proposed [10]

$$r_3 = c_\mathrm{L} k_3(T)\left(a_\mathrm{2MB1} - \frac{a_\mathrm{2MB2}}{K_3(T)}\right) \tag{5.41}$$

For the sake of a simplified illustration, the mixture of isomers 2MB1 and 2MB2 is treated as one pseudo-component isoamylene (IA) so that its mole fraction is $x_\mathrm{IA} = x_\mathrm{2MB1} + x_\mathrm{2MB2}$.

Fig. 5.18 shows residue curve maps of pure distillation of the non-reactive mixture IA/MeOH/TAME. Corresponding to the mixture in the MTBE synthesis, two binary azeotropic points exist: an unstable node between the olefin IA and the alcohol MeOH, and a saddle point between the ether TAME and the alcohol. These two points are linked by a distillation boundary line, which separates the whole composition space into two distillation areas. In the lower one pure TAME is the stable node; in the upper area pure MeOH is the stable node. By increasing the operating pressure p, the two azeotropic points move towards pure MeOH.

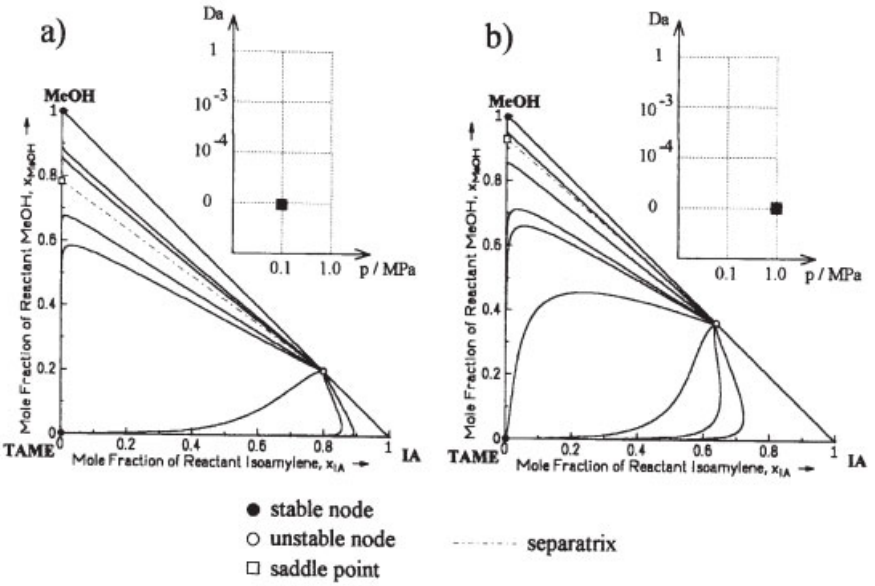

Fig. 5.18. Residue curve maps for distillation without reaction ($Da = 0$) of the mixture IA/MeOH/TAME at two operating pressures ([8], reprinted from *Chem. Eng. Sci.*, Vol 52, Thiel, Sundmacher and Hoffmann, Pages 993–1005, Copyright 1997, with permission from Elsevier Science)

In Fig. 5.19 the residue curve maps of RD for TAME synthesis are displayed. For these results the operating pressure was changed (0.1 MPa, 1.0 MPa) as the second parameter besides the Damköhler number (10^{-4}, 10^{-3}, 1.0). The results calculated with the lower pressure show basically the same characteristics as discussed for the synthesis of MTBE. At a low Damköhler number, Fig. 5.19a, the separation effect is still dominating over the reaction effect so that two stable nodes in MeOH and nearby TAME are developed. A slight enhancement of *Da* leads to Fig. 5.19c, which is qualitatively similar to Fig. 5.19a except that the slower stable point has discharged from the TAME vertex. If *Da* is increased to $Da = 1$, there is a strong influence of the chemical reactions and one stable node disappears and every trajectory runs into the collecting trajectory, which is the only remaining separatrix in the composition space. This separatrix is in the vicinity of the chemical equilibrium line and ends in the MeOH vertex, Fig. 5.19e.

By raising the operating pressure p a new behavior of the system can be studied. A new saddle point appears and at $Da = 10^{-4}$ and $p = 1.0$ MPa three stable points exist (Fig. 5.19b). In addition to the stable node in the MeOH vertex and in the region between chemical equilibrium and TAME vertex a third stable point is built in the isoamylene (IA) vertex. This is remarkable since IA is the light-boiling pure component of the system. In addition, a second saddle point appears.

As in the MTBE system, by use of a continuation method the location of singular points in the TAME residue curve map can be tracked against the Damköhler number *Da*. The calculated results at various operating pressures are given in Fig. 5.20.

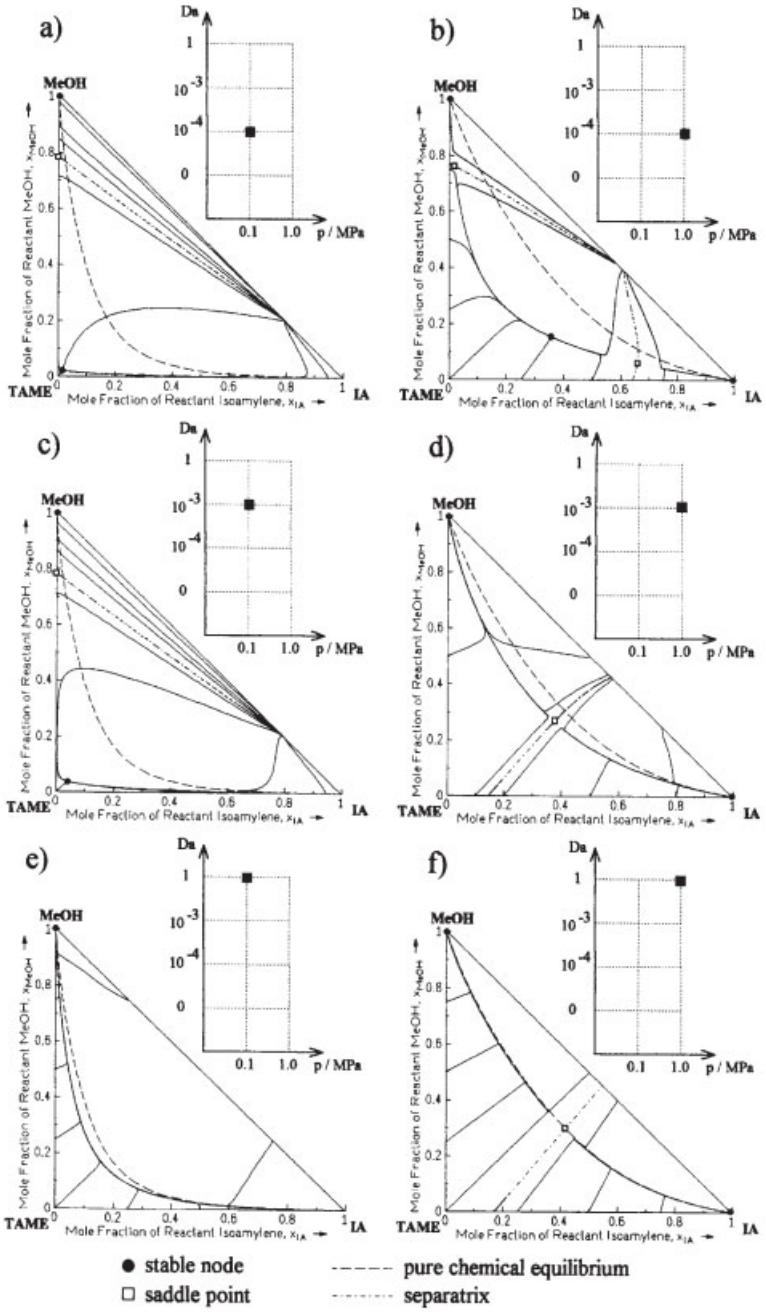

Fig. 5.19. Residue curve maps for heterogeneously catalyzed TAME synthesis at operating pressures $p = 0.1$ MPa and $p = 1.0$ MPa; Damköhler numbers: $Da = 10^{-4}$, 10^{-3}, and 1.0 ([8], reprinted from *Chem. Eng. Sci.*, Vol 52, Thiel, Sundmacher and Hoffmann, Pages 993–1005, Copyright 1997, with permission from Elsevier Science)

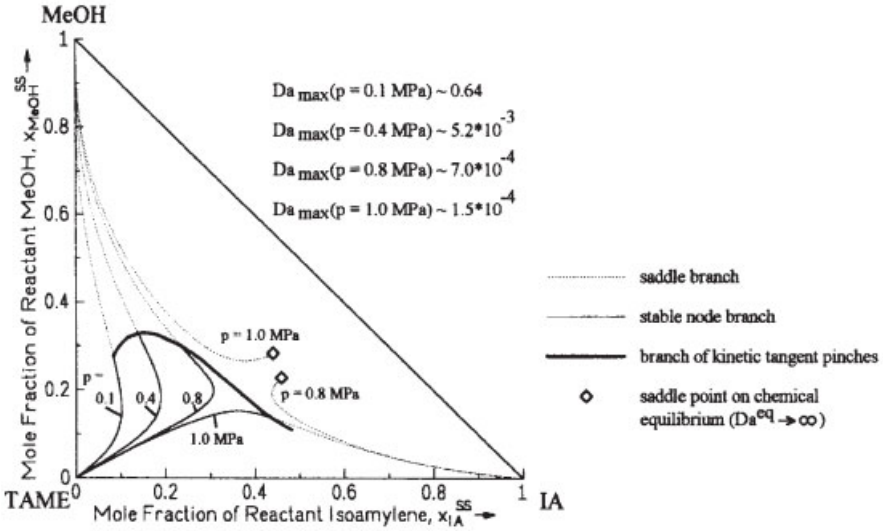

Fig. 5.20. Singular point curves in the TAME system at different operating pressures and branch of kinetic tangent pinches ([8], reprinted from *Chem. Eng. Sci.*, Vol 52, Thiel, Sundmacher and Hoffmann, Pages 993–1005, Copyright 1997, with permission from Elsevier Science)

At an operating pressure p below 1.0 MPa, the curves have a qualitative shape similar to those computed for the MTBE example: a stable node branch moves from the TAME vertex to the kinetic tangent pinch and reaches its maximum Damköhler number Da_{max} here. Then, the stable node branch turns into a saddle branch and runs into the binary azeotropic point between MeOH and TAME. A second saddle branch develops if an operating pressure $p = 0.8$ MPa at the starting point of pure IA is chosen. This saddle branch moves away from the IA vertex and reaches the line of chemical equilibrium at $Da \rightarrow \infty$. This point is marked with a diamond in Fig. 5.20. If p is set to 1.0 MPa the stable node branch does not turn into a saddle branch that ends in the binary azeotropic point between MeOH and TAME, but which runs into pure IA. Consequently, at $p = 1.0$ MPa a second saddle branch, which starts at the binary azeotropic point between MeOH and TAME and arrives in the line of chemical equilibrium at $Da \rightarrow \infty$, can be computed. In addition, in Fig. 5.20 the branch of kinetic tangent pinches is also plotted.

Residue curve maps and parametric dependencies similar to those reported for the MTBE and TAME system were also obtained for the heterogeneously catalyzed synthesis of the alternative fuel ether ETBE from isobutene and ethanol [12].

5.3.4
Systems with Liquid-Phase Splitting

Little research has been done on reacting systems with simultaneous distillation and liquid-phase splitting. Ung and Doherty [13] presented a theory of phase equilibrium in multiple reaction systems, which also covers heterogeneous liquid sys-

tems. Most recent papers dealing with this subject were written on the butyl acetate esterification system and only mentioned phase-splitting behavior as a side phenomenon [14–16]. Westerberg et al. [17] published a survey of the possible combinations of many phenomena including the three involved in this case, but they did not deal in detail with the occurrence of liquid-phase splitting in RD. Gumus and Ciric [18] specifically tried to simulate such a system. Their focus was on the simultaneous reaction/distillation/phase splitting behavior because its prediction is computation-time intensive so that it is ideally suited to show the efficiency of a new numerical algorithm. Recently, Qi et al. [19] developed a model for studying the effects of chemical kinetics on the residue curve maps of pseudohomogeneous and heterogeneous reactive mixtures. The kinetic effects in the two kinds of systems were compared. The special case in which the chemical reaction only occurs in one of the two liquid phases inside the L–L region was also taken into account. As reaction system of technical relevance, these authors considered the liquid-phase hydration of cyclohexene and water to form cyclohexanol

$$\text{cyclohexene} + \text{H}_2\text{O} \overset{+\text{H}^+}{\rightleftharpoons} \text{cyclohexanol} \tag{5.42}$$

For this reaction system, the liquid-phase non-ideality can be described by the UNIFAC activity coefficient model [20]. Panneman and Beenackers [21] studied the reaction kinetics of (5.42) catalyzed by macroporous strongly acidic ion-exchange resins. Based on their results, Qi et al. [19] proposed an activity-based reaction rate expression for this reaction

$$r = c_{\text{L}} k(T) \left(a_{\text{ene}} a_{\text{H}_2\text{O}} - \frac{a_{\text{ol}}}{K(T)} \right) \tag{5.43}$$

with the equilibrium constant and the forward rate constant as functions of temperature

$$K(T) = 2.37 \times 10^{-5} \exp\left(\frac{30.236 \text{ kJ/mol}}{RT} \right) \tag{5.44}$$

$$\frac{k(T)}{1/s} = 2.77 \times 10^{8} \exp\left(\frac{-103.2 \text{ kJ/mol}}{RT} \right) \tag{5.45}$$

The pseudohomogeneous chemical equilibrium (PCE) for the cyclohexanol reaction system is illustrated in Fig. 5.21a and the non-reactive isobaric L–L phase diagram is plotted in Fig. 5.21b. The raffinate phase is very close to the pure water vertex (see enlarged view in the right block). The two L–L envelopes intersect the PCE at two points $\boldsymbol{x}$ = (0.3466, 0.1840) and $\boldsymbol{x}$ = (0.0003, 0.9969). The two parts of the PCE outside the L-L region and the so called 'unique reactive liquid–liquid tie line' [19] comprise the heterogeneous chemical equilibrium line (HCE), which is the bold line in Fig. 5.21b.

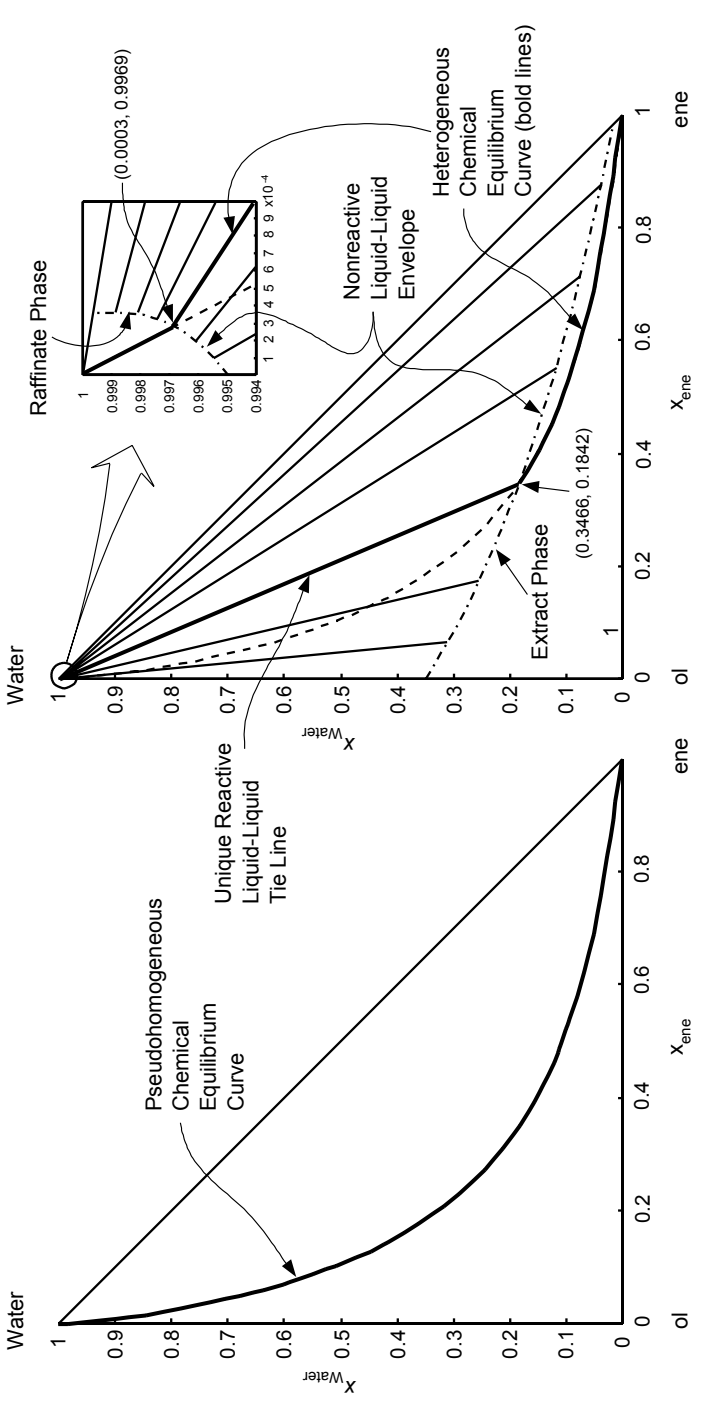

Fig. 5.21. Chemical equilibrium curves for the cyclohexanol synthesis at $p = 0.1$ MPa ([19], reprinted from *Chem. Eng. Sci.*, Vol 57, Qi, Kolah and Sundmacher, Pages 163–178, Copyright 2002, with permission from Elsevier Science)

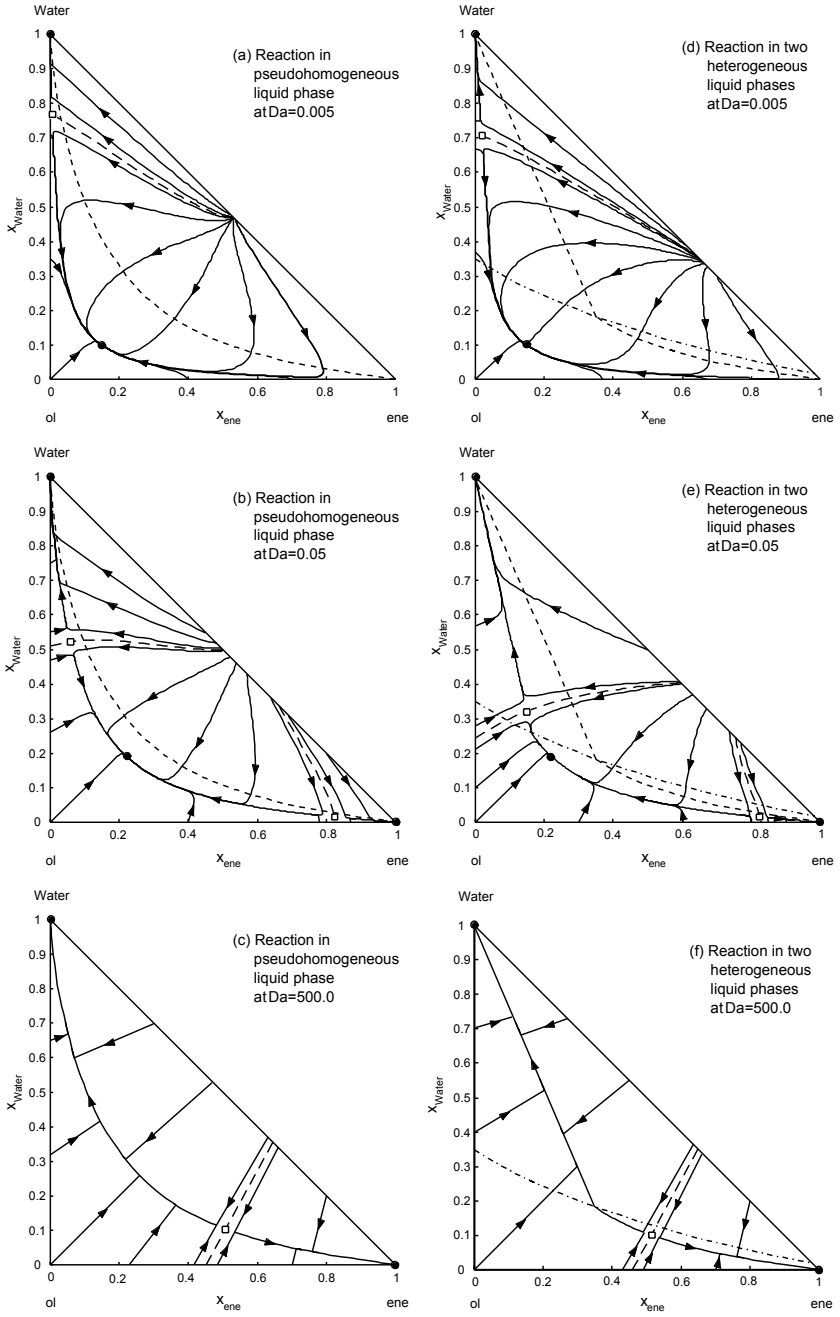

Fig. 5.22. Residue curve maps for heterogeneously catalyzed cyclohexanol synthesis at $p =$ 0.1 MPa: a–c) pseudohomogeneous liquid system, d–f) heterogeneous liquid system ([19], reprinted from *Chem. Eng. Sci.*, Vol 57, Qi, Kolah and Sundmacher, Pages 163–178, Copyright 2002, with permission from Elsevier Science)

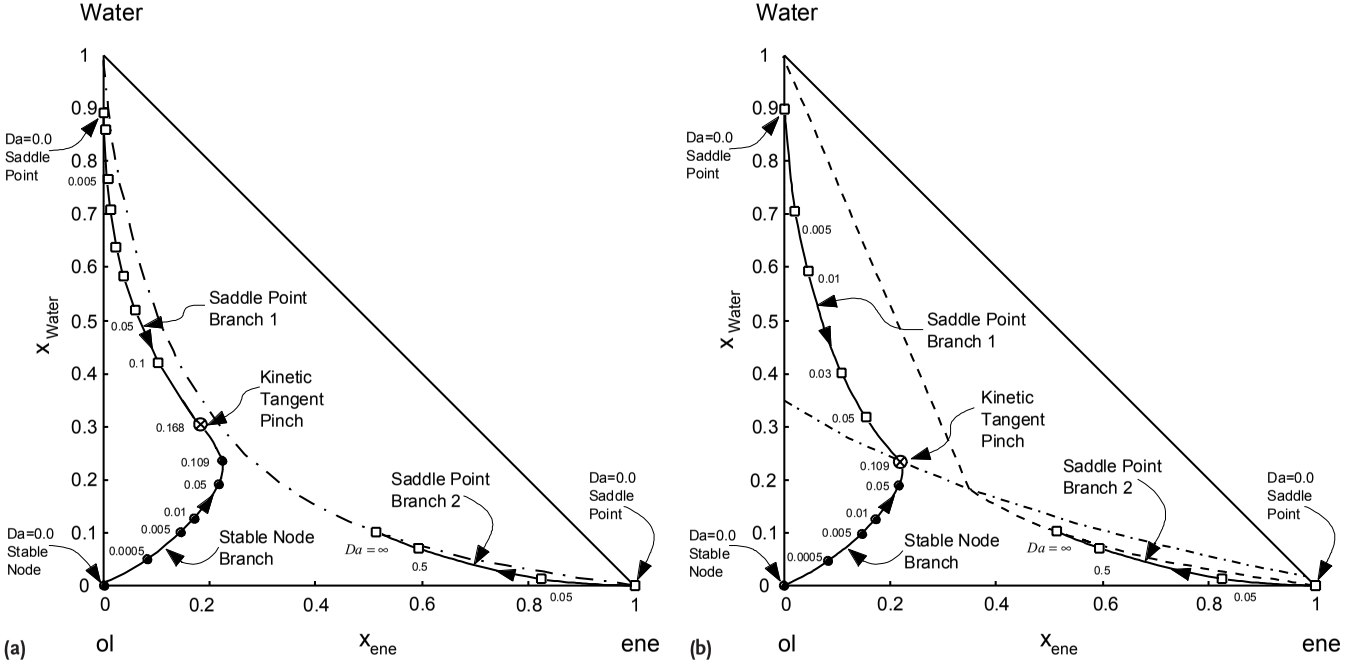

Fig. 5.23. Bifurcation behavior of stable node and saddle point for the cyclohexanol reaction system with respect to the Damköhler number [19]: a) pseudohomogeneous liquid system, b) heterogeneous liquid system ([19], reprinted from *Chem. Eng. Sci.*, Vol 57, Qi, Kolah and Sundmacher, Pages 163–178, Copyright 2002, with permission from Elsevier Science)

The kinetic RCMs for the pseudohomogeneous system and for the heterogeneous system at different Damköhler numbers are shown in Fig. 5.22. For the pseudohomogeneous RCMs, with increasing Damköhler number the saddle point on the water–cyclohexanol edge and the stable node (pure cyclohexanol) move into the composition triangle (Fig. 5.22). There they meet and extinguish each other at the critical Damköhler number $Da = 0.165$. Meanwhile, the saddle point (pure cyclohexene) in the non-reactive RCM also moves into the triangle, shifts towards the PCE and leaves the pure cyclohexene vertex as a stable node (Fig. 5.22b). Fig. 5.22c shows the pseudohomogeneous equilibrium RCM ($Da = 500$). The reactive azeotropes in the two systems are identical because they are located outside the L–L phase splitting region.

For the heterogeneous liquid system, the reaction was assumed to take place in both liquid phases. When we compare the RCMs at the same Da for the pseudohomogeneous and heterogeneous systems, again we can find that the properties (including the reactive azeotrope) of the RCMs outside the L–L region are identical. But they are distinct inside the L–L region because of their different chemical equilibrium curves (compare Fig. 5.21).

Moreover, the bifurcation behavior for the pseudohomogeneous and heterogeneous kinetic RCMs is different, as shown in Figs.5.23. For the heterogeneous case (Fig. 5.23b), the saddle point branch starting from the water–cyclohexanol edge and the stable point branch starting from the pure cyclohexanol vertex meet on the L–L envelope (extract side) at the critical $Da = 0.109$. This point represents the kinetic tangent pinch point of the system. For the pseudohomogeneous system (Fig. 5.23a), bifurcation occurs at the critical Damköhler number $Da = 0.165$.

Recently, Steyer et al. [22] presented an extended analysis of cyclohexanol synthesis and splitting, supposing that the chemical reaction will proceed in the two liquid phases at different rates, that is with different Damköhler numbers. Based on their results, these authors proposed a flow-sheet of two coupled RD columns for the separation of cyclohexene/cyclohexane mixtures.

5.3.5 Systems with Interfacial Mass-Transfer Resistances

Recently, the effect of interfacial mass-transfer resistances on the location of the attainable products of a reactive separation process was analyzed considering the simple model A + B ↔ C [23]. The analysis was based on the calculation of the top and bottom products of a separative reactor of infinite height at infinite reflux ratio (∞,∞-analysis). The products of this reactor are obtained from the following equations in matrix-vector notation

$$\text{Bottom } 0 = -[k^*]\left(y^e(x^B) - x^B\right) + \left(v - x^B v_T\right) \cdot Da \cdot r^*(x^B) \tag{5.46}$$

$$\text{Distillate } 0 = [k^*]\left(y^e(x^D) - x^D\right) + \left(v - y^e v_T\right) \cdot Da \cdot r^*(x^D) \tag{5.47}$$

with the reactor coordinate τ, the vapor phase equilibrium composition y^e, the vector of reaction rates $Da \cdot r^*$, the matrix of multicomponent mass-transfer coefficients $[k^*]$, the matrix of stoichiometric coefficients ν, and vector of total mole changes ν_T. The $[k^*]$ elements can be obtained from the Maxwell–Stefan equations with suitable bootstrap conditions [24].

If $[k^*]$ is a diagonal matrix, the attainable products will not be affected by interfacial mass-transfer phenomena. In contrast, if the off-diagonal elements of the $[k^*]$ matrix are not vanishing, mass transfer can have a strong influence on the products. As a consequence, the attainable product region of a membrane reactor, for instance a pervaporative reactor, can be shifted by tailoring the membrane material and/or its pore structure.

Fig. 5.24 shows some illustrative results of a fixed-point continuation for the reversible reaction A + B ↔ C carried out in a pervaporative reactor with internal reflux. The Damköhler number *Da* is used as continuation parameter. The boiling sequence $p^s_A > p^s_B > p^s_C$ was assumed so that the desired product C is obtainable as a bottom product. The reaction kinetics are described by the power law expression $r^* = x_A x_B - x_C/K$ with the chemical equilibrium constant K as in Section 5.3.2. The role of mass transfer can be studied in terms of the dimensionless quantities k_{AC} and k_{BC}, that is the relative membrane permeabilities between A/C and B/C, respectively. For the ternary system considered, the elements of the mass-transfer coefficient matrix $[k^*]$ are calculated as follows [24]

$$k^*_{AA} = k_{AC}[\gamma_A k_{BC} + (1 - \gamma_A)]/S \tag{5.48a}$$

$$k^*_{AB} = [\gamma_A k_{BC}(k_{AC} - 1)]/S \tag{5.48b}$$

$$k^*_{BA} = [\gamma_B k_{AC}(k_{BC} - 1)]/S \tag{5.48c}$$

$$k^*_{BB} = k_{BC}[\gamma_B k_{AC} + (1 - \gamma_B)]/S \tag{5.48d}$$

where $S = \gamma_A k_{BC} + \gamma_B k_{AC} + \gamma_C$.

When $k_{AC} = k_{BC} = 1$, the off-diagonal elements of $[k^*]$ are equal to zero and the RD process discussed in Section 5.3.2 (case b) is recovered. Then, the location of the attainable product composition only depends on the vapor–liquid equilibria. In Fig. 5.24, singular point curves for the attainable bottom products of the depicted counter-current pervaporative reactor are given as a function of k_{AC} (Fig. 5.24a) and k_{BC} (Fig. 5.24b). For each set of membrane permeabilities there is one curve of possible singular points. The full circles on the singular point curves indicate stable nodes, that is they mark attainable bottom products. For the system considered, stable nodes are only obtained below the chemical equilibrium line.

As can be seen from Fig. 5.24a, by increasing k_{AC} the fixed-point curves move towards the C/B edge until a border line for $k_{AC} \to \infty$ is reached. When k_{AC} is decreased, the fixed points move towards the C/A edge until another border line for $k_{AC} \to 0$ is achieved that cannot be overcome. The gray area between the two border

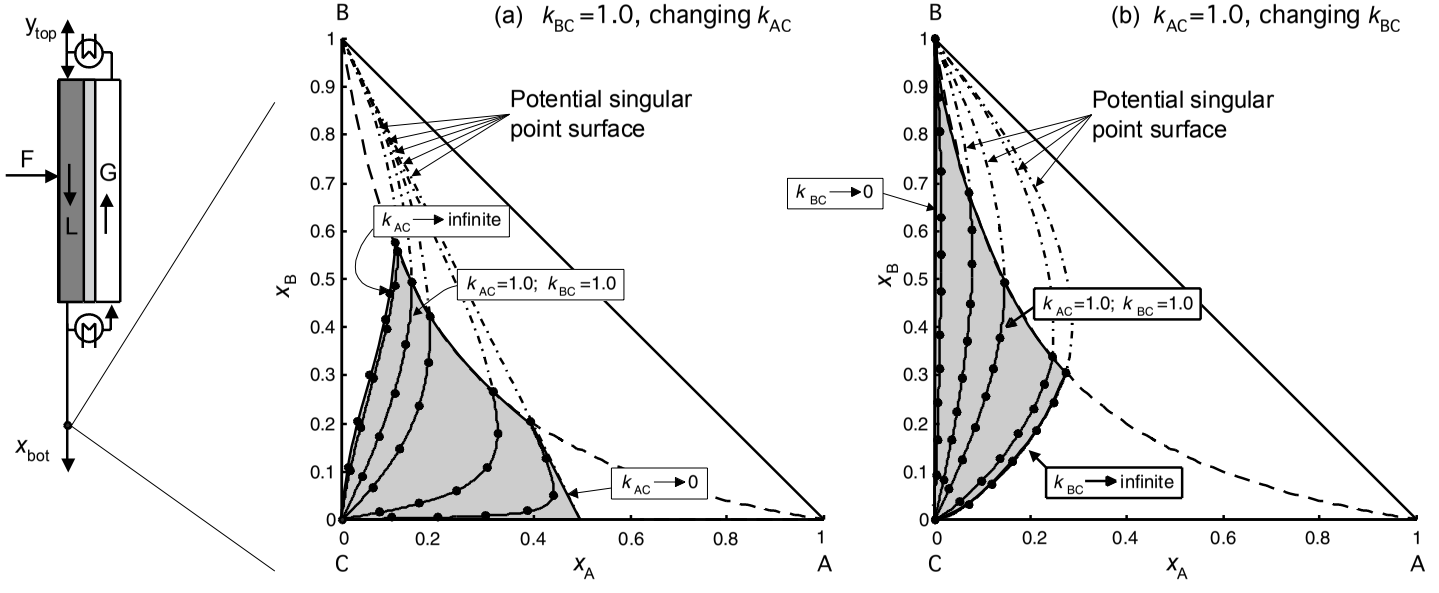

Fig. 5.24. Attainable regions of the bottom products (gray) of a pervaporative reactor (left) at different relative membrane permeabilities (dashed line: chemical equilibrium line at $K = 5$, Damköhler number: $Da = 0 \rightarrow \infty$)

lines and the chemical equilibrium line indicates the resulting attainable region. As illustrated in Fig. 5.24b, a different attainable region is obtained by changing the relative permeability k_{BC}. When k_{BC} decreases, the stable node branch approaches the B/C edge and at $k_{BC} \rightarrow 0$ even includes the pure B vertex.

These results are valid for the bottom products and are based on (5.46). A similar analysis can be carried out for the attainable top products by use of (5.47) [23].

5.4 Determination and Analysis of Reaction Kinetics

We have seen that the kinetics of the chemical reactions carried out play a major role for the performance of RD processes. Therefore, especially for reliable design and operation of counter-current columns, it is important to determine and analyze the reaction rates in detail. In the following, some guidelines are given about how to formulate rate expressions and which transport resistances have to be accounted for when describing the kinetics of reactions under the operating conditions of RD columns.

5.4.1 Physicochemical Transport Phenomena

It is preferable if the reactions in RD columns are catalyzed by heterogeneous catalysts because they are easily kept in the reactor and they allow hybrid RD columns combining reactive and non-reactive sections. Fig. 5.25 illustrates a column randomly packed with supported ion exchangers in rings. Such a heterogeneous cat-

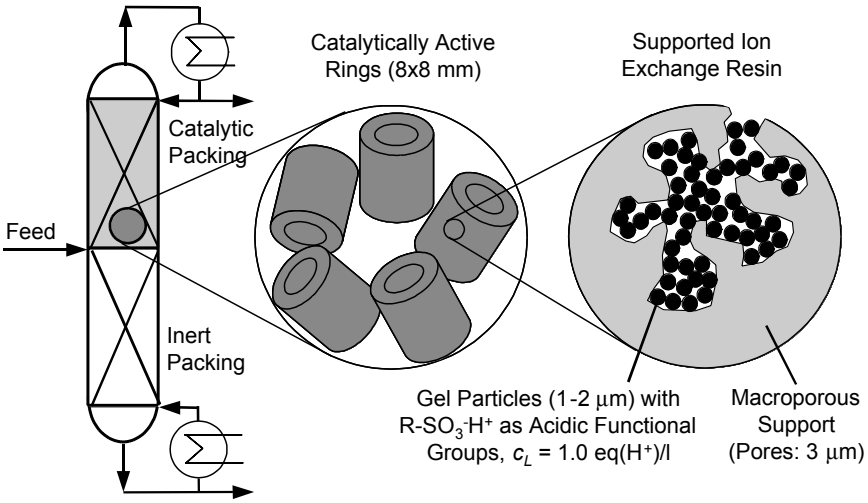

Fig. 5.25. Installation of ring-shaped ion-exchange catalyst in distillation column

alyst was successfully used for the synthesis of the fuel ether MTBE [25], the fuel ether TAME [26, 27], and the ester methyl acetate [28].

Fig. 5.26 gives a schematic representation of the mass and energy transport phenomena occurring in the RD process with a heterogeneous catalyst. In this process, the chemical reaction takes place in the solid catalyst phase. Along the external catalyst surface, the liquid phase trickles down the column. The liquid phase and the rising vapor phase are in counter-current flow. The sketch in Fig. 5.26 assumes the catalyst to be totally wetted at its external surface. Internally the porous catalyst bodies very often are completely wetted due to capillary forces but in some cases this situation can be changed by internal boiling processes [29].

The directions of the mass and energy fluxes between the phases cannot be predicted because of the influence of convection in axial column direction, and due to the fact that multicomponent mass-transport phenomena may result in uphill transport [30]. There are three types of transport resistances present in the considered three-phase (vapor/liquid/solid) process

– transport between the vapor and the liquid phase,
– transport between the liquid and the solid phase,
– intraparticle transport within the solid phase.

If supported macroreticular ion exchangers are used as catalysts, the intraparticle transport processes can be decomposed into gel phase diffusion and macropore diffusion [31]. For a combination of the two mechanisms special catalyst models were proposed [32].

Furthermore, it should be mentioned that for structured packing additional mass-transport resistances may exist between the catalyst particles in the structured wire gauzes of the packing. So far, relatively little is known about these interparticle resistances. However, they may play a major role in RD operations since a

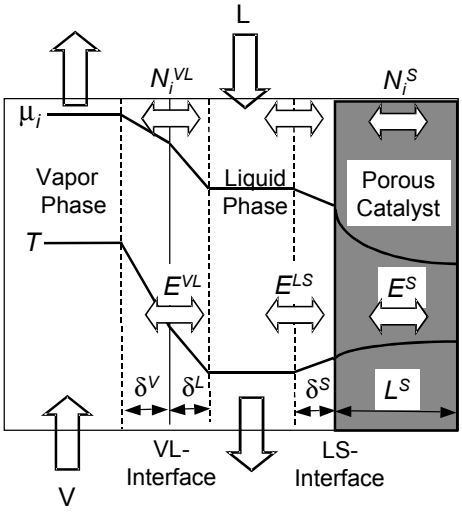

Fig. 5.26. Schematic of the transport phenomena in a column section packed with heterogeneous catalyst

significantly reduced catalyst activity was reported for the splitting of MTBE in an RD column compared with the activity that was observed at the non-packed catalyst particles in a liquid-phase batch reactor (Chapter 3).

5.4.2 Process Evaluation by Dimensionless Numbers

For the reliable prediction of RD process performance it is crucial to identify the dominant local mass and energy transport resistances between the phases in a packed catalytic column section. Dimensionless parameter groups are an efficient tool for this purpose, which allow estimation of the relevance of certain transport resistances from experimental data. Here only the most important qualitative results are given [33].

1. As already used in the preceding subsections, the Damköhler number *Da* evaluates the effective rate of the chemical reaction in comparison to the feed flow rate

$$Da \equiv \frac{k_f V_{cat}}{F} \propto \frac{\text{effective rate of reaction}}{\text{feed flow rate}} \tag{5.49}$$

   In (5.49), k_f represents the effective reaction rate constant including internal transport resistances of the catalyst packing. V_{cat} stands for the catalyst volume installed in the column. For $Da \gg 1$ the chemical reaction approaches chemical equilibrium, for $Da \ll 1$ the reaction is far from its equilibrium.
2. Since the separation in distillation columns is dominated by the vapor–liquid equilibrium, it is a reasonable assumption to neglect the mass-transfer resistances between the vapor phase and the liquid phase. However, in RD columns, the importance of vapor–liquid mass-transport resistances depends on the following dimensionless ratio

$$\frac{NTU_{i,ov}^{V}}{Da} \equiv \frac{c_t^L k_{i,ov}^{V} a}{k_f \varepsilon^S} \propto \frac{\text{VL mass transfer rate}}{\text{effective rate of reaction}} \tag{5.50}$$

   which can be easily derived from a steady-state liquid-phase mass balance. $NTU_{i,ov}^{V}$ is the overall number of mass-transfer units of a selected key component i referred to the vapor phase. For (5.50), the mass-transfer coefficient $k_{i,ov}^{V}$ and the specific mass-transfer area a have to be estimated from literature correlations, for example, from Onda's correlations, which are valid for packed towers [34]. For $NTU_{i,ov}^{V}/Da \gg 1$, the vapor–liquid mass-transfer resistances are negligible in comparison to the chemical reaction resistance. Therefore, only for very fast chemical reactions interfacial mass-transfer phenomena are of major importance.
3. Internal mass transport inside the catalyst particles should be evaluated with the help of the Thiele modulus

$$\phi \equiv \frac{1}{S_V}\sqrt{\frac{r}{c_t^L x_i D_{eff,i}^S}} \propto \frac{\text{rate of chemical reaction}}{\text{rate of intraparticle diffusion}} \tag{5.51}$$

In (5.51), r stands for the intrinsic reaction rate at liquid bulk conditions. For worst-case-estimations, one should use a highest rate value possible in the considered RD column. In this respect it should be kept in mind that the reaction rates under RD conditions strongly depends on the operating pressure that influences the boiling temperatures, that is the reaction temperature. $D_{eff,i}{}^S$ represents the effective diffusion coefficient of a selected reaction component inside the catalyst particles. One should use the component with the lowest mole fraction x_i in the liquid bulk mixture as key component [35]. Its effective diffusion coefficient can be estimated from the diffusion coefficient at infinite dilution: $D_{eff,i}{}^S = (\varepsilon/\tau) D_i^\infty$ with the total porosity ε and the tortuosity τ of the applied catalyst. Based on (5.51) one can say that intraparticle diffusion resistances will be negligible, if $\phi \ll 1$.

4. The importance of external mass transport resistances at the outer surface of the catalyst particles are estimated with the following Biot number

$$Bi_m^{LS} \equiv \frac{(1/S_V) \cdot k_i^{LS}}{D_{eff,i}^S} \propto \frac{\text{rate of LS mass transfer}}{\text{rate of intraparticle diffusion}} \tag{5.52}$$

where k_i^{LS} stands for the liquid–solid mass-transfer coefficient of the key component i, which can be estimated from published correlations [36, 37]. An evaluation of experimental data from different authors reveals that for most RD processes the Biot number is $Bi_m{}^{LS} \approx 10\text{–}100$. Therefore, external mass transport resistances are negligible. Only for extremely fast reactions at an egg-shell type catalyst, the transport of species towards the external catalyst surface may be important.

5. The heat of reaction $(-\Delta_R H^0)$ can lead to a temperature increase/decrease inside the catalyst particles. The significance of this phenomenon is evaluated by means of the Prater number β, which is well known from the reaction engineering literature

$$\beta \equiv \frac{(-\Delta_R H^o) c_t^L x_i D_{eff,i}^S}{\lambda_{eff}^S T^L} \propto \frac{\text{rate of intraparticle diffusion}}{\text{rate of intraparticle heat conduction}} \tag{5.53}$$

Since the Prater numbers of RD processes were found to have values $\beta < 10^{-3}$, the internal heat-transport effects can be neglected. The same is true for external heat transport effects [33].

6. The thermal sensitivity of the chemical reaction kinetics is an important effect that is characterized by the Arrhenius number

$$\gamma \equiv E_A/(RT^L) \tag{5.54}$$

5.4.3 Formulation of Reaction Rate Expressions

For process modeling proposes the effective chemical reaction rate r_{eff} has to be expressed as a function of the liquid bulk composition x, the local temperature T, and the catalyst properties such as its number of active sites per catalyst volume c_L, its porosity ε, and its tortuosity τ. As discussed in Section 5.4.2, the chemical reaction in the catalyst particles can be influenced by internal and external mass transport processes. To separate the influence of these transport resistances from the intrinsic reaction kinetics, a catalyst effectiveness factor η is introduced by

$$r_{eff} = \eta \cdot r \tag{5.55}$$

The catalyst effectiveness factor depends on the parameters defined in Section 5.4.2

$$\eta = \eta(\phi, Bi_m^{LS}, \beta, \gamma) \tag{5.56}$$

In correspondence with the guidelines given above, the catalyst effectiveness is mostly only a weak function of Bi_m^{LS}, β, and γ. Therefore: $\eta \approx \eta(\phi)$. The latter function is available in analytical form for first-order reactions [38]. In the general case, it has to be determined from the numerical solution of the catalyst particle balances, as done for instance in [35, 39–42]. In the case of negative reaction orders, multiple effectiveness factors can be obtained [32]. This is illustrated in Fig. 5.27 for the MTBE synthesis where the rate has a negative order with respect to the educt methanol.

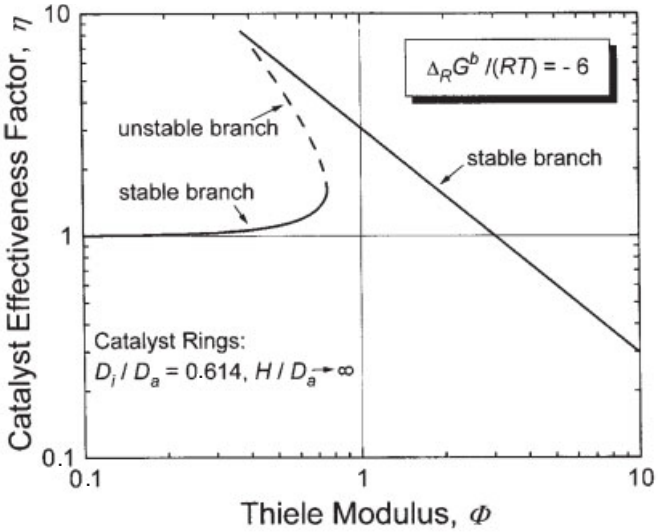

Fig. 5.27 Simulated effectiveness factor of a ring-shaped catalyst body plotted versus the Thiele modulus for MTBE synthesis ([32], reprinted from *Chem. Eng. Technol.*, Vol 21, Sundmacher, Künne and Kunz, Pages 494–498, Copyright 1998, with permission from Wiley-VCH)

In (5.55), r is the intrinsic reaction rate per volume of catalyst at liquid bulk conditions

$$r = c_L \cdot k(T) \cdot f(x) \tag{5.57}$$

where $k(T)$ is the intrinsic reaction rate constant at reaction temperature, and $f(x)$ contains the dependency of r on the liquid-phase composition. The intrinsic rate r has to be determined in the absence of any transport limitations. For this purpose, the use of separate kinetic measurements in a continuous stirred tank reactor [31, 43] or a differential tube reactor [44] are strongly recommended. In order to excluded transport limitations, measurements with increasing stirrer speed (CSTR) or increasing recycling rate (differential reactor), and decreasing catalyst particle size are indispensable [45, 46].

When formulating a microkinetic rate expression $r(T,x)$ one has to account for the sorption equilibria of the reaction components between the liquid phase and the active catalyst phase. For this purpose, since the liquid-phase reaction mixtures have a strongly non-ideal behavior, one should use generalized Langmuir sorption isotherms in terms of liquid-phase activities as proposed first in the pioneer work of Rehfinger and Hoffmann [45]. According to these authors, the sorption equilibria of the N species A_i on one active site S is given by

$$A_i + S \overset{K_{s,i}}{\rightleftharpoons} A_iS \tag{5.58}$$

$$\theta_i = \frac{K_{s,i} a_i}{1 + \sum_{j=1}^{N} K_{s,j} a_j} \tag{5.59}$$

where θ_i is the fraction of active catalyst sites occupied by component A_i, $K_{s,i}$ is the sorption equilibrium constant of A_i, and a_i is the liquid-phase activity at T ($a_i = x_i \gamma_i$) with the activity coefficient γ_i, which can be estimated from the UNIQUAC method, for example.

In order to formulate an expression $f(x)$ in (5.57), the rate determining step of the reaction mechanism has to be identified. For many heterogeneously catalyzed liquid-phase reactions the rate limiting step is found to be the reaction of sorbed molecules. For example, in the synthesis of the fuel ethers MTBE, TAME, and ETBE at acid ion-exchange catalyst the rate limiting step can be expressed as follows

$$\text{Alcohol} \cdot S + \text{Olefin} \cdot S \overset{k_+}{\underset{k_-}{\rightleftharpoons}} \text{Ether} \cdot S + S \tag{5.60}$$

$$r = c_L (k_+ \theta_{\text{Alcohol}} \theta_{\text{Olefin}} - k_- \theta_{\text{Ether}} \theta_o) \tag{5.61}$$

where θ_o is the fraction of unoccupied sites, and k the rate constant of forward (+) and reverse reaction (−). Inserting (5.59) into (5.60) leads to am expression for the reaction rate in terms of the liquid-phase activities, which in turn are dependent on the liquid-phase composition

$$r = c_L \frac{k_+ K_{s,Alcohol} K_{s,Olefin} a_{Alcohol} a_{Olefin} - k_- K_{s,Ether} a_{Ether}}{\left(1 + \sum_{j=1}^{N} K_{s,j} a_j\right)^2} \tag{5.62}$$

Due to the highly selective sorption of the polar alcohol molecules at the acid ion-exchange catalyst, the rate expression in (5.62) can be simplified considerably into

$$r = c_L k(T) \left(\frac{a_{Olefin}}{a_{Alcohol}} - \frac{1}{K_a} \frac{a_{Ether}}{a_{Alcohol}^2}\right) \tag{5.63}$$

The temperature dependence of the reaction rate constant k is given by the Arrhenius equation

$$k(T) = k(T_{ref}) \exp\left(-\frac{E_A}{R}\left(\frac{1}{T} - \frac{1}{T_{ref}}\right)\right) \tag{5.64}$$

where $k(T_{ref})$ is the rate constant at T_{ref} and E_A is the activation energy.

In Fig. 5.28a experimental and simulated rates for the synthesis of MTBE from methanol and isobutene are depicted, which show that the rate expression (5.63) is valid for the MTBE synthesis [45]. Fig. 5.28b illustrates its validity for the ETBE synthesis from ethanol and isobutene [41] compared with experimental data reported by Francoisse and Thyrion [47]. In analogous manner this rate approach can be applied to the synthesis of the fuel ether TAME from methanol and isoamlyenes [43, 46]. Activity-based rate expressions were also applied for other reactions carried out in strongly non-ideal liquid mixtures, for example for butyl acetate synthesis [48] and for dimethyl ether synthesis [49].

5.4.4 Importance of Transport Resistances for Column Operation

For the simulation of RD columns in which the chemical reactions take place at heterogeneous catalysts, it is important to keep in mind that a macrokinetic expression (5.55) has to be applied. Therefore, the microkinetic rate has to be combined with the mass transport processes inside the catalyst particles. For this purpose a model for the multicomponent diffusive transport has to be formulated and combined with the microkinetics based on the component mass balances. This has been done by several authors [50–53] by use of the generalized Maxwell–Stefan equations.

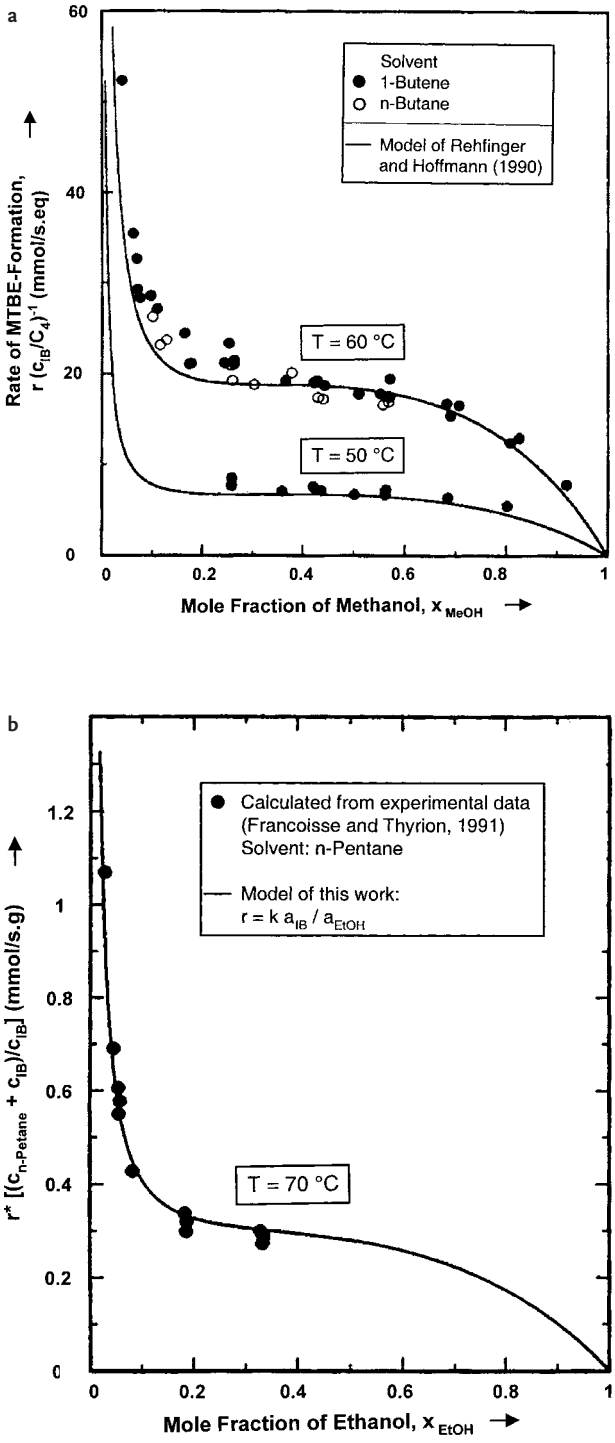

Fig. 5.28. Experimental and modeled intrinsic formation rates of fuel ethers versus mole fraction of alcohol in liquid bulk phase: a) MTBE synthesis ([35], reprinted from *Chem. Eng. Sci.*, Vol 49, Sundmacher and Hoffmann, Pages 3077–3089, Copyright 1994, with permission from Elsevier Science), b) ETBE ([41], reprinted from *Chem. Eng. Technol.*, Vol 18, Sundmacher, Zhang and Hoffmann, Pages 269–277, Copyright 1995, with permission from Wiley-VCH)

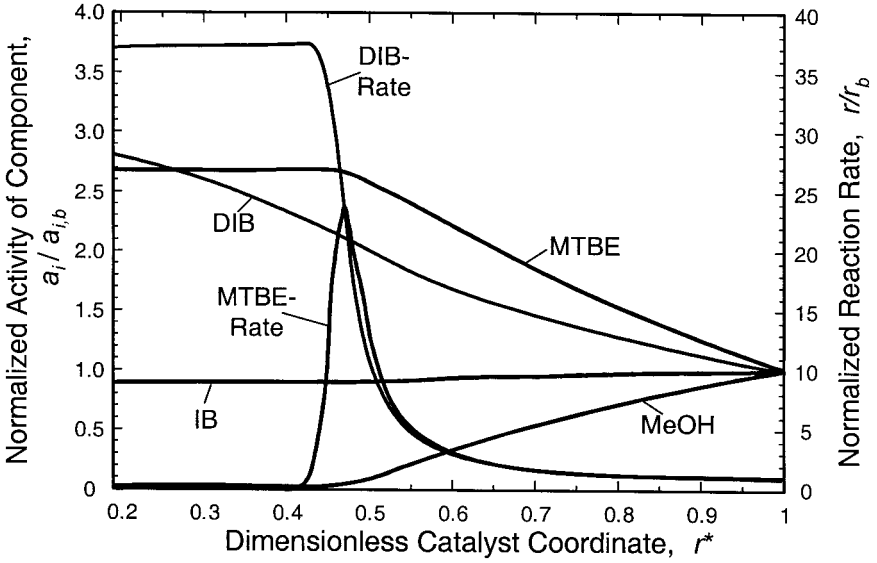

Fig. 5.29. Simulated reaction rates and liquid-phase component activity profiles inside a catalyst particle for MTBE synthesis

For illustration, here we will briefly summarize some phenomena that will originate from the diffusion-reaction interaction at acid ion-exchange catalysts during the MTBE synthesis. In Fig. 5.29 simulated profiles of reaction rates and component activities within a spherical catalyst particle are given, assuming an excess of isobutene in the surrounding bulk phase. As can be seen from this figure, due to internal diffusion limitations the methanol concentration decreases towards the particle center. In contrast, the MTBE-content increases towards the catalyst center. As a result of the methanol decrease, the MTBE-formation rate is increasing, reaches a maximum, and then is sharply decreasing until it drops nearly to zero. The reason for this peculiar phenomenon, is the negative reaction order of the reaction rate (5.63), with respect to the reactant methanol. Consequently, there is a particle core that is nearly free of methanol. This gives rise to an undesired side reaction, that is the dimerization of isobutene and its further reaction to higher oligomers that can deactivate the catalyst [51].

Dimer formation leads to a significant increase of the boiling temperatures along the stripping section of a RD column as can be seen from the experimental data shown in Fig. 5.30. The comparison with two alternative process models reveals that only a heterogeneous column model, that is a model that includes the mass transport phenomena within the catalyst rings, is able to predict the observed steady-state process behavior with respect to axial column temperatures (Fig. 5.30a) as well as with respect to the axial liquid-phase compositions (Fig. 5.30b).

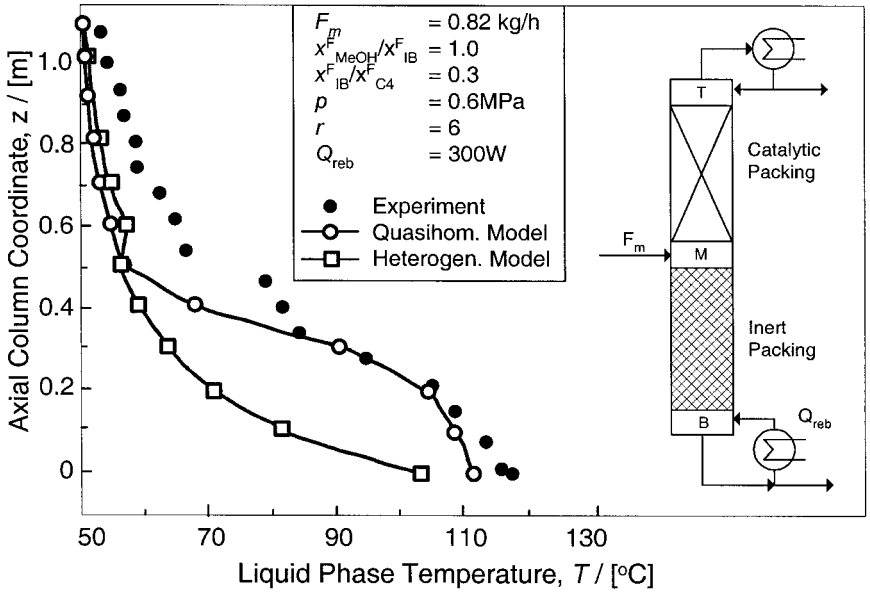

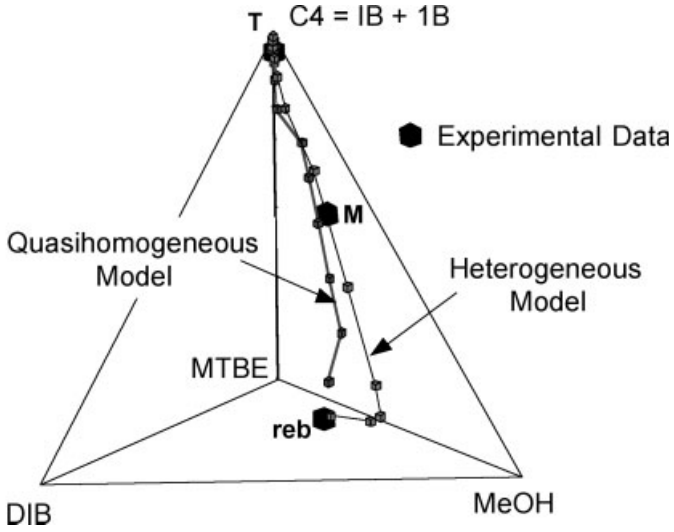

Fig. 5.30. a) Experimental and simulated temperature profiles for packed MTBE RD column. b) Experimental and simulated liquid-phase compositions for MTBE synthesis in a packed RD column

5.5 Conclusions

As has been outlined in the first sections of this chapter, RD processes can efficiently replace reactor–separator flow-sheets by internalization of external recycling loops. This is demonstrated for a simple isomerization reaction in an ideal binary mixture. It is clearly shown that hybrid columns combining non-reactive and reactive sections overcome the restrictions of fully RD columns. The most simple and effective solution for isomerization reactions is a reactive total reboiler with a non-reactive column on top.

The kinetics of a chemical reaction have a significant influence on the products that can be attained from a RD process. The attainable products of counter-current RD columns of infinite height operated at infinite reflux ratio can be obtained as singular points of a reactive reboiler batch process (bottom product) or a reactive condenser batch process (distillate product). The compositions of both products are located on a unique singular point curve. This curve is independent of any special type of reaction kinetics. However, the locations of the top and bottom products on this curve depend on the structure of the rate equation and on the intensity of the reaction (Damköhler number) in the considered reaction system.

In the last sections of this chapter, the determination and analysis of reaction kinetics is discussed. Dimensionless parameter groups are a very efficient tool for evaluating quickly the importance of the physicochemical phenomena occurring in RD columns. Since most of the reactions in RD columns take place in non-ideal liquid mixtures at heterogeneous catalysts, the use of activity-based Langmuir sorption isotherms is recommended. This approach results in microkinetic rate expressions in terms of liquid-phase activities. As a most important advantage, these rate equations coincide with the chemical equilibrium in the limiting case of vanishing reaction rate.

The steady-state process behavior of counter-current RD columns operated with heterogeneous catalysts depends strongly on the reaction macrokinetics. This is illustrated using the formation of MTBE in a packed RD column as an example.

5.6 Acknowledgments

K. Sundmacher thanks all his colleagues and partners from academia and industry who were involved in the research presented in this chapter, especially U. Hoffmann, A. Rehfinger, U. Kunz, C. Thiel, P. Ramund, C. Oost, H. Künne, and G. Uhde, all at Clausthal University of Technology, A. Kienle, K. D. Mohl, and E. D. Gilles from Max-Planck-Institute Magedburg, H. Schoenmakers and B. Bessling from BASF AG, and A. Tuchlenski from Degussa AG. He is also very thankful to two collaborating visiting scientists: L. Rihko-Struckmann from Helsinki University of Technology, Finland, and R. S. Zhang from East China University of Science and Technology in Shanghai, China. The financial support from

different funding organisations (BMBF, VW-Stiftung, DFG, FCI, all in Germany; BriteEuram grant from European Community) during the last 10 years is also gratefully acknowledged.

Z. Qi is very thankful to the Max-Planck Society for the Max-Planck Scholarship that allowed him to start his research activities in reactive distillation when he came to Magdeburg in September 1999.

5.7 Notation

A_1, A_2	educt, product (-)
B	bottom flow rate ($mol \cdot s^{-1}$)
D	distillate flow rate ($mol \cdot s^{-1}$)
Da	Damköhler number (-)
F	feed flow rate ($mol \cdot s^{-1}$)
K	chemical equilibrium constant (-)
k	reaction rate constant ($mol \cdot m^{-3} \cdot s^{-1}$)
L	liquid flow rate ($mol \cdot s^{-1}$)
N	total number of stages (-)
N_{min}	minimum number of stages (-)
n	reaction order (-)
p_i^S	vapor pressure of component i, (Pa)
R	reflux ratio (-)
R_{min}	minimum reflux ratio (-)
r	reaction rate ($mol\ s^{-1} m^{-3}$)
r^*	dimensionless reaction rate (-)
V_R	reaction volume (m^3)
$V_{R,S}$	reaction volume on one stage (m^3)
V	vapor flow rate ($mol \cdot s^{-1}$)
x	mole fraction of A_2 in liquid phase (-)
x_{ce}	mole fraction of A_2 at chemical equilibrium (-)
$x^e(y)$	liquid-phase mole fraction of A_2 at vapor–liquid equilibrium (-)
y	mole fraction of A_2 in vapor phase (-)
$y^e(x)$	vapor phase mole fraction of A_2 at vapor–liquid equilibrium (-)

Greeks

α	relative volatility A_2/A_1 (-)
φ	recycling ratio (-)
π_{reb}	reboiler pole

Subscripts

1, 2	related to components A_1, A_2
crit	critical
π	related to pole location

con	related to condenser
max	maximum attainable value
min	minimum attainable value
reb	related to reboiler
s	related to a single distillation stage
f	forward reaction
ce	chemical equilibrium
cat	catalyst

Superscripts

B, D, F	related to bottom, distillate, feed flow
R	related to outlet of chemical reactor
*	dimensionless
e	at equilibrium
s	saturated state

References

1 K. Sundmacher, Z. Qi, *Chem. Eng. Proc.*, **2002**, in press.
2 W. L. McCabe, J. C. Smith, P. Harriott, *Unit Operations of Chemical Engineering*, McGraw Hill, New York, 5th edn., **1993**, 545–549.
3 N. Chadda, M. F. Malone, M. F. Doherty, *AIChE J.* **2001**, *47*, 590–601.
4 G. A. F. Fien, Y. A. Liu, *Ind. Eng. Chem. Res.* **1994**, *33*, 2505–2522.
5 D. Barbosa, M. F. Doherty, *Chem. Eng. Sci.* **1988**, *43*, 541–550.
6 S. Ung., M. F. Doherty, *Ind. Eng. Chem. Res.* **1995**, *34*, 3195–3202.
7 A. Rehfinger, U. Hoffmann, *Chem. Eng. Sci.* **1990**, *45*, 1605–1617.
8 C. Thiel, K. Sundmacher, U. Hoffmann, *Chem. Eng. Sci.* **1997**, *52*, 993–1005.
9 G. Venimadhavan, G. Buzad, M. F. Doherty, M. F. Malone, *AIChE J.* **1994**, *40*, 279–289.
10 C. Oost, U. Hoffmann, *Chem. Eng. Sci.* **1995**, *51*, 329–340.
11 L. K. Rihko, J. A. Linnekoski, A. O. Krause, *J. Chem. Engng Data* **1994**, *39*, 700–704.
12 C. Thiel, K. Sundmacher, U. Hoffmann, *Chem. Eng. J.* **1997**, *66*, 181–191.
13 S. Ung, M. F. Doherty, *Chem. Eng. Sci.* **1995**, *50*, 3201–3216.
14 G. Venimadhavan, M. F. Malone, M. F. Doherty, *Ind. Eng. Chem. Res.* **1999**, *38*, 714–722.
15 Y. Zhicai, C. Xianbao, G. Jing, *Chem. Eng. Sci.* **1998**, *53*, 2081–2088.
16 S. Löning, C. Horst, U. Hoffmann, *Chem. Eng. Technol.* **2000**, *23*, 789–794.
17 A. W. Westerberg, J. W. Lee, S. Hauan, *Comput. Chem. Eng.* **2000**, *24*, 2043–2054.
18 Z. H. Gumus, A. R. Ciric, *Comput. Chem. Eng.* **1997**, *21*, S983–S988.
19 Z. Qi, A. Kolah, K. Sundmacher, *Chem. Eng. Sci.* **2002**, *57*, 163–175.
20 J. P. Novak, J. Matous, J. Pick, *Liquid–Liquid Equilibria*, Elsevier, Amsterdam, **1987**, 245–253.
21 H. J. Pannemann, A. A. C. M. Beenackers, *Chem. Eng. Sci.* **1992**, *47*, 2635–2640.
22 F. Steyer, Z. Qi, K. Sundmacher, *Chem. Eng. Sci.* **2002**, *57*, 1511–1520.
23 Z. Qi, K. Sundmacher, in *Int. Symp. Chem. Reac. Eng. ISCRE-17*, Hong Kong, 25–28 August **2002**.
24 R. Taylor, R. Krishna, *Multicomponent Mass Transfer*, Wiley, New York, **1993**.

25 K. Sundmacher, *Reaktivdestillation mit katalytisch aktiven Füllkörperpackungen: ein neuer Prozess zur Herstellung der Kraftstoffkomponente MTBE*, CUTEC-Schriftenreihe Nr.17, Clausthal-Zellerfeld, **1995**.

26 U. Hoffmann, H. Krummradt, P. Rapmund, K. Sundmacher, *Chem. Ing. Tech.* **1997**, *69*, 483–487.

27 P. Rapmund, K. Sundmacher, U. Hoffmann, *Chem. Eng. Technol.* **1998**, *21*, 136–139.

28 B. Bessling, J. M. Löning, A. Ohligschläger, G. Schembecker, K. Sundmacher, *Chem. Eng. Technol.* **1998**, *21*, 393–400.

29 K. Sundmacher, U. Hoffmann, *Chem. Eng. Technol.* **1993**, *16*, 279–289.

30 K. Sundmacher, U. Hoffmann, *Chem. Eng. Sci.* **1994**, *49*, 4443–4464.

31 A. Refinger, Reaktionstechnische Untersuchungen zur Flüssigphasesynthese von Methyl-tert-butylether (MTBE) an einem starksauren makroporösen Ionenaustauschharz als Katalysator, PhD Thesis, TU Clausthal, **1988**.

32 K. Sundmacher, H. Künne, U. Kunz, *Chem. Eng. Technol.* **1998**, *21*, 494–498.

33 K. Sundmacher, L. K. Rihko, U. Hoffmann, *Chem. Eng. Comm.* **1994**, *127*, 151–167.

34 K. Onda, H. Takeuchi, Y. Okumoto, *J. Chem. Eng. Jpn.* **1968**, *1*, 56–62.

35 K. Sundmacher, U. Hoffmann, *Chem. Eng. Sci.* **1994**, *49*, 3077–3089.

36 D. W. van Krevelen, J. T. C. Krekels, *Recl. Trav. Chim. Pays-Bas* **1948**, *67*, 512.

37 S. Goto, J. Levec, J. M. Smith, *Catal. Rev. Engng.* **1977**, *15*, 187–247.

38 M. Baerns, H. Hofmann, A. Renken, *Chemische Reaktionstechnik*, Georg Thieme, Stuttgart, **1987**.

39 A. Rehfinger, U. Hoffmann, *Chem. Eng. Sci.* **1990**, *45*, 1619–1626.

40 D. A. Berg, T. J. Harris, *Ind. Eng. Chem. Res.* **1993**, *32*, 2147.

41 K. Sundmacher, R. S. Zhang, U. Hoffmann, *Chem. Eng. Technol.* **1995**, *18*, 269–277.

42 G. Uhde, K. Sundmacher, U. Hoffmann, *Chem. Eng. Technol.* **1999**, *22*, 33–37.

43 L. K. Rihko, A. O. I. Krause, *Ind. Eng. Chem. Res.* **1995**, *34*, 1172–1180.

44 C. Oost, Ein Beitrag zum Umweltschutz: Reaktionstechnische Untersuchungen zur Flüssigphasesynthese des Antiklopfmittels TAME, CUTEC-Schriftenreihe Nr. 14, Clausthal-Zellerfeld, **1995**.

45 A. Rehfinger, U. Hoffmann, *Chem. Eng. Sci.* **1990**, *45*, 1605–1617.

46 C. Oost, U. Hoffmann, *Chem. Eng. Sci.* **1996**, *51*, 329–340.

47 O. Francoisse, F. C. Thyrion, *Chem. Eng. Process.* **1991**, *30*, 141–149.

48 C. E. Leyee, D. F. Othmer, *Ind. Eng. Chem.* **1945**, *37*, 968–977.

49 A. Nisoli, M. F. Malone, M. F. Doherty, *AIChE J.* **1997**, *43*, 374–387.

50 K. Sundmacher, U. Hoffmann, *Chem. Eng. Sci.* **1996**, *51*, 2359–2368.

51 G. Uhde, K. Sundmacher, U. Hoffmann, *Chem. Eng. Sci.* **1999**, *54*, 2839–2847.

52 A. Higler, R. Krishna, R. Taylor, *Ind. Eng. Chem. Res.* **2000**, *39*, 1596–1607.

53 K. D. Mohl, A. Kienle, K. Sundmacher, E. D. Gilles, *Chem. Eng. Sci.* **2001**, *56*, 5239–5254.

Reactive Distillation. Edited by Kai Sundmacher, Achim Kienle

ISBNs: 3-527-30579-3 (Hardback); 3-527-60052-3 (Electronic)

Part III
Process Design

Reactive Distillation. Edited by Kai Sundmacher, Achim Kienle

ISBNs: 3-527-30579-3 (Hardback); 3-527-60052-3 (Electronic)

6
Feasibility and Process Alternatives for Reactive Distillation

S. B. Gadewar, N. Chadda, M. F. Malone, and M. F. Doherty

6.1
Introduction

Reactive distillation (RD) has the demonstrated potential for capital productivity improvements (from enhanced overall rates, by overcoming very low reaction equilibrium constants, and by avoiding or eliminating difficult separations), selectivity improvements (which reduce excess raw material use and by-product formation), reduced energy use, and the reduction or elimination of solvents. Some of these advantages are realized by using reaction to improve separation, such as overcoming azeotropes or reacting away contaminants; others are realized by using separation to improve reactions, for example, overcoming reaction equilibrium limitations, improving selectivity, or removing catalyst poisons. The potential is greatest when both aspects are important. This technology is potentially attractive whenever there is a liquid phase reaction that involves an excess of reactant. Many existing, and potential, applications are discussed by Sharma and Mahajani [40].

Some of the successes of RD are so dramatic that we might ask if all liquid-phase chemical processes should be based on simultaneous reaction and separation instead of more traditional separate steps. The answer is no, because combining reaction and distillation is not always advantageous; in some cases it may not even be feasible! A key question is 'How can we decide quickly whether RD is a good process concept?' This question is addressed mainly by studies in conceptual design, which is the major focus of this chapter.

For conceptual design of RD, systematic methods are needed for deciding its feasibility. We use geometric methods which have been used extensively to assess the feasibility for non-RD. For non-RD, a number of algorithms can be used to find the feasible splits. Stichlmair and Herguijuela [44] calculate the products at total reflux while Wahnschafft et al. [49] and Fidkowski et al. [15] use pinch tracking techniques to estimate the feasible products for finite as well as total reflux. These methods rely on geometric visualization, so have been applied to ternary mixtures. Algorithms building on these ideas, but that do not rely on visualization are described by Safrit and Westerberg [42] and Rooks et al. [38]. These methods can

also be applied in the limit of reaction equilibrium using transformations of the compositions that have properties similar to those of mole fractions in non-reactive mixtures [1, 9, 46]. There is a one-to-one correspondence between the real mole fractions and the transformed variables at chemical equilibrium.

Such one-to-one transformations are not known for kinetically controlled RD although some aspects of these transforms remain useful in the kinetic regime. Studies at finite rates of reaction are important because most RD devices operate in this regime. There are several approaches available that capture some of the effects of finite reaction rates, such as, geometric design methods [2, 3, 34]; mixed integer nonlinear programming (MINLP) methods [6, 28, 36]; attainable region methods [32, 33]; residue curve/bifurcation methods [37, 45, 47, 48]; and difference point methods [30]. However, there are few tools that assess the feasibility of reactive mixtures in the kinetic regime. Giessler et al. use static analysis to determine feasibility of reactive columns operated with large internal flows [17, 18]. Chadda et al. generate feasible product regions at finite rates of reaction for ternary systems [4]. However, that method cannot be extended to treat a larger number of components or multiple reactions.

In this chapter, we describe an algorithm for predicting feasible splits for continuous single-feed RD that is not limited by the number of reactions or components. The method described here uses minimal information to determine the feasibility of reactive columns: phase equilibrium between the components in the mixture, a reaction rate model, and feed state specification. This is based on a bifurcation analysis of the fixed points for a co-current flash cascade model. Unstable nodes ('light species') and stable nodes ('heavy species') in the flash cascade model are candidate distillate and bottom products, respectively, from a RD column. Therefore, we focus our attention on those splits that are equivalent to the 'direct' and 'indirect' *sharp splits* in non-RD. One of the products in these sharp splits will be a pure component, an azeotrope, or a kinetic pinch point; the other product will be in material balance with the first.

The proposed algorithm is based on the following.

- A bifurcation study to predict the distillate and bottoms products for the entire range of reaction rates from the limit of no reaction to the limit of chemical equilibrium. This provides a global view of the *direct* and *indirect split* products from a continuous RD at all rates of reaction.
- Flash calculations and the application of the *lever rule* (overall mass balance relating the feed, distillate and bottoms product streams) to predict feasible *sharp splits* for a given feed condition.

We begin by describing a simple example that demonstrates the advantages gained by combining reaction and separation. These advantages are represented in terms of the attainable region.

6.2 Motivation

A method for assessing the feasibility of reactor systems that has gained prominence in the past decade seeks *attainable regions*. This approach does not assume a reactor network *a priori*, but only the set of fundamental processes (such as reaction, mixing etc.) that can occur. The concept was first proposed by Horn [26] and later developed by Glasser and co-workers. Horn defines the attainable region as the collection of the 'objective variables,' such as recycling flow rate and composition of the product, that corresponds to the totality of physically possible reactors [26]. Glasser et al. define the attainable region as a domain in the concentration space that can be achieved by using any system of steady-flow chemical reactors, that is, by using the processes of *mixing* and *reaction* [19]. This attainable region is sometimes called the 'kinetically attainable region' to distinguish it from the 'thermodynamically attainable region,' determined by equilibrium constraints [43]. Glasser et al. established a set of necessary conditions for the kinetically attainable region [19]. Currently, sufficient conditions for the kinetically attainable region are not known.

Feinberg and Hildebrandt derived properties for the boundary of the attainable region [10]. They showed that the boundary of the attainable region is always accessible by means of elementary reactors (PFR, CSTR etc.) taken in simple combination. Glasser et al. considered combinations of plug-flow, CSTR, and recycle reactors in constructing the attainable region [19]. This analysis was also applied to systems with three dimensional attainable regions [22, 23], to adiabatic systems [20, 24], and to more complex reactor systems [21]. Feinberg showed that a differential side-stream reactor (DSR) can reside on the boundary of the attainable region only if it satisfies specific design equations that govern the precise way of adding side-streams along the length of the reactor, and these equations depend on the reaction chemistry and kinetics [11]. The CSTRs that give rise to extreme points of the attainable region must also conform to certain special design equations [12]. These design equations indicate that for a CSTR to give a point on the boundary of the attainable region, there are only very exceptional values of residence time (which are usually computable). Rooney et al. describe a method for constructing attainable regions of dimensions greater than two by combining two dimensional projections of candidate regions [39]. Smith and Malone applied the concept to polymerization reaction systems for determining the attainable region for number-average molecular weights and polydispersity [41].

One important use of the attainable region concept is in assisting the process of optimization. Lakshmanan and Biegler used the attainable-region properties to formulate a reactor network and optimized it using a MINLP approach [29]. Pahor et al. suggest an iterative procedure using attainable region analysis to update the superstructure in a MINLP formulation [35].

Relatively little has been published on the attainable region for reaction combined with separation. One of the first papers applied the concept of attainable region to find feasible compositions for systems with simultaneous reaction and

separation in co-current devices [33]. The reaction–separation devices considered were CSTR with vapor removal and PFR with vapor removal. However, they did not estimate the conversions achieved using the reaction–separation devices. It is not known how simultaneous separation with reaction in a counter-current device affects the region of feasible compositions. Feinberg [13] showed that for finding bounds on the attainable effluents from reactor-separator systems of arbitrary design, it is sufficient to consider a reaction system with a finite number of CSTRs coupled with a separation system capable of making sharp separations; the number of CSTRs needed to describe the boundary of the attainable region depends on the number of independent reactions in the reaction chemistry.

The aim of this example is to apply the attainable region methodology to a counter-current reaction–separation process. The attainable region for reaction–separation should encompass all possible compositions achievable by using the phenomenon of reaction, separation, and mixing (including those obtained by hybrid devices for reaction–separation). In this example, we focus on specific devices, therefore, the region that we identify should be considered a *feasible region*, which will be a subset of the *attainable region* for reaction–separation. The feasible region gives an estimate of the composition space achievable using a counter-current reaction–separation device and therefore provides an estimate of its potential advantage over conventional reactors and separators.

Consider a system with the elementary irreversible reactions in series

$$A \xrightarrow{k_{f,1}} B \xrightarrow{k_{f,2}} C$$

in an ideal liquid solution. For simplicity, we assume an isothermal case. For this reaction system, a PFR will always give better yield and selectivity to the desired product B than a CSTR [31]. When the rate constants for both the reactions are identical, the attainable region boundary is the PFR trajectory, which is convex. The CSTR locus lies inside the PFR trajectory.

Now consider a two phase CSTR consisting of an isobaric flash separator with a simultaneous chemical reaction in the liquid phase, as shown in Fig. 6.1.

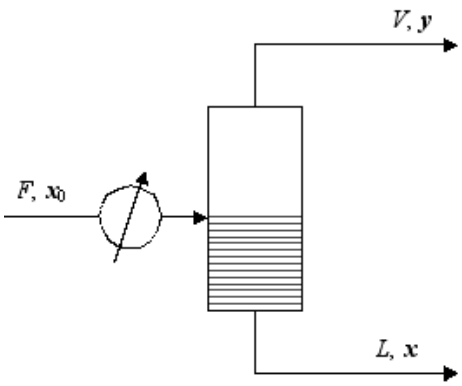

Fig. 6.1 CSTR with vapor removal

We assume the liquid and vapor are in phase equilibrium, and that the volatilities of components B and C relative to A are constant and equal to 5 and 3, respectively. Therefore, the vapor in phase equilibrium with the liquid reaction mixture will have more of the desired product B compared to the liquid phase. It is intuitive that removing vapor from a CSTR will help in removing the desired product from the reaction mixture, and is bound to improve the selectivity for the process. A model was developed by Gadewar et al. for the device in Fig. 6.1 to calculate the yield of B and selectivity to B with the conversion of A [16]. Activity-based rate expressions are used in formulating the model for reasons explained in Nisoli et al. [33].

The overall material balance (Fig. 6.1) is written as

$$F - L - V + \sum_{k=1}^{2} \nu_{T,k} r_k(x) H = 0 \tag{6.1}$$

where $r_k(x)$ is the reaction rate per mole of liquid mixture for the kth reaction, and has the dimensions of moles reacted per mole of mixture per unit time. $\nu_{T,1}$ and $\nu_{T,2}$ are the algebraic sum of the stoichiometric coefficients for the first and second reaction, respectively. The streams F and L are assumed to be saturated liquids. The material balance for the i^{th} component is

$$Fx_{i,0} - Lx_i - Vy_i + \sum_{k=1}^{2} \nu_{i,k} r_k(x) H = 0 \tag{6.2}$$

The vapor compositions are determined by using a constant relative volatility model. Since both reactions are equimolar, $\nu_{T,1} = \nu_{T,2} = 0$. Eliminating L from (6.1) and (6. 2), we get

$$x_i - x_{i,0} = \frac{V}{F}(x_i - y_i) + \frac{H}{F}\sum_{k=1}^{2} \nu_{i,k} r_k(x) \tag{6.3}$$

The Damköhler number [7], $\mathrm{Da} = Hk_{\mathrm{f,\,ref}}/F$, is the ratio of a characteristic liquid residence time (H/F) to the characteristic reaction time $(1/k_{\mathrm{f,\,ref}})$, where, $k_{\mathrm{f,\,ref}}$ is the rate constant for the reference reaction. $\phi = V/F$, is the fraction of liquid feed that is vaporized. Using these parameters in (6.3), we get

$$x_i - x_{i,0} = \phi(x_i - y_i) + Da \sum_{k=1}^{2} \nu_{i,k} \frac{r_k(x)}{k_{\mathrm{f,\,ref}}} \tag{6.4}$$

The difference between the liquid composition vectors $\boldsymbol{x}$ and $\boldsymbol{x}_0$ is given in terms of a separation vector $(\boldsymbol{x} - \boldsymbol{y})$ and a reaction vector $\sum_{k=1}^{2} \nu_k r_k(x)$. Given a value for F, a choice of ϕ sets all of the flows and Da determines the reactor volume. The yield of the desired product B and the conversion of A is found from the combined streams L and V, and the overall outlet composition vector is given by $((1 - \phi)x + \phi y)$. The selectivity to B is simply the ratio of yield of B to conversion of A.

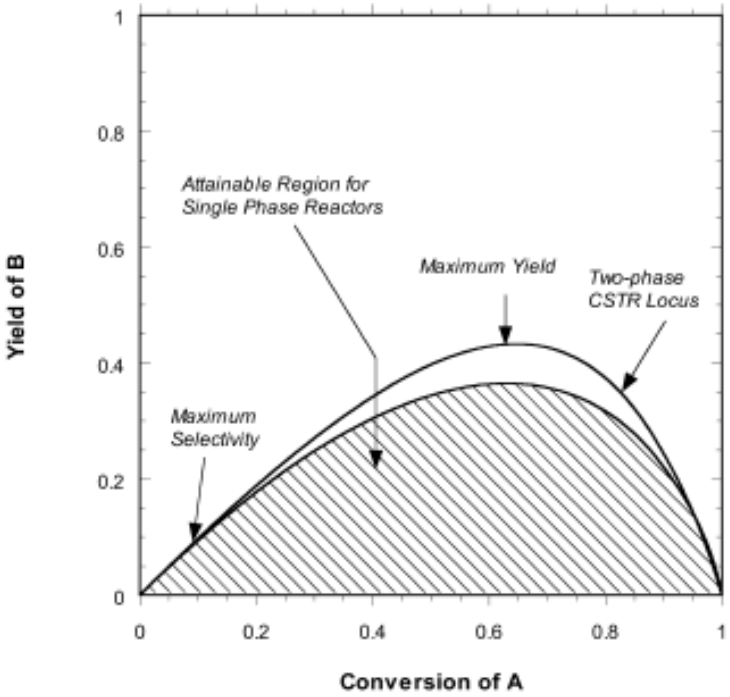

Fig. 6.2 Effect of separation on the attainable region for $A \rightarrow B \rightarrow C$

We use first order reaction rate models for both reactions, where the rates are given as $r_1 = k_{f,1}x_A$ and $r_2 = k_{f,1}x_A - k_{f,2}x_B$. We choose $\phi = V/F = 0.8$, and a liquid feed of pure A to the two-phase CSTR. Assuming that the rate constant for both reactions is identical, $k_{f,1} = k_{f,2} = k_{f,ref}$, the conversion of A, the yield and selectivity to B are determined from the overall composition vector after specifying a value for Da and solving (6.4). The conversion increases monotonically with Da since the characteristic residence time increases for a given characteristic reaction time. Fig. 6.2 shows the yield of B against the conversion of A for the two-phase CSTR. The hatched area is the attainable region for single-phase reactors (CSTR, PFR). The figure shows that using a CSTR with vapor removal gives a larger region of feasible compositions than for single-phase reactors. Fig. 6.3 shows the selectivity to B against the conversion of A.

Good improvement in selectivity is possible by using a two-phase CSTR over a conventional reactor. Since the desired product, B is the lightest boiling component in the mixture, vaporization improves yield and selectivity to B. It is therefore logical to string together a series of CSTRs where the liquid and vapor streams move in a counter-current fashion (Fig. 6.4).

The resulting reactive-separation device greatly increases the feasible region, and dramatically improves the selectivity to B, Figs 6.5 and 6.6.

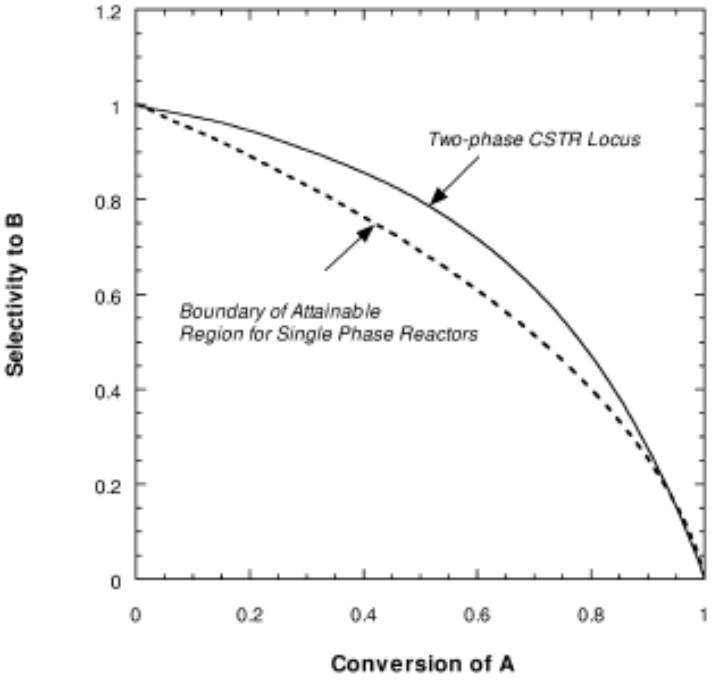

Fig. 6.3 Selectivity to *B* against conversion of *A* for a two-phase CSTR and for the boundary of the attainable region

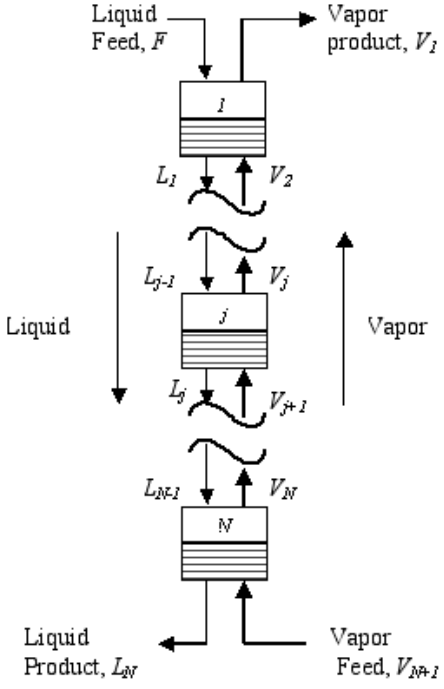

Fig. 6.4 Schematic of a counter-current cascade of two-phase CSTR's

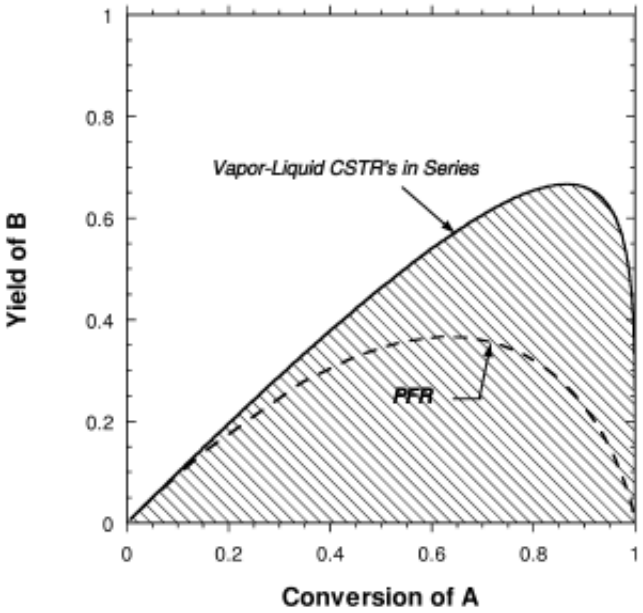

Fig. 6.5 Feasible region (hatched region) for reactions-in-series in a counter-current reactive separator

A comparison of the selectivity of *B* corresponding to the boundary of the feasible region and that for a single phase PFR is shown in Fig. 6.6. The selectivity to *B* is high even at higher conversions by using a counter-current reactive separator. This approach provides an estimate of the raw material savings by using simultaneous reaction–separation in a counter-current device, and therefore the economic incentive for implementing such a configuration. For a 95 % selectivity, the single phase reactor network can be operated at a maximum conversion of about 10 %, however, to achieve the same selectivity, the reactor network consisting of a counter-current cascade can be operated at about 40 % conversion. In plants with recycling (typically continuous processes) higher conversions significantly reduce the recycle flows and also the flow rates entering the separation system of a process. Batch plants without recycle are normally operated near the maximum yield. In this example, the maximum yield for a single phase reactor is about 35 % at a conversion of about 60 %, giving a selectivity of about 58 %. A separative reactor in a counter-current device significantly improves *all* these quantities simultaneously, giving a maximum yield of about 65 % at a conversion of about 90 %, with a selectivity of about 72 %. Therefore, significant savings in raw materials, and significant decrease in waste by-products can be expected by using counter-current reactive separators to carry out the reactions. Such a configuration can also be expected to increase the conversion in equilibrium limited reactions.

The logical next step in device development is to consider a RD column. The feasible products from such a device are estimated using the approach described next.

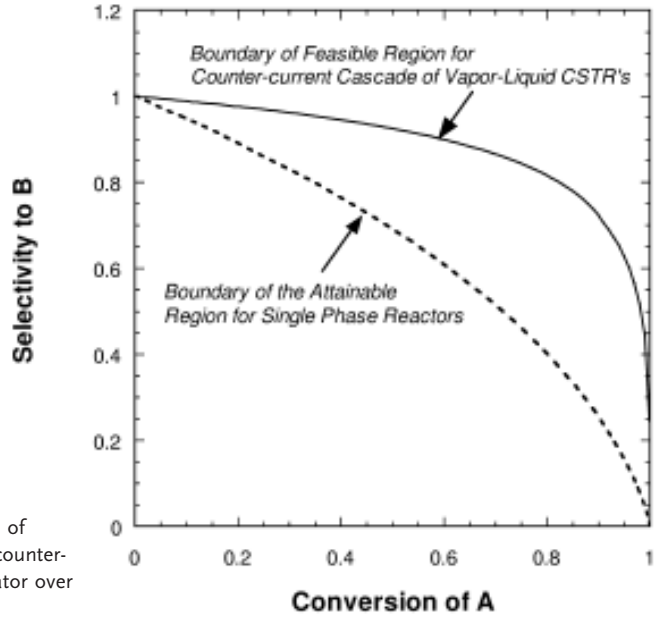

Fig. 6.6 Improvement of selectivity to *B* using counter-current reactive separator over conventional reactors

6.3 Flash Cascade Model

In a distillation column, each section (rectifying or stripping) can be effectively represented by a counter-current cascade of flashes. This cascade can be simplified for the purpose of estimating feasible product compositions, by removing the counter-current recycling of liquid and vapor flows among successive flash units, leaving a co-current arrangement shown in Fig. 6.7. The compositions of the liquid and vapor streams in the flash cascade arrangement are close to those of the counter-current cascade and by extension, to those in a column section. The two arrangements (counter-current against co-current) differ mainly in that the recovery of the key components in the counter-current cascade is much higher than in the flash cascade arrangement [25]. In a feasibility analysis, it is the product compositions that we are trying to estimate, so we use the simpler co-current flash cascades to study the feasibility of reactive mixtures in continuous columns.

We formulate the reactive flash model for an equimolar chemistry. Next, we hypothesize a condition under which the trajectories of the flash cascade model lie in the feasible product regions for continuous RD. This hypothesis is tested for an example mixture at different rates of reaction. The fixed point criteria for the flash cascade are derived and a bifurcation analysis shows the sharp split products from a continuous RD.

A schematic of the co-current flash cascade arrangement is shown in Fig. 6.7. There are two sections. In the rectifying cascade, vapor from each flash reactor

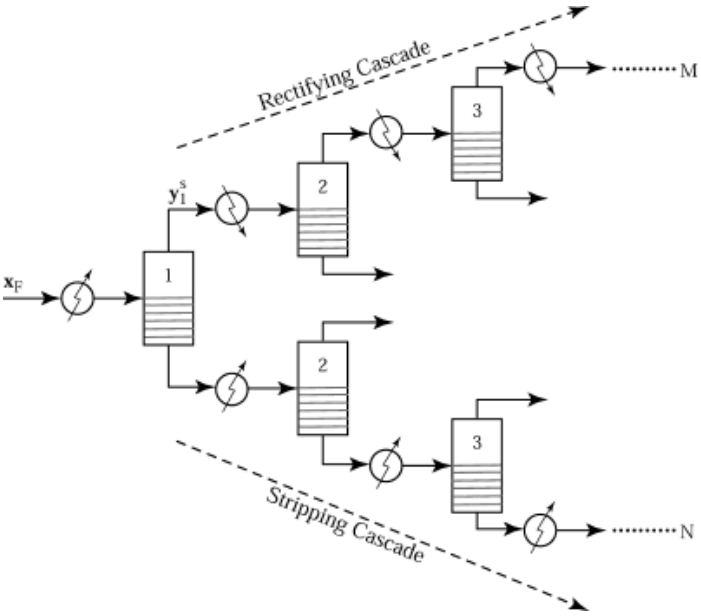

Fig. 6.7 A co-current flash cascades arrangement. The top half is the rectifying cascade and the bottom half is the stripping cascade

is partially condensed and fed to the next unit. This vapor cascade is similar to the rectifying section of a continuous distillation column but without any liquid recycling. The opposite is done for the stripping cascade shown in the bottom half of the figure, where the liquid stream from each flash device is partially vaporized and sent as feed to the next unit in the series.

Each flash device in Fig. 6.7 is a two phase CSTR reactor-separator with chemical reaction occurring only in the liquid phase. For simplicity we begin with a single reaction, an equimolar chemistry, a saturated liquid feed, and steady state conditions [5]. The flash devices operate under isobaric conditions, so that the temperature changes from stage to stage according to the boiling point of the stage composition.

The overall mass balance for the j^{th} unit in the stripping cascade in Fig. 6.1 is

$$L_{j-1} = V_j + L_j \quad (j = 1 \ldots N) \tag{6.5}$$

The material balance for the jth component is

$$L_{j-1}x_{i,j-1} = V_j y_{i,j} + L_j x_{i,j} - v_i k_f H_j r(x_j) \quad (i = 1 \ldots c-1,\ j = 1 \ldots N) \tag{6.6}$$

where L and V are liquid and vapor molar flows; x_i and y_i are the liquid and vapor phase mole fractions for component i; v_i is the stoichiometric coefficient for component i ($v_i < 0$ for reactants, $v_i > 0$ for products); k_f is the forward rate constant

with the dimensions of reciprocal time; H_j is the molar liquid holdup in the jth flash unit and $r(x)$ is the reaction driving force

$$r(x) = \left(\prod_{\text{reac tan ts}} a_i^{-\nu_i} - \prod_{\text{products}} \frac{a_i^{\nu_i}}{K_{\text{eq}}} \right) \tag{6.7}$$

where K_{eq} is the chemical equilibrium constant and a_i is the activity for component i. For liquid phase reactions, activities are represented by the product of the activity coefficient, γ_i and the liquid phase composition, $a_i = \gamma_i\, x_i$.

Eliminating L_j from (6.6) leads to

$$x_{i,j-1} - x_{i,j} = \frac{V_j}{L_{j-1}} (y_{i,j} - x_{i,j}) - \nu_i k_{\text{f}} \frac{H_j}{L_{j-1}} r(x_j) \quad (i = 1 \ldots c-1,\ j = 1 \ldots N) \tag{6.8}$$

We define two dimensionless parameters:

- $\phi_j = V_j / L_{j-1}$, the fraction of feed vaporized in the jth unit.
- $Da_j = (H_j / L_{j-1}) / (1/k_{\text{f, ref}})$, the Damköhler number for unit j.

This is the ratio of the characteristic liquid residence time to a characteristic reaction time. $k_{\text{f, ref}}$ is the forward rate constant at a reference temperature, T_{ref}. No reaction occurs in the limit $Da_j \to 0$ and reaction equilibrium is achieved as $Da_j \to \infty$. At intermediate Da_j, the stage operates in the kinetically controlled regime.

Incorporating ϕ_j and Da_j in (6.8), we find

$$x_{i,j-1} - x_{i,j} = \phi_j (y_{i,j} - x_{i,j}) - \nu_i \left(\frac{k_{\text{f}}}{k_{\text{f, ref}}} \right) Da_j r(x_j) \quad (i = 1 \ldots c-1,\ j = 1 \ldots N) \tag{6.9}$$

ϕ_j and Da_j are two independent parameters for each flash unit. We study the cases in which

the same fraction of feed is vaporized in each stage

- $\phi_1 = \phi_2 = \ldots = \phi_j = \ldots \phi_N = \phi$ (6.10)

each flash stage has the same residence time

- $Da_1 = Da_2 = \ldots = Da_j = \ldots = Da_N = Da$ (6.11)

These two assumptions imply that the vapor rate and the liquid hold-up both decrease along the cascade for a fixed feed flow rate. This produces a policy of decreasing vapor rate along the cascade similar to a decreasing vapor rate policy in simple (batch) distillation, which keeps the instantaneous value of Da approximately constant [47].

The model for the stripping cascade becomes

$$x_{i,j-1} = \phi\, y_{i,j} + (1-\phi) x_{i,j} - \nu_i \left(\frac{k_{\text{f}}}{k_{\text{f, ref}}} \right) Da\, r(x_j) \quad (i = 1 \ldots c-1,\ j = 1, 2 \ldots N) \tag{6.12}$$

where $\boldsymbol{x}_0 = \boldsymbol{x}_{\text{F}}$.

It is convenient to introduce a dimensionless parameter [48]

$$D = \frac{Da}{1 + Da} \tag{6.13}$$

where D varies from 0 for the case of no reaction to unity in the limit of reaction equilibrium.

Including (6.13) in (6.12), gives the final formulation of the stripping cascade

$$x_{i,j-1} = \phi\, y_{i,j} + (1-\phi)x_{i,j} - v_i\left(\frac{k_f}{k_{f,\,ref}}\right)\left(\frac{D}{1-D}\right)r(x_j) \quad (i = 1 \ldots c-1,\ j = 1, 2 \ldots N) \tag{6.14}$$

where $\boldsymbol{x}_0 = \boldsymbol{x}_F$.

Equation (6.14) can be solved recursively for given values of the parameters, ϕ and D starting with the initial condition, $\boldsymbol{x}_0 = \boldsymbol{x}_F$. The solution is a trajectory of liquid compositions for the stripping cascade.

We can also derive a model for the rectifying cascade

$$y_{i,j-1} = \phi\, y_{i,j} + (1-\phi)x_{i,j} - v_i\left(\frac{k_f}{k_{f,\,ref}}\right)\left(\frac{D}{1-D}\right)r(x_j) \quad (i = 1 \ldots c-1,\ j = 2, 3 \ldots M) \tag{6.15}$$

where $\boldsymbol{y}_1 = \boldsymbol{y}_1^s$, and $\boldsymbol{y}_1^s$ is the vapor stream composition from the first flash device of the stripping cascade shown in Fig. 6.7. The solution to (6.15) is a trajectory of vapor phase compositions along the rectifying cascade.

Equations (6.14) and (6.15) model the co-current stripping and rectifying cascades, respectively. For a given feed composition, these cascades are solved recursively for $N,\ M \to \infty$, until there is no change in successive iterates, that is, until a stable fixed point is reached.

We demonstrate the use of this model on an example and then characterize its properties in terms of fixed points and bifurcations.

6.4 Feasibility Hypothesis

The flash cascade provides a two parameter (ϕ and D) model ((6.14) and (6.15)). The iterates depend primarily on the value of D. The pinch points towards which these iterates evolve depend only on a single parameter, (Da/ϕ). Therefore, the solution structure is not dependent on the value of ϕ, and we may choose any value of ϕ (we pick $\phi = 0.5$). This simply rescales the value of Da at which bifurcations occur.

> **Hypothesis:** The trajectories of the flash cascades lie in the feasible product regions for continuous RD.

We test this hypothesis with an example. Consider the esterification of acetic acid with isopropanol at a pressure of 1 atm.

$$\mathrm{IPA} + \mathrm{HOAc} \rightleftharpoons \mathrm{IPOAc} + \mathrm{H_2O} \tag{6.16}$$

We present the kinetics by a homogeneous model.

$$r = k_f \left(a_{\mathrm{HOAc}} a_{\mathrm{IPA}} - \frac{a_{\mathrm{IPOAc}} a_{\mathrm{H_2O}}}{K_{\mathrm{eq}}} \right) \tag{6.17}$$

where k_f is approximately independent of temperature, $(k_f/k_{f,\,\mathrm{ref}}) = 1$, and the reaction equilibrium constant has a value of 8.7 in the temperature range of interest [30]. The vapor–liquid equilibrium (VLE) was modeled using the Antoine vapor pressure equation, the NRTL equation for activity coefficients, and including vapor phase dimerization of acetic acid. The physical property models were taken from Table 3 in Venimadhavan et al. [48].

Solutions of (6.14) and (6.15), the rectifying and stripping cascade flash trajectories, can be represented in mole fraction space (three dimensional for the IPOAc system). However, we represent the solutions in transformed composition space, which is two dimensional for IPOAc system (for a derivation and properties of these transformed variables [46]). This transformed composition space is a projection of a three dimension mole fraction space onto a two dimensional transformed composition subspace for the IPOAc system. Even though the correspondence between real compositions and transformed compositions is not one-to-one in the kinetic regime, we will make use of these transforms because of ease of visualization of the trajectories, and because overall mass balance for reactive systems (kinetically or equilibrium limited) can be represented with a lever rule in transformed compositions. We use this property to assess feasible splits for continuous RD.

If we select IPOAc as the reference component, then the definition given in Ung and Doherty [46] gives the transformed variables

$$\begin{aligned} X_1 &= x_{\mathrm{HOAc}} + x_{\mathrm{IPOAc}} \\ X_2 &= x_{\mathrm{IPA}} + x_{\mathrm{IPOAc}} \end{aligned} \tag{6.18}$$

Similar expressions are obtained for the transformed variables in the vapor phase, Y_i.

The trajectories of the flash cascades for an equimolar feed ($x_{F,\mathrm{HOAc}} = 0.5$, $x_{F,\mathrm{IPA}} = 0.5$), are shown in Fig. 6.8 for $D = 0.25$ and $D = 0.75$. The stripping cascade is solved recursively for this feed composition via (6.14) for a large number of stages until a point is reached where the composition is essentially constant from stage to stage. This pinch point (stable node) is acetic acid. The mole fraction iterates are then converted to the transformed compositions using (6.18). In similar fashion, the rectifying cascade model (6.15) is solved recursively for a large number of stages until a pinch point (stable node) is reached; in this case it is a quaternary mixture. These vapor mole fractions so obtained are then converted to transformed compositions and are shown in Fig. 6.8.

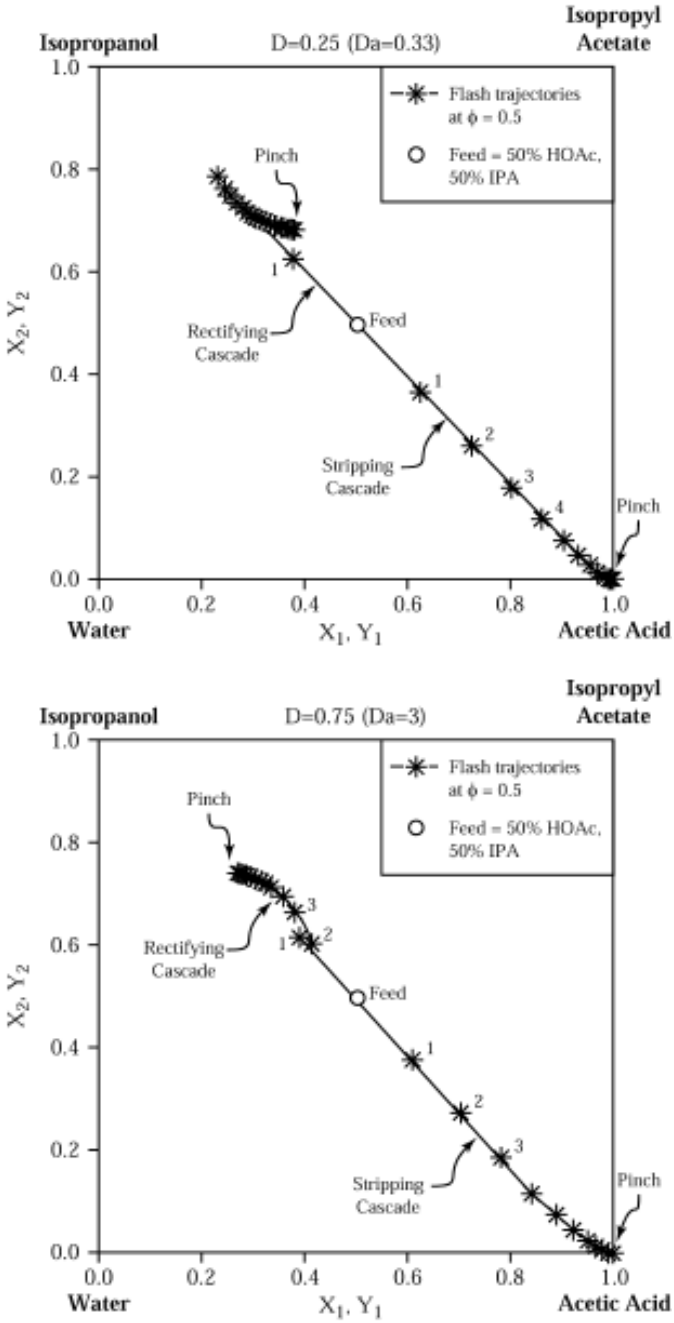

Fig. 6.8 Rectifying and stripping cascade trajectories for a saturated liquid equimolar reactant feed for the IPOAc system at $D = 0.25$ and $D = 0.75$. The trajectories are plotted in transformed mole fraction space. For the stripping cascade, $X_1 = x_{HOAc} + x_{IPOAc}$, $X_2 = x_{IPA} + x_{IPOAc}$ and for the rectifying cascade, $Y_1 = y_{HOAc} + Y_{IPOAc}$, $Y_2 = y_{IPA} + y_{IPOAc}$

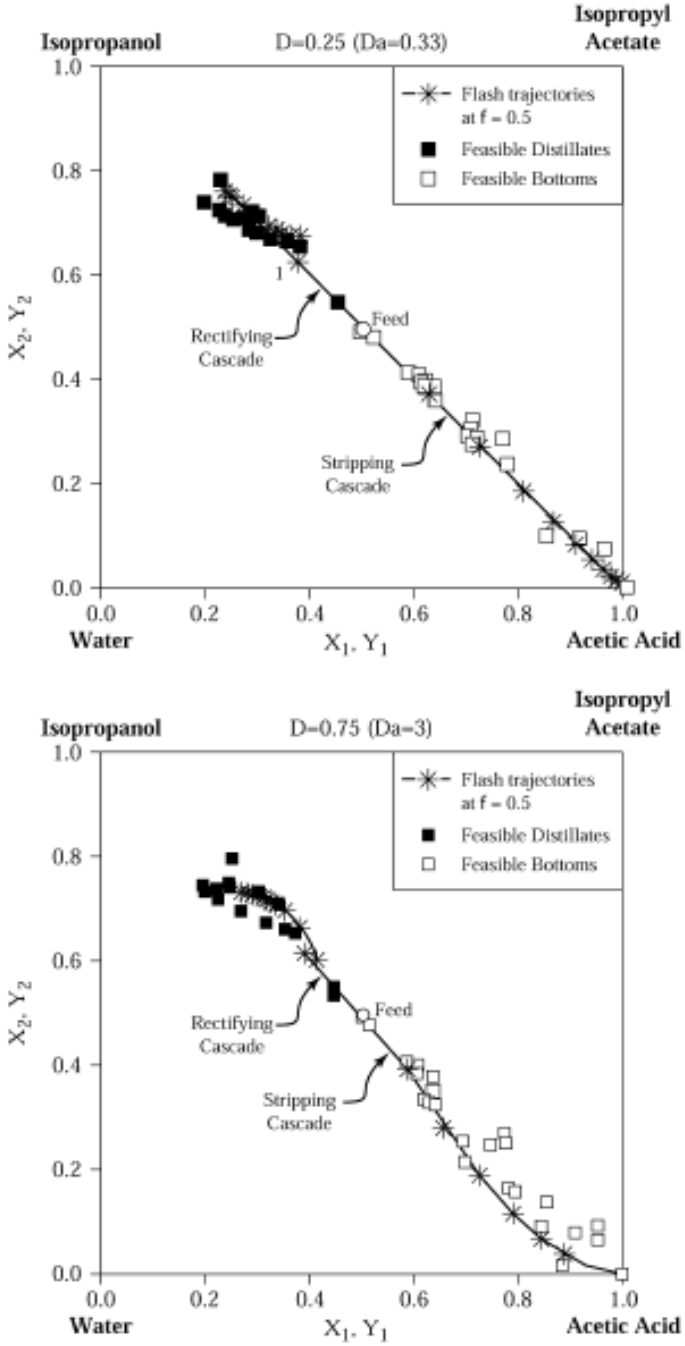

Fig. 6.9 Feasible products from column simulations with different N_T, feed stage location, r, s, and D recorded in transformed variable space. The filled squares represent feasible bottoms and the open squares represent feasible distillates. The rectifying and stripping cascade trajectories from Fig. 6.8 are also shown for comparison

Parametric column simulations for the IPOAc system were performed with different Damköhler numbers, reflux ratios, reboil ratios as well as total number of stages, (N_T) and feed tray location, (f). The distillate and bottoms compositions obtained were recorded in transformed composition space. Fig. 6.9 compares the products obtained from column simulations with 30 stages and using different values of r and s at $D = 0.25$ and $D = 0.75$. The column feed specification is the same as that to the co-current flash cascade. The flash trajectories provide a good estimate of the product compositions from a continuous column. We also compared the product compositions from column simulations with the flash trajectories in mole fraction space. We found that product compositions from column simulations surrounded the flash trajectories, in agreement with the hypothesis that the flash trajectories lie in the feasible product regions for continuous RD.

Note that calculating the flash trajectories at $\phi = 0.5$ does not provide the entire feasible product regions for continuous RD, but instead generates a subset of the feasible products. Selecting an iterate on the stripping cascade trajectory as a potential bottoms and an iterate on the rectifying cascade trajectory as a potential distillate does not guarantee that these products can also be obtained simultaneously from a RD column. This is simply because these product compositions may not simultaneously satisfy the overall mass balance for a reactive column. However, when the flash trajectories are used in conjunction with the lever rule for a continuous reactive column, the feasible splits for continuous RD can be quickly predicted.

Next, we derive the fixed-point criteria for the flash cascades and use bifurcation theory to propose rules to estimate feasible products.

6.5
Bifurcation Analysis of the Flash Cascade Model

The fixed points of the flash cascade model are the solutions of equations (6.14) and (6.15) for $j \to \infty$. In other words, successive liquid and vapor mole fractions reach constant values. The fixed points, $\hat{x}$, for the stripping cascade (6.14) are solutions of

$$(1 - D)(\hat{x}_i - \hat{y}_i) + v_i \left(\frac{k_f}{k_{f,\,ref}}\right)\left(\frac{D}{\phi}\right) r(\hat{x}) = 0 \quad (i = 1 \ldots c - 1) \tag{6.19}$$

where $\hat{x}$ and $\hat{y}$ are in vapor liquid equilibrium with each other.

Similarly, the fixed points, $\hat{y}$, for the rectifying cascade (6.15) are solutions of

$$-(1 - D)(\hat{x}_i - \hat{y}_i) + v_i \left(\frac{k_f}{k_{f,\,ref}}\right)\left(\frac{D}{1-\phi}\right) r(\hat{x}) = 0 \quad (i = 1 \ldots c - 1) \tag{6.20}$$

The fixed points obtained by solving (6.15) for a large number of iterates are stable nodes in the rectifying cascade. The same fixed points will form a subset of solu-

tions to equation (6.20). However, to have an analogy between this work and the earlier work done in non-reactive and equilibrium limited RD, we rewrite equation (6.20) as

$$(1 - D)(\hat{x}_i - \hat{y}_i) - \nu_i \left(\frac{k_f}{k_{f,\,ref}}\right)\left(\frac{D}{1-\phi}\right) r(\hat{x}) = 0 \quad (i = 1 \ldots c - 1) \tag{6.21}$$

where $\hat{x}$ and $\hat{y}$ are in vapor liquid equilibrium with each other.

Equation (6.21) has the same fixed points as (6.20); *except that their stability is reversed*. Thus, a fixed point which is a stable node in equation (6.20) becomes an unstable node for equation (6.21).

The solutions for equations (6.19) and (6.21) behave as follows. At $D = 0$ (the non-reactive limit), the fixed point criteria for both the rectifying and stripping cascades reduce to the same equation

$$\hat{x}_i - \hat{y}_i = 0 \quad (i = 1 \ldots c - 1) \tag{6.22}$$

Equation (6.22) is the fixed point criteria for simple distillation and also for a continuous column at total reflux and total reboil. Since there is a symmetry in the rectifying and stripping maps, we can find the fixed points for *both* the rectifying and stripping cascades from equation (6.22). Thus, in this limit, our model recovers the criterion for fixed points in the well-known limit of no-reaction. At $D = 1$ (the chemical equilibrium limit), the fixed point criteria reduce to a single equation

$$r(\hat{x}) = 0 \tag{6.23}$$

Equation (6.23) implies that fixed points lie on the reaction equilibrium surface. Equation (6.23), however, is just a necessary condition; the sufficient condition for fixed points of the rectifying and stripping cascades can be written in terms of transformed variables by writing either (6.19) or (6.21) for component i and a reference component, k and adding the two, giving

$$\hat{X}_i - \hat{Y}_i = 0 \quad (i = 1 \ldots c - 2) \tag{6.24}$$

The solutions of equation (6.24) are fixed points for simple RD at chemical equilibrium and also for a continuous RD at total reflux and total reboil. As in the non-reactive case, the fixed point criteria for the rectifying and stripping cascades are the same and is given by equations (6.23) and (6.24). Once again our model reduces to the well-known criteria for chemical equilibrium fixed points.

For $0 < D < 1$ (kinetically controlled regime), (6.19) gives the fixed points of the stripping cascade and (6.21) the fixed points of the rectifying cascade. Therefore, in the kinetic regime, there are *different* fixed point criteria for the rectifying and stripping cascades, a fact that has not been previously recognized. The solutions of equation (6.19) at $\phi = 1$ are the fixed points for simple RD [48], but the structure of the solutions to equation (6.21) has not been reported. As we shall see, it can be

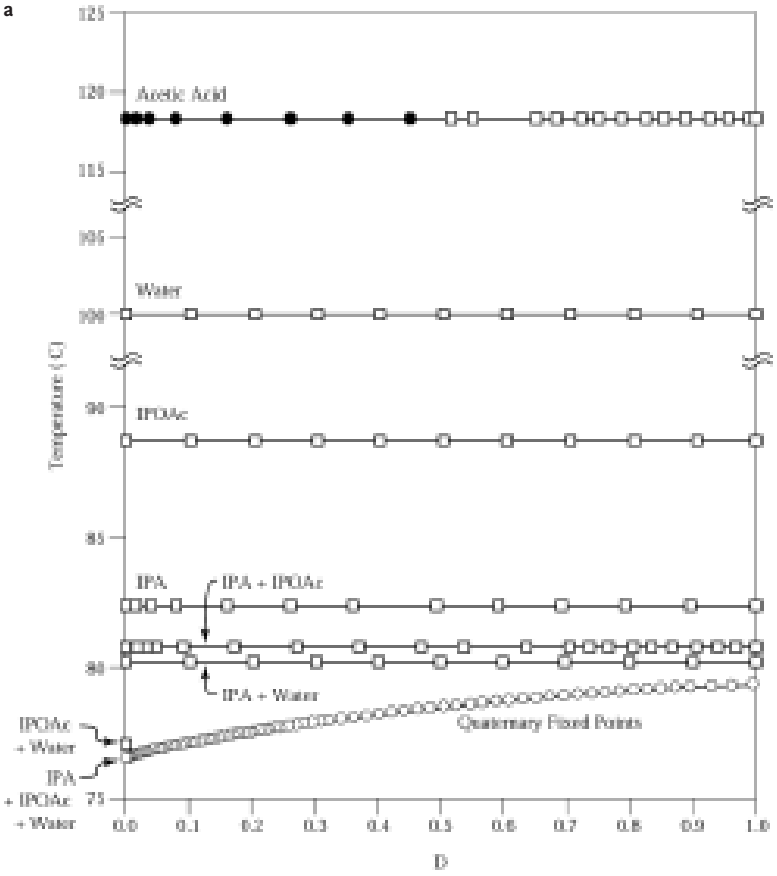

Fig. 6.10 Bifurcation diagrams for the (a) rectifying and (b) stripping cascades. The filled circles denote stable node branches, open circles denote unstable node branches, and the open squares denote saddle branches

quite different than for equation (6.19). Since fixed points for simple RD are equivalent to the fixed points of the stripping cascade at $\phi = 1$, they can only provide information about the potential bottoms product from a continuous column. *Therefore, the distillate product composition from a continuous column for $0 < D < 1$ cannot be inferred from a knowledge of fixed points of simple RD.* However, it is possible to estimate potential distillates from the fixed points of the rectifying flash cascade (equation (6.21)).

We are interested in investigating the fixed-point branches of the flash cascade model for $0 \leq D \leq 1$ at $\phi = 0.5$. A systematic approach is by a bifurcation analysis of the solutions, $\hat{x}(D)$, for (6.19) and (6.21). The starting points for the analysis are the solutions at $D = 0$; to calculate these points, a homotopy continuation method is available [14]. We use the mixture boiling point, $T(\hat{x}(D))$, to represent the solu-

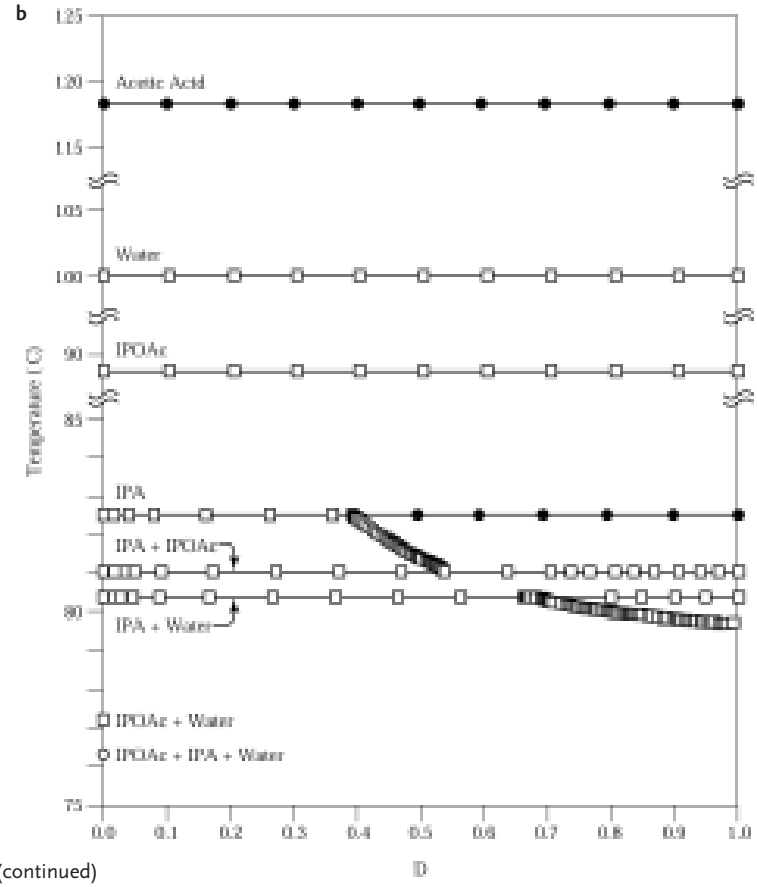

Fig. 6.10 (continued)

tion. The branches of fixed points were calculated using the pseudo-arclength continuation method in Auto [8].

For the IPOAc system, the fixed point branches are shown in bifurcation diagrams for the rectifying and stripping cascades in Fig. 6.10. The left edge of the diagrams ($D = 0$) represents the limit of no reaction. Here, there is a minimum boiling ternary azeotrope containing isopropanol, isopropyl acetate, and water, which is an unstable node; six intermediate boiling fixed points (all saddles); acetic acid is the heaviest species (stable node). Starting from these initial conditions, fixed point branches are tracked for both the rectifying and stripping cascades.

The branches of interest are the unstable nodes in the rectifying bifurcation diagram and the stable nodes in the stripping cascade bifurcation diagram. These node branches are shown separately in a *feasibility diagram*, Fig. 6.11.

The feasibility diagram provides a global view of the feasible products to expect from a continuous distillation at any rate of reaction (D). For any feed composition and for D in the range, $0 \leq D \leq 0.395$, it is possible to obtain acetic acid as bot-

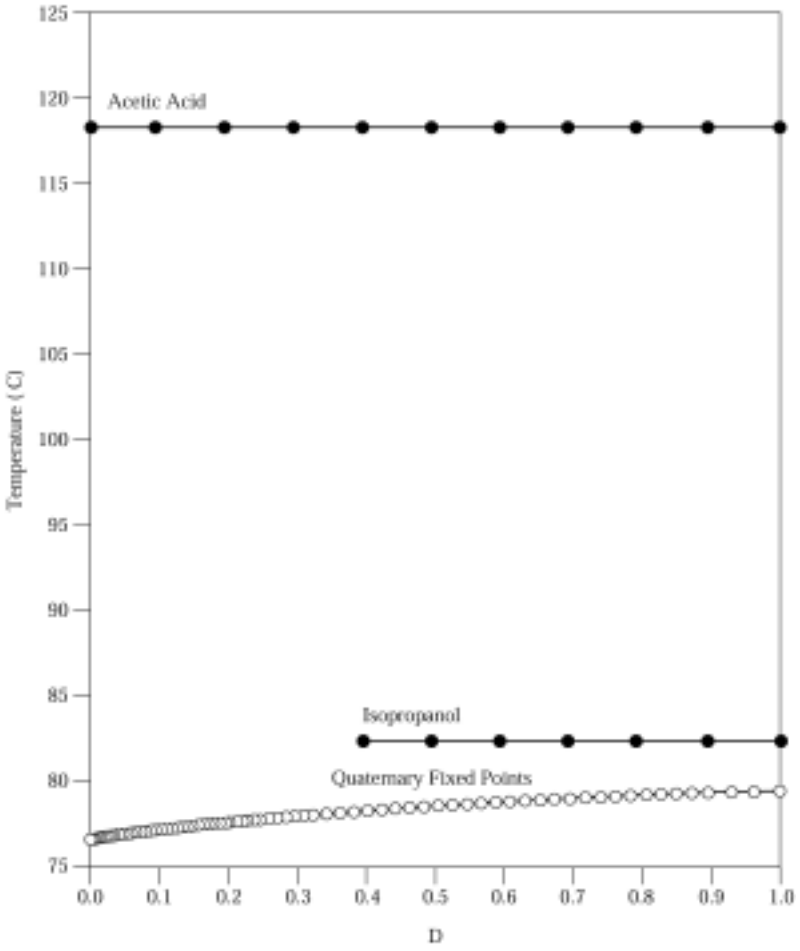

Fig. 6.11 Feasibility diagram showing the feasible distillates (unstable nodes) and feasible bottom products (stable nodes) from the rectifying and stripping cascade bifurcation diagrams, respectively

toms from a continuous RD. However, for $0.395 \leq D \leq 1$ we can obtain either isopropanol or acetic acid as the bottoms product depending on the feed composition. The potential distillates are all quaternary mixtures, with compositions that depend on D. Thus, different splits are feasible for different ranges of the Damköhler number. Conversely, any given split may or may not be feasible as the reaction rate or residence time is changed, so that the feasibility of a given separation may depend on production rates, catalyst levels, and liquid holdup. The results mean that IPOAc cannot be obtained as a pure product from a single-feed fully reactive column, no matter what rate of reaction the column is operated at.

Thus, we propose the following rule.

Rule for Feasible Products: Unstable node branches in the feasibility diagram represent potential distillates while the stable node branches represent the potential bottoms from a continuous RD column.

Chadda et al. [5] have compared the predictions made by this approach with detailed column simulations at values of $D = 0.25$ and $D = 0.75$ using the methods described in Huss et al. [27], and find the predictions to be in good agreement with the simulations.

6.6 Conclusions

Geometric methods provide a useful framework for assessing the process opportunities of combining reaction and separation. The attainable region can be used to estimate the incentive for developing process technology based on single-stage, and multi-stage vapor-liquid reactors. In some instances, this may lead to process alternatives based on RD.

A flash cascade model is developed to estimate feasible products from a continuous single-feed RD column. An important finding is that the fixed point structures for the rectifying and stripping cascades are *different* for the kinetically controlled regime. The fixed point structure of the flash cascade model is helpful in determining the reaction regime in which the column must be operated to get the desired products. We used a feasibility diagram to depict possible *direct* and *indirect split* products as a function of production rate, catalyst level, and liquid holdup. With this diagram one can quickly determine if a desired product can be obtained from a single-feed reactive column.

Feasibility analysis for RD has advanced to the point that useful engineering methods can be implemented relatively easily. Attainable region methods, however, are still relatively new and there remains significant potential for developing a framework to generate process alternatives with combined reaction and separation using this approach. If these methods could be developed further, it should be possible to link attainable region methods to feasibility methods to build a useful design tool (synthesis methodology) for generating and screening process alternatives for multifunctional reactor-separator devices.

6.7 Notation

a_i	activity of i
c	total number of components
D	scaled Damköhler number, dimensionless
Da	Damköhler number, dimensionless
f	feed stage location in a continuous distillation column

F molar flow rate
H_j liquid holdup in unit j, mol
K_{eq} reaction equilibrium constant
k_f forward reaction rate constant, 1/time
$k_{f,\,ref}$ forward reaction rate constant at the reference temperature
L liquid flow rate, (mol/time)
P system pressure
M index for rectifying cascade flash unit
N index for stripping cascade flash unit
N_T total number of stages in a continuous distillation column
$r(\boldsymbol{x})$ driving force for the reaction
r reflux ratio
s reboil ratio
T temperature
V vapor flow rate, mol/time
$\boldsymbol{x}$ state vector
x_i mole fraction of i in the liquid phase
X_i transformed mole fraction of i in the liquid phase
y_i mole fraction of i in the vapor phase
Y_i transformed mole fraction of i in the vapor phase

Greeks

γ_i liquid activity coefficient
v_i stoichiometric coefficient for i
v_T summation of all stoichiometric coefficients
ϕ_j fraction of feed vaporized in jth flash unit

Subscripts and superscripts

0 initial condition
B bottoms
D distillate
F feed
T total
eq equilibrium
f forward reaction
i component index
j stage index for flash cascade
k reference component
ref reference
$\wedge$ pinch composition

References

1 Barbosa, D.; Doherty, M. F. *Chem. Eng. Sci.* **1988**, *43*, 1523.
2 Buzad, G.; Doherty, M. F. *Chem. Eng. Sci.* **1994**, *49*, 1947.
3 Buzad, G.; Doherty, M. F. *Comp. Chem. Eng.* **1995**, *19*, 395.
4 Chadda, N.; Malone, M. F.; Doherty, M. F. *AIChE J.* **2000**, *46*, 923.
5 Chadda, N.; Malone, M. F.; Doherty, M. F. *AIChE J.* **2001**, *47*, 590.
6 Ciric, A. R.; Gu, D. *AIChE J.* **1994**, *40*, 1479.
7 Damköhler, G. *Chem. Ing. Tech.* **1939**, *12*, 469.
8 Doedel, E. *AUTO: Software for Continuation and Bifurcation Problems in Ordinary Differential Equations*. Dept. of Mathematics, California Institute of Technology, Pasadena, CA, **1986**.
9 Espinosa, J.; Aguirre, P. A.; Perez, G. A. *Ind. Eng. Chem. Res.* **1995**, *34*, 853.
10 Feinberg, M.; Hildebrandt, D. *Chem. Eng. Sci.* **1997**, *52*, 1637.
11 Feinberg, M. *Chem. Eng. Sci.* **2000**, *55*, 2455.
12 Feinberg, M. *Chem. Eng. Sci.* **2000**, *55*, 3553.
13 Feinberg, M. submitted to *Ind. Eng. Chem. Res.* **2000**.
14 Fidkowski, Z. T.; Doherty, M. F.; Malone, M. F. *Comp. Chem. Eng.* **1992**, *17*, 1141.
15 Fidkowski, Z. T.; Doherty, M. F.; Malone, M. F. *AIChE J.* **1993**, *39*, 1303.
16 Gadewar, S. B.; Malone, M. F.; Doherty, M. F. submitted to *AIChE J.* **2001**.
17 Giessler, S.; Danilov, R. Y.; Pisarenko, R. Y.; Serafimov, L. A.; Hasebe, S.; Hashimoto, I. *Ind. Eng. Chem. Res.* **1998**, *37*, 4375.
18 Giessler, S.; Danilov, R. Y.; Pisarenko, R. Y.; Serafimov, L. A.; Hasebe, S.; Hashimoto, I. *Ind. Eng. Chem. Res.* **1999**, *38*, 4060.
19 Glasser, D.; Hildebrandt, D.; Crowe, C. *Ind. Eng. Chem. Res.* **1987**, *26*, 1803.
20 Glasser, B.; Hildebrandt, D.; Godorr, S. *Ind. Eng. Chem. Res.* **1992**, *31*, 1541.
21 Glasser, D.; Hildebrandt, D.; Godorr, S. *Ind. Eng. Chem. Res.* **1994**, *33*, 1136.
22 Godorr, S. A.; Hildebrandt, D.; Glasser, D. *Chem. Eng. J.* **1994**, *54*, 175.
23 Hildebrandt, D.; Glasser, D. *Chem. Eng. Sci.* **1990**, *45*, 2161.
24 Hildebrandt, D.; Glasser, D.; Crowe, C. *Ind. Eng. Chem. Res.* **1990**, *29*, 49.
25 Henly, E. J.; Seader, J. D. *Equilibrium Stage Separation Operations in Chemical Engineering*, John Wiley, **1981**.
26 Horn, F. in *Proc. Eur. Symp. Chemical Reaction Engineering*, Pergamon Press, New York, **1964**, 293.
27 Huss, R. S.; Chen, F.; Malone, M. F.; Doherty, M. F. *Comp. Chem. Eng.* **1999**, S1955..
28 Ismail, S. R.; Pistukopolous, E. N.; Papalexandri, K. P. *Chem. Eng Sci.* **1999**, *54*, 2721.
29 Lakshmanan, A.; Biegler, L. T. *Ind. Eng. Chem. Res.* **1996**, *35*, 1344.
30 Lee, L.-S.; Kuo, M.-Z. *Fluid Phase Equilib.* **1996**, *123*, 147.
31 Levenspiel, O., *Chemical Reaction Engineering*, 2nd edn, John Wiley, New York, **1972**, Ch. 7.
32 McGregor, C.; Glasser, D.; Hildebrandt, D. *Distillation and Absorption, '97, IChemE Symposium Series*. **1997**, *142*, 663.
33 Nisoli, A.; Malone, M. F.; Doherty, M. F. *AIChE J.* **1997**, *43*, 374.
34 Okasinski, M. J.; Doherty, M. F. *Ind. Eng. Chem. Res.* **1998**, *37*, 2821.
35 Pahor, B.; Irsic, N.; Kravanja, Z. *Comp. Chem. Eng.* **2000**, *24*, 1403.
36 Papalexandri, K. P.; Pistukopolous, E. N. *AIChE J.* **1996**, *42*, 1010.
37 Rev, E. *Ind. Eng. Chem. Res.* **1994**, *33*, 2174.
38 Rooks, R. E.; Julka, V.; Doherty, M. F.; Malone, M. F. *AIChE J.* **1998**, *44*, 1382.
39 Rooney W. C.; Hausberger, B. P.; Biegler, L. T.; Glasser, D. *Comp. Chem. Eng.* **2000**, *24*, 225.
40 Sharma, M. M.; Mahajani, S. M. in *Reactive Distillation* (Eds Sundmacher, K.; Kienle, A.), Wiley-VCH, Weinheim, Germany, **2002**.

41 Smith, R. L.; Malone, M. F. *Ind. Eng. Chem. Res.* **1997**, *36*, 1076.
42 Safrit, B. T.; Westerberg, A. W. *Ind. Eng. Chem. Res.* **1997**, *36*, 1841.
43 Shinnar, R.; Feng, C. A. *Ind. Eng. Chem. Fundam.* **1985**, *24*, 153.
44 Stichlmair, J. G.; Herguijuela, J. R. *AIChE J.* **1992**, *38*, 1523.
45 Thiel C.; Sundmacher, K.; Hoffmann, U. *Chem. Eng. Sci.* **1997**, *52*, 993.
46 Ung, S.; Doherty, M. F. *Ind. Eng. Chem. Res.* **1995**, *34*, 2555.
47 Venimadhavan, G.; Malone, M. F.; Doherty, M. F. *AIChE J.* **1994**, *40*, 1814. Correction: *AIChE J.* **1995**, *41*, 2613.
48 Venimadhavan, G.; Malone, M. F.; Doherty, M. F. *AIChE J.* **1999**, *45*, 546.
49 Wahnschafft, O. M.; Koehler, J. W.; Blass, E.; Westerberg, A. W. *Ind. Eng. Chem. Res.* **1992**, *31*, 2345.

Reactive Distillation. Edited by Kai Sundmacher, Achim Kienle

ISBNs: 3-527-30579-3 (Hardback); 3-527-60052-3 (Electronic)

7
Hardware Selection and Design Aspects for Reactive Distillation Columns

R. Krishna

7.1
Introduction

Most of the published literature on reactive distillation (RD) has been focussed mainly on aspects such as conceptual design with the aid of residue curve maps, steady-state multiplicity and bifurcations, and development of equilibrium (EQ) stage and rigorous non-equilibrium (NEQ) steady-state and dynamic models [1, 2]. Relatively little attention has been paid to hardware design. In this chapter the concepts underlying the selection of the appropriate hardware for RD columns are discussed. For RD column design, detailed information on hydrodynamics and mass transfer for the chosen hardware is required, but this information is often lacking. Modern tools such as computational fluid dynamics (CFD) can be invaluable aids in hydrodynamic and mass-transfer studies.

7.2
Hardware for Homogeneous Reactive Distillation

First consider RD columns in which the reaction takes place in the liquid phase, without the use of a solid catalyst. For homogeneous RD processes, counter-current vapor-liquid contact, with a sufficient degree of staging in the vapor and liquid phases, can be achieved in a multitray column (Fig. 7.1) or in a column with random or structured packing (Fig. 7.2). The packing in this case is inert (i. e., non-reactive and with no catalytic properties) and serves only to provide even liquid distribution in the column and to suppress liquid-phase back-mixing. The Hatta number for most RD applications is expected to be less than unity [3] and therefore there is no enhancement of mass transfer due to chemical reaction. From the point of view of increasing the productivity of the RD column, therefore, it is important to maximize the liquid hold-up in the column. Packed columns (Fig. 7.2) usually have a much lower liquid hold-up than tray columns, so for homogeneous RD, tray columns are preferred.

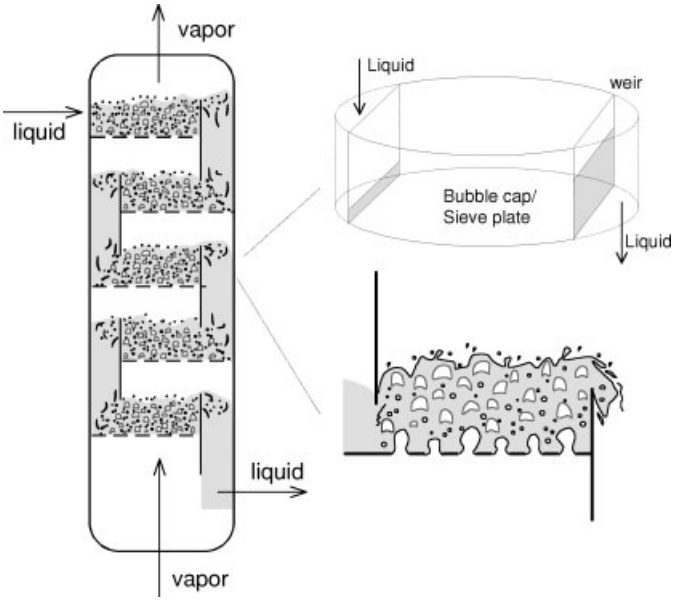

Fig. 7.1 Counter-current vapor–liquid contact in multistage tray columns. Animations of CFD simulations of flows on the tray can be viewed on our web site: http://ct-cr4.chem.uva.nl/sievetrayCFD

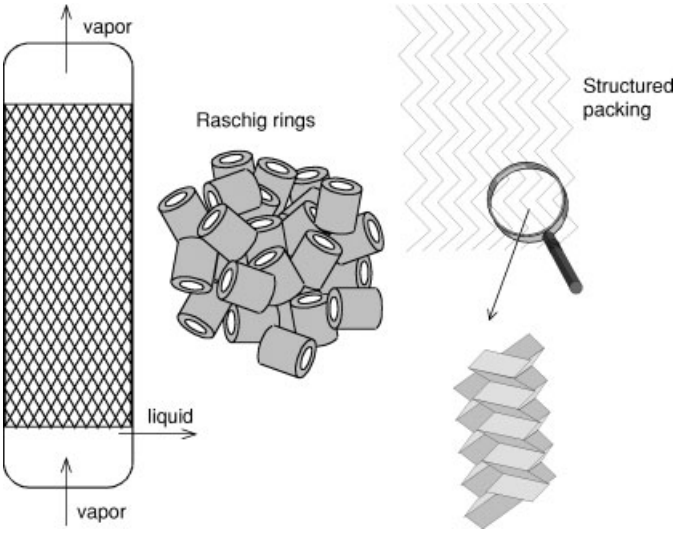

Fig. 7.2 Counter-current vapor–liquid contact in packed columns, either randomly packed (e. g., Raschig rings) or with structured packing (e. g., Sulzer BX)

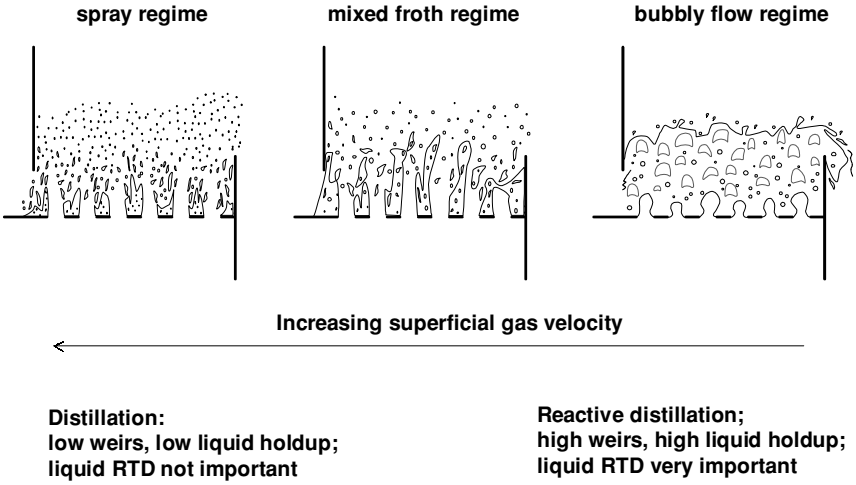

Fig. 7.3 Choice of hydrodynamic flow regimes on reactive and non-reactive trays

A tray column can be operated in the spray, mixed froth, or bubbly flow regimes (Fig. 7.3). Conventional (i. e., non-reactive) distillation columns usually operate at high superficial vapor velocities in the spray or froth regime. This is because of the desire to increase throughput in the column and to increase the vapor–liquid interfacial area. There is no need to aim for maximum liquid hold-up in conventional distillation. The situation with respect to RD is quite different. The reaction takes place in the liquid phase and in order to allow more 'room' for chemical reaction we should aim for high liquid hold-ups and liquid-phase residence times. Therefore the preferred regime of operation is the bubbly flow regime, which is achieved by operating at much lower superficial vapor velocities. The choice of higher weirs ensures higher liquid hold-up on the trays. Bubble cap trays are appropriate choices for RD columns, as these have greater liquid holding capacity than sieve trays. Furthermore, there is no danger of weeping of the liquid phase from bubble cap trays. Reverse-flow trays with additional sumps can be used to increase the liquid residence time; a specially designed tray for maximizing liquid hold-up is used in the Eastman process for methyl acetate manufacture [4].

Though the hydrodynamics of distillation tray columns is well researched and documented [5, 6], the available information is usually not sufficient for RD tray design. This is because liquid-phase residence time distribution (RTD) is not usually relevant for conventional distillation but is of crucial importance in RD tray design. Baur et al. [7] have studied the influence of tray hardware design on the conversion, and selectivity, of hydration of ethylene oxide (EO) to ethylene glycol (EG); one of their simulation results (using a rigorous NEQ stage model) is shown in Fig. 7.4.

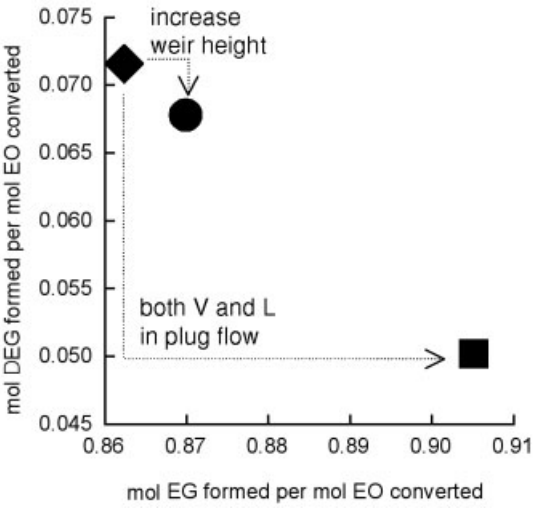

Fig. 7.4 Yield of EG (desired product) against yield of by-product DEG in an RD column for hydration of EO: simulation results of Baur et al. [7]. NEQ model calculation results are shown for three different configurations

The base case configuration is a sieve tray with a 80 mm weir height, in which the liquid and vapor phases are both considered to be well mixed. The yield of EG is plotted on the *x*-axis and the yield of by-product diethylene glycol (DEG) is plotted on the *y*-axis. The performance of the base case configuration is indicated by the large black diamond. EG production is increased and DEG production is lowered when both the liquid and vapor phases are considered to be in plug flow (large black square). Increasing the weir height from 80 to 100 mm also has a beneficial effect of increasing EG yield while decreasing DEG yield. A clever choice of hardware can enhance conversion and selectivity in RD. We need to

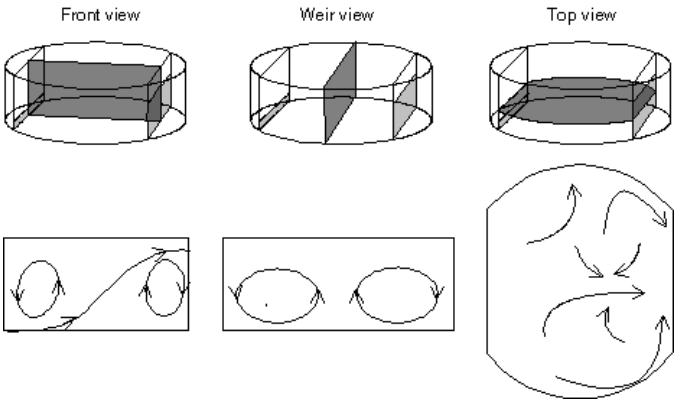

Fig. 7.5 Simplified 'snapshots' of the front, weir, and top views of sieve tray simulations at a superficial gas velocity, $U_G = 0.7$ m/s; weir height $h_w = 80$ mm; liquid weir load $Q_L/W = 1.2 \times 10^{-3}$ m^3/s/m. An animation of the simulation can be viewed on our web site: http://ct-cr4.chem.uva.nl/sievetrayCFD. The arrows indicate the liquid velocity vectors

ensure plug flow of liquid, and vapor, phases on the tray and minimize the danger of liquid phase bypassing and dead zones. Such detailed information on flows is not usually available in the literature. One way to obtain this information is to use CFD simulations [8–11]. For a sieve tray of 0.3 m diameter operating at a superficial gas velocity of $U = 0.7$ m/s in the bubbly flow regime, CFD simulations [9] underline the chaotic behavior of the liquid and gas flows and show the existence of several recirculating liquid flow patterns, as sketched in Fig. 7.5. The liquid RTD is far removed from the plug-flow conditions desired in practice. One could envisage the installation of flow straighteners in the liquid path to suppress back-mixing. CFD simulations are invaluable aids in screening various hardware configurations because they are able to capture the circulation patterns. It is, however, essential to perform fully transient 3D simulations, which are computationally expensive.

7.2.1 Case Study for Methyl Acetate Production

We shall illustrate some of the tray hardware design issues by considering a case study of the production of methyl acetate in which the reaction is catalyzed by H_2SO_4, added to the liquid phase [1]. In the RD process for methyl acetate, invented by the Eastman Chemical Company [3, 12], the entire process is carried out in a single column, as shown in Fig. 7.6. In this single column, high-purity methyl acetate is made with no additional purification steps and with no unconverted reactant streams to be recovered. By flashing off the methyl acetate from the reaction mixture, conversion is increased without using excess reactants. The reactive column has stoichiometrically balanced feeds and is designed so that the lighter reactant MeOH is fed at the bottom and the heavier acetic acid is fed at the top. The column consists of three sections. The reaction takes place predominantly in the middle section. The bottom section serves to strip off the MeOH from water and return it to the reaction zone. The vapors leaving the reactive section consists of the MeOAc–MeOH azeotrope, which is 'broken' in the rectifying section by addition of AcOH, which acts as entrainer. The RD column represents an entire chemical plant, costs one-fifth of the capital investment of the conventional process, and consumes only one-fifth of the energy. Following the design study of Doherty and Malone [1], we take each of the molar feed flows of MeOH and AcOH to be 280 kmol/h, on the stages 5 and 40. The reflux ratio is set at 1.9. The column operates at a pressure of 1 atm. We employed a partial reboiler and a total condenser. The non-reactive section contains 10 theoretical stages and 33 catalytically (homogeneous) active theoretical stages in the reactive section. Simulations of the liquid composition profiles, using the EQ stage model are shown in Fig. 7.6.

We set the column specifications, and the desired conversion and purities of MeOAc and water, to a value of 98.5 %. These specifications are only fulfilled for a fairly small range of reboil ratios: see calculations in Fig. 7.7a. For low reboil ratios, the reactants cannot be recycled efficiently and high water purities in the

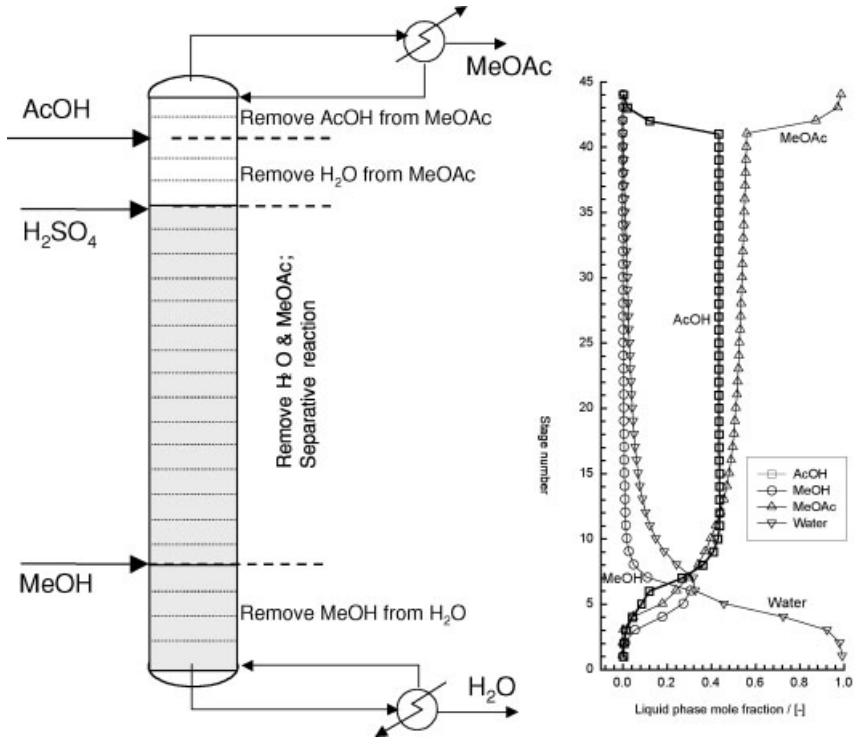

Fig. 7.6 The Eastman RD process for methyl acetate manufacture. Adapted from Agreda et al. [4]. The column composition profiles sketched on the right were obtained with an EQ model

bottom stream cannot be reached. On the other hand, if the reboil ratio is too high then the residence time in the reactive section decreases, reducing conversion. The sensitivity of the AcOH conversion to volumetric hold-up at each stage, V_{stg}, is shown in Fig. 7.7b.

If the value of V_{stg} is less than about 2 m^3, it is impossible to achieve the target AcOH conversion of 98.5 %. For a reboil ratio of, say, 1.4 it is necessary to ensure a V_{stg} of at least 2.75 m^3. Let us examine the hardware design factors that would meet this hold-up requirement. Fig. 7.8a presents the calculations for the clear liquid height and the volumetric liquid hold-up V_{stg} for a 5.7 m diameter column, operating at a range of superficial vapor velocities. We see from Fig. 7.8a that to achieve a value $V_{stg} = 2.75$ m^3, we need to operate at a superficial vapor velocity as low as 0.27 m/s, keeping the weir height at a high value of 140 mm. The operation of the reactive section is in the bubbly flow regime. For the non-reactive section at the top of the RD column, there is no corresponding requirement of liquid hold-up and a much higher superficial vapor velocity of 1.27 m/s can be chosen, along with a smaller column diameter of 2.8 m and a lower weir height of 80 mm: see Fig. 7.8b. The operation of the column is close to the transition between froth and spray regimes.

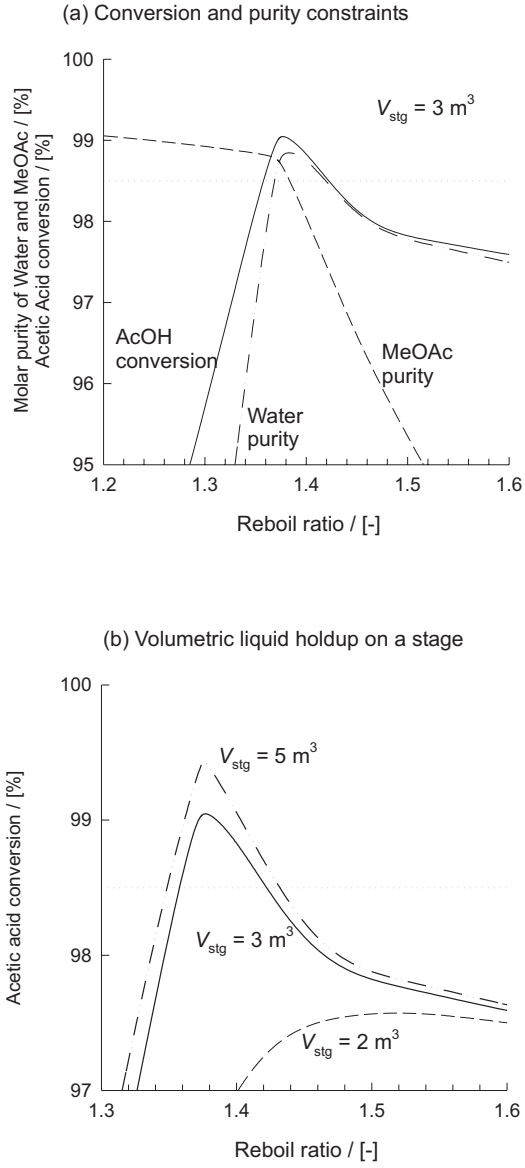

Fig. 7.7 a) Acetic acid conversion and purities of MeOAc and water in leaving product streams as a function of reboil ratio. The volumetric liquid hold-up on each reactive stage V_{stg} is set at 3 m^3. b) Acetic acid conversion as a function of the reboil ratio for various liquid hold-ups on each reactive stage

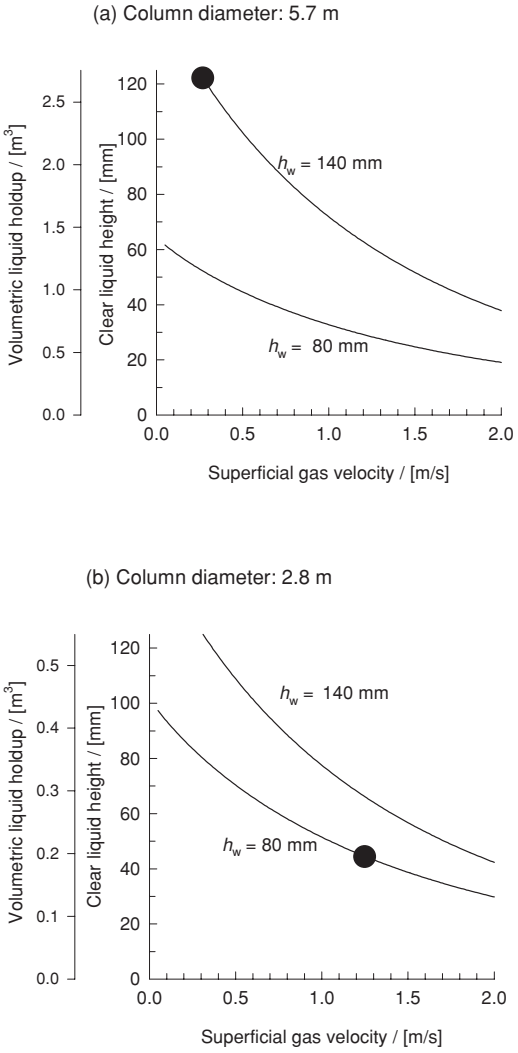

Fig. 7.8 The clear liquid height, and volumetric liquid hold-up on a tray, as a function of the superficial vapor velocity for: a) 5.7 m diameter column; b) 2.8 m diameter column. The calculations have been carried out for two weir heights $h_w = 80$ and 140 mm. The large black circles denote the chosen design conditions

Fig. 7.9 summarizes the hardware design of the RD column. Despite the large column diameter required in the reactive section (5.7 m), it is interesting to note that only 25 % of the column volume is available for 'holding up' the liquid and carrying out the reaction. The rest of the column volume is taken up by freeboard above the tray that is necessary to minimize liquid entrainment to the tray above that, causes flooding. Distillation tray columns are not efficient devices for carrying out slow liquid-phase reactions.

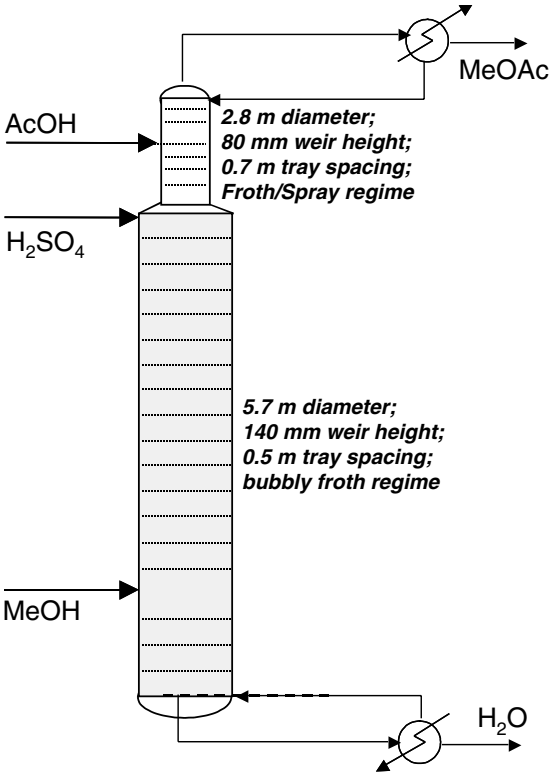

Fig. 7.9 Column configuration and tray hardware design for RD column for methyl acetate manufacture

7.3
Hardware for Heterogeneous Reactive Distillation

7.3.1
Different Hardware Configurations

For heterogeneously catalyzed processes, hardware design poses considerable challenges. The catalyst particle sizes used in such operations are usually in the 1–3 mm range. Larger particle sizes lead to intra-particle diffusion limitations. To overcome the limitations of flooding, the catalyst particles have to be enveloped within wire gauze. Most commonly the catalyst envelopes are packed inside the column. Almost every conceivable shape of catalyst envelope has been patented: some basic shapes are shown in Figs 7.10–7.12.

These structures are the following.

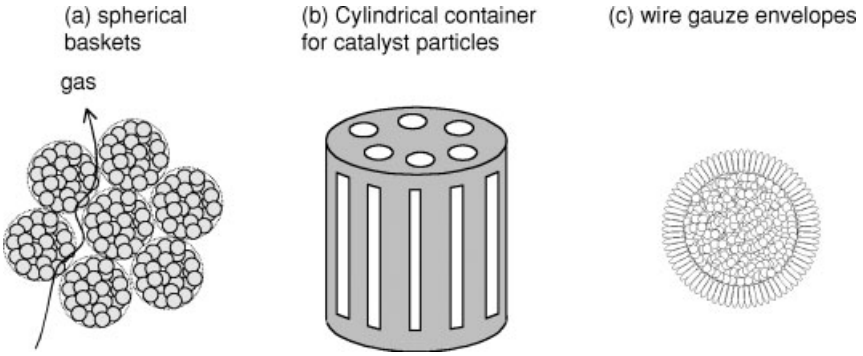

Fig. 7.10 Various 'tea-bag' configurations. Catalyst particles need to be enveloped in wire gauze packing and placed inside RD columns

- Porous spheres filled with catalyst [13, 14], Fig. 7.10a.
- Cylindrical envelopes [14], Fig. 7.10b.
- Wire gauze envelopes with various shapes: spheres, tablets, doughnuts [15], Fig. 7.10c.
- Horizontally disposed wire mesh tubes containing catalyst [13, 16, 17], Fig. 7.11.
- Catalyst particles enclosed in cloth wrapped in the form of bales [18–20]. This is the configuration used by Chemical Research & Licensing (CR&L) in their RD technology. Pockets are sewn into a folded cloth and then solid catalyst is loaded into the pockets. The pockets are sewn shut after loading the catalyst and the resulting belt or 'catalyst quilt' is rolled with alternating layers of steel mesh to

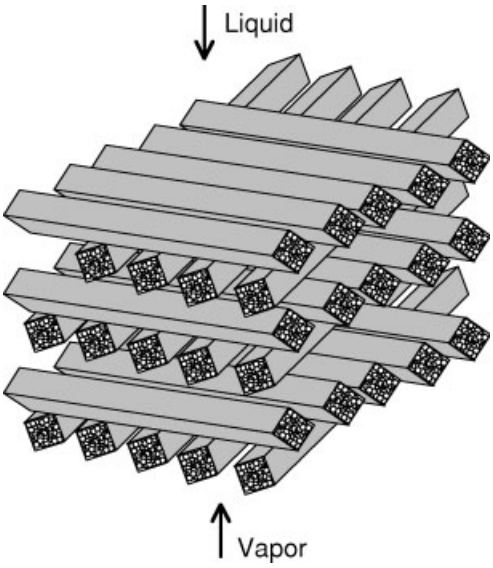

Fig. 7.11 Wire gauze tubes containing catalyst

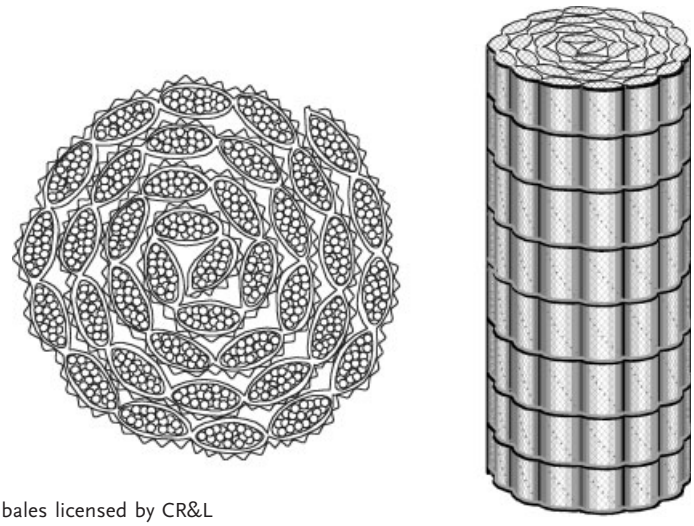

Fig. 7.12 Catalyst bales licensed by CR&L

form a cylinder of 'catalyst bales' as shown in Fig. 7.12. The steel mesh creates voids to allow vapor traffic and vapor–liquid contact. Scores of these bales are installed in the reactive zone of a typical commercial RD column. Bales are piled on top of each other to give the required height necessary to achieve the desired extent of reaction. When the catalyst is spent, the column is shut down and the bales are removed and replaced with fresh ones. Improvements to the catalyst bale concept have been made over the years [14, 21]. The hydrodynamics, kinetics, and mass-transfer characteristics of bale-type packing have recently been published [22–26].

- Catalyst particles sandwiched between corrugated sheets of wire gauze [18, 27–29], see Fig. 7.13. Such structures are being licensed by Sulzer (Katapak-S) and Koch-Glitsch (Katamax). They consist of two pieces of rectangular crimped wire gauze sealed around the edge, thereby forming a pocket of the order of 1–5 cm wide between the two screens. These catalyst 'sandwiches' or 'wafers' are bound together in cubes. The resulting cubes are transported to the distillation column and installed as a monolith inside the column to the required height. When the catalyst is spent, the column is shut down and the packing is removed and replaced. Information on the fluid dynamics, mixing, and mass transfer in such structures is available [30–34]. The important advantage of the structured catalyst sandwich structures over the catalyst bales is with respect to radial distribution of liquid. Within the catalyst sandwiches, the liquid follows a criss-crossing flow path. The radial dispersion is about an order of magnitude higher than in conventional packed beds [32].

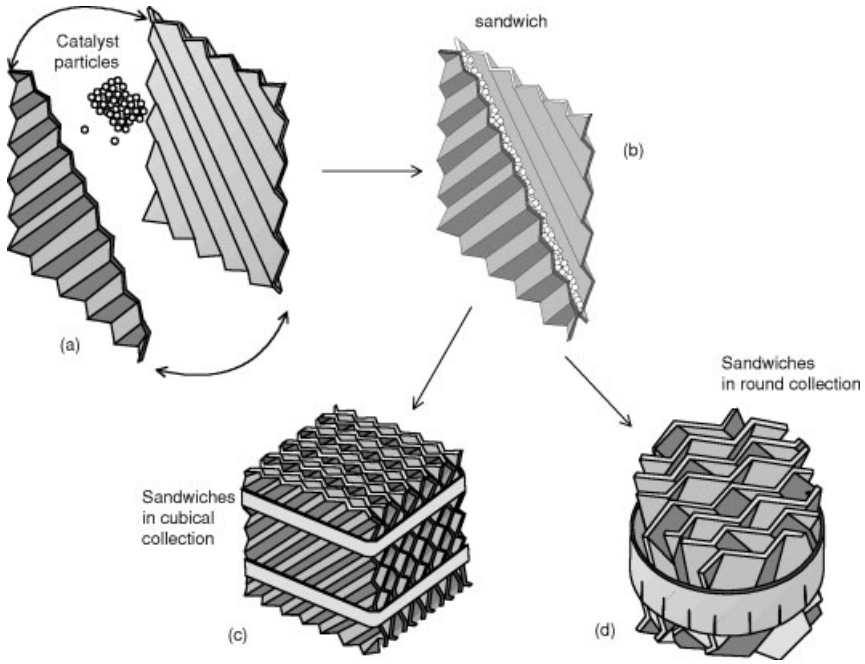

Fig. 7.13 Structured catalyst-sandwiches: a) catalyst sandwiched between two corrugated wire gauze sheets; b) the wire gauze sheets are joined together and sewn on all four sides; c) the sandwich elements arranged into a cubical collection; d) the sandwich elements arranged in a round collection. Photographs of the structure, along with CFD simulations of the liquid flow within the sandwiches can be viewed at: http://ct-cr4.chem.uva.nl/strucsim

Another possibility is to make the packing itself catalytically active. This is the strategy adopted by Flato and Hoffmann [35] and Sundmacher [36]. Raschig ring-shaped packing is made catalytically active, Fig. 7.14. The catalyst rings can be prepared by block polymerization in the annular space. Their activity is quite high, however, osmotic swelling processes can cause breakage by producing large mechanical stresses inside the resin. An alternative configuration is the glass-supported precipitated styrene-divinylbenzene copolymer, which is subsequently activated by chlorsulphonic acid.

A further possibility is to coat structured packing with zeolite catalysts [37], Fig. 7.15a. This concept has not been put into practice for the following reasons [38].

- The amount of catalyst that can be loaded in a column in this manner is small compared with addition of catalyst pills or homogenous catalyst.
- Coating or impregnation of catalyst materials on metal surfaces is expensive.
- Production of catalyst materials in the shape of distillation packing is also expensive.
- There is presently no generic manufacturing method that can produce different catalyst materials as coatings or structured packing economically.

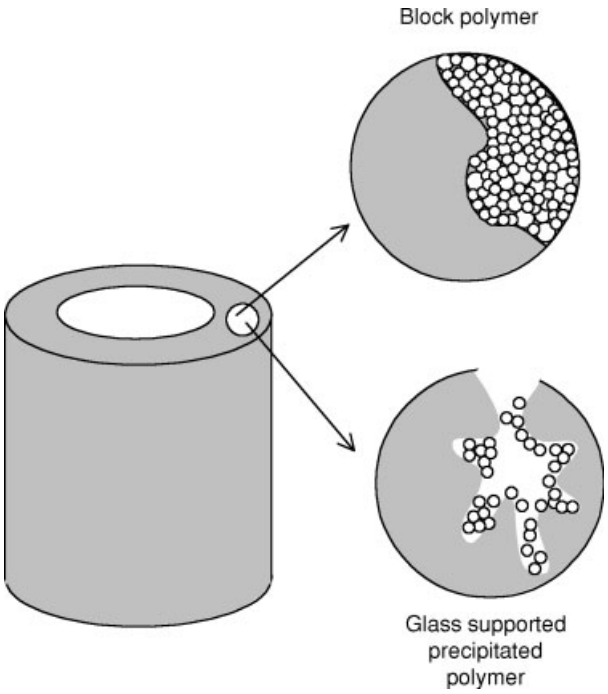

Fig. 7.14 Catalytically active Raschig ring. Adapted from Sundmacher [36]

The catalyst can also be 'cast' into a monolith form and used for counter-current vapor–liquid contact, Lebens et al. [39] have developed a monolith construction consisting of fluted tubes, Fig. 7.15b. The monolith construction has good gas–liquid mass-transfer characteristics.

Catalyst envelopes can also be placed in an RD tray column and many configurations have been proposed. Vertically disposed catalyst-containing envelopes can be placed along the direction of the liquid path across a tray [40], Fig. 7.16. These envelopes are almost completely immersed in the froth on the tray, ensuring

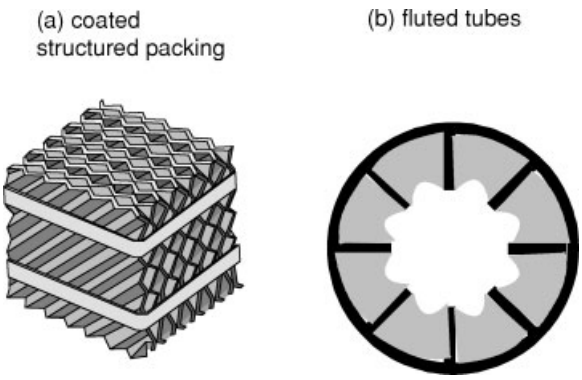

Fig. 7.15 a) Structured packing coated with catalyst; b) fluted catalyst monolith tubes

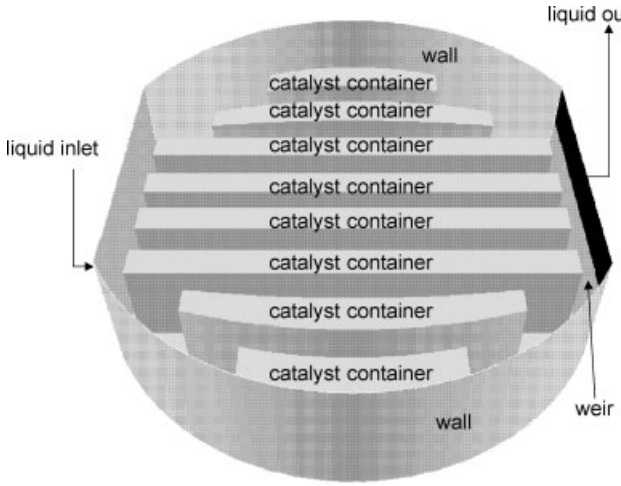

Fig. 7.16 Catalyst envelopes placed along the liquid flow path. For photographs of this configuration, along with CFD animations of the flow visit the web site: http://ct-cr4.chem.uva.nl/kattray

good contact between liquid and catalyst. Furthermore, since the vapor and liquid phase pass along the packed catalyst in the envelopes, and not through them, the pressure drop is not excessive. The catalyst containers also serve to ensure plug flow of liquid across the tray. CFD simulations have been used to study the hydrodynamics of such structures [10, 11].

Catalyst envelopes can be placed within the downcoming stream, or at the exit of the downcoming stream [41, 42], Fig. 7.17. The primary drawback is the limited

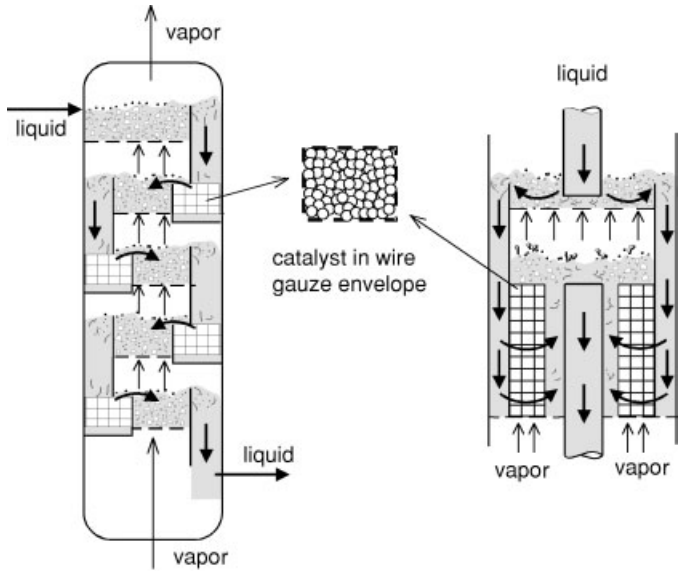

Fig. 7.17 Counter-current vapor–liquid–catalyst contact in trayed columns: catalyst in envelopes inside, and at the exit of downcoming stream

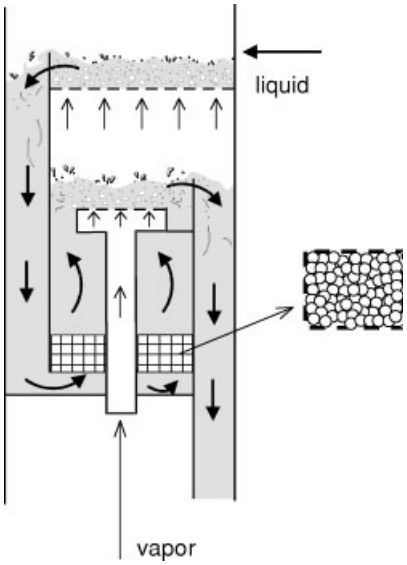

Fig. 7.18 Alternating packed layers of catalyst and non-reacting trays

volume available for catalyst inventory. The vapor does not pass through the catalyst envelopes.

Trays and packed catalyst sections can also be used on alternate stages [43, 44], Fig. 7.18. The vapor flows through the packed section up a central chimney without contacting the catalyst. The liquid from the separation trays is distributed evenly into the packed reactive section below by a distribution device.

Other designs have been proposed for tray columns with catalyst-containing pockets or regions that are fluidized by the upflowing liquid [44–47]. Catalyst attrition is a concern in a fluidized environment, but this can be taken care of by filtration of the liquid and by the make-up of the catalyst.

7.3.2 Hardware Selection Aspects

The 'ideal' hardware configuration is one that offers: maximum catalyst hold-up in the column, good gas–liquid and liquid–solid contact and mass transfer, and low pressure drop. These three requirements cannot all be met by the same packing and most hardware choices represent compromises. Consider, for example, use of the active Raschig rings in the reactive section of an RD column. This packing provides intimate contact between gas, liquid, and catalyst and, as a consequence, the pressure drop is extremely high. In structures such as catalytic bales and Katapak-S, preferential passages ('open' channels) are offered for flow of gas while the liquid is forced through the catalyst-containing envelopes. The vapor only comes into contact with the liquid at the cloth surface and some entrained liquid drops within the open channels. Consequently the pressure drop is low, but the

vapor–liquid mass transfer is also low. The gas–liquid contact is much poorer than for Raschig rings: low pressure drop is not compatible with good mass transfer.

To illustrate the quantitative differences, we present the calculations of Baur and Krishna [48] for Raschig rings, of 1 in. size, and catalytic bales for use in the reactive section of an RD column for synthesis of *tert*-amyl ether (TAME), Fig. 7.19. Correlations for pressure drop and mass transfer were taken from literature sources [22, 23, 49, 50]. From Fig. 7.19a we conclude that with Raschig rings, to avoid danger of flooding, the column diameter has to be much higher than for bales. However, from Fig. 7.19b we note that the mass-transfer performance of bales is about a factor three times lower than that of Raschig rings; therefore the height of the reactive section has to be higher in order to meet the require-

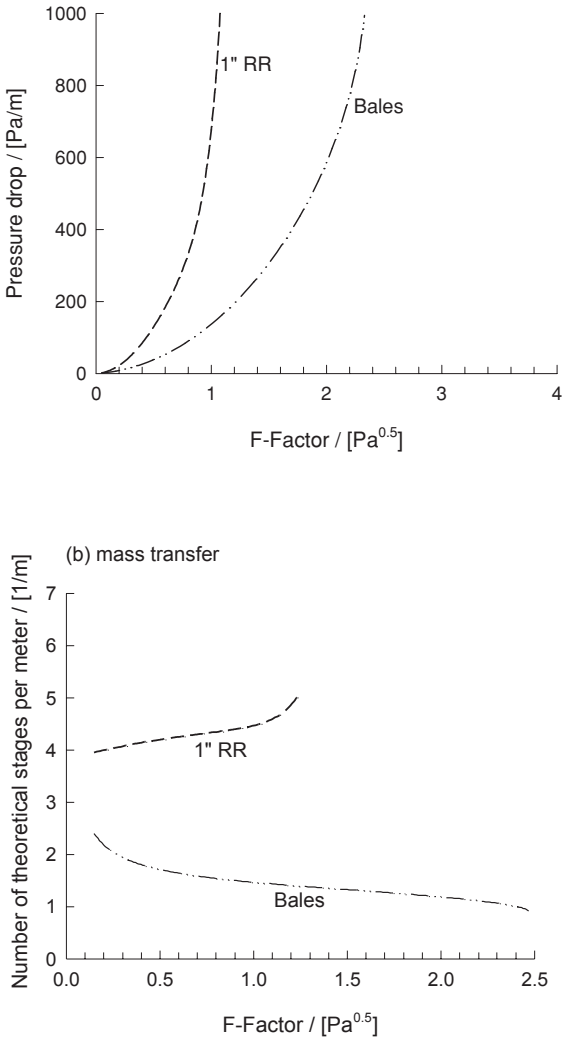

Fig. 7.19 Comparison of the pressure drop and mass-transfer performance of 1 in. Raschig rings with catalytic bales: a) pressure drop against F-Factor at constant maximum liquid load; b) number of theoretical stages per meter against F-factor. The liquid load is kept constant at a value of 0.05 m^3/s. Calculations of Baur and Krishna [48]

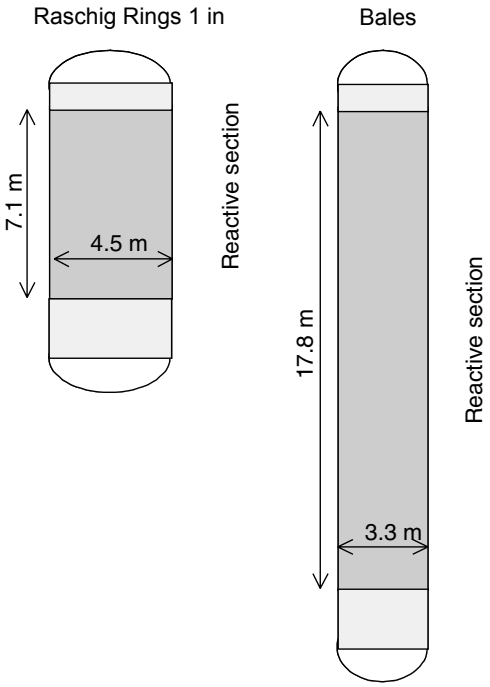

Fig. 7.20 Schematic of column configurations for TAME synthesis with Raschig rings and Bales in the reactive sections. Adapted from Baur and Krishna [48]

ments of in-situ separation. Two column configurations for TAME, with Raschig rings and bales, both designed for the same yield and product purity, are shown in Fig. 7.20. In general, we would prefer to build tall slim columns rather than short fat ones, because the primary column cost determinant for high-pressure systems, excluding internal column cost, depends on the column diameter not the height.

7.4 The Side-Reactor Concept

One approach to solving the incompatibility in the requirements of reaction (high liquid or catalyst hold-up) and separation (high vapor–liquid interfacial area) is to employ the side-reactor or external reactor concept [51], Fig. 7.21. The liquid is withdrawn from stage j, passes through the side reactor, and is fed back to the column at stage k. The amount of liquid pumped around, $L_{RPA} = R_{PA}\, L_j$, where R_{PA} is the pump-around ratio. By providing adequate residence time for reaction, equilibrium conversion is achieved in the side reactor.

For the production of MeOAc, let us compare the RD column with a distillation column with either three or five side reactors, Fig. 7.22. The side-reactor could be a tubular reactor, packed with, say, Amberlyst-15 for acid catalysis. It could also be a homogeneous liquid-phase tubular reactor, catalyzed by H_2SO_4. Clearly the location

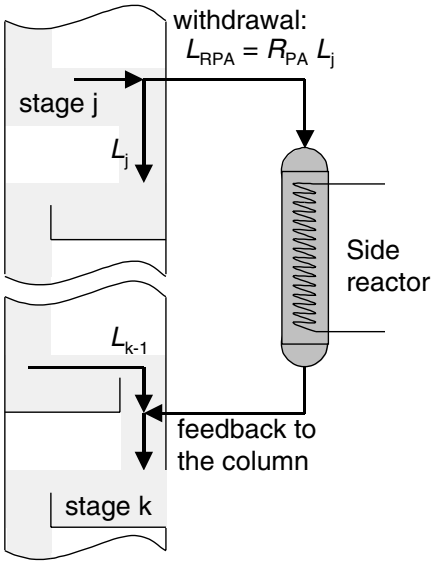

Fig. 7.21 A side reactor linked to a distillation column

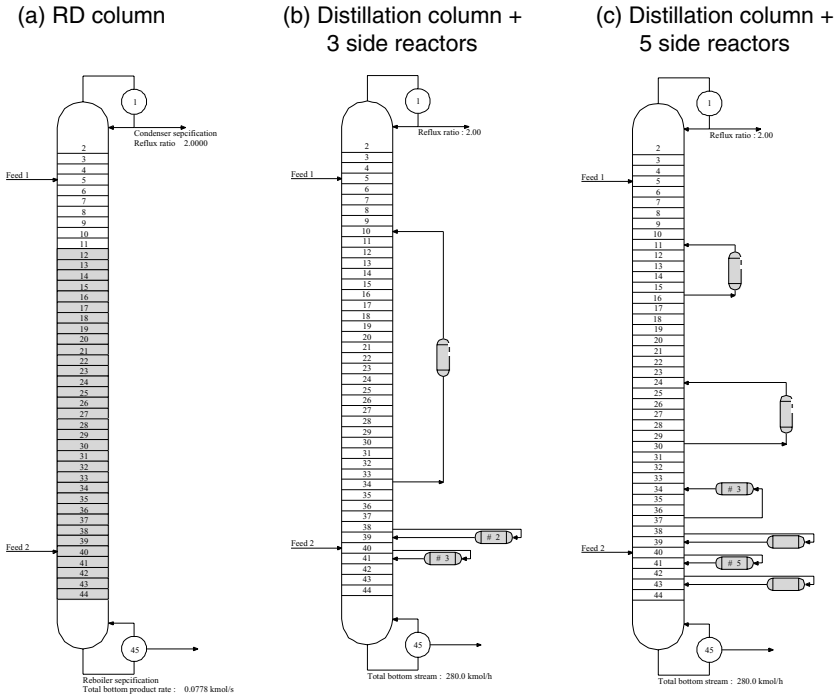

Fig. 7.22 Alternative configurations for MeOAc production: a) RD column; b) distillation column with three side reactors; c) distillation column with five side reactors

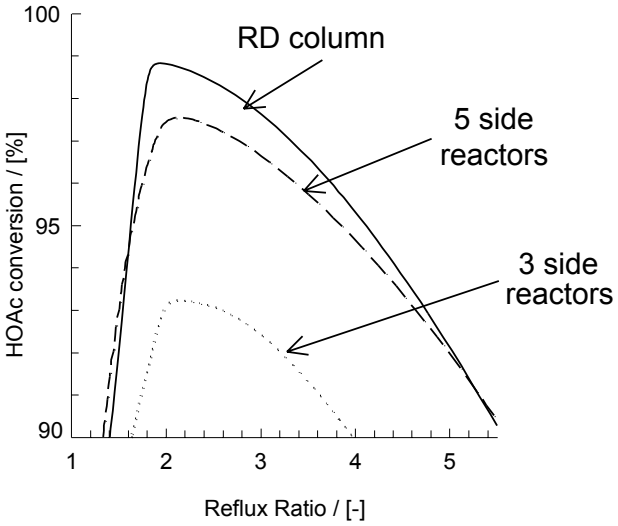

Fig. 7.23 Comparison of the acetic acid conversion obtained in the configurations shown in Fig. 7.22 as a function of the reflux ratio

and positioning of the side-reactors needs to be optimized; the optimum solutions are indicated in Fig. 7.22b and c, taking $R_{PA} = 1$. For these three- and five-side-reactor configurations, the AcOH conversions are compared in Fig. 7.23 with that of the RD column, for a range of reflux ratios. We note that maximum conversion achievable in the side-reactor concept is lower than for the RD configuration. Use of a higher pump-around ratio $R_{PA} = 5$, makes the five-side-reactor configuration approach the performance of an RD column.

The (non-reactive) distillation columns linked to the side reactors can be much smaller in diameter than the RD column and no specially designed trays (e. g., with higher weirs or additional sumps) or proprietary devices such as Katapak-S are necessary. The side-reactor concept is particularly attractive when the conversion requirements are not as stringent as assumed in the MeOAc case study above.

7.5 Conclusions

The hardware selection and design aspects for RD columns are not the same as for conventional distillation columns. In RD columns we need to aim for high liquid or catalyst hold-ups in the column, whereas in conventional distillation columns we usually aim for high throughput and high vapor–liquid interfacial area. For homogeneous RD, we would prefer to operate the tray column at very low superficial vapor velocities in the bubbly flow regime. For heterogeneous RD columns, the choice of hardware is even more difficult because it is nearly impossible to reconcile the conflicting requirements of high catalyst hold-up, low pressure drop and good vapor–liquid contact.

Many of the conflicting hardware issues can be resolved by de-coupling the separation and reaction function by employing the side-reactor concept.

7.6 Acknowledgments

R. K. would like to express his appreciation to Dr. R. Baur for carrying out most of the simulation work presented in this chapter and assistance in the preparation of this paper. R. K. also acknowledges financial support from the Netherlands Organization for Scientific Research (NWO) in the form of a '*programmasubsidie*' for development of novel concepts in reactive separations.

References

1 Doherty, M. F.; Malone, M. F. *Conceptual Design of Distillation Systems*, McGraw-Hill, New York, **2001**.
2 Taylor, R.; Krishna, R. *Chem. Eng. Sci.* **2000**, *55*, 5183–5229.
3 Sundmacher, K.; Rihko, L. K.; Hoffmann, U. *Chem. Eng. Commun.* **1994**, *127*, 151–167.
4 Agreda, V. H.; Partin, L. R.; Heise, W. H. *Chem. Eng. Prog.* **1990**, 40–46.
5 Lockett, M. J. *Distillation Tray Fundamentals*, Cambridge University Press, Cambridge, UK, **1986**.
6 Stichlmair, J. G.; Fair, J. R. *Distillation Principles and Practice*, Wiley-VCH, New York, **1998**.
7 Baur, R.; Higler, A. P.; Taylor, R.; Krishna, R. *Chem. Eng. J.* **2000**, *76*, 33–47.
8 Krishna, R.; Van Baten, J. M.; Ellenberger, J.; Higler, A. P.; Taylor, R. *Chem. Eng. Res. Des., Trans. I. Chem. E.* **1999**, *77*, 639–646.
9 van Baten, J. M.; Krishna, R. *Chem. Eng. J.* **2000**, *77*, 143–152.
10 van Baten, J. M.; Ellenberger, J.; Krishna, R. *Catal. Today* **2001**, *66*, 233–240.
11 van Baten, J. M.; Ellenberger, J.; Krishna, R. *Chem. Eng. Technol.* **2001**, *24*, 1077–1081.
12 Siirola, J. J. *Adv. Chem. Eng.* **1996**, *23*, 1–62.
13 Buchholz, M.; Pinaire, R.; Ulowetz, M. A. **1995**, EP 448884B1.
14 Johnson, K. H. **1993**, US Patent 5189001.
15 Smith Jr., L. A. **1984**, US Patent 4443559.
16 Groten, W. A.; Booker, D.; Crossland, C. S. **1998**, US Patent 5730843.
17 Hearn, D. **1993**, US Patent 5266546.
18 Johnson, K. H.; Dallas, A. B. **1994**, US Patent 5348710.
19 Smith Jr., L. A. **1985**, EP 008860B1.
20 Smith Jr., L. A. **1980**, US Patent 4215011.
21 Crossland, C. S.; Gildert, G. R.; Hearn, D. **1995**, US Patent 5431890.
22 Subawalla, H.; Gonzalez, J. C.; Seibert, A. F.; Fair, J. R. *Ind. Eng. Chem. Res.* **1997**, *36*, 3821–3832.
23 Subawalla, H.; Fair, J. R. *Ind. Eng. Chem. Res.* **1999**, *38*, 3606–3709.
24 Akbarnejad, M. M.; Safekordi, A. A.; Zarrinpashne, S. *Ind. Eng. Chem. Res.* **2000**, *39*, 3051–3058.
25 Xu, X.; Zhao, Z.; Tian, S-J. *Chem. Eng. Res. Des., Trans. I. Chem. E. A* **1997**, *75*, 625–629.
26 Xu, X.; Zhao, Z.; Tian, S. *Chem. Eng. Res. Des., Trans. I. Chem. E. A* **1999**, *77*, 16–20.
27 Stringaro, J. P. **1991**, EP 433222A1.
28 Stringaro, J. P. **1995**, US Patent 5470542.

29 Gelbein, A. P.; Buchholz, M. **1991**, US Patent 5073236.
30 Ellenberger, J.; Krishna, R. *Chem. Eng. Sci.* **1999**, *54*, 1339–1345.
31 Moritz, P.; Hasse, H. *Chem. Eng. Sci.* **1999**, *54*, 1367–1374.
32 van Baten, J. M.; Ellenberger, J.; Krishna, R. *Chem. Eng. Sci.* **2001**, *56*, 813–821.
33 van Baten, J. M.; Krishna, R. *Catalysis Today* **2001**, *69*, 371–377.
34 van Baten, J. M.; Krishna, R. *Chem. Eng. Sci.* **2002**, *57*, 1531–1536.
35 Flato, J.; Hoffmann, U. *Chem. Eng. Technol.* **1992**, *15*, 193–201.
36 Sundmacher, K. PhD thesis, Universität Clausthal, **1995**.
37 Oudshoorn, O. L. PhD thesis, Delft University of Technology, Delft, **1999**.
38 Towler, G. P.; Frey, S. J. Chapter 2 in *Reactive Separation Processes* (ed. S. Kulprathipanja), Taylor & Francis, Philadelphia, **2002**.
39 Lebens, P. J.; Kapteijn, F.; Sie, S. T.; Moulijn, J. A. *Chem. Eng. Sci.* **1999**, *54*, 1359–1365.
40 Jones, E. M., Jr. **1985**, US Patent 4536373.
41 Asselineau, L.; Mikitenko, P.; Viltard, J. C.; Zuliani, M. **1994**, US Patent 5368691.
42 Sanfilipo, D.; Lupieri, M.; Ancilloti, F. **1996**, US Patent 5493059.
43 Nocca, J. L.; Leonard, J.; Gaillard, J. F.; Amigues, P. **1991**, US Patent 5013407.
44 Quang, D. V.; Amigues, P.; Gaillard, J. F.; Leonard, J.; Nocca, J. L. **1989**, US Patent 4847430.
45 Marion, M. C.; Viltard, J. C.; Travers, P.; Harter, I.; Forestiere, A. **1998**, US Patent 5776320.
46 Jones, E. M., Jr. **1992**, US Patent 5130102.
47 Jones, E. M., Jr. **1992**, EP 0 402 019 A3.
48 Baur, R.; Krishna, R. *Chem. Eng. & Proc.* **2002**, *41*, 445–462.
49 Taylor, R.; Krishna, R. *Multicomponent Mass Transfer*, John Wiley, New York, **1993**.
50 Onda, K.; Takeuchi, H.; Okumoto, Y. J. *Chem. Eng. Japan* **1968**, *1*, 56–62.
51 Schoenmakers, H .G.; Buehler, W. K. *German Chemical Engineering* **1982**, *5*, 292–296.

Reactive Distillation. Edited by Kai Sundmacher, Achim Kienle

ISBNs: 3-527-30579-3 (Hardback); 3-527-60052-3 (Electronic)

8
Development of Unstructured Catalytic Packing for Reactive Distillation Processes

U. Kunz and U. Hoffmann

8.1
Introduction

The introduction of lead-free gasoline brought about a new technical process on a large scale: reactive distillation (RD). Although the principle of this process had been known for many years [1], the need to produce huge quantities of ethers as antiknock enhancers caused rapid development of this technique: more than 14×10^6 tonnes/year of ethers are produced. The catalysts for the production of methyl-*t*-butylether (MTBE), *t*-amylmethylether (TAME), or ethyl-*t*-butylether (ETBE), which are the main products for the fuel market, are acidic ion-exchange resins. The most important type is based on cross-linked polystyrene that is sulfonated to create the active acid sites. These resins are produced as beads of less than 3 mm in a suspension polymerization process.

In an RD process, two operations are coupled and run simultaneously. One operation is chemical synthesis and the other is separation by distillation, enabling a shift in composition to drive equilibrium-limited reactions to higher conversion. In this chapter we summarize some of our published papers and extend the work to other applications of polymer carrier composite materials and components.

8.2
Requirements for RD Catalytic Packing

Before we started our work on catalyst development, we examined the requirements for catalytic packing in RD columns. From the standpoint of chemical synthesis, high activity per volume is favorable, activity and selectivity of the catalyst should be high, good accessibility of the active sites is required, and stability with regard to chemical aspects and mechanical strength is necessary. For good distillation performance the catalyst needs to have a large geometrical surface area for enhanced mass transfer, low pressure drop, good separation properties, good wetability, and good mechanical strength, to mention the most important proper-

ties. A cost-effective and easy production process is required by both. The integration of chemical synthesis in a distillation column will always be a compromise between the requirements of the two unit operations.

8.3 State of the Art: Catalytic Packing for RD Processes

8.3.1 Commercial Packing

Commercial catalytic packing for RD processes is done by wrapping: ion-exchange resin beads are sewn into glass-fiber cloth and rolled into bales (CDTech, Passadena, Texas) or put into wire mesh or perforated metal sheets (Sulzer, Winterthur, Switzerland, similar to the methods of Koch Engineering or Montz). Fig. 8.1 and Fig. 8.2 show examples [2, 3].

This packing fits the column diameter or a few pieces of packing are arranged across the column diameter; Fig. 8.3 shows an RD column equipped with catalytic bales [4].

In addition to commercially available packing there are other approaches to wrapping ion-exchange resins. One idea is to use small tetrahedral wire packages: this was also patented by the CDTech company, Fig. 8.4 [5].

The benefit of wrapping is that a wide variety of catalysts can be used, but production is rather complicated and expensive. The pressure drop is relatively low compared with packed beds, but the mass-transfer characteristics are poorer, leading to longer columns. Filling and removing this packing into and out of the columns causes relatively long shut-off times. The catalyst particles are not anchored to the packing, so they can move. This can lead to abrasion damage, allowing the catalyst to leave the desired section of the column, which can only be prevented by using very fine mesh, but this has adverse effects on mass transfer between the fluid phase and the catalyst.

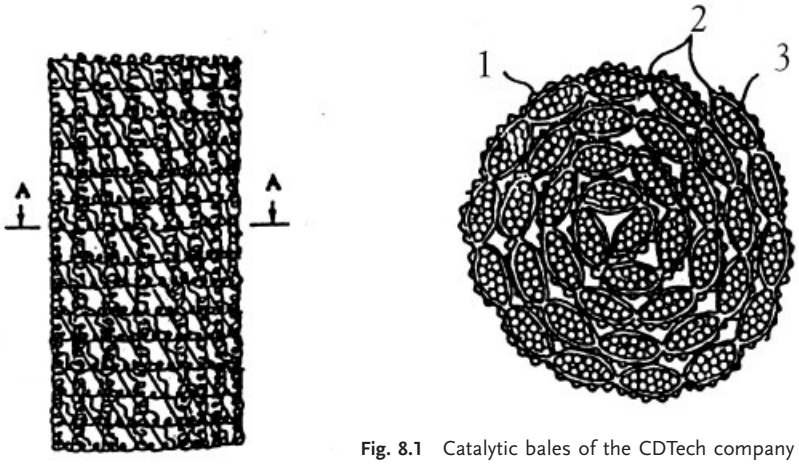

Fig. 8.1 Catalytic bales of the CDTech company

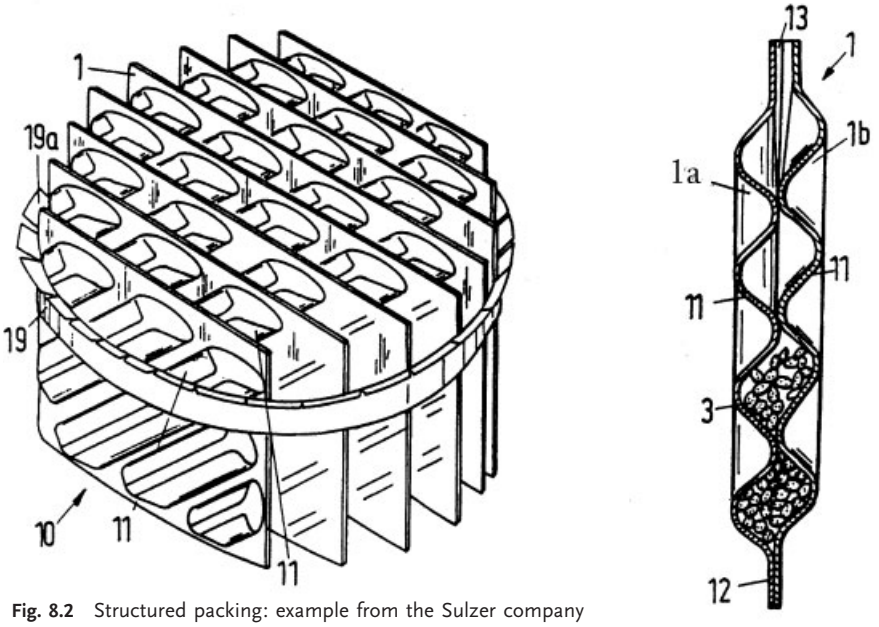

Fig. 8.2 Structured packing: example from the Sulzer company

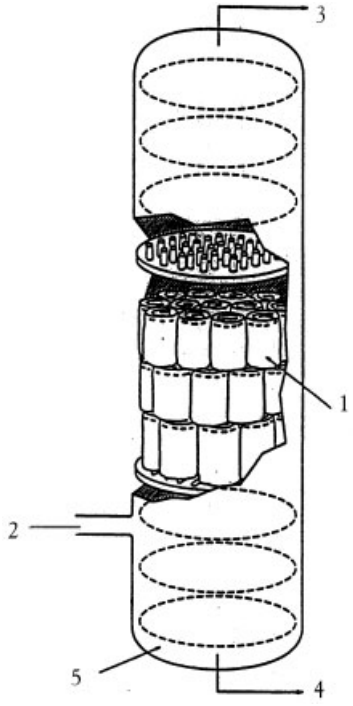

Fig. 8.3 RD column with catalytic bales

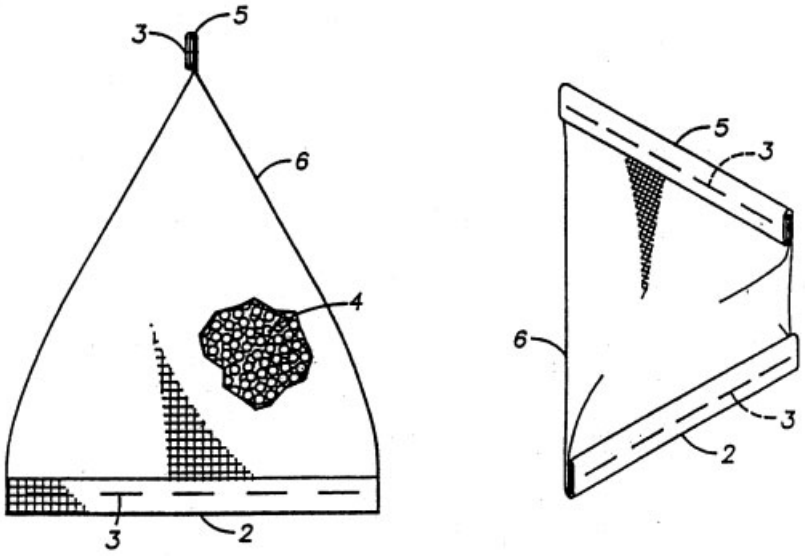

Fig. 8.4 Wire mesh filled with catalyst

8.3.2 Alternative Concepts

In addition to commercial packing there are several other methods described in the literature for preparing catalytic packing materials for RD purposes; the concepts can be divided into two approaches.

- Catalysts made of pure catalytic material.
- Catalysts supported on carrier materials.

8.3.2.1 Catalysts Made of Pure Catalytic Material

All catalysts used in the wrapping technique described above belong to the first group. The beads are pure polymer, completely sulfonated.

To avoid wrapping, Spes was the first to prepare monoliths of polymer with acidic properties [6]. He mixed ion-exchange beads with inert thermoplastic polymer and sintered this mixture. The temperature control of the sintering process is critical: if it is too hot the resin beads are plugged by the molten thermoplastic polymer. To stabilize the bodies during sintering, activated carbon or other structural promoters are needed. To ensure accessibility of the active sites, sodium chloride was used as a pore-forming agent, but after removing the salt by washing, the catalyst has to be transformed to the hydrogen form. The size of the porous bodies was several centimeters. Mechanical stability was not good because of swelling.

The low mechanical stability is caused by the large dimensions of the bodies prepared by Spes. To avoid this, Fuchigami decreased the size of the sintered bodies

[7]. He prepared 7 mm diameter tablets, but these are too small for RD processes because of the pressure drop. Both authors suggested methylacetate decomposition as a field of application.

Chaplits prepared similar products in an extruder [8]. The main difference was that he extruded copolymers consisting of cross-linked polystyrene with a thermoplastic polymer. As a pore-forming agent water was used in the extrusion process. Acid sites are created by sulfonation of the cut extrudates. As an application, *t*-butanol production from water and isobutylene was suggested.

Yoshioka prepared fibers with ion-exchange properties [9, 10]. Polypropylene and polystyrene were melted and fibers produced. Then the fibers were cross-linked and functionalized by treatment with paraformaldehyde, acetic acid, and sulfuric acid. The fibers can be woven into fabrics that can be used in RD processes.

Rehfinger prepared Raschig rings by copolymerization of styrene and divinylbenzene [11]. To create a macroporous resin he used organic solvents as the pore-forming agent. The polymerization was performed in a mold, resulting in a tube that was cut into Raschig rings. After sulfonation, acidic ion-exchange resin was obtained. The rings were used for MTBE synthesis. As for all pure polymer catalysts, they have the disadvantage that swelling forces (unavoidable in different reaction mixtures) cause a change in volume. The swelling forces can be sufficient to fracture the catalyst.

8.3.2.2 **Catalysts Supported on Carrier Materials**

Supported catalysts were prepared by Smith [2]. Carrier materials of various shapes were coated with solutions of monomers, which were then polymerized by UV light, creating a surface film. Mechanical stability was poor. Swelling forces led to crumbling of the film, loss of adhesion, and loss of polymer. The ion-exchange capacity was poor because only the outer surface of the carrier is available for polymer attachment.

Childress evaporated solutions of polymers on the surface of carrier materials [12]. To avoid removal of the polymer by swelling forces, he heated the polymer above the melting point. This led to a non-porous polymer coating on the outer surface of the carrier.

Hiramatsu also prepared films on a carrier material [13]. Halogenated polymers containing noble metals were prepared on the carrier surface. These catalysts had no acidic properties; they were used in hydrogen peroxide synthesis.

Bareis et al. and Eiceman impregnated porous powders with polymers and sulfonated them to get an acidic ion-exchange catalyst [14, 15]. The powders were used in chromatographic applications. The resins were non-porous, so pore-forming agents were not used.

Dromard impregnated porous inorganic carrier materials (4 μm–5 mm) with solutions of monomers and polymers [16]. After evaporation of the solvent, films on the carrier surface were obtained. These catalysts can be activated with sulfonic or phosphonic acid groups. The catalysts were used for the production of silicones. The preparation procedure seems to be problematic, because during polymeriza-

tion the carrier material particles adhere to each other leading to difficulties in removing them from the polymerization reactor.

We tried to sulfonate polystyrene tubes, but this led to unstable products. The sulphonic acid group needs a space in the polymer resulting in breakage of the tubes. Pre-swelling in solvents did not solve this problem.

We tried coating inorganic carrier materials by gluing commercial resin beads to the carrier surface, but this was not successful. Most glues are not stable in organic solvents, so the beads leave the carrier material and glue enters the reaction mixture. Even if the glue is stable in the solvent, the swelling of the ion-exchange beads prevents them remaining attached. The swelling forces in ion-exchange resins can reach several hundred bar, making it impossible to keep the resin beads anchored to a surface by gluing.

To summarize the state of the art reported in the literature: all the methods described do not take into consideration the requirements of RD processes. The methods result in films on carrier surfaces not adhering to the support over a long time. The films are not porous, so mass transfer will be slow. The preparation procedures require the handling of highly viscous polymer mixtures or solutions, resulting in agglomeration of the carrier material particles during preparation. In principle thin films allow only small polymer load on the support, leading to low ion-exchange capacities not attractive for technical processes. With one exception [11] the fact that all resins for MTBE synthesis are macroporous was not implemented in the preparation procedures.

8.4 New Catalyst Concept: Porous Polymer/Carrier Composite

To develop a new catalyst for etherification reactions in RD processes we tried to use all the information available in the literature. The first aim was to develop a catalyst for the production of MTBE from isobutylene and methanol.

The general formula for the etherification reaction of olefins with alcohols is given in Fig. 8.5.

From the literature it is well known that this etherification reaction requires an acidic catalyst. In industrial processes ion-exchange resins with sulfonic acid groups are in use. The structure of this cross-linked resin is depicted in Fig. 8.6

To have a catalyst that can compete with the existing materials we decided to prepare a catalyst that also contains sulfonic acid groups. To compile the requirements for the new catalyst, kinetic data for MTBE synthesis [11, 17] and information on chemical [18] and mechanical [19] stability of ion-exchange resins under the reac-

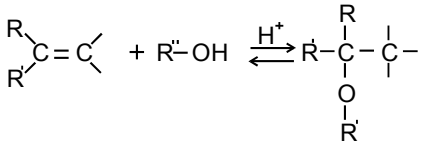

Fig. 8.5 Etherification of olefins with alcohols

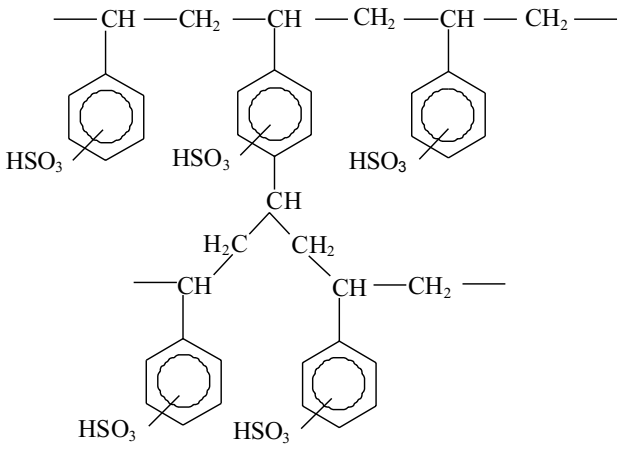

Fig. 8.6 Structure of sulfonic acid catalysts based on sulfonated styrene-divinylbenzene copolymers

tion conditions of RD columns were evaluated. In [11] the rate equation for the MTBE synthesis is given in activities, the first approach to do this for a process of industrial relevance.

It is known that the kinetics of the MTBE synthesis has a negative reaction order with respect to methanol. That means that at lower concentrations of methanol the reaction towards MTBE becomes faster. A faster reaction means that the concentration of the reactant methanol decreases inside the catalyst. On the other hand the concentration of isobutylene increases inside the catalyst. If this happens, the side reaction of dimerization of isobutylene occurs, lowering the selectivity towards MTBE. This effect can also be seen if the size of the catalyst particles is decreased. Smaller particles are more selective than large ones; large particles are deactivated by plugging the catalyst with dimer, starting from the center of the particle. Only an outer shell is the active part of the catalyst particle.

To produce a highly selective catalyst it is necessary to prepare the catalyst as a fine powder or to prepare a catalyst in which only the outer surface contains active sites. The decrease in size will cause problems with an RD column as reactor. Fine powders can only be handled in a slurry reactor, but this is not advantageous because we have a reaction that is equilibrium limited. For such a reaction a distillation column is superior. So the catalyst particles should be large enough to give a low pressure drop. The preparation of a shell catalyst will result in high selectivity but also in low activity because the outer surface of suitable catalyst particles is too low to make this concept attractive for an industrial application.

Commercial catalysts for MTBE synthesis are macroporous. The diffusion of methanol inside the macropores of the catalyst is the rate-determining step of the reaction to MTBE. In the gel phase of the catalyst there is no mass-transport limitation [11]. A factor influencing macroporosity is the degree of cross-linking. The higher the cross-linker concentration, the more of the polar compound enters the catalyst. So cross-linking is a factor influencing selectivity. The higher cross-linking is, the higher selectivity should be. The degree of cross-linking can only

be adjusted between certain limitations. At very high cross-linking the polymer becomes brittle, and catalyst damage by mechanical forces can happen easily. A compromise is to use a medium cross-linker concentration of 5–20 %.

We mentioned that MTBE synthesis has a special kinetic behavior. Depending on the concentration of methanol in the feed, the reaction rate can be very fast at low methanol concentrations or rather fast at high methanol concentrations (a range from about 2 to 160 $mol/m^3\ s^{-1}$ is covered). The reasons for this are mass-transport effects in the pores of the catalyst. To avoid this, the pores in the new catalyst should be large: larger than in commercial macroporous resins.

Styrene-divinylbenzene cross-linked resins with sulfonic acid groups can be used up to 110–120 °C. Exceeding this temperature range will result in a loss of acid groups. Desulfonation will occur at elevated temperatures. Resins with higher cross-linking will deactivate faster than those with low cross-linking because the concentration of acidic sites is higher (lower swelling at higher cross-linking). A high concentration of acidic sites means a high concentration of that catalyst that catalyses the desulfonation. The acidic sites catalyze their own deactivation. So the degree of cross-linking should be low for good chemical stability at elevated temperatures.

From this evaluation, taking an RD column as a reactor into consideration, the resulting requirements for the new catalyst can be summarized in Table 8.1.

As a result it is clear that the new catalyst can not be prepared easily. Some requirements are contradictory. A compromise is necessary to produce a product that fulfils the technical requirements.

As mentioned in Table 8.1, the catalyst should have small particle size to enhance selectivity. The smallest size that one can imagine is a monomolecular layer of active sites on a large pore support. From the literature it is known that silanes can react with silanol groups of inorganic carrier materials [20]. Suitable carrier materials are silica or glass. So we calculated what ion-exchange capacity can be obtained if the surface of megaporous glass Raschig rings is covered with trichlorophenylsilane. Reaction of the chloro groups with the silanol groups of

Table 8.1 Requirements and reasons for the requirements for a reactive distillation catalyst

Requirement	***Reason for the requirement***
Small catalyst particles	high selectivity for MTBE
High ion-exchange capacity	high activity per volume
Large pores	high reaction rate
Sulfonic acid groups as active sites	well known active etherification catalyst
Shape of a Raschig ring	reactor is reactive distillation column
Large size	low pressure drop
High mechanical stability	resistance to swelling forces

the glass will lead to a chemically bound aromatic ring that can be sulfonated. Taking the data from the literature for the density of silanol groups on silica and the technical data of the Raschig rings (40 m^2/L), it is clear that the obtainable ion-exchange capacity is very low. Even if silica with high surface area is used only ion-exchange capacities in the range of some microequivalents H^+/g are obtainable [21]. This is not attractive for a technical application. In addition the pores of silica are smaller compared with macroreticular ion-exchange resins, probably causing even more problems with mass-transfer effects.

So we decided to establish a catalyst concept that makes use of the pore volume to incorporate ion-exchange resins. The information obtained from the literature revealed that it is not wise to try to anchor the catalytic polymer to the surface because swelling forces will break this linkage. Only the concept that makes use of the pore volume to attach the polymer allows high ion-exchange capacities suitable for technical processes.

8.4.1 Requirements for the Carrier Materials

The first step was the choice of suitable carrier materials. Supports with pores in the nanometer range were discounted, mass-transfer limitations could occur. The task is to incorporate fine polymer particles into the pore volume of the carrier. Polymer particles from known preparation methods are rather large, so this also requires large pores. The requirements for a suitable carrier material are given in Table 8.2.

Table 8.2 Desired properties of the carrier materials

Large pore volume
Open, interconnected pores
Large pores in the micrometer range
High mechanical strength
Inert in the polymerization step
Stability during all preparation steps

Suitable materials are ceramics and glass. In principle natural materials are also possible, for example pumice. That would be a very cheap material, but natural minerals could contain ions that could interfere with the active sites of the incorporated resin. So this is not a good material choice. In Table 8.3 a compilation of selected materials is given.

The pore diameter covers a wide range and is larger than for standard catalyst supports; such materials are called ‘megaporous’ [22].

Table 8.3 Selected carrier materials suitable for the preparation of polymer/carrier catalysts

Carrier material	*Shape*	*Pore diameter*	*Pore volume*
Mullit ceramic	structured packing	0.15 µm	35 %
Porous glass	Raschig ring 9 mm	60–300 µm	55–60 %
Alumina foam	X-size 2 × 1 × 1 cm	0.1 mm	85 %
Glass foam	Irregular pieces 2 cm	0.2 mm	75 %
Silicon carbide foam	Irregular pieces 2 cm	1.5 mm	80 %

8.4.2 Requirements for the Polymerization Process

Our aim was to incorporate small polymer particles into the pore volume of the carrier. So the next step was the evaluation of polymerization methods to reach that aim. The requirements for the polymerization process are listed in Table 8.4.

Commercial ion-exchange resin beads are produced in a suspension polymerization, in which small droplets of monomer are dispersed in water and radical initiators in the monomer start the polymerization. This method can not be used for our intended catalyst preparation because it is not possible to stir a suspension in the pores of a carrier. The particles from suspension polymerization are too big for our purposes.

Emulsion polymerization gives very small polymer particles, but the use of an emulsifier keeps the particles separated. The polymer particles are removed by convective flow through the carrier, so this process also is not suitable.

Polymerization in solution leads to a solution of the polymer in the chosen solvent. To prepare a polymer phase inside pores, evaporation of the solvent would be necessary. This leads to a polymer film on the surface of the carrier that does not adhere firmly on the surface.

Table 8.4 Requirements for the Polymerization process of polymer/carrier catalysts

Application inside the porous structure of a carrier
Homogeneous polymer distribution inside the carrier material
Adjustable polymer load
High degree of polymer dispersion
Easy removability of additives from the polymerization reaction
Extension of the preparation process to different monomers
Low residues of additives from the polymerization reaction
High reproducibility
Easy and cost effective

Finally we decided to use precipitation polymerization (dispersion polymerization). This gives small polymer particles. In classical dispersion polymerization a detergent is used to keep the reaction mixture stirable and to produce isolated single particles, but we omitted the detergent to interconnect the particles by polymer bridges. This results in a stable polymer phase consisting of small particles that are interconnected.

8.5
Preparation of Sulfonated Ion-Exchange Polymer/Carrier Catalysts

The precipitation polymerization takes place in a batch reactor. Azoisobutyronitrile is used as the radical initiator, and styrene and divinylbenzene were chosen as monomers. A solution of the monomers in a long-chain hydrocarbon liquid is prepared [23]. After a clear solution has formed the megaporous glass Raschig rings are immersed in the solution, vacuum was used to remove the air from the pores, and the polymerization was initiated by heating. Fig. 8.7 shows the course of the precipitation polymerization in the pore volume of the carrier.

At first there is a homogeneous solution of the monomers in the solvent; heating initiates chain growth. After about 3 h the macromolecules formed are no longer soluble in the solvent (the solvent needs to be a good solvent for the monomers but a bad solvent for the polymer). First polymer particles are formed: the concentra-

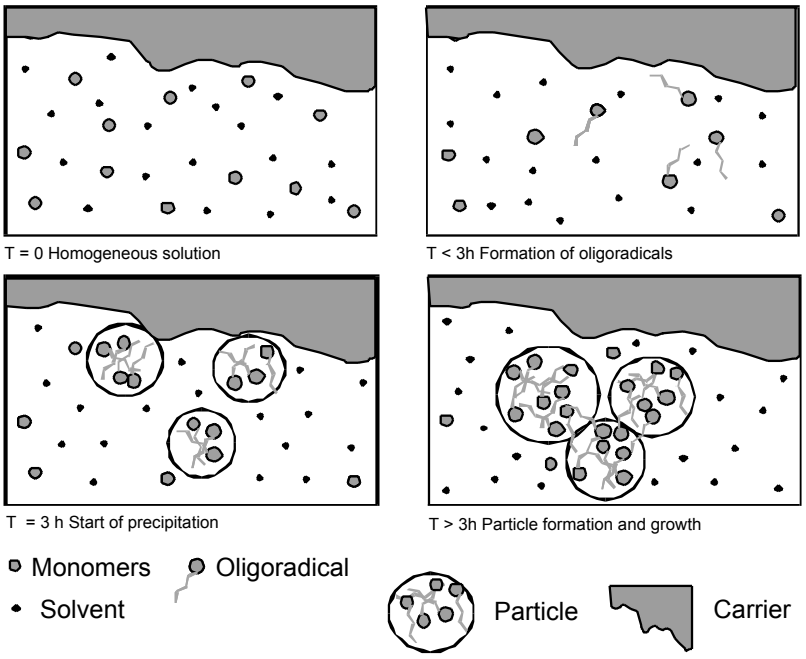

Fig. 8.7 Course of precipitation polymerization inside carrier materials

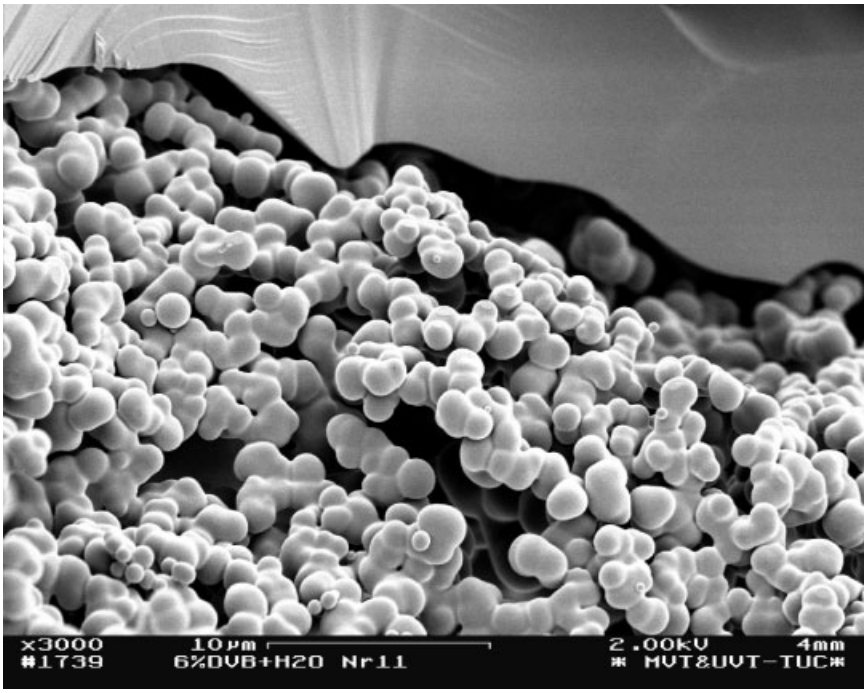

Fig. 8.8 SEM image of a polymer/carrier composite

tion of the monomers is still high. Monomer molecules diffuse to the existing particles and there is further growth. When the particles have reached a certain size they touch each other. Still monomers diffuse to the particles and are added to the particles by the polymerization reaction. This leads to the polymer bridges we can see in Fig. 8.8. In Fig. 8.9 typical dimensions of the polymer/carrier composite materials are given.

Fig. 8.10 shows a comparison between the smallest available fraction of commercial resin beads (50–500 µm) and the particles from our preparation method. The dark areas in the picture are the pores, the white area is the glass carrier. The small white dots in the dark area are the polymer particles. This SEM image shows that the size of the polymer particles is several micrometers. This is much smaller than commercial resin beads. Between the particles are large pores with a diameter in the micrometer range. This morphology is beneficial for good mass transfer

It is evident that the small size of the polymer particles will lead to better active site accessibility. The pores between the particles are megapores, enabling convective flow through the catalyst at low pressure gradients.

After the polymerization step the styrene–divinylbenzene copolymer is activated by sulfonation with chlorosulfonic acid. The result is a polymer/carrier composite material that is a universal heterogeneous catalyst with the shape of a Raschig ring, well-suited for RD purposes.

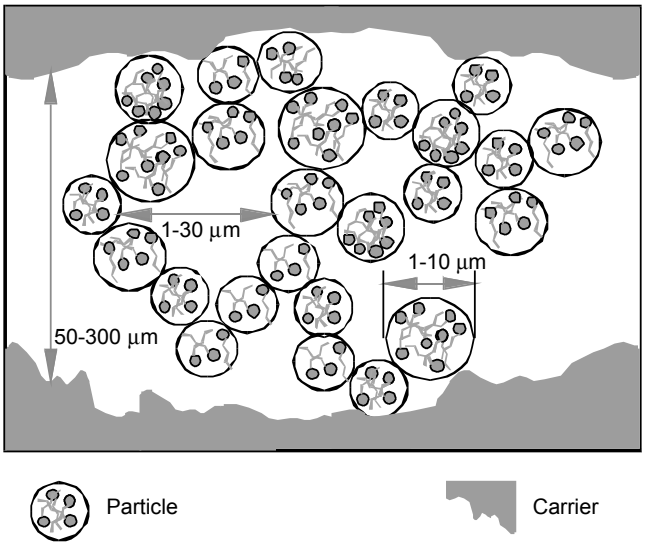

Fig. 8.9 Typical dimensions inside polymer/carrier composite materials

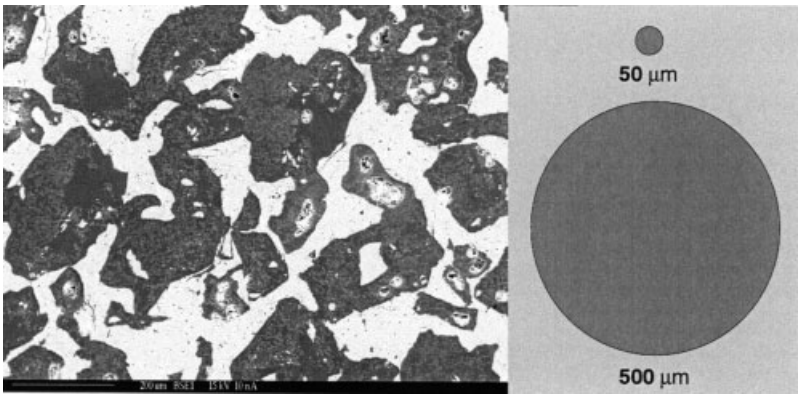

Fig. 8.10 Comparison of polymer particle size of polymer/carrier composites with commercial resin beads

Table 8.5 compares technical data of the new catalyst with a well-known Amberlyst ion-exchange resin.

Table 8.5 Comparison of amberlyst 15 with polymer/glass Raschig rings

Parameter	*Amberlyst 15*	*Polymer/glass Raschig ring*
Shape	bead	Raschig ring
Diameter [mm]	0.3–1.2	9 × 9 × 2
Polymer load [wt.-%]	100	10–30
Crosslinking [wt.-%]	20	2–20
Capacity [meq H^+/g]	5	0.5–1.4
BET surface area [m^2/g]	50	about 0.7
Pore diameter [nm]	29	1000–10 000
Microparticle diameter [nm]	80	500–5000

8.6 Performance of Polymer/Carrier Catalysts

By precipitation polymerization polymer/carrier catalysts with different properties were prepared. Table 8.6 gives properties of some samples.

As a test a continuous stirred tank reactor was used. Pressure was adjusted to keep the reactants in the liquid phase (2.0 MPa) and the reactants were fed at temperatures of 60–90 °C at a flow rate of 20 mL/min. The isobutylene concentration was kept constant at 6 mol/L. The methanol concentration was varied from 0.1 to 8.6 mol/L.

Table 8.6 Properties of the prepared and tested polymer/carrier-catalysts. The degree of crosslinking is 7.5 % by weight for all samples, balanced with styrene

	GFP-15	*GFP-2*	*GFP-12*	*GFP-10*
Steps of precipitation	1	1	2	2
Concentration of monomers [mol/l]	1.3	1.8	1.4	1.8
Content of resin [wt.-%]	11	17	24	30
Ion exchange capacity [meq H^+/g]	0.5	0.8	1.2	1.4
Ion exchange capacity of resin content [meq H^+/g]	4.9	4.8	4.9	4.8

8.6.1
Influence of Polymer Content and Reactant Concentration

In Fig. 8.11 the global observed reaction rate against methanol concentration is depicted for four catalyst samples with different polymer content. In general, higher polymer content leads to lower activity for MTBE synthesis per active site. Only at a very low polymer content is the typical MTBE kinetic pattern observed. This difference from regular MTBE kinetics, as measured by Rehfinger and others [11, 17], is because the transport of isobutene may become mass-transport limited, as well as the mass-transport limitations of methanol within the macropores of the catalyst. The reason for mass-transfer limitations for isobutene may be gel phase diffusion inside the polymer particles. The polymer spheres formed during precipitation polymerization are non-porous particles much bigger than the microspheres in commercial ion-exchange resins. By increasing the polymer content, larger particles are formed. However, the polymer spheres of the new catalysts are much smaller than commercial ion-exchange resin beads.

The dimerization of isobutene (DIB formation) is the only observed side reaction. Fig. 8.12 shows the influence of methanol concentration on DIB formation, which increases with decreasing methanol concentration. In general this is expected, because at low methanol concentration active sites are available for this side reaction. In commercial macroporous ion-exchange catalysts (such as Amberlyst 15) the by-product formation starts when MTBE synthesis reaches its maximum rate. This is only the case for the GFP-15 catalyst with the lowest polymer content. At higher polymer content the behavior changes. The reaction shows no ignition behavior. In general the dimerization rate falls with increasing polymer content. This indicates a mass-transfer limitation for isobutene in the polymer spheres.

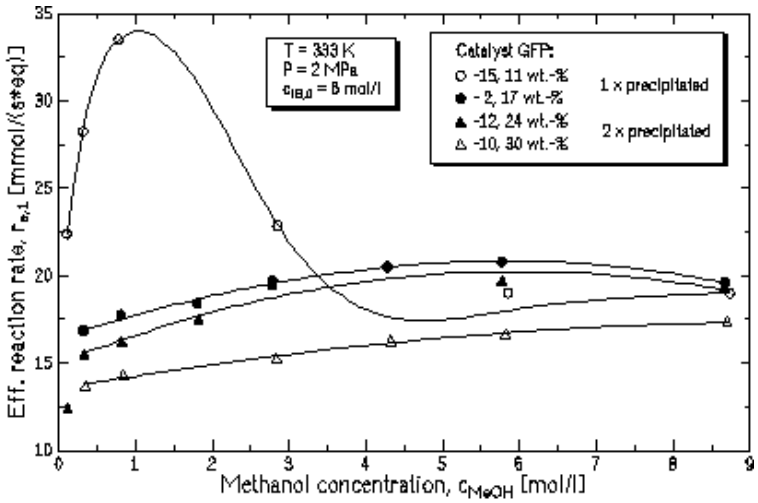

Fig. 8.11 Effect of polymer load on MTBE synthesis using a polymer/carrier catalyst

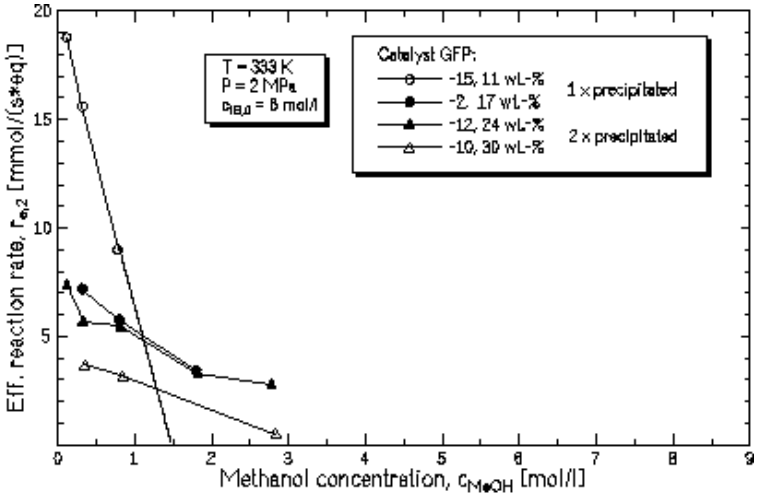

Fig. 8.12 Influence of polymer load on the formation of isobutene dimer

8.6.2 Influence of Reaction Temperature

In RD processes isothermal operation of the catalyst bed is not possible. At the top of the column temperatures in the range of 60 °C are common, with higher temperature towards the bottom. Higher temperatures enhance the reaction more than mass transfer. Therefore mass-transport phenomena will have more pronounced effects at higher temperatures. We tested the catalysts at temperatures of 60, 75, and 90 °C. The results are shown in Fig. 8.13 and Fig. 8.15 for polymer/carrier catalysts with different polymer content. GFP-15 is a catalyst with low polymer content; GFP-12 has twice the polymer content of GFP-15. GFP-15 was chosen because it shows the classical MTBE kinetic pattern. GFP-12 was tested in an RD column.

As expected the maxima for GFP-15 are shifted towards higher methanol concentrations with increasing temperature. GFP-12 shows no maximum: rising temperature and increasing methanol concentration lead to higher reaction rates. At low methanol concentration both catalysts give a lower reaction rate.

To estimate the operating region of the catalysts, activation energies were measured. For GFP-12 the effective activation energy is 42 kJ/mol, for GFP-15 the value is 74 kJ/mol. This indicates that internal mass-transport phenomena influence the observed reaction rates. The activation energy for MTBE synthesis without internal mass-transport limitations should have a value of 92 kJ/mol [11].

At 90 °C the GFP-15 has observed rates more than twice the rate of GFP-12. Despite having only half the polymer content per volume fraction of GFP-12, GFP-15 has the same catalytic performance in MTBE synthesis. Regarding selectivity, it is more advantageous to use GFP-12 in the region of low methanol concentration and

high temperature. This can be seen in Fig. 8.13, Fig. 8.14, and Fig. 8.15. So we recommend the use of a low polymer content polymer/carrier catalyst at the top of the tower and a high polymer content polymer/carrier catalyst at the bottom.

Polymer/carrier Raschig rings have shown high activity and selectivity during tests in a laboratory RD column. Detailed investigations on this new catalyst have been reported [24].

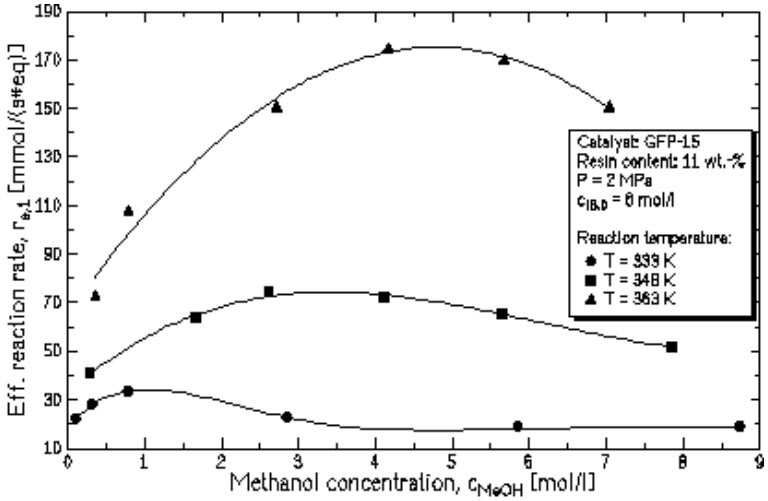

Fig. 8.13 Influence of temperature on MTBE synthesis with polymer/carrier catalysts

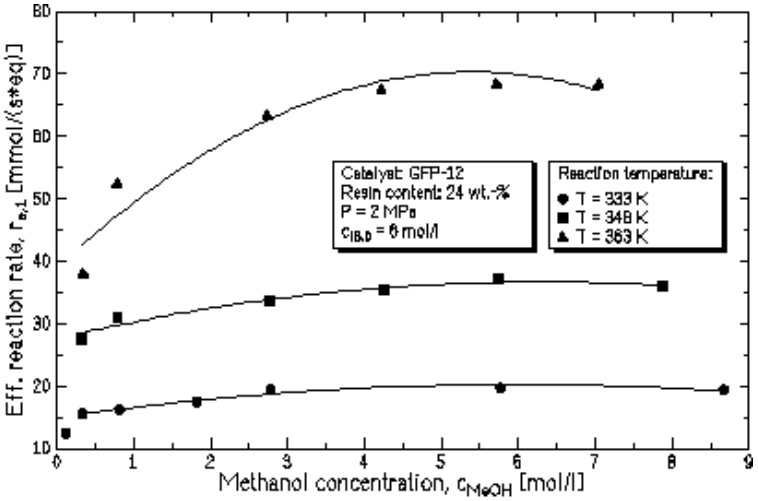

Fig. 8.14 Influence of temperature on MTBE synthesis with polymer/carrier catalysts

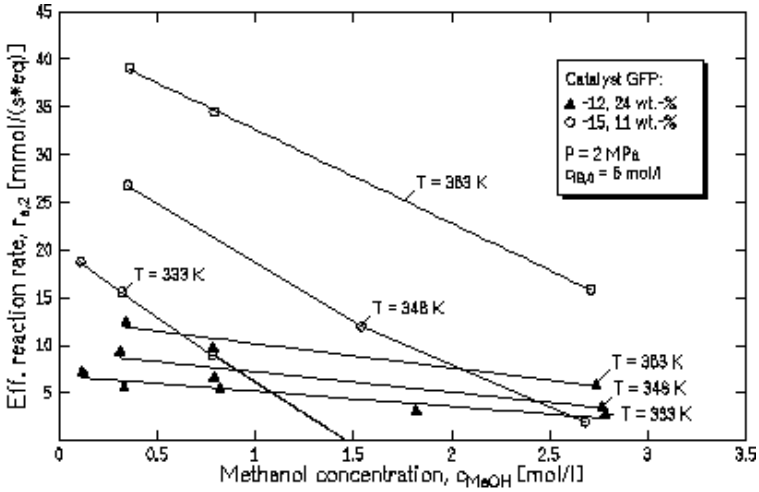

Fig. 8.15 Influence of temperature on the formation of diisobutene by using polymer/carrier catalysts with different polymer load

8.6.3
Influence of Cross-Linking

To investigate the influence of cross-linking and polymer content, samples with two different amounts of cross-linking and different polymer loading were prepared. This was done by varying the monomer concentration in the precipitation polymerization step. The lower polymer content was 11 %, the upper content was 24 %.

8.6.4
Influence of Cross-Linking at Low Polymer Content

Fig. 8.16 shows the effective reaction rate for the synthesis of MTBE for three catalyst samples with different cross-linking and a low polymer content of 11 %. More cross-linking shifts the expected maximum of the MTBE reaction rate to lower methanol concentrations. In general, with more cross-linking the ratio of the polar compound to the non-polar reactant will rise. For MTBE synthesis this means that a high cross-linked resin contains more methanol. In the kinetics of MTBE synthesis methanol has a negative reaction order, resulting in reaction rate curves with a maximum [11, 17]. In addition, high cross-linking results in low swelling of the polymer. This causes larger pores and higher porosity compared with less cross-linked resins. Large pores limit methanol transport less. This behavior is observed for the new catalyst also, but only at low polymer loading. For the activity in the catalytic reaction this means that cross-linking is a parameter that can be used to adjust the catalytic activity in MTBE synthesis for a given bulk fluid composition. However, this parameter influences selectivity. The main side

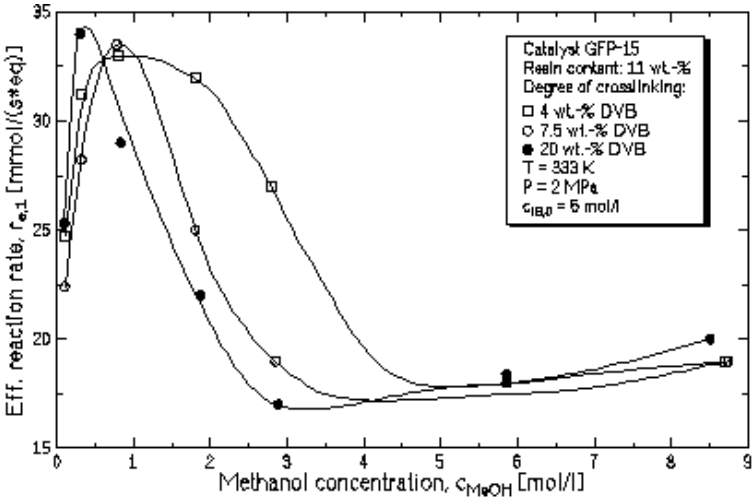

Fig. 8.16 Influence of cross-linking of polymer/ceramic ion-exchange catalysts on the activity of the MTBE synthesis at low polymer loading

reaction in MTBE synthesis is DIB formation. Fig. 8.17 shows the influence of cross-linking on this side reaction. By-product formation starts earlier with low cross-linking. At high cross-linking this reaction arises later, but with a steeper slope. The reason for this behavior is that at low cross-linking the catalyst is rich in isobutene promoting the side reaction. As mentioned above, porosity is also influenced, leading to higher selectivity for MTBE at high cross-linking. At very low methanol concentrations (below 0.25 mol/L) the ratio changes: low cross-linking leads to higher MTBE selectivity.

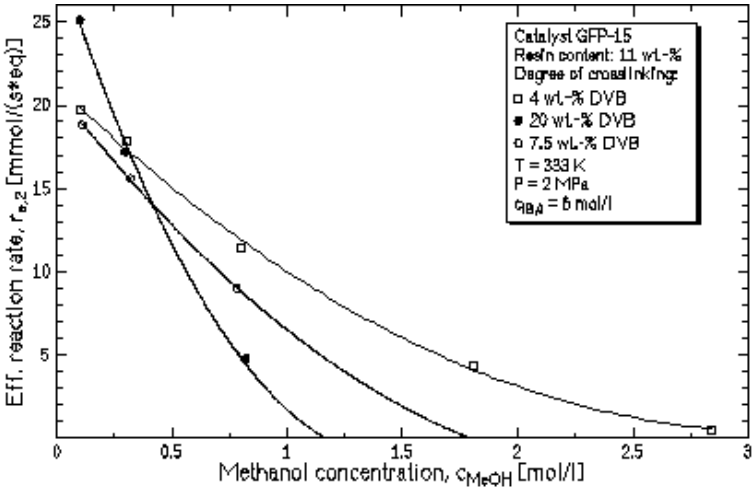

Fig. 8.17 Influence of cross-linking of polymer/ceramic ion-exchange catalysts for the dimerization of isobutene during MTBE synthesis at low polymer loading

8.6.5
Influence of Cross-Linking at High Polymer Content

As mentioned above, low polymer loading gives reaction rate curves with the shape observed for commercial macroporous catalysts (maximum for the reaction rate in the region of low methanol concentration).

Different behavior was observed for the samples with higher polymer content. These curves show no maximum (Fig. 8.18). For all tested catalysts, activity for MTBE is nearly the same. Cross-linking in these cases is of minor importance. At low methanol concentrations the rate drops for all samples. The reason for this is that the polymer loading in the pore volume of the carrier causes a transport limitation for isobutene. So the typical activity pattern for macroporous resins cannot be observed. For the operation of an RD column this is beneficial; drastic changes in the rate caused by fluid phase concentration changes do not occur. The whole packing in the column can be approximated with one rate, especially in the concentration range of industrial plants.

As measured for the samples with low polymer content, the selectivity for MTBE rises with increasing cross-linking (Fig. 8.19). Selectivity is in general lower compared with the catalysts with low polymer content. In the methanol concentration range of industrial RD processes, selectivity is high and no by-products were detected. The highly cross-linked catalyst differs from the two other samples. At first no dimer was formed, but when dimerization started it increases with a steeper slope. This behavior is the same as for the low polymer loaded catalyst. A possible reason is the different swelling of the polymer particles resulting in a more swollen resin at low cross-linking. Mass transport of isobutene may become limited in the larger gel particles.

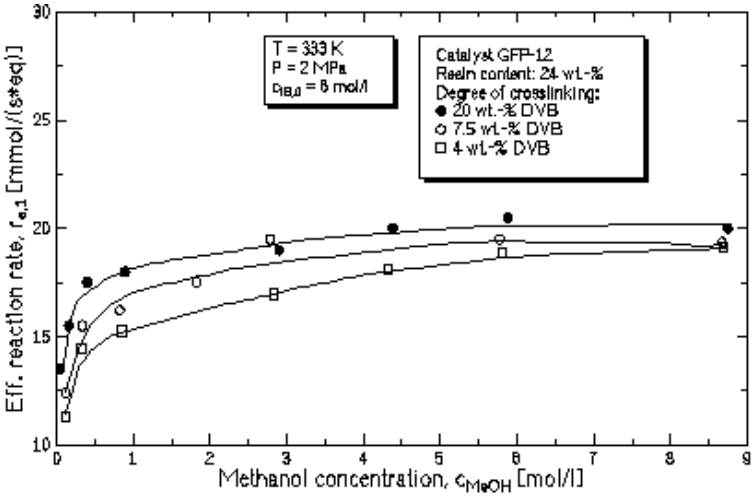

Fig. 8.18 Influence of cross-linking of polymer/ceramic ion-exchange catalysts on the activity of the MTBE synthesis at high polymer loading

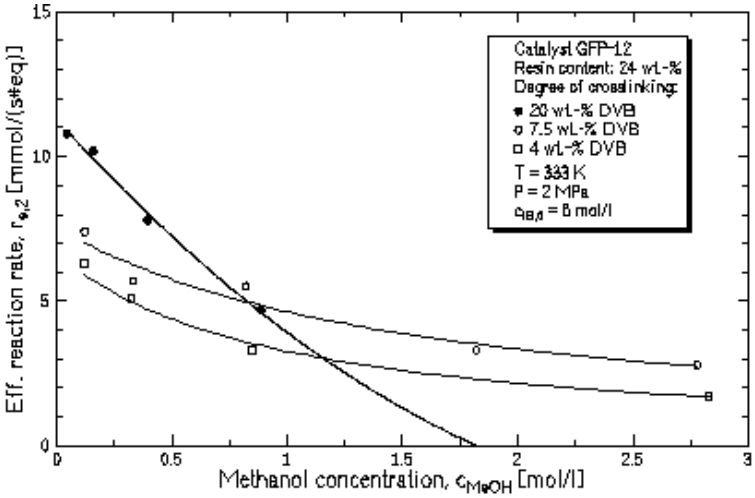

Fig. 8.19 Influence of cross-linking of polymer/ceramic ion-exchange catalysts for the dimerization of isobutene during MTBE synthesis at high polymer loading

8.7
Outlook: Extension to Other Synthetic Processes With Integrated Separation

After having tested samples of polymer/carrier catalysts with varied polymer load and cross-linking in the MTBE reaction and successfully used the Raschig rings in a TAME column [25] we extended the application to other chemical syntheses.

8.7.1
Reactive Stripping

In a reactive stripping process one disadvantage of RD can be avoided. If in an RD process the pressure is chosen, the temperature is a result of this pressure. Pressure and temperature are always coupled because all of the reactants are heated until evaporation occurs, which means that the reaction temperature is determined by the pressure or vice versa. This coupling of temperature and pressure does not happen in a reactive stripping process. In such a process the reactants are feed as a liquid to the top of a column and trickle over the catalyst bed downwards. During the flow to the bottom of the column chemical reaction and separation occur. This process is useful for fine chemical production, in which the reactants may not be heated to their boiling points as is very often the case in organic synthesis [26]. Polymer/carrier Raschig rings were tested successfully for the esterification of fatty acids with long chain alcohols. The operating temperature was up to 120 °C. The Raschig rings changed in color into deep dark brown, but ion-exchange capacity measurements revealed that the capacity did not change during operation for several weeks. This observation might be explained by the fact that desulfonation occurs fast if water is present, but in the stripping process of esterification the by-

product water was removed by the stripping gas hydrogen. The product ester leaves the column at the bottom; water and hydrogen leave the column at the top. The use of hydrogen as stripping gas might be a rare choice, but there are two reasons: one is the high diffusion coefficient of water vapor in hydrogen and the other is that the hydrogen can be used for hydrogenation of double bonds in a bifunctional catalyst.

8.7.2 Reactive Chromatography

Based on our experience with the preparation of Raschig rings, we succeeded in making monolithic rods. We prepared samples with diameters of 5.3 and 12 mm and lengths of 110 and 200 mm. The sulfonated monoliths were tested in tetrahydrofuran synthesis from 1,4-butandiol in which water is formed as a by-product of this cyclization etherification. The two products have different sorption behavior from the resin particles, which can be used to separate the products if the catalyst is operated as a chromatographic column [27]. As a reactor the rod was encapsulated in a fiber-reinforced epoxy resin casing allowing operation at pressures up to 100 bar. The casing was equipped with HPLC fittings: Fig. 8.20 shows a cross-section of this column.

This microreactor was heated to the desired reaction temperature and dioxan was pumped through the reactor. If a pulse of 1,4-butandiol is injected into the flowing dioxan, the diol forms tetrahydrofuran and water on the acidic polymer particles inside the channels of the rod. Water is adsorbed strongly: tetrahydrofuran leaves the reactor first, followed by water. Fig. 8.21 gives a calculated chromatogram based on sorption data.

The production of water-free tetrahydrofuran is possible using this method [28], but this is only a model reaction. No one will produce a bulk chemical like tetrahydrofuran in a microreactor. But products with higher value have similar reaction behavior, for example the esterification of end-terminated long-chain hydroxycarbon acids. An inner ester forms by cyclization leading to macrocyclic compounds, which can be used in the flavor and fragrance industry.

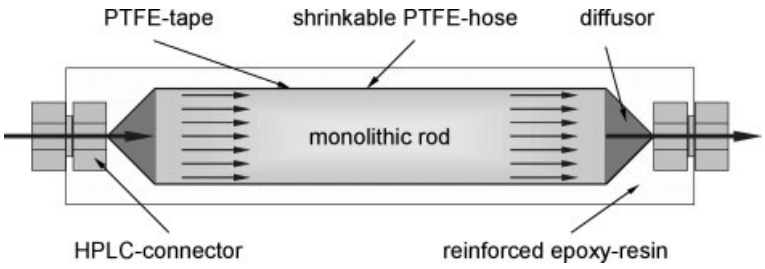

Fig. 8.20 Cross sectional drawing of a monolithic reactor

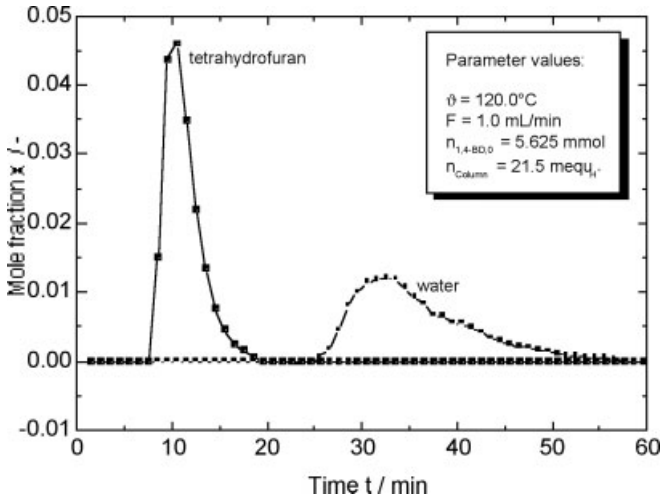

Fig. 8.21 Conversion of 1,4-butanediol with simultaneous separation of the products tetrahydrofuran and water on a monolithic reactor: column length = 180 mm; column diameter = 12 mm

8.7.3
Polymer-Assisted Solution-Phase Organic Synthesis

Another very interesting field of application is polymer-assisted solution-phase synthesis. In this synthetic approach one of the reactants is fixed on the solid polymer support and the other reactant is added in solution [29]. Detailed review papers concerning aspects of polymer design for synthetic purposes have been published, but solid phase synthesis as a convenient laboratory method in organis synthesis emerged only recently [30–32]. The advantage of this method is that purification of the product mixture is simplified. By-products stay on the resin phase whereas the product solution leaves the reactor. To enhance the convenience of this method we developed microreactors consisting of a monolithic rod with a basic ion-exchange resin inside the pore volume [33]. These microreactors were used as batch reactors in recycling mode. In co-operation with others, several organic reactions could be performed covering reductions, oxidations, and nucleophilic substitutions, as described in a paper published recently [34].

8.8
Conclusions

In this chapter we summarize results from our work on RD catalysts, which we started in the early 1980s [11, 24, 25, 35–43]. The concept of polymer/carrier materials in the shape of Raschig rings, rods, discs, or other shapes has demonstrated its benefits in a number of applications. Starting from the requirements for RD

processes a new class of materials was developed that allowed the extension to other processes like reactive stripping, membrane reactors, chromatographic reactors, or microreactors for the preparation of potential pharmaceuticals. The main advantages of the new materials are the small size of the interconnected polymer particles ensuring high accessibility of the active sites, the large pores of the megaporous carriers allowing enhanced mass transfer by convective flow through the polymer phase, and the dimensional stability of the polymer phase under swelling/shrinking conditions. With this new technique even monolithic microreactors for fine chemical production are possible. Fig. 8.22 shows the materials and the fields of application are compiled. As can be seen many applications are possible by this type of new materials. Commercialization of polymer/carrier materials is done by the Chelona company, Potsdam, Germany.

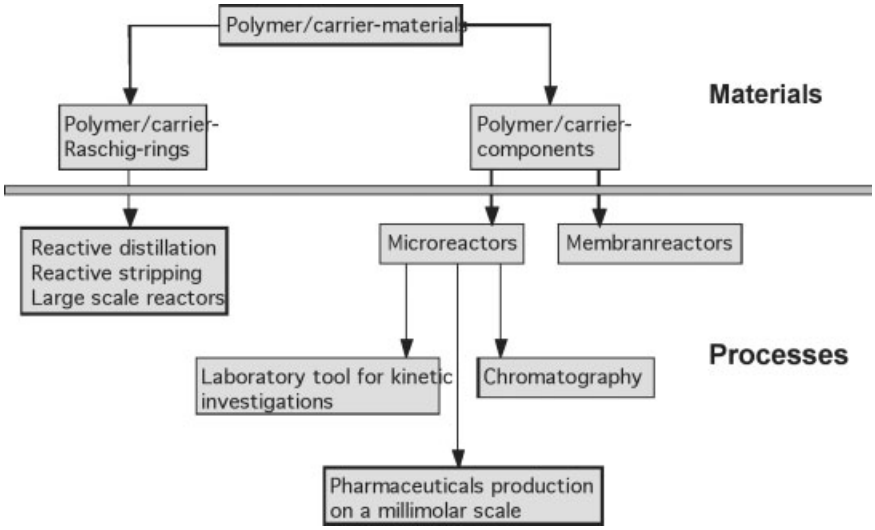

Fig. 8.22 Polymer/carrier materials and components and their fields of application

References

1 Spes, H. **1966**, German Patent 1 285 170.
2 Smith, L. A. **1981**,US Patent 4 250 052.
3 Stringaro, J. P. **1993**, EP 0 631 813 A1.
4 Rock, K.; Smith, L.; Chen, J., in *AIChE Spring Meeting*, New Orleans, Louisiana, USA, 29 March, **1992**.
5 Hearn, D. **1993**, WO 94/00235.
6 Spes, H. **1970**, DE 1 300 233.
7 Fuchigami, Y. *J. Chem. Eng. Japan* **1990**, *23*, 354–359.
8 Chaplits, D. N. **1977**, US Patent 4 012 456.
9 Yoshioka, T.; Shimamura, M. *Bull. Chem. Soc. Japan* **1983**, *56*, 3726–3729.
10 Yoshioka, T. *Bull. Chem. Soc. Japan* **1985**, *58*, 2618–2625.
11 Rehfinger, A. PhD Thesis, TU Clausthal, **1988**.
12 Childress, D. L.; Tasset, E. L.; Weaver, J. D. **1987**, Int. Patent 0 503 688 A2.
13 Hiramatsu, Y. D. S. F.; Ishiushi, Y.; Nagashima, H. **1990**, Int. Patent 0 492 064 A1.
14 Bareis, E.; Büchel, U.; Elias, H. G. *Angewand. Chemie* **1976**, *55*, 129–139.
15 Eiceman, G. A. *J. Chromatogr.* **1982**, *242*, 267–274.
16 Dromard, A.; Millet, C. **1982**, Int. Patent 0 065 925 A1.
17 Ancillotti, F.; Massi Mauri, M.; Pescarollo, E.; Romagnoni, L. *J. Mol. Catal.* **1978**, *4*, 37–48.
18 Helfferich, F. *Ion Exchange*, Mc Graw Hill, LCCCN 61-15435, **1962**.
19 Dorfner, K. *Ion Exchangers*, de Gruyter, ISBN 3-11-010341-9, **1991**.
20 Iler, R. K. *The Chemistry of Silica*, John Wiley, ISBN 0-471-02404-X, **1979**.
21 Weigand, N.; Sebastian, I.; Halarz, I. *J. Chromatogr.* **1974**, *102*, 325–332.
22 Richardson, J. T.; Twigg, M. V., in *Preparation of Catalysts VI*, Elsevier, ISBN 0-444-82078-7, **1995**.
23 Hoffmann, U.; Kunz, U.; Bruderreck, H.; Gottlieb, K.; Schädlich, H. K.; Becker, S. **1993**, WO 94/08713.
24 Sundmacher, K. PhD Thesis, TU Clausthal, **1995**.
25 Krummradt, H. PhD Thesis, TU Clausthal, **1995**.
26 Kunz, U.; Hoffmann, U. **1996**, EP 0 859 653 B1.
27 Kunz, U.; Hoffmann, U.; Altwicker, C.; Limbeck, U. **1999**, DE 199 29 073.3.
28 Kunz, U.; Altwicker, C.; Limbeck, U.; Hoffmann, U. *J. Mol. Catal.*, accepted for publication.
29 Kirschning, A.; Monenschein, H.; Wittenberg, R. *Angewand. Chemie Int. Ed.* **2001**, *40*, 650–679.
30 Guyot, A., in *Synthesis and Separations using Functional Polymers*, D. C. Sherington, P. Hodge (Eds.), John Wiley, **1988**.
31 Hudson, D. *J. Combin. Chem.* **1999**, *1* (I), 333–360.
32 Hudson, D. *J. Combin. Chem.* **1999**, *1* (II), 403–457.
33 Kunz, U.; Kirschning, A.; Hoffmann, U., **2001**, PCT/DE01/01092.
34 Kunz, U.; Kirschning, A., in *5th Int. Conf. Microreaction Technology, IMRET 5*, Strasbourg, France, 27–30 May **2001**.
35 Kunz, U. CUTEC-Schriftenreihe Nr. 34, Clausthal-Zellerfeld, **1998**.
36 Flato, J. PhD Thesis, TU Clausthal, **1990**.
37 Oost, C. PhD Thesis, TU Clausthal, **1995**.
38 Künne, H. PhD Thesis, TU Clausthal, **1996**.
39 Rappmund, P. PhD Thesis, TU Clausthal, **1998**.
40 Thiel, C. PhD Thesis, TU Clausthal, **1997**.
41 Limbeck, U. PhD Thesis, TU Clausthal, **2000**.
42 Löning, S. PhD Thesis, TU Clausthal, **2001**.
43 Altwicker, C. PhD Thesis, TU Clausthal, **2001**.

Reactive Distillation. Edited by Kai Sundmacher, Achim Kienle

ISBNs: 3-527-30579-3 (Hardback); 3-527-60052-3 (Electronic)

Part IV
Modeling and Process Control

Reactive Distillation. Edited by Kai Sundmacher, Achim Kienle

ISBNs: 3-527-30579-3 (Hardback); 3-527-60052-3 (Electronic)

9
Modeling of Homogeneous and Heterogeneous Reactive Distillation Processes

R. Taylor and R. Krishna

9.1
Introduction

This chapter is concerned solely with the modeling of RD processes. The widely used equilibrium stage model is described first, followed by a discussion of the variety of non-equilibrium models needed to model these complicated processes. A perspective on the use of these models in RD process design concludes this chapter.

We make no attempt to be comprehensive in our citation of the relevant literature since to do so would significantly lengthen the chapter. Instead, readers are referred to our recent review of the literature on modeling reactive distillation in which we tried to be nearly completely comprehensive in our coverage [1]. That review updates an earlier one by Doherty and Buzad [2], which is partially responsible for the surge in interest in reactive distillation. Of the more than 300 papers cited in our review, more than half appeared after 1992 [1]! The recent textbook of Doherty and Malone also contains an excellent introduction to the subject of reactive distillation and a fairly extensive bibliography [3].

9.2
Equilibrium Stage Models

The development and application of the equilibrium (EQ) stage model for conventional (i. e., non-reactive) distillation has been described in several textbooks [4]. Here we are concerned with the extension of this standard model to distillation accompanied by chemical reaction(s).

A schematic diagram of an equilibrium stage is shown in Fig. 9.1a. Vapor from the stage below and liquid from the stage above is brought into contact on the stage together with any fresh or recycled feeds. The vapor and liquid streams *leaving* the stage are *assumed* to be in equilibrium with each other. A complete separation process is modeled as a sequence of s of these equilibrium stages (Fig. 9.1b).

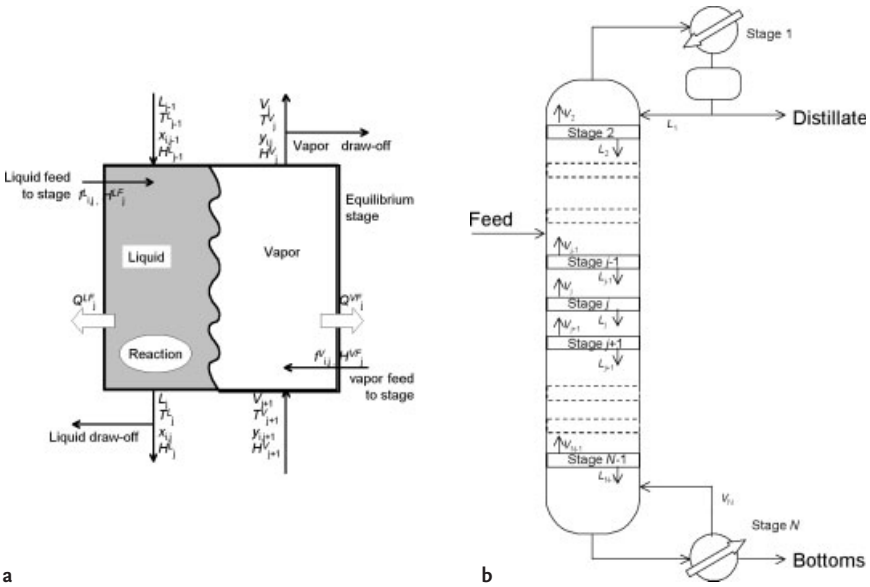

Fig. 9.1 a) The equilibrium stage; b) multi-stage distillation column

The equations that model equilibrium stages are known as the MESH equations, MESH being an acronym referring to the different types of equation. The M equations are the material balance equations; the total material balance takes the form

$$\frac{\mathrm{d}U_j}{\mathrm{d}t} = V_{j+1} + L_{j-1} + F_j - (1 + r_j^{\mathrm{V}})V_j - (1 + r_j^{\mathrm{L}})L_j + \sum_{m=1}^{r}\sum_{i=1}^{c} \nu_{i,m} R_{m,j} \varepsilon_j \tag{9.1}$$

U_j is the hold-up on stage j. With very few exceptions, U_j is considered to be the hold-up only of the liquid phase. It is, however, important to include the hold-up of the vapor phase at higher pressures. The component material balance (neglecting the vapor hold-up) is

$$\frac{\mathrm{d}U_j x_{i,j}}{\mathrm{d}t} = V_{j+1}y_{i,j+1} + L_{j-1}x_{i,j-1} + F_j z_{i,j} - (1+r_j^{\mathrm{V}})V_j y_{i,j} - (1 + r_j^{\mathrm{L}})L_j x_{i,j} + \sum_{m=1}^{r} \nu_{i,m} R_{m,j} \varepsilon_j \tag{9.2}$$

In the material balance equations given above, r_j is the ratio of sidestream flow to interstage flow

$$r_j^{\mathrm{V}} = S_j^{\mathrm{V}}/V_j; \quad r_j^{\mathrm{L}} = S_j^{\mathrm{L}}/L_j \tag{9.3}$$

$\nu_{i,m}$ represents the stoichiometric coefficient of component i in reaction m and ε_j represents the reaction volume.

The E equations are the *phase* equilibrium relations

$$y_{i,j} = K_{i,j} x_{i,j} \tag{9.4}$$

Chemical reaction equilibrium is not considered in many of the early papers because it is more difficult to model. There are, however, some exceptions to this statement and such works are noted in [1].

The S equations are the summation equations

$$\sum_{i=1}^{c} x_{i,j} = 1; \quad \sum_{i=1}^{c} y_{i,j} = 1 \tag{9.5}$$

The enthalpy balance is given by

$$\frac{\mathrm{d}\, U_j H_j}{\mathrm{d}t} = V_{j+1} H_{j+1}^{\mathrm{V}} + L_{j-1} H_{j-1}^{\mathrm{L}} + F_j H_j^{\mathrm{F}} - (1 + r_j^{\mathrm{V}}) V_j H_j^{\mathrm{V}} - (1 + r_j^{\mathrm{L}}) L_j H_j^{\mathrm{L}} - Q_j \tag{9.6}$$

The superscripted H are the enthalpies of the appropriate phase. The enthalpy in the time derivative on the left-hand side represents the total enthalpy of the stage but, for the reasons given above, this will normally be the liquid phase enthalpy. Some authors include an additional term in the energy balance for the heat of reaction. However, if the enthalpies are referred to their elemental state then the heat of reaction is accounted for automatically and no separate term is needed.

Under steady-state conditions all of the time derivatives in the above equations are equal to zero.

Some authors include additional equations in their (mostly unsteady-state) models. For example, pressure drop, controller equations, and so on.

Much of the early literature on RD modeling is concerned primarily with the development of methods for solving the steady state EQ stage model. For the most part such methods are more or less straightforward extensions of methods that had been developed for solving conventional distillation problems. The number of examples that illustrate most of the early papers usually is rather limited, both in number as well as in the type of RD process considered (quite often it is an esterification reaction). Only rarely is there any attempt to compare the results of simulations to experimental data. More and more of the more recent modeling studies are carried out using one or other commercial simulation package: Aspen Plus, Pro/II, HYSYS, and SpeedUp are the packages mentioned most often in the published literature [1].

It is well known that real distillation processes do not operate at equilibrium. The conventional way out of this difficulty is to introduce an efficiency factor in to the model equations. There are many different definitions of the stage efficiency; that of Murphree is most often used in EQ stage simulation

$$E_j^{\mathrm{MV}} = \frac{\overline{y_{i\mathrm{L}}} - y_{i\mathrm{E}}}{y_i^* - y_{i\mathrm{E}}}; \quad i = 1, 2, \ldots n \tag{9.7}$$

where $\overline{y_{iL}}$ is the average composition of the vapor leaving the tray, y_{iE} is the composition of the vapor entering the tray, and y_i is the composition of the vapor in equilibrium with the liquid leaving the tray. Since the mole fractions add to unity, only $(n - 1)$ of the Murphree component efficiencies are independent. For distillation of systems with three or more species, the component efficiencies are almost always unequal to one another and these can routinely assume values greater than unity or less than zero [5].

For packed columns it is common to use the HETP (height equivalent to a theoretical plate). The behavior of HETPs in multi-component mixtures is closely related to the behavior of stage efficiencies.

There are no fundamentally sound methods for estimating either efficiencies or HETPs in RD operations, in which the presence of chemical reactions will have an influence on the component efficiencies. If an efficiency factor of any kind is used it is more often than not treated as an adjustable parameter (or set of parameters) for fitting experimental data. Some authors have obtained good agreement with experimental data in this way [6].

9.3 Non-equilibrium Stage Modeling

In recent years the evidence has been growing that distillation (and related) operations are better simulated with non-equilibrium (NEQ) models that take account of mass (and energy) transfer (and sometimes of fluid-flow patterns) in a manner that is more rigorous than is possible with the EQ stage models.

9.3.1 The Conventional NEQ Model

It will be helpful to begin with a brief review of the NEQ model of Krishnamurthy and Taylor [7] for conventional distillation and absorption operations. A schematic representation of the NEQ stage is shown in Fig. 9.2. This NEQ stage may represent a tray or a cross section of a packed column.

The component molar balances for the vapor and liquid phases are

$$V_j y_{i,j} - V_{j+1} y_{i,j+1} - f_{j,j}^{V} + N_{i,j}^{V} = 0 \tag{9.8}$$

$$L_j x_{i,j} - L_{j-1} x_{i,j-1} - f_{j,j}^{L} - N_{i,j}^{L} = 0 \tag{9.9}$$

$N_{i,j}$ are the interfacial mass-transfer rates: the product of the molar fluxes and the net interfacial area. The overall molar balances are obtained by summing Eqs. (9.8) and (9.9) over the total number (c) of components in the mixture. At the vapor–liquid interface we have the continuity equations

$$N_i^{V}|_I = N_i^{L}|_I = 0 \tag{9.10}$$

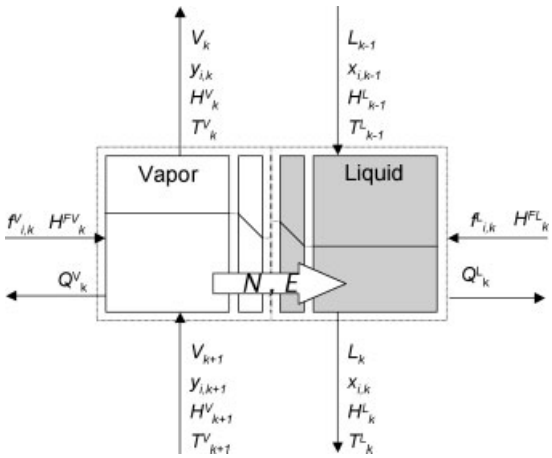

Fig. 9.2 The non-equilibrium stage (cell) for homogeneous liquid phase reaction

The enthalpy balances for both vapor and liquid phases are

$$V_j H_j^{\mathrm{V}} - V_{j+1} H_{j+1}^{\mathrm{V}} - F_j^{\mathrm{V}} H_j^{\mathrm{VF}} + E_j^{\mathrm{V}} + Q_j^{\mathrm{V}} = 0 \tag{9.11}$$

$$L_j H_j^{\mathrm{L}} - L_{j-1} H_{j-1}^{\mathrm{L}} - F_j^{\mathrm{L}} H_j^{\mathrm{LF}} + E_j^{\mathrm{L}} + Q_j^{\mathrm{L}} = 0 \tag{9.12}$$

E_j are the interphase energy transfer rates, the product of the energy fluxes and the net interfacial area. We also have continuity of the energy transfer rates at the interface.

$$E^{\mathrm{V}}|_{\mathrm{I}} = E^{\mathrm{L}}|_{\mathrm{I}} \tag{9.13}$$

The most fundamentally sound way to model mass transfer in multi-component systems is to use the Maxwell–Stefan theory [5, 8]. The Maxwell–Stefan equations for mass transfer in the vapor and liquid phases respectively are given by

$$\frac{y_i}{\mathrm{R}T^{\mathrm{V}}} \frac{\partial \mu_i^{\mathrm{V}}}{\partial z} = \sum_{k=1}^{c} \frac{y_i N_k^{\mathrm{V}} - y_k N_i^{\mathrm{V}}}{c_t^{\mathrm{V}} Đ_{i,k}^{\mathrm{V}}} \tag{9.14}$$

and

$$\frac{x_i}{\mathrm{R}T^{\mathrm{L}}} \frac{\partial \mu_i^{\mathrm{L}}}{\partial z} = \sum_{k=1}^{c} \frac{x_i N_k^{\mathrm{L}} - x_k N_i^{\mathrm{L}}}{c_t^{\mathrm{L}} Đ_{i,k}^{\mathrm{L}}} \tag{9.15}$$

where x_i and y_i are the mole fractions of species i in the liquid and vapor phases respectively. The N_i are the molar fluxes of species i, and the $Đ_{i,k}$ represent the corresponding Maxwell–Stefan diffusivity of the $i-k$ pair in the appropriate phase. Only $c - 1$ of the Eqs. (9.14) and (9.15) are independent; the mole fraction of the last component is obtained by the summation equations for both phases.

The energy flux is related to conductive and convective contributions as follows

$$E_j^{\mathrm{L}} = -\lambda_j^{\mathrm{L}} \frac{\partial T^{\mathrm{L}}}{\partial \eta} + \sum_{i=1}^{c} N_{i,j}^{\mathrm{L}} H_{i,j}^{\mathrm{L}} \tag{9.16}$$

Eqns. (9.16, 9.18) form a system of nonlinear, coupled differential equations that must be solved numerically in most cases. In practice, at least for non-reactive separations, the $N_{i,j}$ are obtained from the Maxwell–Stefan equations (9.16) modified as follows

$$\frac{x_{i,j}}{\mathrm{R}T_j} \frac{\partial \mu_{i,j}^{\mathrm{L}}}{\partial \eta} = \sum_{k=1}^{c} \frac{x_{i,j} N_{k,j}^{\mathrm{L}} - x_{k,j} N_{i,j}^{\mathrm{L}}}{c_{t,j}^{\mathrm{L}} (\kappa_{i,k}^{\mathrm{L}} a)_j} \tag{9.17}$$

with a similar relation for the vapor phase. The $\kappa_{i,k}^{\mathrm{L}}$ represents the mass-transfer coefficient of the $i-k$ pair in the liquid phase; this coefficient is estimated from information on the corresponding Maxwell–Stefan diffusivity $Đ_{i,k}^{\mathrm{L}}$ using the standard procedures discussed in Taylor and Krishna [5]. a is the interfacial area.

Equation (9.17) is based on a film model of interphase transport. For this model Eqs. (9.14, 9.15) may be solved analytically, subject to some simplifying assumptions, of course [5].

The energy transfer rates are given by

$$E_j^{\mathrm{L}} = -h_j^{\mathrm{L}} a \frac{\partial T^{\mathrm{L}}}{\partial \eta} + \sum_{i=1}^{c} N_{i,j}^{\mathrm{L}} H_{i,j}^{\mathrm{L}} \tag{9.18}$$

with a similar relation for the vapor phase. h_j^{L} is the heat transfer coefficient in the liquid phase.

At the vapor–liquid interface we assume phase equilibrium

$$y_{i,j}|_{\mathrm{I}} = K_{i,j} x_{i,j}|_{\mathrm{I}} \tag{9.19}$$

where the subscript I denotes the equilibrium compositions and $K_{i,j}$ is the vapor–liquid equilibrium ratio for component i on stage j. The K-values are evaluated at the temperature, pressure, and composition of the interface from appropriate thermodynamic models (the same models used in conventional equilibrium stage models).

Furthermore, in the NEQ model we take account of the pressure drop across a stage

$$p_j - p_{j-1} - (\Delta p_{j-1}) = 0 \tag{9.20}$$

where p_j and p_{j-1} are the stage pressures and Δp_{j-1} is the pressure drop per tray from stage $(j-1)$ to stage j. The pressure drop over the stage is considered to be a function of the stage flows, the physical properties, and the hardware design. In the NEQ model, hardware design information must be specified so that mass-

transfer coefficients, interfacial areas, liquid hold-ups, and so on can be calculated. The NEQ model requires thermodynamic properties, not only for calculation of phase equilibrium but also for calculation of driving forces for mass transfer. In addition, physical properties such as surface tension, diffusion coefficients, and viscosities, for calculation of mass (and heat) transfer coefficients and interfacial areas are required. The steady-state model equations most often are solved using Newton's method or by homotopy-continuation. A review of early applications of NEQ models is available [5].

9.3.2 NEQ Modeling of Reactive Distillation

Building an NEQ model of a reactive separation process is not as straightforward as it is for the EQ stage model, in which we simply (or not so simply) add a term to account for reaction to the liquid phase material balances. It must be recognized that no single model can deal with all possible situations; separate models are needed depending on the way in which the reaction is brought into the process. We can identify two very different types of reactive separation process: a homogeneous system in which the reaction (catalyzed or not) takes place only in the liquid phase, or a heterogeneous system in which a solid phase is present to catalyze the reaction. We consider each type of system in turn.

9.3.3 Homogeneous Systems

If the reaction occurs in the liquid phase (without any solid catalyst present), as is the case in some reactive separations, then we must consider the following steps in the transport process as depicted in Fig. 9.3:

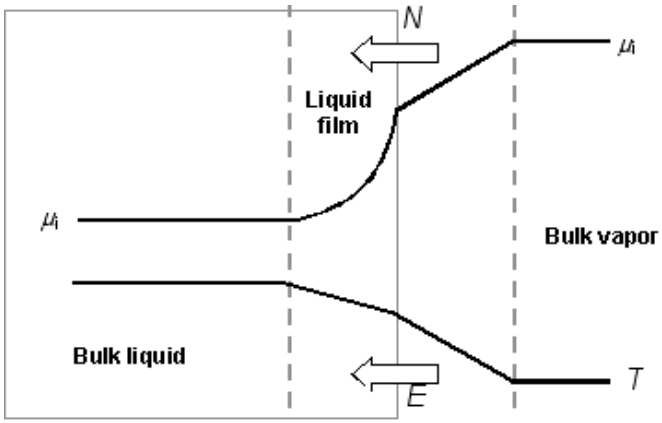

Fig. 9.3 Transport processes in homogeneous liquid phase reactive distillation

– mass transfer through the vapor film,
– mass transfer with reaction in the liquid film, and
– reaction in the bulk liquid.

There are two limiting cases of practical importance:

– homogeneous slow liquid phase reaction and
– homogeneous rapid liquid phase reaction.

If the reaction rate is very slow then the reaction takes place essentially only in the bulk liquid and the non-equilibrium model of Krishnamurthy and Taylor [7] will suffice with the modification of the bulk phase material balances to account for the chemical reactions.

$$L_j x_{i,j} - L_{j-1} x_{i,j-1} - f_{i,j}^{\mathrm{L}} - N_{i,j}^{\mathrm{L}} - \sum_{m=1}^{r} \nu_{i,m} R_{m,j} \varepsilon_j = 0 \tag{9.21}$$

where $R_{m,j}$ is the rate of reaction m on stage j, $\nu_{i,m}$ represents the stoichiometric coefficient of component i in reaction m, and ε_j represents the reaction volume on stage j. For homogeneous reactions this is given by the total liquid hold-up on stage j and, in an NEQ model, is obtained directly from the column internals specifications and appropriate hydrodynamic correlations. No modification of the interface mass transfer or equilibrium equations is needed. In other words, we may safely ignore the influence of reaction in the liquid film.

If it is sufficiently rapid, the reaction will also take place in the liquid film adjacent to the phase interface, and very fast reactions may occur only in the film. In either case the continuity equations for the film are required for taking into account the effect of the reaction on the interphase mass-transfer rates

$$\frac{\partial N_i}{\partial z} = \sum_{m=1}^{r} \nu_{i,m} R_m \tag{9.22}$$

For most reactive distillations the change in the fluxes through the film will not be significant because the Hatta numbers are smaller than unity. The composition profile within the film will be approximately linear. For other reactive separation processes (e. g., reactive absorption) the composition change in the film will be very important. It will not always be clear in advance, in which regime a particular process will be operating, and the regime may even vary from stage to stage. Thus, the most general approach is to solve the MS and continuity equations simultaneously for all cases involving homogeneous reactions. In this case the combined set of MS and continuity equations usually must be solved numerically.

The phase equilibrium equations for the interface may also need to be modified for the influence of additional species on the thermodynamic properties at the interface. A case in point is sour water stripping, in which reactions in the liquid phase create additional species (including ions), which affect the interfacial equilibrium. Enhancement factors have been derived for many cases and there is no sin-

gle model that can be used in all cases. Indeed, each process must be considered on its merits. Almost never is the mass-transfer process treated rigorously using the Maxwell–Stefan equations since to do so would involve numerical solution of a coupled system of differential equations. Instead, an effective diffusivity model is used, which can be solved analytically. Such models are strictly valid only for dilute systems in the absence of significant mass transfer by convection. Fortunately, some of the systems to which these models are applied are of this type so such simplified models are not entirely without value.

9.3.4 Heterogeneous Systems

If a solid catalyst influences the reaction then we must consider the nature of the catalyst as well. Two kinds of solid catalyst need be considered [9]:

- non-porous (e. g., coated sheet metal) or
- porous (e. g., Raschig rings made of Amberlyst).

In some processes the catalyst is present as a coating on a more or less standard form of structured packing. In this case we must consider the following steps in the transport process depicted in Fig. 9.4:

- transport of reactants from the bulk vapor to the bulk liquid,
- transport of reactants from the bulk liquid to the catalyst surface,
- reaction at the surface,
- transport of reaction products from the catalyst surface to the bulk liquid, and
- transport of the reaction products from the bulk liquid to the bulk vapor.

The first two and last two of these steps should be modeled using the Maxwell–Stefan equations as discussed above. The surface reaction provides the surface boundary

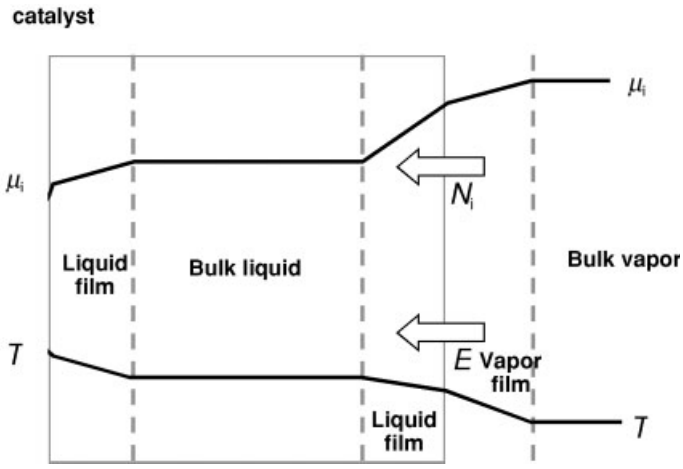

Fig. 9.4 Transport processes in RD with a solid non-porous catalytic packing

condition on the liquid–solid mass-transfer process. In some cases one or more of these steps may be rate determining allowing some simplification in the modeling of the transport and reaction processes.

In many more cases, however, the cases we have a porous catalyst that is supported in some structure within the walls of the column. In these processes the list of transport and reaction processes is even longer than that above. As illustrated in Fig. 9.5, we must consider:

- transport of reactants from the bulk vapor to the bulk liquid,
- transport of reactants from the bulk liquid to the catalyst surface,
- diffusion with simultaneous reaction within the porous catalyst,
- transport of reaction products from the catalyst surface to the bulk liquid, and
- transport of the reaction products from the bulk liquid to the bulk vapor.

The first of these steps can be modeled using the Maxwell–Stefan equations as already discussed above. There are two approaches to modeling the remaining steps: a pseudo-homogeneous model or a heterogeneous model.

The first, and simplest, approach is to treat the reaction pseudo-homogeneously, whereby catalyst diffusion (including diffusion to the catalyst surface) and reaction are lumped into an overall reaction term. For heterogeneous reactions that are modeled in this way the liquid phase material balance is as given above and ε_j is given by the total amount of catalyst present on the stage under consideration. In this case, one only needs to specify catalyst mass and activity.

A more rigorous approach to modeling heterogeneous systems involving porous catalyst particles (Fig. 9.5) would require a complete description of mass transport to the catalyst and diffusion and reaction inside the catalyst particles.

Modeling multi-component mass transfer in porous media is complicated when the mean-free-path length of the molecules is of the order of magnitude of the pore diameter. The difficulties posed by this case may be circumvented by a method

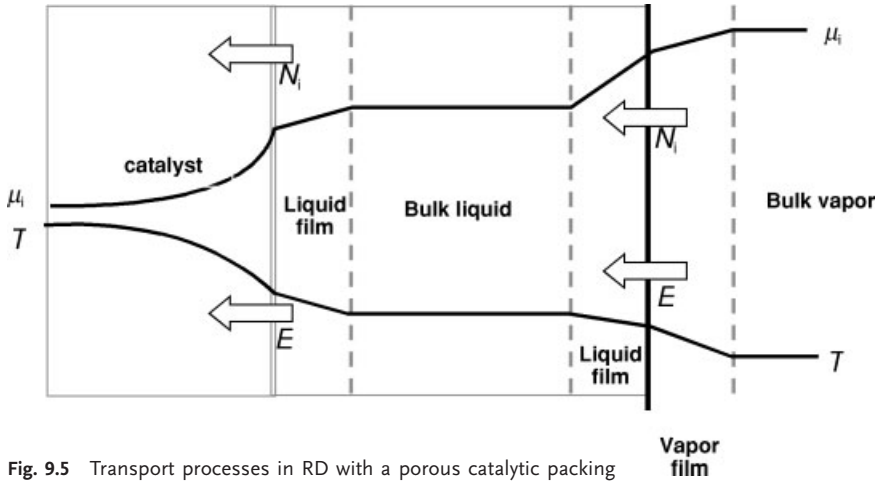

Fig. 9.5 Transport processes in RD with a porous catalytic packing

originally introduced by Maxwell in 1866 and developed further by Mason et al. [10]. Maxwell suggested that the porous material itself be described as a supplementary 'dust' species, consisting of very large molecules that are kept motionless by some unspecified external force. The Chapman–Enskog kinetic theory is then applied to the new pseudo-gas mixture, in which the interaction between the dust and gas molecules simulates the interaction between the solid matrix and the gas species. In addition, one is no longer faced with the problem of flux and composition variations across a pore and problems related to catalyst geometry.

The dusty fluid model as developed by Krishna and Wesselingh [8] is a modification of the dusty gas model so as to be able to model liquid phase diffusion in porous media. For a non-ideal mixture we have

$$\frac{x_i}{RT}\frac{\partial \mu_i}{\partial z} + \frac{x_i}{RT}\overline{V}_i\frac{\partial p}{\partial z} + \frac{x_i}{\eta}\frac{B_0}{D_{i,e}} = \sum_{k=1}^{c}\frac{x_i N_k - x_k N_i}{c_t \mathcal{D}^e_{i,k}} - \frac{N_i}{c_t D^e_i} \tag{9.23}$$

D^e_i is the effective Knudsen diffusion coefficient for species i in the porous catalyst.

The mass-transfer rates are obtained by multiplying the fluxes by the interfacial area of the catalyst particles. This is not as straightforward, as it looks, since, depending on the geometry of the catalyst, the cross-sectional area can change along the diffusion path. It is necessary to take catalyst geometry into account in the solution of these equations.

The dusty gas model is often used as the basis for the calculation of a catalyst effectiveness factor in chemical reactor analysis. The extension to non-ideal fluids noted above and its application in RD modeling has not been used as often, partly because of the somewhat greater uncertainty in the parameters that appear in the equations [1, 11].

9.3.5 NEQ Cell Model

An issue that is not adequately addressed by most models (EQ and NEQ) is that of vapor and liquid flow patterns on distillation trays or maldistribution in packed columns. Since reaction rates and chemical equilibrium constants are dependent on the local concentrations and temperature, they may vary along the flow path of liquid on a tray, or from side to side of a packed column. For such systems the residence time distribution could be very important, as well as a proper description of mass transfer. On distillation trays, vapor will rise more or less in plug flow through a layer of froth. The liquid will flow along the tray more or less in plug flow, with some axial dispersion caused by the vapor jets and bubbles. In packed sections, maldistribution of internal vapor and liquid flows over the cross-sectional area of the column can lead to loss of interfacial area.

To deal with this shortcoming of earlier non-equilibrium models, both steady state and dynamic NEQ cell models have been developed [12–15]. The distinguishing feature of this model is that stages are divided into a number of *contacting cells*, as shown in Fig. 9.6. These cells describe just a small section of the tray or packing,

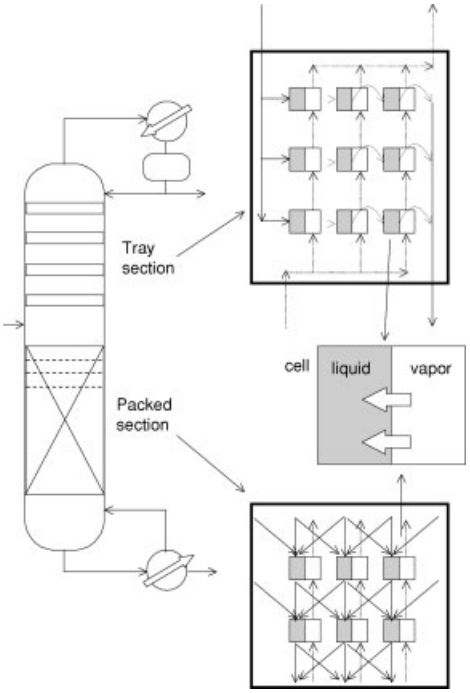

Fig. 9.6 The non-equilibrium cell model

and by choosing an appropriate set of cell connections, one can very easily study the influence of flow patterns and maldistribution on the distillation process.

Flow patterns on distillation trays are modeled by choosing an appropriate number of cells in each flow direction. A column of cells can model plug flow in the vapor phase, and multiple columns of cells can model plug flow in the liquid phase as depicted in Fig. 9.7. Back-mixing may also be taken into account by using an appropriate number of cells. This may be derived from calculating an equivalent number of cells from eddy diffusion models. Flow patterns in packed columns are evaluated by means of a natural flow model. The flows are split up according to the ratio of the cell surface areas between the cells. Other flow patterns may be approximated using different flow splitting policies.

The unit cell for homogeneous systems (and for heterogeneous systems modeled as though they were homogeneous) is depicted in Fig. 9.8. The equations for each cell are given in Table 9.1.

A schematic diagram of the unit cell for a vapor–liquid–porous catalyst system is shown in Fig. 9.9. Each cell is modeled essentially using the NEQ model for heterogeneous systems described above. The bulk fluid phases are assumed to be completely mixed. Mass-transfer resistances are located in films near the vapor–liquid and liquid–solid interfaces, and the Maxwell–Stefan equations are used for calculation of the mass-transfer rates through each film. Thermodynamic equilibrium is assumed only at the vapor–liquid interface. Mass transfer inside the porous catalyst may be described with the dusty fluid model described above.

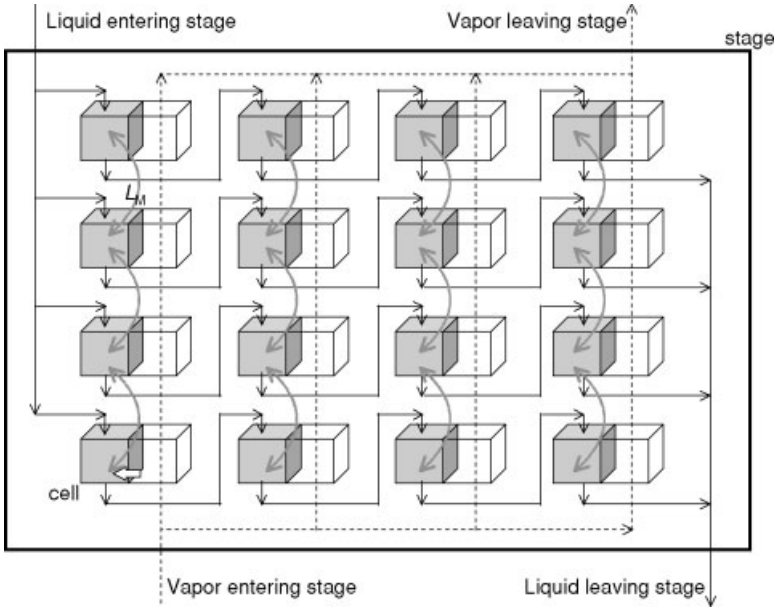

Fig. 9.7 Details of flows in and out of multiple cells used to model the hydrodynamics of trayed columns

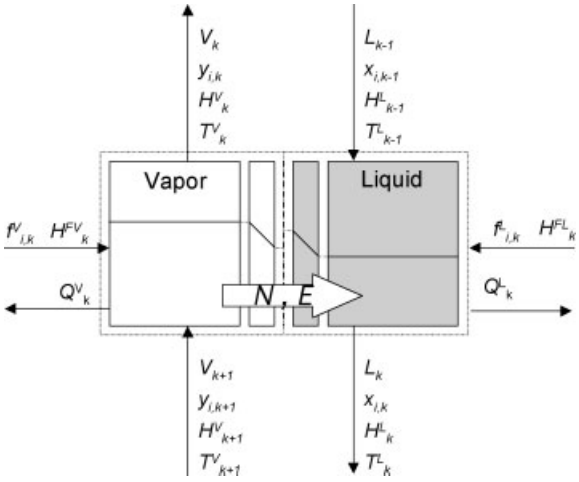

Fig. 9.8 The non-equilibrium stage (cell) for homogeneous catalyzed reaction

Table 9.1 Equations describing dynamic NEQ cell model

Equation type and number	***Liquid phase***	***Vapor phase***
Equations describing conservation laws for an NEQ cell		
Molar component balance (1)	$\frac{dM_i^L}{dt} = L_{in}x_{i,in} - Lx_i + N_i^L + \sum_{k=1}^{r} v_{i,k}R_k\varepsilon^L$	$\frac{dM_i^V}{dt} = V_{in}y_{i,in} - Vy_i - N_i^V$
Total molar hold-up (2)	$\frac{dM^L}{dt} = L_{in} - L + \sum_{k=1}^{c} N_i^L + \sum_{i=1}^{c}\sum_{k=1}^{r} v_{i,k}R_k\varepsilon^L$	$\frac{dM^V}{dt} = V_{in} - V - \sum_{k=1}^{c} N_k^V$
Mole fractions (3)	$x_i = M_i^L/M^L$	$y_i = M_i^V/M^V$
Summation (4)	$\sum_{k=1}^{c} x_k = 1$	$\sum_{k=1}^{c} y_k = 1$
Energy balance (5)	$\frac{dE^L}{dt} = L_{in}\frac{E_{in}^L}{M_{in}^L} - L\frac{E^L}{M^L} + E^L$	$\frac{dE^V}{dt} = V_{in}\frac{E_{in}^V}{M_{in}^V} - V\frac{E^V}{M^V} - E^V$
Energy hold-up (6)	$E^L = H^L M^L$	$E^V = H^V M^V$
Equations describing conservation laws with diffusion "films" (for cell)		
Molar component balance (7)	$\frac{\partial N_i^{Lf}(\eta^{Lf})}{\partial\eta^{Lf}} + \sum_{k=1}^{r} v_{i,k}R_k(\eta^{Lf})A\delta^{Lf} = 0$	$\frac{\partial N_i^{Vf}(\eta^{Vf})}{\partial\eta^{Vf}} = 0$
Maxwell-Stefan relations (8)	$\frac{x_i^{LF}}{RT^{Lf}}\frac{\partial\mu_i^{Lf}}{\partial\eta} = \sum_{k=1}^{c}\frac{x_i^{LF}N_k^{Lf} - x_k^{LF}N_i^{Lf}}{c_t^{Lf}\kappa_{i,k}^{Lf}A}$	$\frac{y_i^{VF}}{RT^{Vf}}\frac{\partial\mu_i^{Vf}}{\partial\eta} = \sum_{k=1}^{c}\frac{y_i^{VF}N_k^{Vf} - y_k^{VF}N_i^{Vf}}{c_t^{Vf}\kappa_{i,k}^{Vf}A}$
Summation equations (9)	$\sum_{k=1}^{c} x_{i,j}^{LF} = 1$	$\sum_{k=1}^{c} y_{i,j}^{VF} = 1$
Energy balance (10)	$\frac{\partial E^{Lf}}{\partial\eta^{Lf}} = 0$	$\frac{\partial E^{Vf}}{\partial\eta^{Vf}} = 0$
Energy transfer rate (11)	$E^{Lf} = -h^{Lf}A\frac{\partial T^{Lf}}{\partial\eta} + \sum_{i=1}^{c} N_i^{Lf}H_i^{Lf}$	$E^{Vf} = -h^{Vf}A\frac{\partial T^{Vf}}{\partial\eta} + \sum_{i=1}^{c} N_i^{Vf}H_i^{Vf}$

Table 9.1 (continued)

Equation type and number	***Liquid phase***	***Vapor phase***
Relations at interface between vapor and liquid for cell		
Vapour-liquid equilibrium (12)		$y_i\Big\vert_{\mathrm{I}} = K_i x_i\Big\vert_{\mathrm{I}}$
Temperature equilibrium (13)		$T^{\mathrm{V}f}\Big\vert_{\mathrm{I}} = T^{\mathrm{L}f}\Big\vert_{\mathrm{I}}$
Continuity of molar fluxes (14)		$N_i^{\mathrm{V}f}\Big\vert_{\mathrm{I}} = N_i^{\mathrm{L}f}\Big\vert_{\mathrm{I}}$
Continuity of energy fluxes (15)		$E^{\mathrm{V}f}\Big\vert_{\mathrm{I}} = E^{\mathrm{V}f}\Big\vert_{\mathrm{I}}$
Calculation of NEQ stage parameters by summing the outgoing streams from NEQ cells (total number of m cells in liquid flow path, n cells in vapor flow path, mm and nn are running indices in these paths)		
Molar flows leaving stage (16)	$\sum_{nn}^{n} L_{m,nn} = L_j$	$\sum_{mm}^{m} V_{mm,n} = V_j$
Mole fractions of flows leaving stage (17)	$\sum_{nn}^{n} x_{i,m,nn} L_{m,nn} = x_{i,j} L_j$	$\sum_{mm}^{m} y_{i,mm,n} V_{mm,n} = y_{i,j} V_j$
Enthalpy of flows leaving stage (18)	$\sum_{nm}^{n} \frac{E^{\mathrm{L}}_{m,nn}}{M^{\mathrm{L}}_{m,nn}} L_{m,nn} = H_j^{\mathrm{L}} L_j$	$\sum_{mm}^{m} \frac{E^{\mathrm{V}}_{mm,n}}{M^{\mathrm{V}}_{mm,n}} V_{mm,n} = H_j^{\mathrm{V}} V_j$
Hydrodynamics of trays		
Calculation of volumetric liquid and vapor hold-ups (19)	$\frac{1}{c^{\mathrm{L}}_{t,j}} M_j^{\mathrm{L}} \equiv \varepsilon_j^{\mathrm{L}} = h_{\mathrm{cl},j} A_{\mathrm{bub},j}$	$\frac{1}{c^{\mathrm{V}}_{t,j}} M_j^{\mathrm{V}} \equiv \varepsilon_j^{\mathrm{V}} = \left(h_t - h_{\mathrm{cl},j}\right) A_{\mathrm{bub},j}$

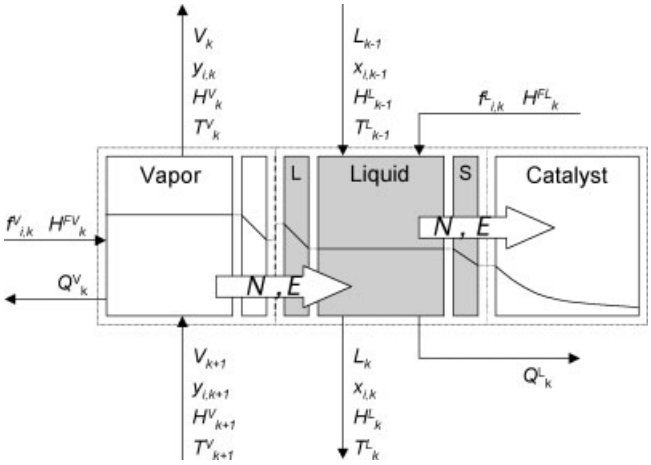

Fig. 9.9 The non-equilibrium stage (cell) for heterogeneous catalyzed reaction

9.3.6
Properties, Hydrodynamics, and Mass Transfer

The EQ model requires reaction kinetic parameters and thermodynamic properties; the latter for the calculation of phase equilibrium and taking into account the effect of non-ideal component behavior in the calculation of reaction rates and chemical equilibrium constants.

NEQ models also require thermodynamic properties, not only for calculation of phase equilibrium but also for calculation of driving forces for mass transfer. In addition, physical properties such as surface tension, diffusion coefficients, viscosities, and so on for calculation of mass (and heat) transfer coefficients and interfacial areas are required.

Equipment design information also must be specified in the NEQ model so that mass-transfer coefficients, interfacial areas, liquid hold-ups, and pressure drops can be calculated.

9.4
Comparison of EQ and NEQ Models

Applications of the EQ and NEQ models to RD were reviewed by Taylor and Krishna [1]. Most papers do not compare the two models directly (or even indirectly). Here, we wish to highlight a few studies that reveal the differences between these fundamentally different types of model.

Kreul et al. [16] used an NEQ model of homogeneous RD and, via a series of case studies, studied the importance of various model simplifications. They found little difference between the full MS description of multi-component mass transfer and

a much simpler effective diffusivity models. However, they also conclude that there can be significant differences between EQ and NEQ models, and that the additional effort of the more complicated NEQ approach is justified.

Baur et al. [17] have compared the EQ and the NEQ models for the MTBE process. They underlined some counter-intuitive features of RD processes. For example, for a methanol feed location yielding a low-conversion steady state, the introduction of mass-transfer resistance (i. e., use of the NEQ model), leads to a conversion higher than that predicted by the EQ model). The introduction of a mass-transfer resistance alleviates a 'bad situation' and has the effect of improving conversion.

Lee and Dudukovic [18] described an NEQ model for homogeneous RD in tray columns. The Maxwell–Stefan equations are used to describe interphase transport, with the AIChE correlations used for the binary (Maxwell–Stefan) mass-transfer coefficients. Newton's method and homotopy continuation are used to solve the model equations. Close agreement between the predictions of EQ and NEQ models were found only when the tray efficiency could correctly be predicted for the EQ model. In a subsequent paper Lee and Dudukovic [19] presented a dynamic NEQ model of RD in tray columns. The DAE equations were solved by use of an implicit Euler method combined with homotopy continuation. Murphree efficiencies calculated from the results of an NEQ simulation of the production of ethyl acetate were not constant with time.

Sundmacher et al. [20] used both EQ stage (with Murphree efficiency) and NEQ models to simulate the MTBE and TAME processes. The reactions were handled using both quasi-homogeneous and heterogeneous methods. Simulation results were compared to experimental data obtained in two laboratory-scale columns. A detailed NEQ model was needed to describe the TAME process, but both NEQ and the EQ stage (with an efficiency of 0.8) model could adequately represent the MTBE process.

Multiple steady states (MSS) in conventional distillation have been known from simulation and theoretical studies dating back to the 1970s and has been a topic of considerable interest in the distillation community. Taylor and Krishna [1] cite the papers highlighting MSS in RD. We single out just a few of these papers for mention here.

Mohl et al. [21, 22] implemented a dynamic EQ model (with Murphree type efficiencies) in the DIVA simulator and carried out a numerical bifurcation and stability analysis on the MTBE and TAME processes. They also show that the window of opportunity for MSS to actually occur in the MTBE process is quite small. For the TAME process MSS occur in the kinetic regime and vanish when chemical equilibrium prevails. The window of opportunity for MSS in the TAME process is larger than for the MTBE process.

Experimental confirmation of MSS in RD was provided by Thiel et al. [23] and by Rapmund et al. [24]. Mohl et al. [1] used a pilot scale column to produce MTBE and TAME. MSS were found experimentally when the column was used to produce TAME, but not in the MTBE process. The measured steady state temperature profiles for the low and high steady states for the TAME process are shown in

Fig. 9.10a. For a column operating at the low steady state, a pulse injection of pure TAME for a short period resulted in a shift from the low to the higher steady state (Fig. 9.10b).

The MSS observed in these experiments can be reproduced using the NEQ model in which the reaction is treated as pseudo-homogeneous and the Wilson model is used to describe the liquid phase non-ideality. A reasonable match of the column temperature profiles also is shown in Fig. 9.10a; these profiles are

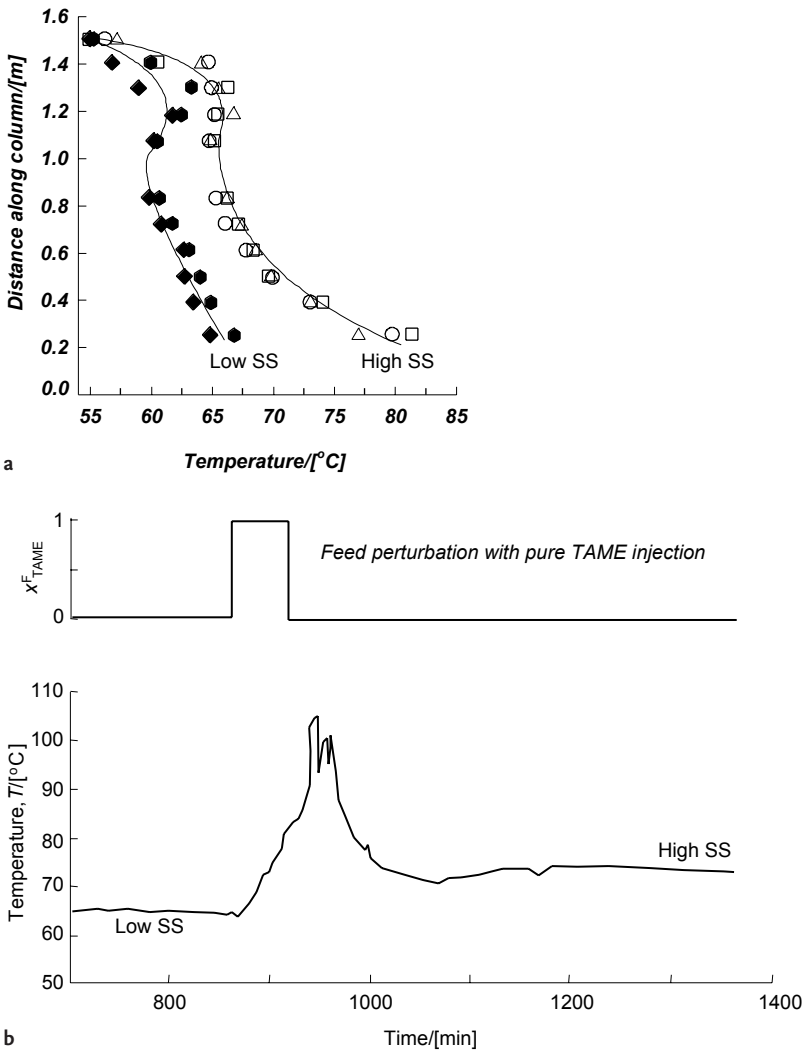

Fig. 9.10 a) Multiple steady states in TAME synthesis. Experimental data on low- and high-conversion steady states. b) Response of TAME column to injection of pure TAME in the feed during the period 860–920 min. The column shifts from a low steady-state to the higher one. Measurements of Mohl et al. [25]

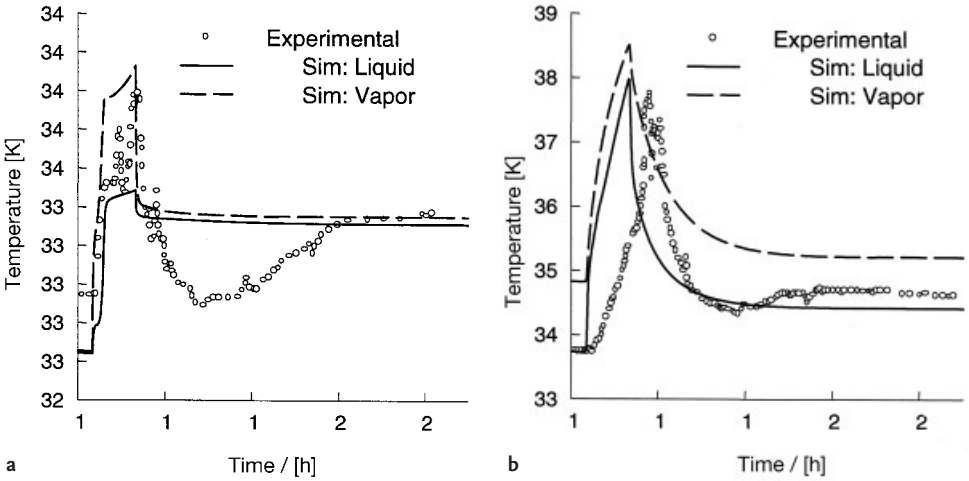

Fig. 9.11 Responses to switching of feed to pure TAME calculated with NEQ model: a) at the bottom of the reactive section; b) at the bottom of the stripping section. Experimental data of Mohl et al. [25]

in good agreement with simulations reported by Mohl et al. [25]. The details of the steady state simulation procedure were published earlier [11]. The dynamic behavior of the laboratory column is strongly influenced by the high liquid hold-up in the porous catalyst [21]. A pseudo-homogeneous model is not able to describe intra-particle mass transfer, energy, and mass storage. The model also does not account for the possible influence of, for example, changes in operating pressure when switching feed or responses of controllers. As a result, the simulations predict a rapid temperature and composition change at the beginning and end of the perturbation. Despite these limitations, the essential features of the steady state transitions are reproduced (see Fig. 9.11, adapted from Baur et al. [26]).

The recent work by Baur et al. [17], comparing the EQ and NEQ models for hydration of ethylene oxide to ethylene glycol, throws more light on the phenomena on MSS and the importance of using the NEQ model. For an ethylene glycol column, three steady states are found with both EQ and NEQ models: SS-1 (high conversion), SS-2 (intermediate conversion), and SS-3 (low conversion). The desired high-conversion steady state solution (SS-1) corresponds to high column temperatures and lowest molar flow rate of the vapor up the column. For a column of 1.7 m diameter, only one solution, SS-1, can be realized. The other solutions SS-2 and SS-3 could not be realized in the NEQ model because the column floods on some (SS-2) or all (SS-3) of the stages; the flooding boundaries are drawn in Fig. 9.12. It is also shown that if the column diameter was chosen to be 3 m, only the lowest conversion steady state can be realized!

NEQ simulations also show that the dynamic response of a RD column is also sensitive to the hardware choice (tray or packing type). The open loop dynamics are predominately influenced by the storage capacities (at steady state) and resi-

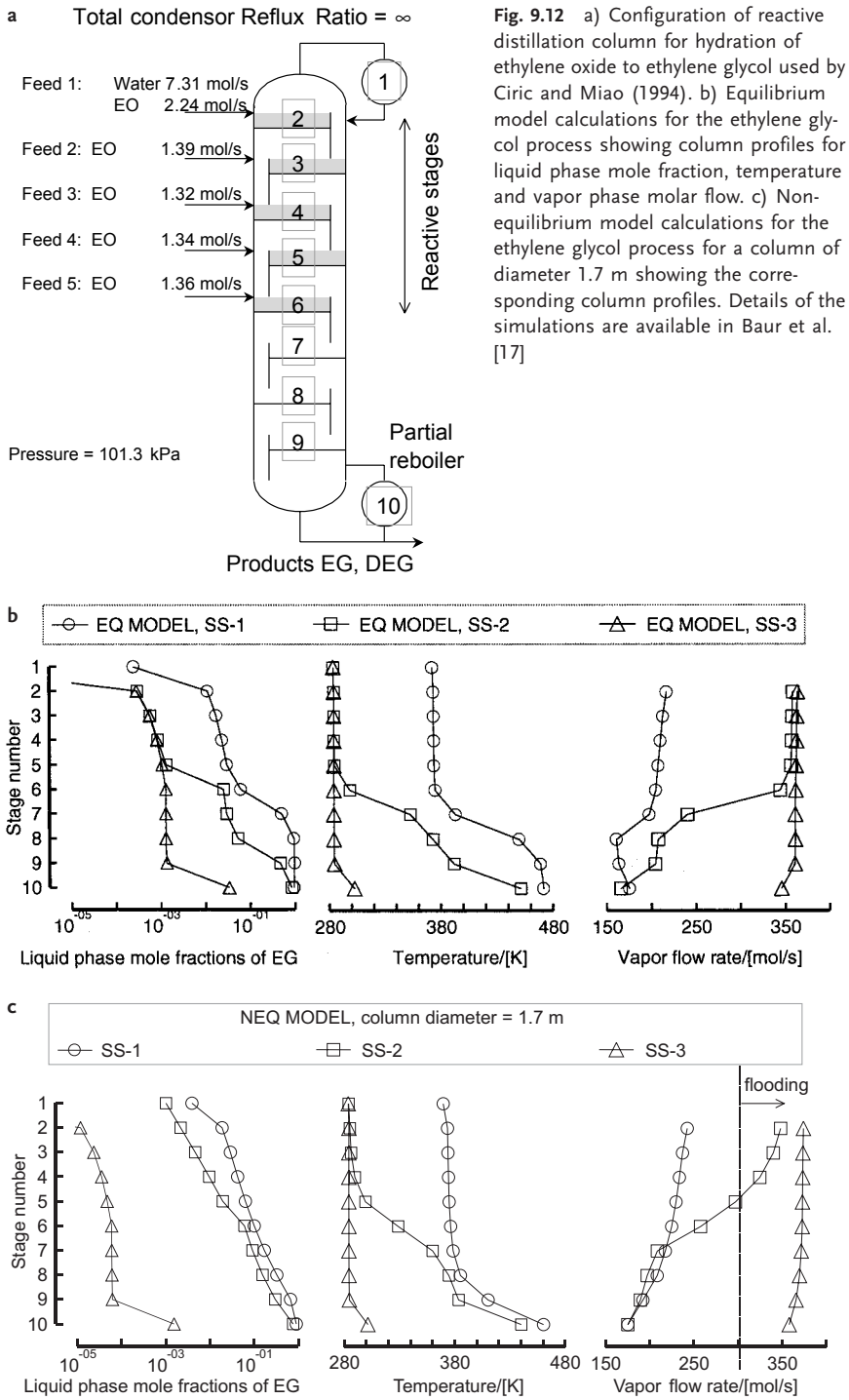

Fig. 9.12 a) Configuration of reactive distillation column for hydration of ethylene oxide to ethylene glycol used by Ciric and Miao (1994). b) Equilibrium model calculations for the ethylene glycol process showing column profiles for liquid phase mole fraction, temperature and vapor phase molar flow. c) Non-equilibrium model calculations for the ethylene glycol process for a column of diameter 1.7 m showing the corresponding column profiles. Details of the simulations are available in Baur et al. [17]

dence times in particular when focussing on hybrid columns. It is clear that the control strategies to be adopted will also be determined by the precise configuration of the reactive section.

9.5 A View of Reactive Distillation Process Design

We close with some comments on the use of these models in RD process design. There are many different types of model now available in the literature for screening, analysis, design, and optimization of RD columns. Below is an outline of a stepwise approach to RD process design:

1. feasibility of RD concept,
2. preliminary design,
3. choose column hardware,
4. equipment sizing,
5. check preliminary design using NEQ models,
6. process dynamics and control.

Determining the feasibility of a process (step 1) is a relatively straightforward task that can be carried out using residue curve maps [2, 3]. Equilibrium stage models are useful for the preliminary design (step 2). This involves determination of the number of theoretical stages in the reactive, stripping, and rectifying sections; the catalyst load in the reactive section(s); and some optimization of operating parameters such as the reboiler load and reflux ratio [2, 3].

The design of the equipment for the non-reactive sections should not pose too great a challenge since existing methods of estimating efficiencies or HETP that are based on key-components could be used. For the reactive section, however, the estimation of HETPS and efficiencies is more problematic. There is no easy way to identify key components. Chemical reactions influence component efficiencies in an unpredictable manner (Fig. 9.22 in [1]). Of course, like the rest of the RD community, we could behave like ostriches and bury our heads in the sand while assuming equal component efficiencies (say, 70 %) for individual species and hope for the best!

Column hardware choice can have a significant influence on the conversion and selectivity; such aspects can be properly described only by the NEQ cell model, or by a still more sophisticated model based on computational fluid mechanics (such models have yet to be developed). It is insufficiently realized in the literature that, say, for tray RD columns, the tray design can be deliberately chosen to improve conversion and selectivity. Even less appreciated is the fact that the design methodology for RD tray columns is fundamentally different from that of conventional trays. Liquid residence time and residence time distributions are more important in RD. The froth regime is to be preferred to the spray regime for RD applications; this is opposite to the design wisdom normally adopted for conventional distillation. For relatively fast reactions, it is essential to properly model intra-particle dif-

fusion effects. Pseudo-homogeneous reaction models may be inadequate for fast reactions. RD columns using dumped (random) packing are susceptible to maldistribution and there is a case to be made for choosing regular structured packing. For proper description of the column dynamics, it is essential to adopt the NEQ model.

Though sophisticated NEQ design models are available already, detailed information on the hydrodynamics and mass-transfer parameters for many available hardware configurations is woefully lacking in the open literature. For some internals types the information available is contradictory, for still others there is no mass-transfer data at all. Paradoxically, such information has vital consequences for the conversion and selectivity of RD columns. There is a crying need for research in this area. It is perhaps worth noting here that modern tools of computational fluid dynamics could be invaluable in developing better insights into hydrodynamics and mass transfer in RD columns.

Besides more research on hydrodynamics and mass transfer, there is a need for more experimental work with the express purpose of model validation. In such process studies, parameters need to be measured along the height of RD columns. Too often measurements are confined to feed and product stream conditions. Such data cannot serve as a reliable discriminant of computer-based process models.

9.6 Notation

a	interfacial area, m^2
B	bottom flow, mol s^{-1}
B_0	permeability, m^2
c	number of components, dimensionless
c_t	total concentration, mol m^{-3}
D	distillate flow, mol s^{-1}
$D_{i,eff}$	effective Fick diffusivity, m^2 s^{-1}
$Đ_i^e$	effective Knudsen diffusivity in porous catalyst, m^2 s^{-1}
$Đ_{i,k}$	Maxwell–Stefan diffusivity, m^2 s^{-1}
E	energy flux, W m^{-2}
E	energy transfer rate, J s^{-1}
E_i^{MV}	overall Murphree tray efficiency, dimensionless
F^V	vapor feedstream, mol s^{-1}
F^L	liquid feedstream, mol s^{-1}
f	component feed stream, mol s^{-1}
H	molar enthalpy, J mol^{-1}
h	heat transfer coefficient, W m^{-2} K^{-1}
K	vapor–liquid equilibrium constant, dimensionless
L	liquid flow rate, mol s^{-1}
L_M	interchange liquid flow rate between horizontal rows of cells, mol s^{-1}

N_i molar flux of species i, mol m^2 s^{-1}
N mass-transfer rate, mol s^{-1}
p_j stage pressure, Pa
Q heat duty, J s^{-1}
r number of reactions, dimensionless
r_j ratio of side stream flow to interstage flow on stage j, dimensionless
r_j^* transformed reflux ratio, dimensionless
$R_{m,j}$ reaction rate, mol m^{-3} s^{-1}
R gas constant, J mol^{-1} K^{-1}
s_j^* transformed stripping ratio, dimensionless
S side draw-off, mol s^{-1}
t time, s
T temperature, K
U molar hold-up, mol
V vapor flowrate, mol s^{-1}
x mole fraction in the liquid phase, dimensionless
y mole fraction in the vapor phase, dimensionless
z mole fraction in either vapor or liquid phase, dimensionless

Greeks

ε reaction volume, m^3
γ_i activity coefficient of species i, dimensionless
κ mass-transfer coefficient, m s^{-1}
μ chemical potential, J mol^{-1}
ν stoichiometric coefficient, dimensionless
η viscosity of fluid mixture, Pa s
η distance along diffusion path, dimensionless

Subscripts

cl clear liquid
eff effective
i component index
I referring to interface
j stage index
k alternative component index
m reaction index
t total

Superscripts

F referring to feed stream
L referring to liquid phase
V referring to vapor phase

List of Abbreviations

DAE differential-algebraic equations
EQ equilibrium
HETP height of a theoretical plate
MS Maxwell–Stefan
NEQ non-equilibrium
RD reactive distillation

References

1 Taylor, R.; Krishna, R. *Chem. Eng. Sci.* **2000**, *55*, 5183–5229.
2 Doherty, M. F.; Buzad, G. *Chem. Eng. Res. Des., Trans. I. Chem. E. A* **1992**, *70*, 448–458.
3 Doherty, M. F.; Malone, M. F. *Conceptual Design of Distillation Systems*, McGraw-Hill, New York, **2001**.
4 Seader, J. D.; Henley, E. J. *Separation Process Principles*, John Wiley, New York, **1998**.
5 Taylor, R.; Krishna, R. *Multicomponent Mass Transfer*, John Wiley, New York, **1993**.
6 Pöpken, T.; Steinigeweg, S.; Gmehling, *J. Ind.Eng.Chem. Res.* **2001**, *40*, 1566–1574.
7 Krishnamurthy, R.; Taylor, R. *AIChE J.* **1985**, *32*, 449–465.
8 Krishna, R.; Wesselingh, J. A. *Chem. Eng. Sci.* **1997**, *52*, 861–911.
9 Krishna, R., in *Proc. 1st Int. Max-Planck Workshop on Reactive Distillation*, Magdeburg, Germany, 2–3 July **2001**.
10 Mason E. A.; Malinauskas, A. P. *Gas Transport in Porous Media: The Dusty Gas Model*, Elsevier, Amsterdam, **1983**.
11 Higler, A.; Krishna, R.; Taylor, R. *Ind. Eng. Chem. Res.* **2000**, *39*, 1596–1607.
12 Higler, A.; Krishna, R.; Taylor, R. *Ind. Eng. Chem. Res.* **1999**, *38*, 3988–3999.
13 Higler, A.; Krishna, R.; Taylor, R. *AIChE J.* **1999**, *45*, 2357–2370.
14 Baur, R.; Taylor, R.; Krishna, R. *Chem. Eng. Sci.* **2000**, *55*, 6139–6154.
15 Baur, R.; Taylor, R.; Krishna, R. *Chem. Eng. Sci.* **2001**, *56*, 1721–1729.
16 Kreul, L. U.; Gorak, A.; Barton, P. I. *Chem. Eng. Sci.* **1999**, *54*, 19–34.
17 Baur, R.; Higler, A. P.; Taylor, R.; Krishna, R. *Chem. Eng. J.* **2000**, *76*, 33–47.
18 Lee J. H.; Dudukovic, M. P. *Comp. Chem. Eng.* **1998**, *23*, 159–172.
19 Lee J. H.; Dudukovic, M. P., in *Proc. AIChE National Meeting*, Dallas, **1999**.
20 Sundmacher, K.; Uhde, G.; Hoffmann, U. *Chem. Eng. Sci.* **1999**, *54*, 2839–2847.
21 Mohl, K. D.; Kienle, A.; Gilles, E. D.; Rapmund, P.; Sundmacher, K.; Hoffmann, U. *Comput. Chem. Eng.* **1997**, *21*, S989–S994.
22 Mohl, K. D.; Kienle, A.; Gilles, E. D. *Chem. Eng. Technol.* **1998**, *21*, 133–136.
23 Thiel, C.; Rapmund, P.; Sundmacher, K.; Hoffmann, U.; Mohl, K. D.; Kienle, A.; Gilles, E. D., in *Proc. 1st Eur. Congr. Chem. Eng. – ECCE-1*, 4–7 May **1997**, Florence, 1423–1426.
24 Rapmund, P.; Sundmacher, K.; Hoffmann, U. *Chem. Eng. Technol.* **1998**, *21*, 136–139.
25 Mohl, K. D.; Kienle, A.; Gilles, E. D.; Rapmund, P.; Sundmacher, K.; Hoffmann, U. *Chem. Eng. Sci.* **1999**, *54*, 1029–1043.
26 Baur, R.; Taylor, R.; Krishna, R. *Chem. Eng. Sci.* **2001**, *56*, 2085–2102.

Reactive Distillation. Edited by Kai Sundmacher, Achim Kienle

ISBNs: 3-527-30579-3 (Hardback); 3-527-60052-3 (Electronic)

10
Nonlinear Dynamics and Control of Reactive Distillation Processes

A. Kienle and W. Marquardt

10.1
Introduction

Reactive distillation (RD) processes can result in an economically attractive alternative to conventional process designs, where reaction and separation are carried out in different processing units. Successful industrial examples include esterification [1] and etherification [96] processes. Numerous additional potential applications of RD are compiled in Chapter 1. Consequently, there has been a lot of interest in this type of integrated processes during recent years. Emphasis has been on steady-state modeling, on the development of new processes and on the foundations of RD column design [62, 84, 106]. Still, comparably little work has been done on nonlinear dynamics and control of RD processes, although these processes can sometimes show an intricate nonlinear dynamic behavior including input as well as output multiplicities and sustained oscillations. A profound understanding of these phenomena as well as their reliable prediction is not only of scientific interest, but also a necessary prerequisite for improved process design and control of industrial processes.

The objective of this contribution is to give an overview on the present knowledge on nonlinear dynamics and control of RD processes. We will try to elucidate the various nonlinear phenomena identified so far and to relate them to the various chemical and physical elementary processes interacting in an RD column. For this purpose, we will study different concrete reactive systems, which are favorably processed in an RD column. These reaction systems include classical esterification and etherification reactions as well as more complex reaction networks with parallel and consecutive steps. We will start our analysis with strongly simplified model problems to facilitate fundamental insights into the causes of certain observed nonlinear effects. Next, rigorous dynamic process models of varying degree of detail will be analyzed by numerical means. Last but not least we will try to generalize the findings from the case studies to the extent possible.

The outline of the chapter is as follows. First, we present some basic terminology in nonlinear dynamics in the next section. We also introduce the process configurations to be studied and the analytical and numerical tools to be used. Some remarks on the analysis of nonlinear dynamics in chemical process systems will be made to provide essential background information without trying to give a comprehensive review. Sections 10.3, 10.4, and 10.5 discuss multiplicity and self-sustained oscillations of selected esterification and etherification processes as well as processes involving more complex parallel-consecutive reaction networks. Section 10.6 attempts a unifying generalization based on the examples studied. Section 10.7 introduces the phenomenon of a traveling wave. Such a spatiotemporal structure cannot only be observed in temperature or concentration profiles in distributed chemical reactors and distillation columns but also in RD processes. Section 10.8 discusses some aspects of monitoring and control of RD columns before we conclude with a summary.

10.2
Multiplicity and Oscillations in Chemical Process Systems

A process model of any chemical process system is given by a system of differential-algebraic equations, which depend on some parameters. The steady state solution branches can be traced out in the parameter space. An exemplary situation is shown in Fig. 10.1 where some norm of the steady states $\boldsymbol{x}$ is plotted above the plane spanned by two selected parameters p_i and p_j. In the triangular shaped region in the parameter space, three steady states can coexist for the same set of para-

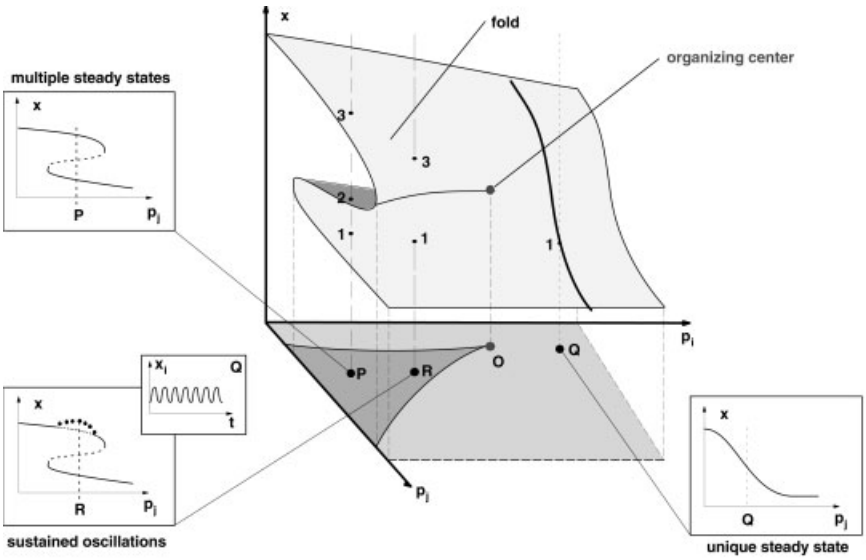

Fig. 10.1 Steady-state multiplicity and sustained oscillations

meters (e. g., at point *P* in the figure). In the remainder of the parameter space, a unique steady state exists (e. g., point *Q* in the figure). There is a distinct point (point *O* in the figure) that is most degenerate in the following sense: All different types of qualitative behavior of the system can be observed in the vicinity of *O*, which is therefore sometimes called the organizing center. In addition to steady state multiplicity, dynamic bifurcations may occur leading to regions in parameter space with self-sustained oscillations. An example is shown in Fig. 10.1 at point *R* where sustained oscillations are present in a certain interval of parameter p_j for fixed p_i. The filled symbols indicate the amplitude of the oscillations around a locally unstable steady represented by the dotted part of the upper branch of the steady-state solution plot. A detailed introduction into nonlinear dynamics may be found in textbooks [30, 81, 94].

The multiplicity in the vicinity of *P* in Fig. 10.1 is termed *output multiplicity*, since it occurs when a set of given inputs (parameters or manipulated variables) results in different values of the output variables (measured quantities) corresponding to different steady states. In RD, inputs are, for example, the reflux rate at the top of the column or the reboiler duty at the bottom of the column, whereas outputs are usually some temperatures inside the column or the product compositions at the bottom or the top, respectively. In case of output multiplicity, usually some of the steady states are open loop stable, while others are open loop unstable. The latter are indicated by the dashed line in the inserts of Fig. 10.1. Depending on the history (e. g., startup strategy) the column settles either down to the upper stable steady state or to the lower stable steady state for parameters at point *P*. This implies that a suitable startup strategy is required to operate the column into the desired steady state. Further, when operating the column in one of the stable steady states, the column may 'jump' onto the other, undesired stable steady state branch after some disturbance. This is easily avoided by some suitable control for disturbance rejection. Moreover, it is also possible to operate the column at an unstable steady state, if desirable, when stabilizing control is applied. Finally, it is worth noting that output multiplicity and open loop stability do not depend on the choice of output or measured variables.

In contrast, *input multiplicity* [46] can occur when different sets of input variables produce the same set of output variables. This input multiplicity will depend on the choice of output or measured variables. It is associated with the so-called zero dynamics of the system, which can be observed by an unexpected inverse response of the outputs after a step change has been applied to the inputs. Therefore, it can have severe implications for closed loop control [46]. We will come back to this point in Section 10.8.

The analysis of nonlinear dynamics of chemical process systems has a long tradition. Most emphasis has been on chemical reactors initiated by the seminal work of Bilous and Amundson [10], van Heerden [109], and Aris and Amundson [3]. Comprehensive reviews have been given by Razon and Schmitz [86] or Elnashaie and Elshishini [19]. Multiplicity analysis of non-RD can be traced back to the paper of Rosenbrock [91] where stability and hence uniqueness of steady-states of a binary distillation column is demonstrated under quite general assumptions.

The numerical study of Magnussen et al. [61] has raised a lot of attention and triggered the analysis of multiplicity in distillation [8, 17, 46–48, 54, 55]. Reviews on dynamics and control of non-RD columns can be found in the literature [50, 60, 95].

RD columns share some common features with chemical reactors on the one hand and with distillation columns on the other hand. The behavior of these multifunctional processes may be either close to that of non-RD columns or to chemical reactors. Further, new patterns of behavior can be introduced by the superposition of reaction and separation in a single processing unit. Hence, another interesting question that will be addressed in this chapter, is under what conditions and in what sense is the dynamic behavior of an RD column similar to that of a chemical reactor or to that of a non-RD column.

Most emphasis has been on output multiplicity as well as on sustained oscillations in chemical process systems. The role of input multiplicity compared to output multiplicity has been treated for RD processes in [26, 98], and the notion of pseudomultiplicity was introduced in [98]. This corresponds to a situation where '...molar inputs (rather than mass or volume inputs that would result from control valves) produce an output multiplicity'. Since this behavior can only be observed via simulation and is not associated with actually operating columns we will focus in this chapter on input and output multiplicity and do not treat pseudomultiplicity.

In order to facilitate the analysis and to gradually build up our understanding of the causes for the observed phenomena with respect to the chemical system and the process configuration, we study different model problems. The most simple is comprised by a continuous stirred tank reactor. If a reboiler and a reflux condenser is added, we obtain a one-stage column, where the whole column is lumped into one stage. Another simple configuration is a very long column section with a large number of trays. Such a configuration will be most favorable for the analysis of wave propagation in Section 10.7. Closely related is a column with an infinite number of trays operated under total reflux: an assumption that simplifies the (so-called ∞/∞) analysis tremendously. Finally, we study a full-scale RD column with various kinds of mathematical models differing in the level of detail.

The mathematical tools we are going to employ are of various types, too. We employ singularity theory [30] and attempt to directly compute the most degenerate point (i. e., the organizing center) of the steady state manifold [22, 23]. Due to the computational complexity, this method is still restricted to fairly small-scale problems [11]. ∞/∞-analysis originally introduced by Petlyuk and Avetyan [82] and further developed by Bekiaris et al. [8] is a simple method to study the qualitative behavior of complete non-reactive and RD columns under some limiting assumptions. Numerical bifurcation analysis by means of continuation and an integrated analysis of the stability behavior of the steady state solutions [94] is used to study the behavior of the large-scale differential-algebraic models [53, 63] describing full scale RD columns. Last but not least, wave front analysis [50, 65] will be employed to study the spatiotemporal patterns in column sections.

10.3 Methyl Formate Synthesis

The synthesis of methyl formate is a typical esterification reaction with a conversion limitation due to chemical equilibrium. Such reactions are suitably carried out in an RD column [1, 13, 62]. Methanol (MeOH) and formic acid (FA) are converted to methyl formate (MF) and water (W) according to the reversible reaction scheme

$$CH_3OH + CHOOH \rightleftharpoons HCOOCH_3 + H_2O \quad . \tag{10.1}$$

In contrast to other esterifications, a significant extent of reaction can be reached even without a catalyst though the reaction equilibrium constant is approximately one. A compilation of the major physical property data can be found elsewhere [25, 87]. Fig. 10.2 shows the residue curve map in transformed coordinates as introduced by Doherty and coworkers [108] at a pressure of 1.013 bar. Due to a single maximum azeotrope, there are two distillation regions. The concentration profile in a single feed, two product lab-scale column with 45 bubble cap trays is also displayed in Fig. 10.2. The column is fed with a stoichiometric feed of formic acid and methanol and operated at a reflux ratio of 5. Water and the desired methyl formate are recovered at purities of about 97 % molar concentration in the bottoms and at the top, respectively.

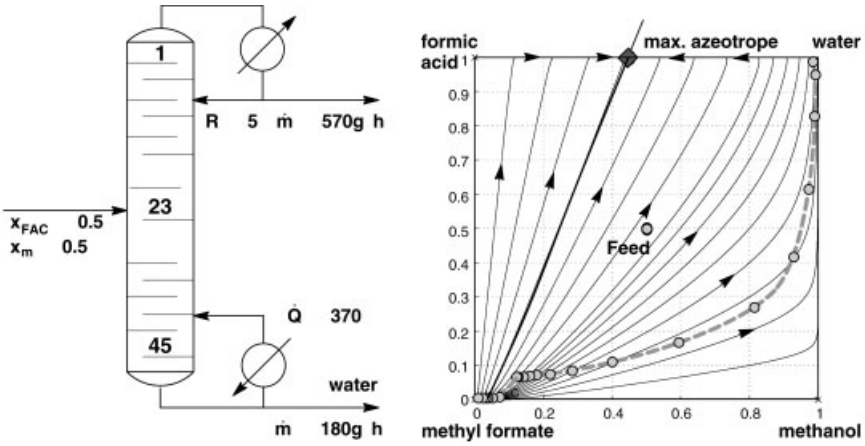

Fig. 10.2 Residue curve map of methyl formate system at $p = 1.013$ bar and concentration profile (right) of lab-scale column (left). The filled symbols on the dashed line correspond to the simulated tray compositions

10.3.1
Singularity Analysis of a One-Stage Column

As a first step towards a better understanding of the nonlinear behavior of such a distillation column, we study a one-stage column by means of singularity theory. The model equations and details of the analysis can be found elsewhere [22, 23]. An organizing center of codimension two can be found for a stoichiometric feed of $x_{FA} = 0.5$ and $x_{MeOH} = 0.5$ for the parameters $Da = 0.001$, $L/F = 4.685$, $Q/(\Delta H_V F) = 4.636$. Fig. 10.3, left, shows the organizing center together with the singularity set in the parameter plane spanned by the reflux L/V and the boiler duty $Q/(\Delta H_V F)$. The multiplicity regions are not only limited by the singularity set but also by the feasibility boundaries dictated by the total mass balance. Two or three steady states may occur simultaneously. Fig. 10.3, right, shows a bifurcation diagram for fixed reflux in the vicinity of the organizing center that has been computed by numerical continuation. Obviously, the region with three multiple steady states is quite small. The predictions found from a singularity analysis of the one-stage column have been confirmed by numerical bifurcation analysis of the lab-scale column using a rigorous column model.

Due to the simplicity of the model, the phenomena causing multiplicity can easily be verified. The multiplicity is caused by the relations between the heat of vaporization and the boiling points of the educts, which are $T_{B,MeOH} < T_{B,FA}$ and $\Delta H_{V,MeOH} > \Delta H_{V,FA}$. Such relations have also been identified by Jacobsen and Skogestad [48] to cause multiplicity in a separation of non-reacting binary mixtures in a one-stage column. Hence, multiplicity is not caused by the reaction but is just the result of the separation only in methyl formate synthesis. Similar results have also been found for the esterification of ethanol with acetic acid [25, 50].

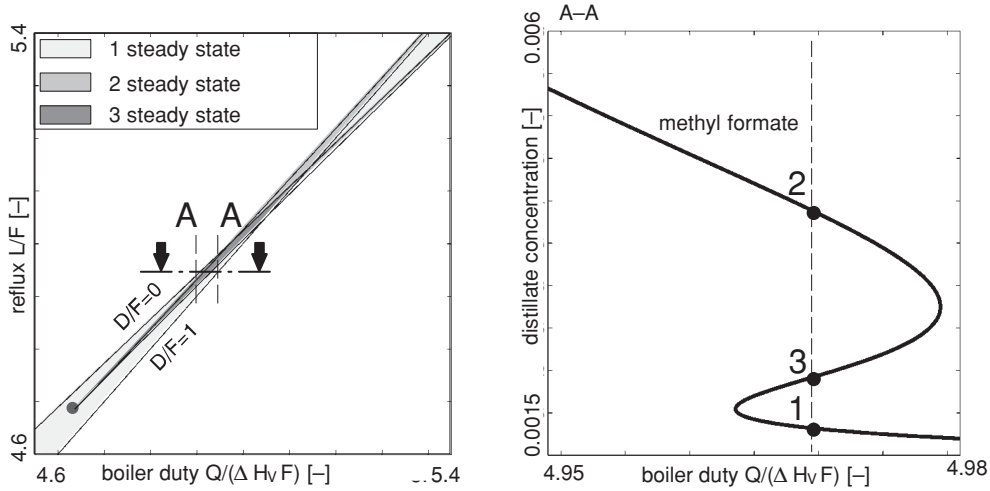

Fig. 10.3 Singularity set with organizing center for the methyl formate one stage column (left). Bifurcation diagram for the methyl formate one-stage column for a fixed reflux ratio, cross section A–A (right)

10.3.2 ∞/∞-Analysis of Lab-Scale Column

Another simple model problem can be stated by assuming an infinite number of stages and an infinite reflux ratio. This ∞/∞-analysis has been introduced originally by Petlyuk and Avetyan [82] and extensively applied for the analysis of non-reactive and RD columns by Morari and coworkers [8, 34, 35] and Marquardt and Müller [76]. If applied to RD, not only phase equilibrium but also chemical equilibrium have to be assumed.

Reder et al. [88] have applied this analysis technique to study distillation of the methyl formate system. They report unique steady state solutions for all possible feeds, if distillation of the (hypothetical) non-reactive quaternary system MeOH/FA/MF/W is considered. In contrast, steady state multiplicity can be found for the reactive system in the distillation region formed by MF, MeOH, W and the binary azeotrope but not for the distillation region formed by FA, MeOH and the binary azeotrope. In fact, an infinite number of steady states with different distillate concentrations can be found for some critical bottom flow rate B. Fig. 10.4 shows the distillate concentration as a function of B varying from zero to its maximum value.

The infinite number of steady states occurring in the limit of the ∞/∞-analysis is not peculiar to the methyl formate system. Rather, a similar situation can be expected for other kinds of esterifications with a similar topology in the space of transformed concentrations.

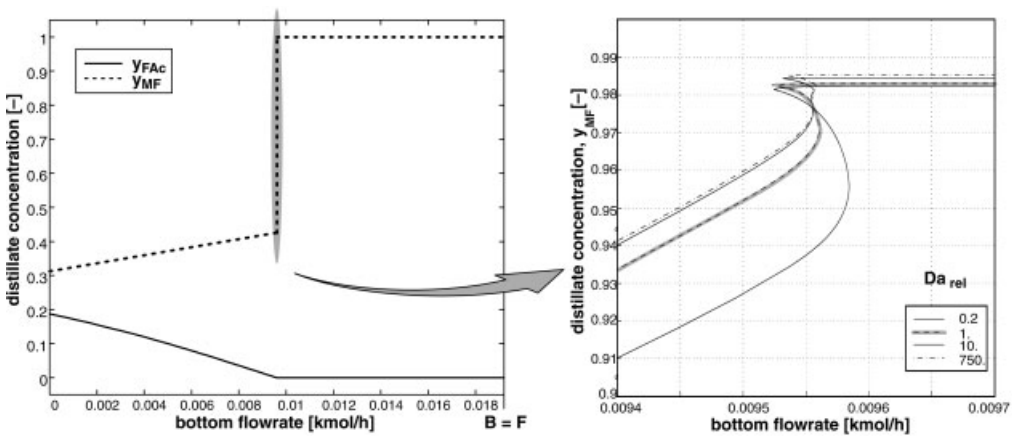

Fig. 10.4 Bifurcation diagram for methyl formate distillation column. Infinite number of trays and infinite reflux ratio (left). Real column, 45 trays, feed on tray 23, reflux ratio 5, Murphree efficiency 0.65 (right)

10.3.3
Continuation Analysis of Lab-Scale Column

Obviously, the infinite number of steady states will most likely not occur in a real column. An extensive numerical bifurcation analysis of the lab-scale distillation column has been carried out by Gehrke et al. [25], Reder [87], and Gehrke [22] employing the continuation algorithms provided in the process simulator DIVA [53, 63]. They find three multiple steady states in the real column for roughly the same bottoms flow rate giving rise to an infinite number of steady state solutions in the column with an infinite number of trays at infinite reflux ratio. Fig. 10.5 shows an exemplary result of the analysis. The methyl formate concentration in the distillate is plotted as a function of the bottoms flowrate F. Three steady states can coexist in a small region of bottom flowrates. The region of multiplicity is first enlarged if the Damköhler number Da is reduced. For very low Da, a unique but parametrically sensitive solution (not shown in the figure) results. The region of multiplicity reduces and at the same time tends to display an increasing number of steady states if Da is increased above the real value attained in the lab-scale process to approach reaction equilibrium in the limit. Three multiple steady states persist in a large range of reflux ratios and for a wide range of trays. In particular, the multiplicity only vanishes at very low reflux ratios or for columns with a small number of trays.

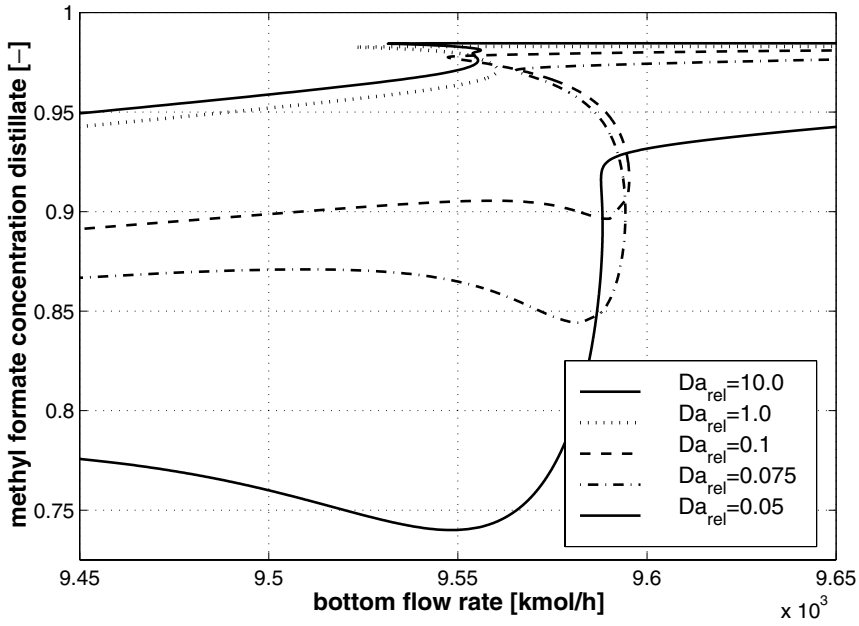

Fig. 10.5 Bifurcation diagram for methyl formate distillation column with 45 trays, feed at tray 23, reflux ratio 5, Murphree efficiency 0.65, and a kinetically controlled reaction with different relative Damköhler numbers $Da_{rel} = Da_{sim}/Da_{real}$

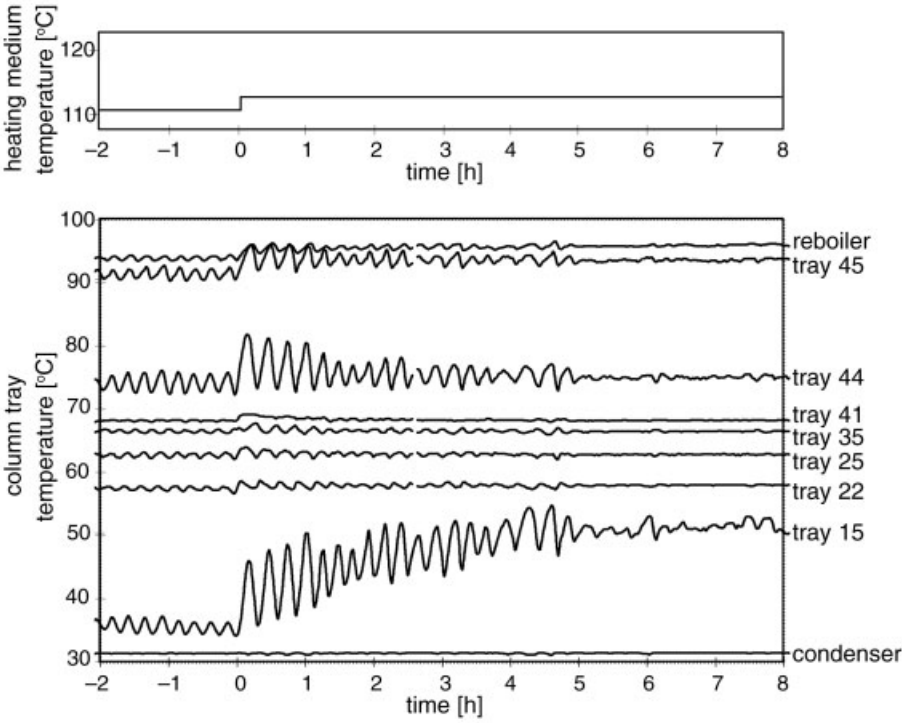

Fig. 10.6 Oscillations observed in an experiment with a lab-scale methyl formate column: 45 bubble cap trays, feed at tray 23

Sustained oscillation could not be found by means of continuation analysis for the lab-scale methyl formate column. However, oscillations have been observed during experimental investigations by Reder [87] as displayed in Fig. 10.6. Various temperature readings in the reboiler and on different trays are shown in the lower diagram. A step change in heat duty is applied at time 0. Large amplitude temperature oscillations with a period of about 0.3 h can be observed before and after the step change. The oscillations have been reproducible in various experiments. No source of external excitation could be located. An explanation of the phenomenon has not yet been achieved, however.

10.4 Ethylene Glycol Synthesis

RD may also be a favorable alternative if complex reactions comprising consecutive and parallel reaction steps are considered. A prototypical reaction system for further study is the synthesis of ethylene glycol (EG) from ethylene oxide (EO) and water (W) according to

$$H_2O + C_2H_4O \rightarrow C_2H_6O_2 \quad ,$$

$$C_2H_6O_2 + C_2H_4O \rightarrow C_4H_{10}O_3 \quad .$$

The first reaction leads to the desired product whereas di-ethylene (DEG) and higher order glycols are formed in consecutive reactions as undesired by-products. The reaction rate constants of the consecutive reactions are higher than that of the main reaction. Hence, an appropriate process has to be devised in order to achieve satisfactory conversion and selectivity.

A number of studies have been carried out to investigate RD as an alternative to the classical process comprising a reactor–separator–recycle [14, 16, 79]. According to our own investigations [24], which have also been confirmed by industrial studies [92], ethylene glycol synthesis by RD is not a viable economical alternative to a reactor-separator-recycle process with a tightly heat-integrated separation system. Nevertheless, the ethylene glycol process may be considered a model problem to facilitate the study of nonlinear dynamics in RD with complex reaction networks. Subsequently, we only consider the first two reaction steps thus resulting in a mixture of four components with volatilities decreasing in the sequence EO, W, EG, and DEG. The mixture does not form any non-reactive azeotrope.

As in the case of the esterification process presented before, we study first a one-stage column by singularity analysis to gain some physical insight and then continue with a numerical bifurcation study of an industrial size RD column.

10.4.1 Singularity Analysis of a One-Stage Column

A model of a one-stage distillation process for ethylene glycol synthesis is reported by Gehrke and Marquardt [23]. Singularity analysis reveals a codimension 4 singularity for a Damköhler number $Da = 0.0247$, a heat duty $Q/(\Delta H_V F) = 0.2871$ and feed concentrations $x_W = 0.4597$, $x_{EG} = 0.072$, $x_{EO} = 0.3961$, $x_{DEG} = 0.072$. However, there is no indication yet that there will not exist any higher codimension singularity in addition. Fig. 10.7, left, shows the regions of multiplicity in the vicinity of the codimension 4 singularity in a cross section of the space of parameters. The typical butterfly type singularity can be observed giving rise to a maximum of five steady states. A bifurcation diagram is displayed in Fig. 10.7, right. The bifurcation diagram shows largely the large-scale three branch multiplicity indicating a saddle-node bifurcation, but with some perturbation close to a turning point to result in a region with five steady states. The region of five steady states is however confined to a fairly small parameter interval.

An analysis of the physical reasons for this behavior can be carried out by studying different kinds of models accounting for different physicochemical phenomena. For example, if all the consecutive reactions are neglected, a codimension 4 singularity can also be identified. Hence, the consecutive reaction(s) are not necessary to devise five steady states. They may rather give rise to higher codimension singularities indicating an even more degenerate behavior. This conjecture is

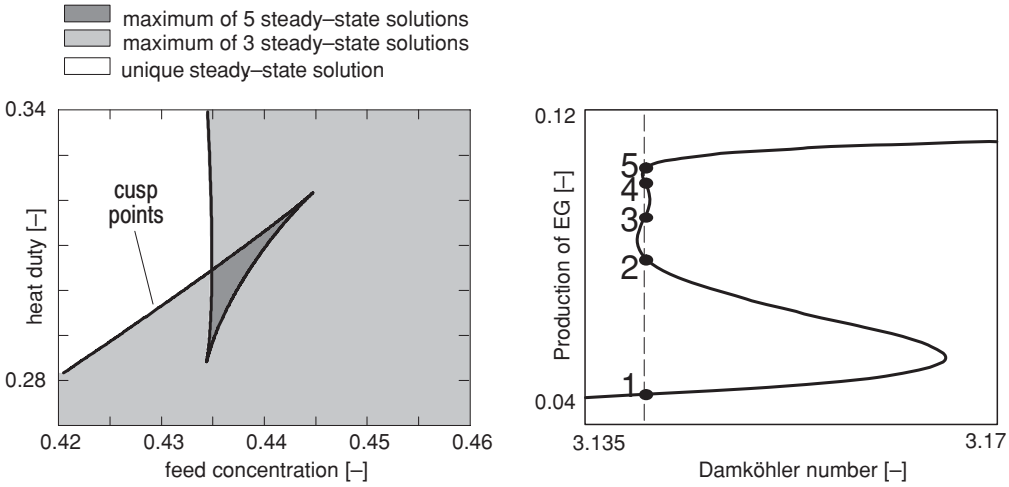

Fig. 10.7 Singularity set for the ethylene glycol one-stage column (left). Bifurcation diagram for the ethylene glycol one-stage column (right)

backed by the fact that there are up to seven steady states for two consecutive exothermic reactions in a CSTR whereas only three steady states can coexist if just a single exothermic irreversible reaction is considered [9].

The physical reasons for the observed steady state multiplicity can be traced back to the interplay between chemical reaction and vapor–liquid equilibrium if an analysis of the one-stage column is carried out just with the main reaction. The multiplicity is mainly caused by a self-accelerating behavior due to an increasing rate of reaction with increasing conversion. This is due to the increasing boiling temperature of the mixture with increasing conversion, since $T_{B,\mathrm{EO}} < T_{B,\mathrm{W}} < T_{B,\mathrm{EG}}$. Since only three steady states occur for a single exothermic reaction in a CSTR, the more complex behavior can be attributed to the cooperative effects of reaction and separation. Surprisingly, the heat of reaction does only contribute to the nonlinear behavior to a lesser extent. An analysis with a very small (positive) heat of reaction or even with a negative heat of reaction does not change the qualitative nonlinear behavior.

10.4.2
Continuation Analysis of Industrial Size Distillation Column

The findings from singularity analysis of the one-stage column will be checked for their relevance for the nonlinear behavior of an industrial size RD column by means of numerical bifurcation analysis using DIVA [53, 63]. The model used is of moderate complexity. The major assumptions are constant liquid holdup on every tray, negligible vapor holdup, constant heat capacities and heats of vaporization of all the species, ideal gas phase, almost ideal liquid phase, perfect mixing on

trays, and kinetically controlled reaction and mass transfer. As a case study, we consider the column design reported by Ciric and Gu [14]: The column has 10 stages, water is added on stage 10 at the top, ethylene oxide is added on stage 5. The holdups of the reactive stages 5–10 have been set according to [14]. The column is operated at total reflux and at a boilup ratio of 0.958. A ternary mixture of water and two of the glycols (EG, DEG) is withdrawn at the bottom.

Fig. 10.8 shows the multiplicity behavior of the distillation column in comparison to the multiplicity of the one-stage column. The production rate of ethylene glycol is plotted as a function of the residence time, which has been changed by multiplying the holdups on every tray by a constant continuation parameter. The qualitative behavior of both, the one-stage and the ten-stage column, is remarkably similar. In both cases the overall behavior is dominated by a large-scale three branch bifurcation diagram with three steady states. There is, however, a small

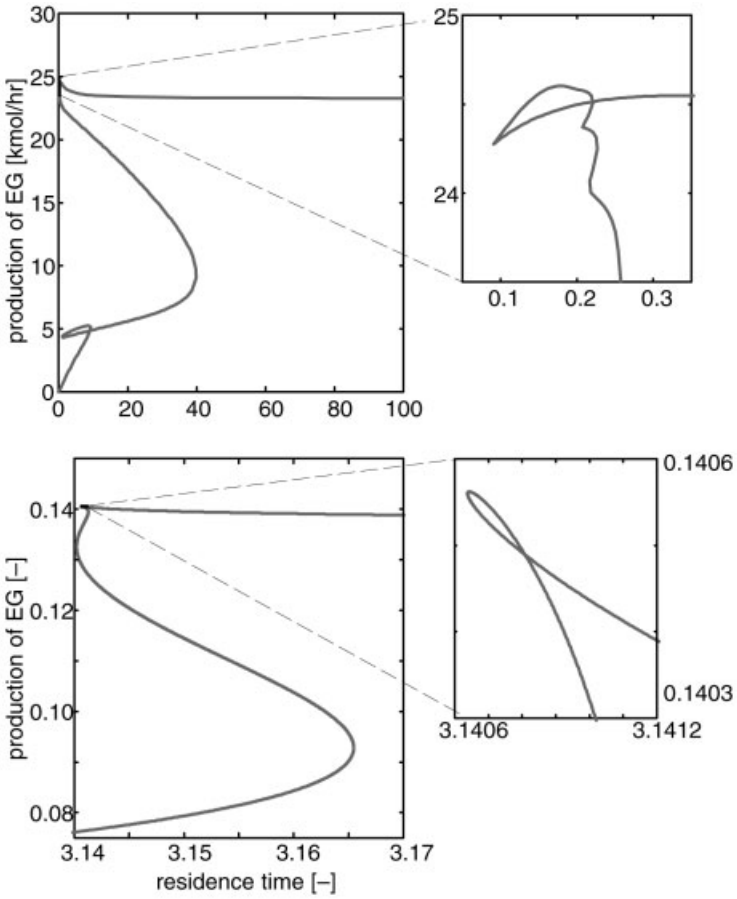

Fig. 10.8 Bifurcation diagrams for ethylene glycol synthesis: one-stage column (bottom) and ten-stage distillation column (top)

region with a more complex multiplicity pattern for low residence times in both cases. Hence, numerical bifurcation analysis of a ten-stage distillation column largely confirms the findings from singularity analysis of the one-stage column. Therefore, we may conclude that the multiplicity behavior is largely determined by the properties of the chemical system and that it is influenced to a much lesser extent by the details of column design. Though, due to the potential stage-wise multiplication of the multiplicity found for a single tray, much higher order multiplicity may be faced for a distillation column.

Our findings are confirmed by the studies of other authors. Ciric and Miao [15] have carried out intensive numerical investigations using a homotopy continuation technique to trace out the parameter dependent steady state solution branches. Their model assumes phase equilibrium on the trays and simplifies the energy balance; it is therefore slightly simpler as the model used in our studies. However, their findings largely coincide with ours indicating that the intricate multiplicity behavior with seven steady states is most likely not an artifact of certain modeling assumptions. They conclude that the large-scale three solution branch of the bifurcation diagram is sensitive to vapor–liquid equilibrium and the bimolecular irreversible reaction. Further, these authors also showed that it is not due to the consecutive reactions or to the exothermicity of the main reaction. Also, the influence of the details of the column design (e. g., the number and location of feed streams) on the qualitative nonlinear behavior is negligible. On the other hand, the details in the bifurcation diagram giving rise to higher order multiplicity is sensitive to the reaction mechanism and kinetics. Further studies of this RD process by Kumar and Daoutidis [58] confirm these results. They show, that the solution curve between the upper and lower stable branches changes completely, if the reactive trays are also extended into the stripping section.

The three solution branch dominating the nonlinear behavior of the process can also be observed in a conventional process with a reactor-separator recycle as recently reported by Blagov et al. [12]. This flowsheet is analogous to a column with one reactive and one non-reactive column section with a single product stream, the multiplicity behavior of which has been studied Cerafimov and coworkers [49, 83]. In these papers it is shown that this type of output multiplicity is a generic phenomenon for reaction systems with competing irreversible reactions and a similar distribution of volatilities between reactants and products.

However, a careful analysis is always recommended if the behavior of a concrete process is of interest. Baur et al. [5], for example, show in a recent study, that multiplicity will most likely not occur in this particular example column for ethylene glycol synthesis, since only a single steady state complies with the fluid dynamics operating envelope of a tray column. This is due to the fact that the flow rates inside the column differ significantly for the different steady states. It is however expected that this behavior only occurs for highly exothermic reactions like the ethylene glycol reaction. In these cases, the flow rates strongly depend on the reaction rates because of the exothermicity of the reaction. The findings in [5] have only been possible through continuation analysis with a very detailed non-equilibrium cell model capturing the details of the tray design.

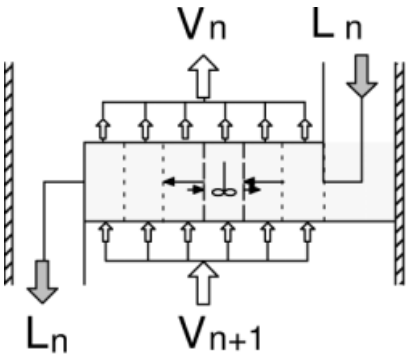

Fig. 10.9 Cell model to represent cross-flow pattern on distillation tray

So far, our bifurcation study has been assuming ideal mixing on the individual trays of the RD column. However, the fluid dynamic behavior of real trays with large holdups (as they are required for ethylene glycol production) will significantly differ from an ideally mixed state. Since residence time distribution of the tray will influence the selectivity of a complex reaction network, we might expect also an influence on the multiplicity behavior. For this purpose a single tray has been studied employing a cell model [25] to represent the cross-flow pattern on a real tray (compare Fig. 10.9). A common backmixing model [69] has been employed to account for dispersion between adjacent cells. This model does not capture fluid dynamics and heat and mass transfer at the level of detail presented later in [6], but covers the most significant effects.

The results of a numerical continuation study for a single tray are shown in Fig. 10.10. The top row of diagrams presents a comparison of a well-mixed and a cross-flow situation for the ethylene glycol system. In case of perfect mixing, three steady states may coexist for a certain holdup region, whereas up to eight steady can occur for a cross-flow tray modeled by four cells (corresponding to a Peclet number of about 8). Further study reveals an increasing number of steady states with an increasing number of cells to approximate the cross-flow pattern. Hence, there is evidence that much more complicated nonlinear behavior may arise for real flow situation as compared to the case of an ideally mixed tray as usually assumed in simulation studies.

The bottom row of diagrams in Fig. 10.10 show the results of a comparable study for methyl formate synthesis. There is always a unique steady state, regardless the assumptions on the flow pattern on a tray. Hence, the flow pattern on a tray seems to influence the qualitative behavior of a column tray only in those cases, when complex reaction networks with strongly nonlinear reaction models are considered.

The results of a similar continuation study for a complete RD column with perfectly and imperfectly mixed trays is shown in Fig. 10.11 for ethylene glycol synthesis. In contrast to a single tray, where the qualitative behavior for perfect and imperfect mixing differs significantly (compare Fig. 10.10), roughly the same behavior is observed for the column as displayed in the two diagrams on the left of Fig. 10.11. A multiplicity of order three occurs in a large region of the parameter

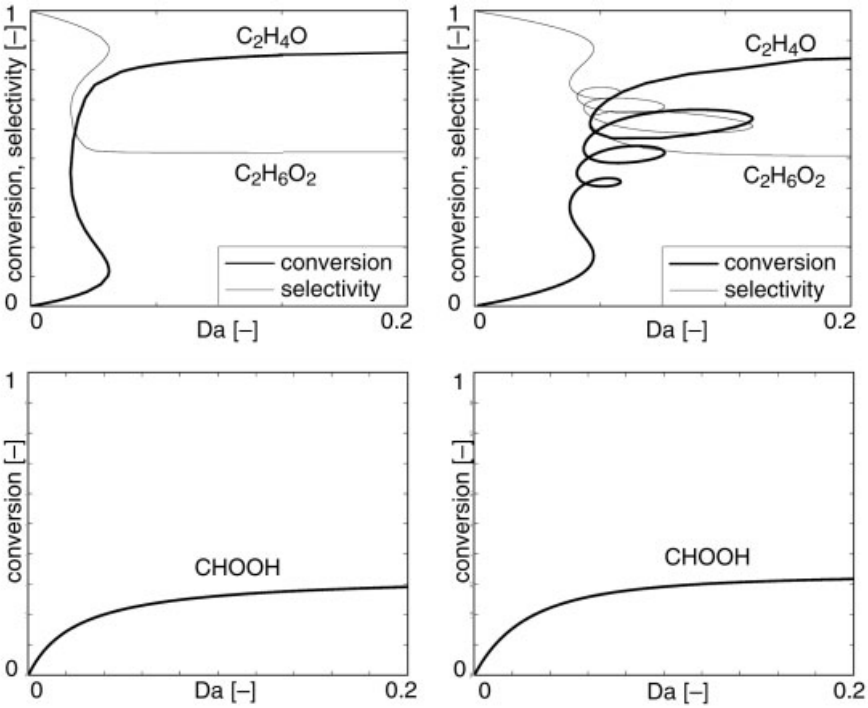

Fig. 10.10 Cell model to represent cross-flow pattern on distillation tray. Ethylene glycol synthesis (top row), methyl formate synthesis (bottom row). Well-mixed liquid (left) and liquid plug flow with dispersion for four cells (right)

space regardless of mixing. In contrast to this structurally stable situation, the multiplicity of order seven in a small region of the parameter space vanishes if imperfect mixing is taken into account.

Stability and the dynamic behavior of an ethylene glycol column has been studied in the region of multiplicity by means of dynamic equilibrium models by several authors [26, 58, 70]. In addition to the steady state bifurcation discussed so far, self-sustained oscillation also may occur in the ethylene glycol process if both consecutive reactions are considered. Kienle et al. [56] not only reported multiple steady states of order three for a column design with a distributed feed [15] but also found a region with a Hopf bifurcation. Fig. 10.12 shows an exemplary result. These oscillations seem to be closely related to the energy balance since no oscillatory behavior could have been identified if the energy balance is neglected. A more systematic study aiming to identify the causes of the oscillations and the sensitivity to modeling assumptions is however largely missing.

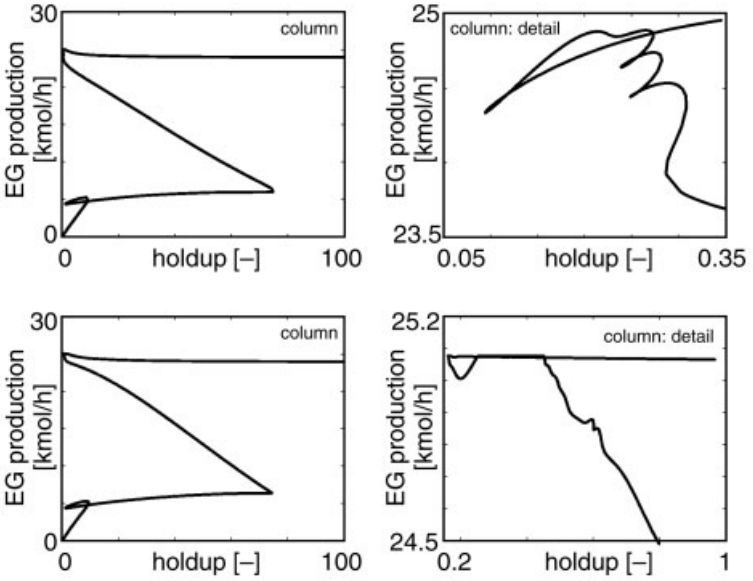

Fig. 10.11 Influence of mixing on the multiplicity behavior of an RD column for ethylene glycol synthesis. Perfect mixing (top row), imperfect mixing (bottom row). The diagrams on the right show the detail in the vicinity of the upper left turning point of the diagrams on the left

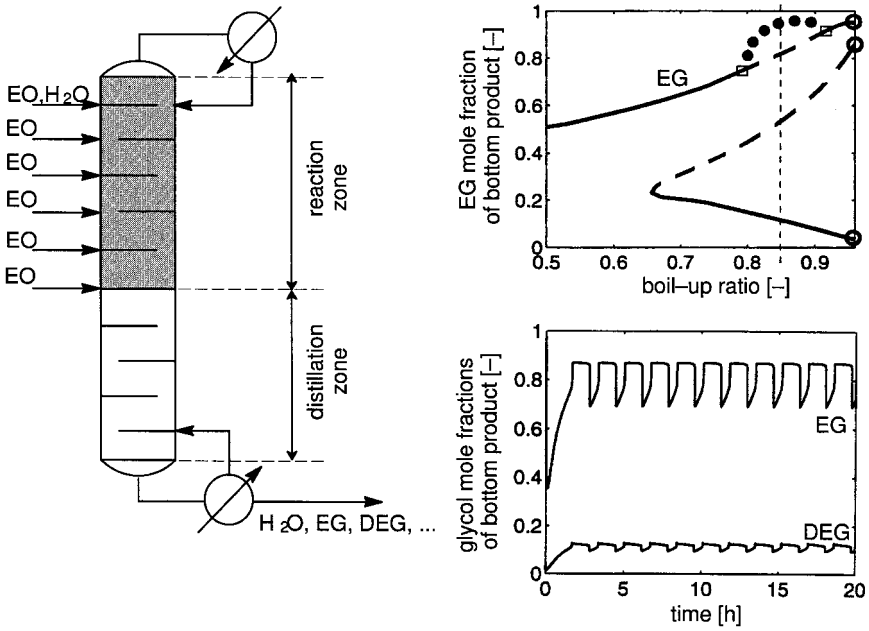

Fig. 10.12 Hopf bifurcation and saddle-node bifurcation for ethylene glycol column, sustained oscillations for a boilup ratio of 0.85

10.5 MTBE and TAME Synthesis

A third class of RD processes that are known to show intricate nonlinear behavior, are processes for the production of fuel ethers methyl *tert*-butyl ether (MTBE) and *tert*-amyl methyl ether (TAME). These are produced by etherification of iso-olefins with methanol according to

$$\text{iso-olefin} + \text{methanol} \rightleftharpoons \text{tert-ether} \tag{10.2}$$

The reactions are catalyzed by strong acid ion-exchange resins and are usually carried out in the presence of inert components. For MTBE synthesis the iso-olefin is isobutylene and for TAME synthesis the iso-olefins are 2-methyl-1-butene and 2-methyl-2-butene. Further details on the chemistry of etherification processes are given in Chapter 5.

10.5.1 MTBE Synthesis

First simulation results on steady state multiplicity of etherification processes were obtained for the MTBE process by Jacobs and Krishna [45] and Nijhuis et al. [78]. These findings attracted considerable interest and triggered further research by others (e. g., [36, 80, 93]). In these papers, a column pressure of 11 bar has been considered, where the process is close to chemical equilibrium. Further, transport processes between vapor, liquid, and catalyst phase as well as transport processes inside the porous catalyst were neglected in a first step. Consequently, the multiplicity is caused by the special properties of the simultaneous phase and reaction equilibrium in such a system and can therefore be explained by means of reactive residue curve maps using ∞/∞-analysis [34, 35]. A similar type of multiplicity can occur in non-reactive azeotropic distillation [8].

However, it was shown that for the above conditions the multiplicity regions in the space of the adjustable operating parameters are fairly small for the MTBE process [73]. This is illustrated in Fig. 10.13 for the pilot plant column treated in [72, 73]. The bifurcation parameters are the heating rate Q and the reflux ratio R, which can be directly adjusted at the real plant. The parameter range is further decreased if a finite mass transfer between the vapor and the liquid phase is taken into account as shown in [5, 40] for the column configuration of Jacobs and Krishna [45]. Moreover, the multiplicity regions even seem to disappear entirely, when finite transport processes are taken additionally into account inside the catalyst [39]. Hence, practical relevance seems to be low.

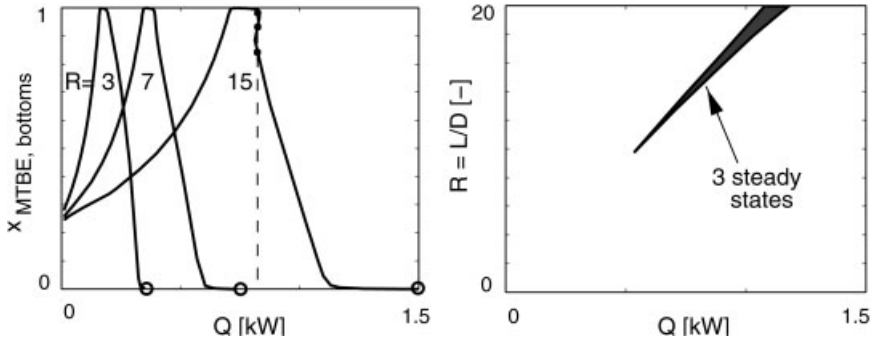

Fig. 10.13 MTBE process at $p = 11$ bar. Bifurcation diagram for different reflux ratios R (left), O denotes total reboil. Multiplicity region in the R/Q parameter plane (right)

10.5.2 TAME Synthesis

Despite the similar reaction mechanism, a completely different type of behavior was found for the TAME process [71–73]. This is due to the fact that the rate of reaction is one order of magnitude slower for TAME synthesis compared to MTBE synthesis. The behavior of the TAME process is illustrated in Fig. 10.14. In contrast to the MTBE process the TAME column is operated in the kinetic regime of the chemical reaction at a pressure of 2 bar. Under these conditions large parameter ranges with multiple steady states occur. The more detailed analysis by Mohl et al. [73] reveals that steady state multiplicity of the TAME process is caused by self-inhibition of the chemical reaction by the reactant methanol, which is adsorbed preferably on the catalyst surface. Steady state multiplicity is therefore caused by the nonlinear concentration dependence of the chemical reaction rate. Consequently, a similar type of behavior can be observed for an isothermal CSTR. This effect is further in-

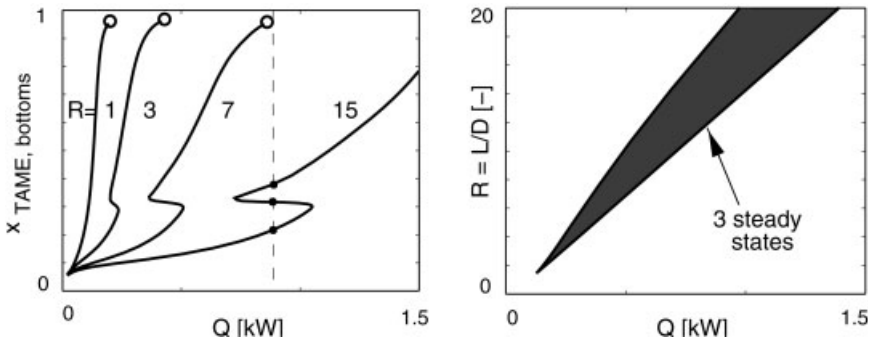

Fig. 10.14 TAME process at $p = 2$ bar. Bifurcation diagram for different reflux ratios R (left), O denotes total reboil. Multiplicity region in the R/Q parameter plane (right)

creased for an RD column with simultaneous reaction and separation. A comparison of the multiplicity regions of an isothermal CSTR, a one-stage RD column, and the pilot plant column shown in Fig. 10.14 has been given [73].

Because of the large multiplicity regions, multiple steady states of the TAME process were also verified experimentally as illustrated in Fig. 10.15 [71, 73, 85]. For this purpose suitable startup strategies were developed by means of dynamic simulation to operate the column directly into the desired steady state. Further, it was

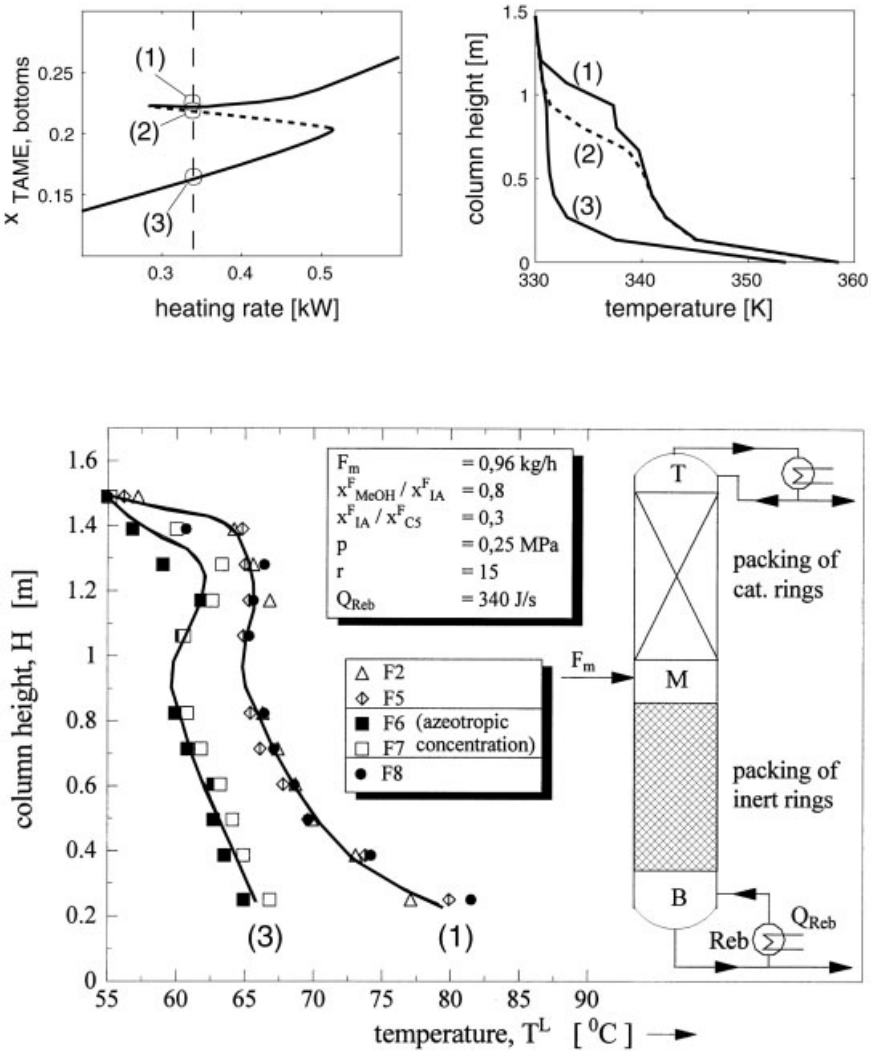

Fig. 10.15 Multiple steady states of the TAME process. Comparison between theoretical predictions (top) and experimental results (bottom)

demonstrated that the column operating at the low steady state is shifted into the higher steady state after a pulse injection of pure TAME for a short period. This dynamic behavior was reproduced with dynamic simulation of a detailed non-equilibrium model by Baur et al. [7] (see also Chapter 9).

Comparison between theoretical predictions and experimental results showed, that, in contrast to the MTBE process, transport processes inside the catalyst were negligible for the TAME process. This is again due to the fact that the microkinetic rate of reaction is one order of magnitude slower than in the MTBE case and is therefore dominating for the operating conditions considered in this study. This was confirmed more rigorously in a recent paper by Higler et al. [39].

10.5.3
Kinetic Instabilities for Finite Transport Inside the Catalyst

More complex patterns of behavior can be found for finite transport resistances inside the porous catalyst [74]. Here, kinetic instabilities occur on two different length scales. On a first, macroscopic scale, multiplicity is induced by ignition and extinction of every single reactive column tray. On a second, microscopic scale, multiplicity comes from isothermal multiplicity of the single catalyst pellet, which is due to the finite transport resistance inside the catalyst.

In tray columns the first mechanism is dominant. This can lead to a large number of different steady state solutions for a given set of operating conditions. If N is the number of steady states (typically an odd number). Then $(N + 1)/2$ of these steady states are stable. This can lead to complex multi-stable dynamic behavior during column startup and set-point or load changes. These phenomena were observed for vanishing as well as for finite intra-particle mass transfer resistance. An example with a total number of six trays (two reactive and two non-reactive trays plus reboiler and condenser) is shown in Fig. 10.16 for the well-known MTBE process. In contrast to the previous section, the column is now operated in the kinetic

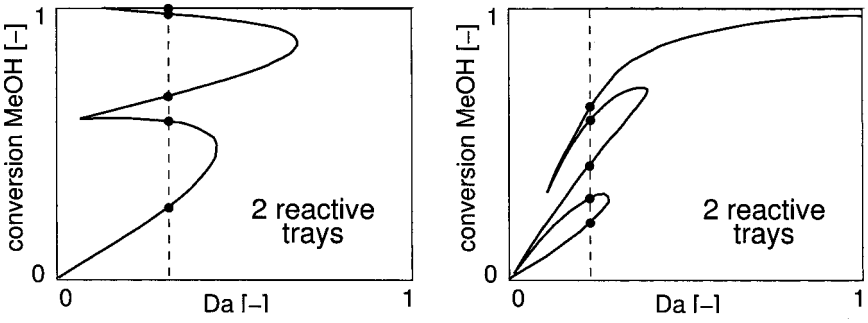

Fig. 10.16 Multiple steady states for MTBE synthesis in a tray column at a pressure of 7 bar: negligible intraparticle diffusion for small particles (left) and finite intraparticle diffusion for large particles (right)

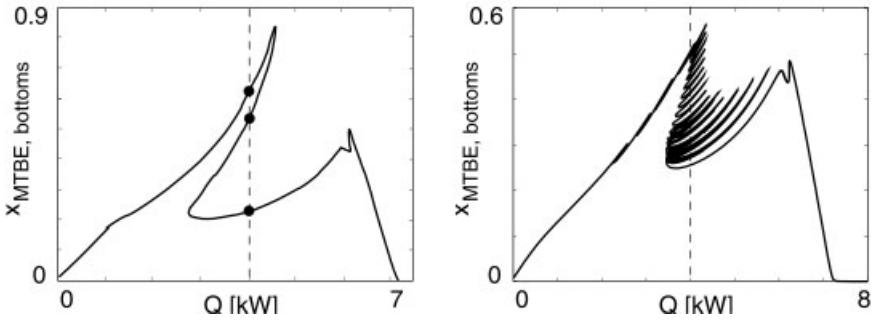

Fig. 10.17 Multiple steady states for MTBE synthesis in a packed column at a pressure of 7 bar: negligible intraparticle diffusion for small particles (left) and finite intraparticle diffusion for large particles (right)

regime with a column pressure of 7 bar and high feed rates: further details are available elsewhere [74].

In case of packed columns, a qualitatively different behavior can be found for finite and infinite intra-particle mass transfer resistance. For vanishing mass transfer resistance inside the catalyst a 'small' number of solutions, typically three, can be observed. Note, that this is consistent with the TAME case discussed above. Instead, for finite transport inside the catalyst a *very* large number of solutions can be observed. An example is shown in Fig. 10.17, right. It was conjectured by Mohl et al. [74], that this behavior is caused by isothermal multiplicity of the single catalyst pellet and is therefore similar to the well-known fixed-bed reactor [38, 77]. However, further research is required to verify this hypothesis. Further, it was shown by Mohl et al. [74] that in both cases the number of solutions may crucially depend on the discretization of the underlying continuously distributed parameter system. A detailed discussion is given by Mohl et al. [74].

In all cases, kinetic multiplicity can be avoided by an increase of the Damköhler number, that is an increase of the number of active sites on the catalyst, or a decrease of the feed rate. Moreover, multiplicity will vanish if the column pressure is increased. In all cases the column gets closer to chemical equilibrium. This is consistent with previous experimental studies for the MTBE process at 7 bar and low feed rates [103] where no multiplicity was found.

10.5.4 Oscillatory Behavior

For the MTBE process also oscillatory behavior was reported in the literature. Potential sources for such an oscillatory behavior are either unwanted periodic forcing (e. g., by badly tuned controllers), fluid dynamic instabilities, or instabilities of the concentration dynamics.

Fluid dynamic instabilities were reported for the MTBE process by Sundmacher and Hoffmann [104]. The cycle times for fluid dynamic oscillations are typically in

the order of minutes. They may occur in the reactive as well as in the non-reactive case.

In contrast to this, for concentration instabilities the cycle times are typically in the order of hours depending on the size of the column. Concentration instabilities for the MTBE system were reported by Schrans et al. [93] and by Hauan et al. [37]. Again, operating conditions were considered with the MTBE process close to chemical equilibrium. A more detailed analysis reveals, that the regions with oscillatory behavior in the space of the adjustable operating parameters are fairly small, again. This is in contrast to the ethylene glycol process considered above. Further, it is worth noting, that, as expected, no concentration oscillations were found for MTBE as well as TAME production in the kinetic regime of the chemical reaction [73, 74].

10.6 Classification

In the last sections three different types of chemical systems that can favorably be processed by means of RD have been presented. Most of the known results on multiplicities and oscillations have been obtained from an analysis of these systems. These results indicate that multiplicities and oscillations may occur quite frequently in RD. Depending on the characteristics of the reaction system and operating conditions these multiplicities and oscillations can have different sources. In principal, each of the individual unit operations 'distillation' and 'reaction' combined in an RD process has it's own sources, which can also be relevant for RD. Further, the combination of both unit operations can give rise to new phenomena.

For a classification of different patterns of behavior let us first focus on systems with a *single reversible reaction*. Today, these constitute the most important class of applications of RD technology in industries. Typical examples are esterification and etherification processes as treated above. For large Damköhler numbers (fast reaction and/or high residence time) the reaction is close to *chemical equilibrium*. In first approximation, such a process can be can be analyzed and explained by means of reactive residue curve maps using ∞/∞-analysis [34, 35]. This procedure is completely analogous to the non-reactive case. Consequently, similar phenomena can be observed as in non-reactive azeotropic distillation including multiple steady states and self-sustained oscillations. However, the regions in the space of the adjustable operating parameters with multiple steady state or oscillatory behavior are small and are typically further reduced if finite inter- or intraphase transport is taken into account. Hence, practical relevance seems to be low. Typical examples are the autocatalytic methyl formate system and the heterogeneously catalyzed MTBE system at high pressures as treated above. Other examples from the literature are the homogeneously catalyzed ethanol and butanol esterifications.

By decreasing the rate of reaction or decreasing the residence time we enter the *kinetic regime* of the chemical reaction. In an RD column, the rate of reaction is decreased by decreasing the column pressure or by decreasing the amount of catalyst.

In the kinetic regime, the nonlinear temperature and concentration dependence of the reaction rate becomes dominant. If the *boiling temperatures* of the different components *lie in the same range*, the temperature is almost fixed by the pressure and only the nonlinear concentration dependence of the reaction rate is important. Typical examples are the TAME and the MTBE system at sufficiently low pressures as treated above. If, in addition, the intraparticle diffusion inside the catalyst is fast compared to the rate of reaction, similar patterns of behavior can be observed as in an isothermal CSTR [73]. The latter has been studied intensively in chemical reaction engineering and two different sources have been identified for isothermal steady state multiplicity (e. g., [18, 68]). The first is self-inhibition by the reactants. The second is autocatalysis by the products. In the open literature only little is known about the application of RD technology to autocatalytic systems. Although there seems to be some potential in such applications [84]. In contrast to this, self-inhibition of the reactants is frequently observed in heterogeneously catalyzed RD. Typical examples are the etherification processes that were treated above. Other examples are hydration processes for the production of *tert*-alcohols [31, 32, 84]. The multiplicity regions can be fairly large like for the TAME process. Therefore, practical relevance can be high and particular attention has to be given to these phenomena when designing and operating these type of processes. The number of steady states can further increase if the diffusional transport inside the porous catalyst is not negligible compared to the rate of reaction. This can be avoided by reducing the size of the catalyst particles to overcome intraparticle diffusional transport resistances or by increasing the pressure or total amount of catalyst to overcome kinetic limitations of the chemical reaction.

According to the investigations in Mohl et al. [73] oscillations are unlikely to occur in the kinetic regime of the chemical reaction for systems with close boiling points.

A different pattern of behavior occurs in the *kinetic regime* of an equilibrium limited reaction or more complex multi reaction systems, if the *boiling points* of the individual components *differ significantly*. This can introduce a positive feedback between reaction and separation via nonlinear temperature dependence of the reaction rate also giving rise to multiplicities and instabilities. It should be noted, that this situation is different from a single phase non-isothermal CSTR. In the single phase CSTR temperature represents a dynamic degree of freedom. Instead, in the two phase region temperature is fixed by the boiling point condition and therefore depends algebraically on the composition. A prototypical example for this class of processes is the ethylene glycol system, which has a more complex reaction mechanism involving consecutive reaction steps. Because this type of reaction mechanism is in particular sensitive to backmixing, additional complexity in the nonlinear behavior is introduced by non-ideal flow patterns on the column trays of an RD column.

Finally, it should be noted that this classification is not complete but represents the authors present point of view based on the experience with the RD systems from above. Certainly, new patterns of behavior will be identified, when applying RD technology to more complex reaction systems or within more complex plant configurations involving mass and energy recycles.

10.7 Nonlinear Wave Propagation

Another nonlinear type of dynamic behavior found in many chemical processes is spatiotemporal pattern formation of the concentration and temperature profiles [66]. This phenomenon is also termed as nonlinear wave propagation. Nonlinear waves are particularly useful to understand and predict the qualitative dynamic behavior without any tedious calculations.

In this section some basic features of nonlinear wave propagation in non-reactive and RD processes will be illustrated and compared with each other. The simulation results presented are based on simple equilibrium or non-equilibrium models [51, 65] for non-reactive separations. In the reactive case, similar models are used, assuming either kinetically controlled chemical reactions or chemical equilibrium. We focus on concentration (and temperature) dynamics and neglect fluid dynamics. Consequently, for equimolar reactions constant flows along the column height are assumed. However, qualitatively similar patterns of behavior are also displayed by more complex models [28, 57, 65] and have been confirmed in experiments [41, 59, 89, 107] for non-reactive multi-component separations. First experimental results on nonlinear wave propagation in reactive columns are presented subsequently.

For an introduction into the subject, we first focus on non-reactive columns. For the case of binary distillation, Marquardt [64] as well as Hwang and Helfferich [42] independently showed by means of the theory of quasi-linear hyperbolic systems that there is a single wave front connecting two pinch regions in a distillation column section without side streams. Hence, a single concentration (and temperature) front may occur in a column section indicating the region of intense mass transfer between the phases. For ideal mixtures, the concentration front is of the constant pattern type. After a disturbance, the front will travel through the column with initially constant shape and velocity. The propagation velocity w of the front can be computed approximately from

$$w \approx \frac{V}{L} \cdot \frac{\Delta y}{\Delta x} - 1 \quad , \tag{10.3}$$

where V, L, Δx, and Δy represent the molar flow rates and the pinch concentration differences in both phases. The boundaries of the column section act as repellors. Hence, the propagation velocity is gradually reduced to zero when the front approaches the section boundary to settle down to a new steady state. Fig. 10.18 shows such a situation. A concentration wave propagates to the top of a rectifying section separating methanol and 1-propanol after a step change of the reflux rate L.

The analysis can be extended to the multi-component case [43, 44, 51, 65, 66]. The number of the fronts is directly related to the number of components n_c in the mixture. For ideal and moderately non-ideal mixtures the concentration and temperature profiles consist of $n_c - 1$ fronts connecting two pinch points. Again, constant pattern waves occur for ideal and moderately non-ideal mixtures. Addi-

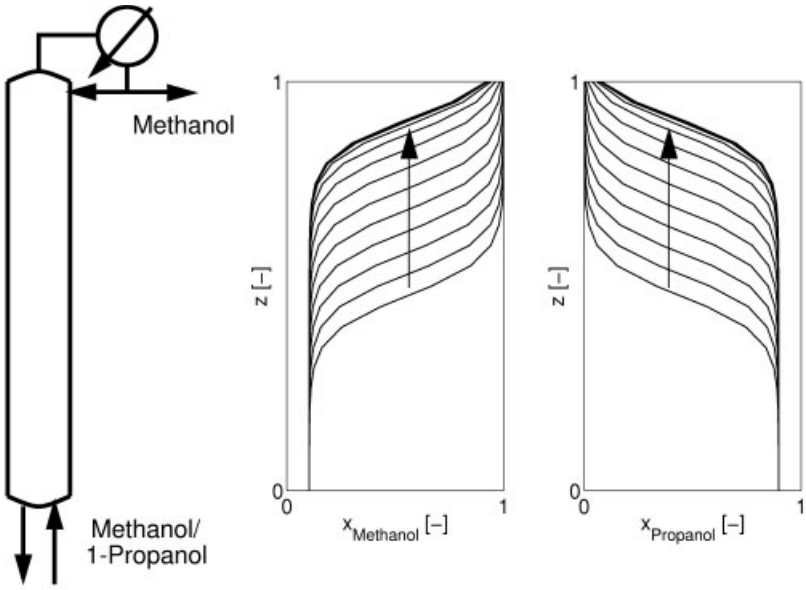

Fig. 10.18 Concentration wave front propagating after a step change in reflux rate to the top of the rectifying section of a binary, non-reactive separation

tional fronts may be possible for highly non-ideal, azeotropic mixtures [50]. Further, for this class of mixtures, so-called combined waves are possible where only a part of the wave front represents a constant pattern wave, whereas the other part has a variable shape. Constant pattern waves travel at the same velocity given by

$$w^{(i)} \approx \frac{V}{L} \cdot \left(\frac{\Delta y}{\Delta x}\right)^{(i)} - 1, \quad i = 1, \ldots, n_c - 1 \quad , \tag{10.4}$$

where

$$\left(\frac{\Delta y}{\Delta x}\right)^{(i)} = \frac{\Delta y_1}{\Delta x_1} = \ldots = \frac{\Delta y_{n_c-1}}{\Delta x_{n_c-1}} \quad . \tag{10.5}$$

Under steady state conditions, at most one of these wave fronts can be located in the middle of a column section, whereas the others are located at either one of the boundaries, where they can overlap and interact. A multicomponent example [51] is shown in Fig. 10.19. Initially, two distinct constant pattern waves can be identified in the concentration profiles of both components traveling at the same velocity to the top of the rectifying section. Close to the upper boundary, the waves start to interact and form some combined steady state pattern.

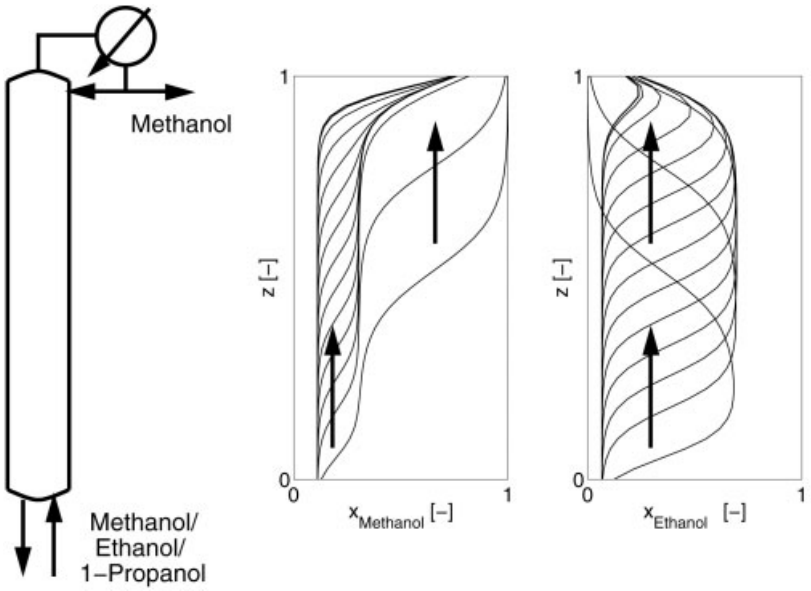

Fig. 10.19 Concentration wave fronts propagating after a step change in reflux rate to the top of the rectifying section of a ternary, non-reactive separation

Similar behavior can also be observed for RD processes. First investigations in this direction have been made by Marquardt and coworkers [25]. They considered the reversible reaction A + B ↔ C for different Damköhler numbers *Da*. Fig. 10.20 shows the variation of the wave front pattern. A single front is obtained in the limit for large *Da*. A similar trend can be observed for the propagation velocity, which

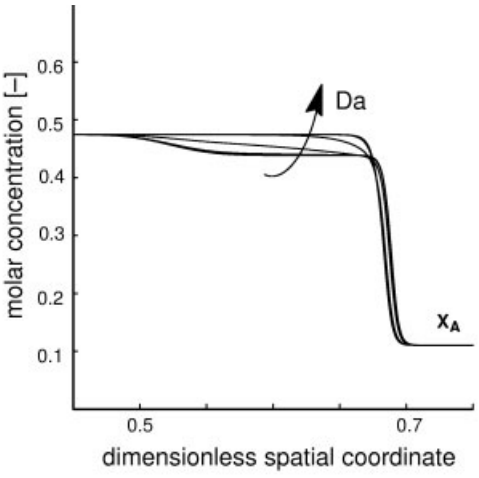

Fig. 10.20 Nonlinear waves in reactive separation. Propagating constant pattern concentrations waves. Sensitivity of wave pattern with respect to Damköhler number

approaches the one for the non-reactive case if the reaction is close to chemical equilibrium. In fact, the equation for w obtained for the non-reactive case is perturbed by an additive term indicating the deviation from reaction equilibrium in the reactive case.

For high *Da* the column is close to chemical equilibrium and behaves very similar to a non-RD column with $n_c - n_r - 1$ components. This is due to the fact that the chemical equilibrium conditions reduce the dynamic degrees of freedom by n_r, the number of reversible reactions in chemical equilibrium. In fact, a rigorous analysis [52] for a column model assuming an ideal mixture, chemical equilibrium and kinetically controlled mass transfer with a diagonal matrix of transport coefficients shows that there are $n_c - n_r - 1$ constant pattern fronts connecting two pinches in the space of transformed coordinates [108]. The propagation velocity is computed as in the case of non-reactive systems if the physical concentrations are replaced by the transformed concentrations. In contrast to non-RD, the wave type will depend on the properties of the vapor–liquid *and* the reaction equilibrium as well as of the mass transfer law.

Despite the analogy between reactive and non-RD, the type of wave pattern may not necessarily comply for similar types of mixtures. In particular, combined waves as described above for non-ideal non-reactive mixtures might occur for ideal, reactive mixtures. Conversely, constant pattern waves may arise for highly non-ideal reactive mixtures.

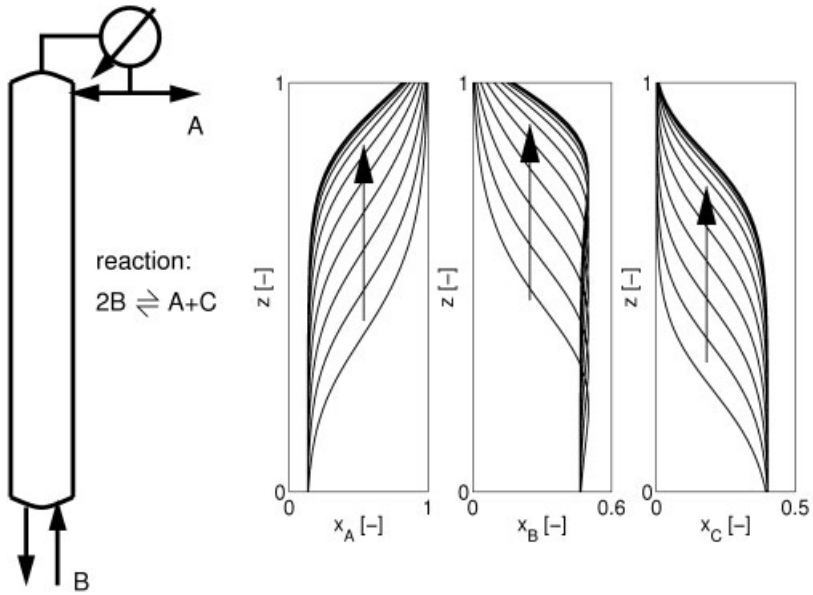

Fig. 10.21 Concentration wave fronts in a reactive ternary separation after a step change in reflux rate. Ideal vapor–liquid equilibrium, kinetically controlled mass transfer, reversible chemical reaction close to chemical equilibrium

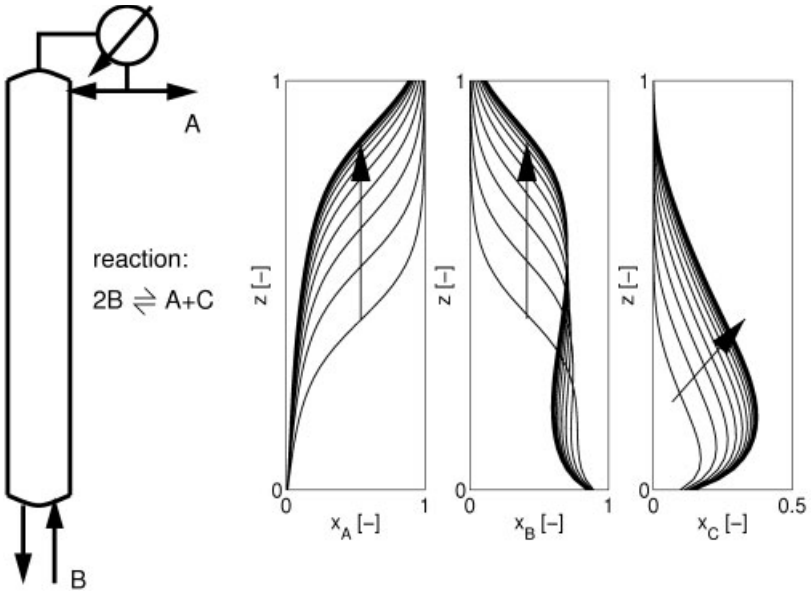

Fig. 10.22 Concentration wave fronts in a reactive ternary separation after a step change in reflux rate. Case as in Fig. 10.21, but reaction in kinetically controlled regime

An example of wave propagation in an RD column is shown in Figs. 10.21 and 10.22. Constant pattern waves can be observed in case of ideal phase equilibrium, kinetically controlled mass transfer and a single reversible reaction close to chemical equilibrium (compare Figs. 10.21). In contrast, at low *Da* in the kinetically controlled regime of the chemical reaction a different, more complex type of dynamic behavior can be observed (compare Fig. 10.22). The behavior in the kinetic regime is not sufficiently understood today and needs further research.

Nonlinear waves in RD have been studied by Balasubramhanya and Doyle III [4] who treat an idealized esterification system, and by Grüner et al. [33] who study a fairly complex, industrial multireaction process. An experimental study of methyl formate synthesis has been carried out by Reder [25, 87] using the lab-scale column introduced above (Fig. 10.2). In all cases the columns are close to chemical equilibrium and therefore behave similar to non-reactive separations.

Fig. 10.23 shows simulated temperature waves in the lab-scale column. A comparison with experimental data is shown for a steady state in Fig. 10.24 showing a satisfactory fit. Clearly, the experiments confirm the pattern of the waves in the rectifying as well as in the stripping section. The flows in the column have been chosen such that the waves are sitting at the lower boundary of the column sections (i. e., close to the feed tray and close to the reboiler).

The extreme sensitivity of the lab-scale column to small variations in the heat duty of the reboiler is shown in Fig. 10.25. The upper left diagram shows the steady state concentrations of the key components in the distillate and in the bottoms

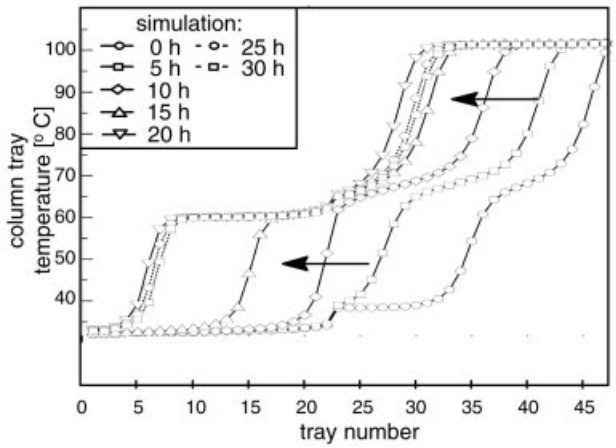

Fig. 10.23 Simulated temperature waves in lab-scale methyl formate column

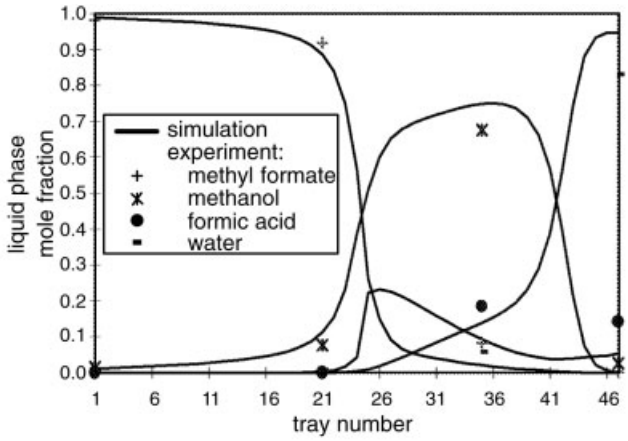

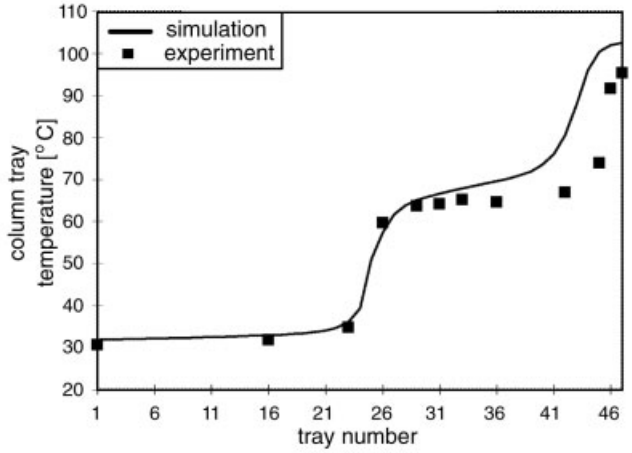

Fig. 10.24 Steady state concentration (top) and concentration waves (bottom) in lab-scale methyl formate column. Simulation (lines) and experiment (symbols)

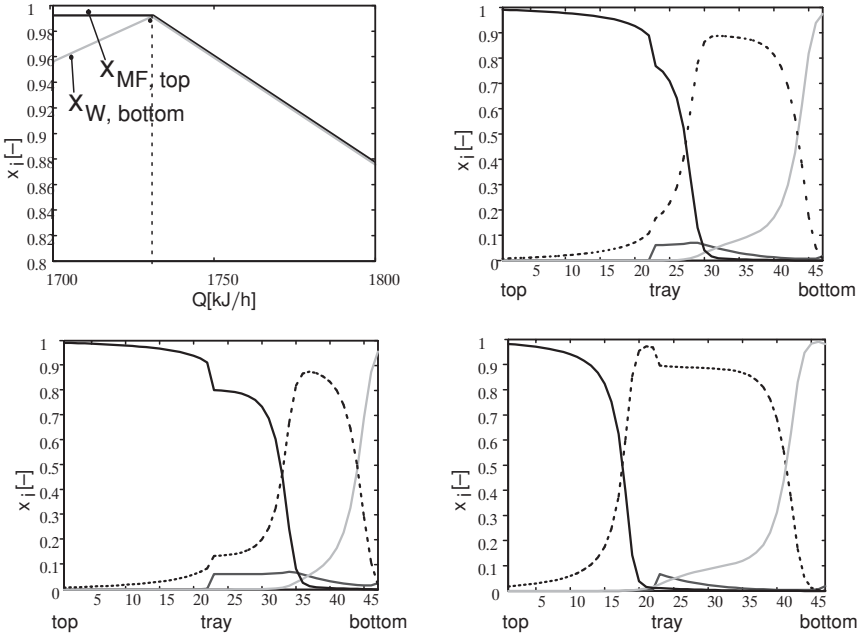

Fig. 10.25 Sensitivity of lab-scale methyl formate column. Concentrations of key components in both product streams (upper left). Nominal steady state (upper right) and disturbed steady states (bottom row)

product as a function of the heat duty. Obviously, there is virtually only a single heat duty, which at the same time results in a high methyl formate and a high water concentration in both products. The concentration profiles at this favorable operating point are shown in the upper right diagram of Fig. 10.25. The diagrams below show a significant shift of the steady state concentration profiles if the heat duty is just varied by 1 % from the nominal value. Control is essential to stabilize the desired operating point.

Nonlinear waves are very useful for a qualitative understanding of the concentration and temperature dynamics in an RD column. So far, only an incomplete understanding of the relation between the physicochemical complexity of the mixture, the design and operation of the column, and the observed spatiotemporal patterns is available. Much research is required to resolve the open issues. In addition, the phenomenon of a propagating wave can also be exploited to derive a simplified quantitative description of the column dynamics in the non-reactive [27, 67] as well as in the reactive [4, 51, 52] case. These reduced nonlinear models are most suitable to design and implement advanced model based control systems as discussed in the next section.

10.8 Control

In general, two different modes of operation are possible for distillation columns, no matter whether reactive or non-reactive. The first is the continuous and the second is the batch mode of operation. Focus in this section is on control of continuously operated RD columns. For optimal operation and control of batch columns we refer to the literature [4, 20, 75, 101, 110].

So far, only little work on RD column control is available in the open literature. Most of this work is concerned with case studies for esterification and etherification processes. Furthermore, the ethylene glycol process has received some attention because of its interesting dynamic behavior, which was summarized and illustrated above. A recent review on control case studies is available in [2]. Only very few general guidelines are available for RD column control including the work of Sneesby et al. [97] and Alarfaj and Luyben [2].

Like in non-RD, a hierarchy of different control tasks exists. On the lowest level, column pressure and the levels in the reboiler at the bottom and the accumulator at the top of the column have to be controlled. On a higher level, product purities have to be controlled. For single product columns only one product composition has to be controlled (one-point control), whereas for two product columns we usually want to control the specifications of both product streams (two-point control). Pressure and level control are similar to non-RD and can be achieved with standard methods. However, composition control of an RD column may introduce some additional complexities as will be illustrated subsequently. In the remainder focus is on two-point composition control.

Control system design consists of two steps: control structure selection includes the choice of suitable manipulated and measured variables as well as their pairing; design and parameterization of some control algorithm defines the computation of the required values of the manipulated variables from the measurements and given set-points. Let us first focus on the control structure selection problem.

10.8.1 Control Structure Selection

Possible candidates for manipulated variables are essentially the same as in non-RD, including reflux, distillate flow rate or reflux ratio at the top of the column and heating rate, bottoms flow rate, or reboil ratio at the bottom of the column. In addition, dosing of the reactants can be an interesting choice in RD, if this is compatible with the upstream processing of the plant. Possible candidates for measured variables are either product compositions or column temperatures. However, online measurement of concentrations is usually slow, expensive, and often not very reliable. Therefore inferential control schemes are preferred, where the product compositions are inferred from temperature measurements. However, the relationship between product compositions and column temperatures is frequently non-unique in RD [26, 98] and this can lead to severe problems as will be illustrat-

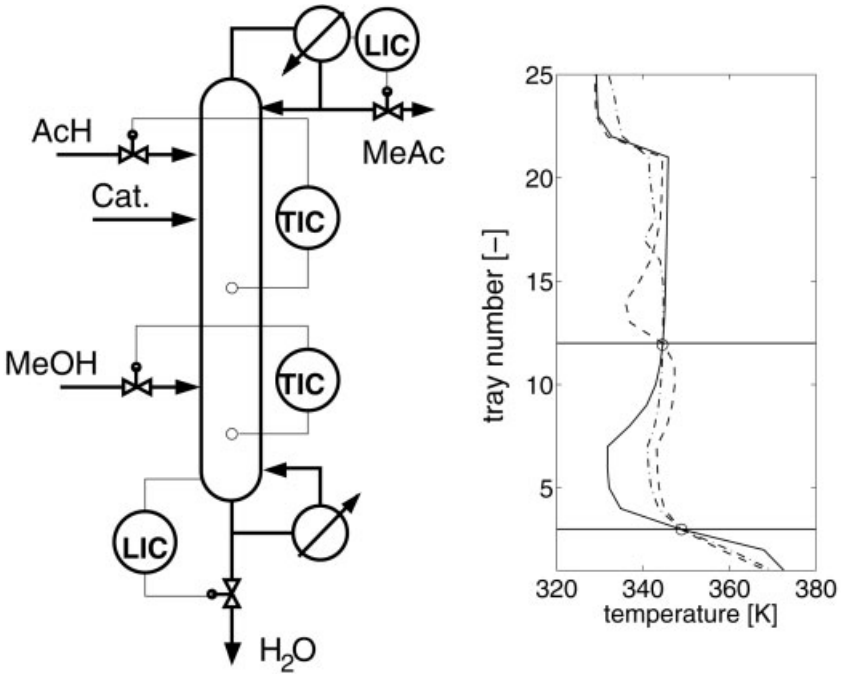

Fig. 10.26 Closed loop steady state temperature profiles for RD column producing methyl acetate with control scheme 1

ed in a first case study. This case study is inspired by the paper of Roat et al. [90] and is concerned with a pilot plant column for producing methyl acetate.

A first control scheme proposed in [90] is shown in Fig. 10.26. In this scheme, product purities of methyl acetate (MeAC) and water (H_2O) are inferred from temperatures on trays 3 and 12, respectively, and the feed rates of methanol (MeOH) and acetic acid (AcH) are used as manipulated variables. For this configuration, three different temperature profiles exist with identical temperature values at the sensor locations but different feed rates and completely different product compositions. The solid line in Fig. 10.26 represents the desired temperature profile with high conversion. This situation corresponds to *input multiplicity* as introduced at the beginning of section 10.2 on multiplicity and oscillations. Here, the same set of output variables (temperatures) is produced by (three) different sets of input variables (feed rates). Because the steady state values of the output variables are fixed by the given setpoint of the controllers, this input multiplicity will lead to steady state multiplicity of the closed loop system as illustrated in Fig. 10.27.

Fig. 10.27 shows the time plots of the input variables (feed rates), the output variables (temperatures on trays 3 and 12) and the product purities of methyl acetate in the distillate and water in the bottoms for two different pulse disturbances of the heating rate. Initially the column is at the desired steady state with high product purity. After a small disturbance, indicated by the dashed line, the column returns

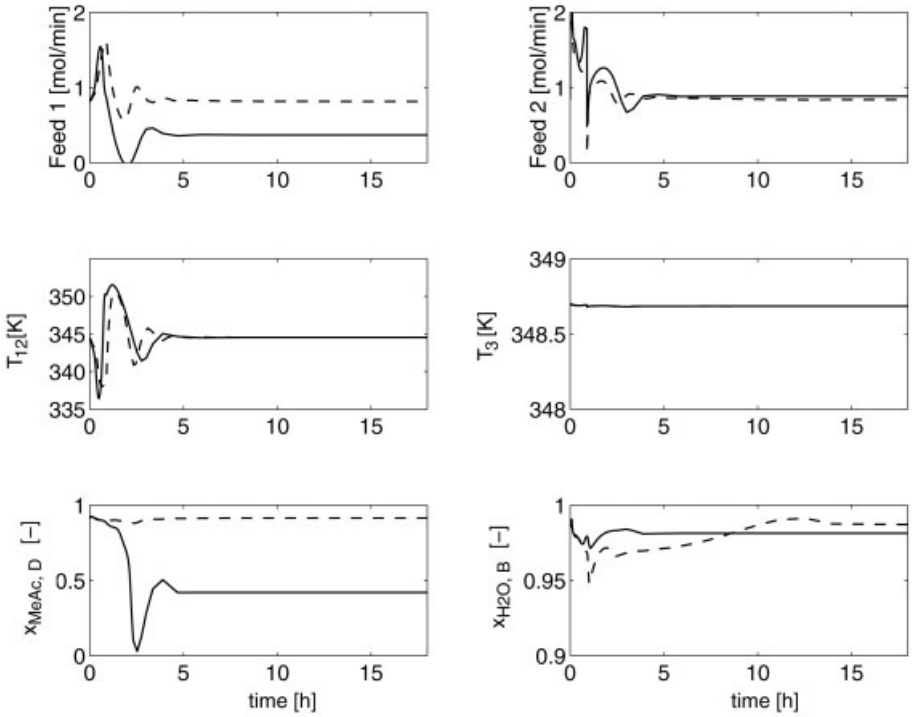

Fig. 10.27 Dynamic transient behavior for control scheme 1 in Fig. 10.26 after a small (dashed line) and a large (solid line) pulse disturbance of the heating rate

to the desired steady state. After a large disturbance, indicated by the solid line, the column suffers an undesired transition to a different steady state with low product purity. In both cases the controlled variables (temperatures on trays 3 and 12) are finally forced to their given setpoints by the controllers.

Because input multiplicity depends on the choice of the output variables, it can be avoided by selecting a suitable control configuration. In the present case, this problem is easily solved by taking a third temperature measurement into account as proposed in [90] and illustrated in Fig. 10.28. The difference between the two temperature measurements in the reaction zone is an indirect measure for the conversion of the chemical reaction and therefore leads to a unique steady state with good control characteristics. Similar control schemes, with direct and indirect inference of conversion were proposed in [99, 100, 105] for etherification processes.

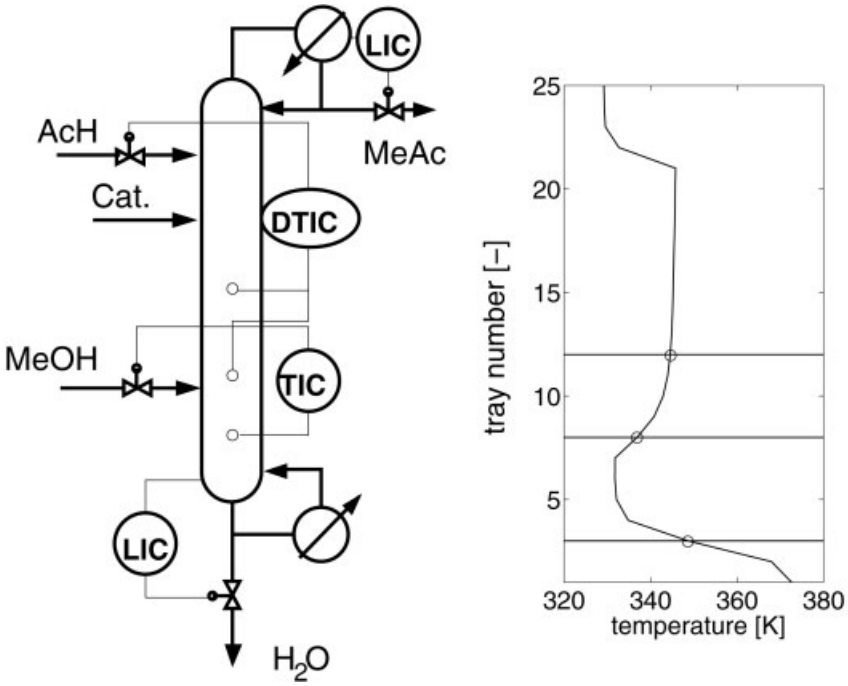

Fig. 10.28 Closed loop steady state temperature profiles for RD column producing methyl acetate with control scheme 2

10.8.2 Control Algorithms

In the previous case study, the focus was on control structure selection. As control algorithms standard linear PI-controllers were used. In a second case study, the focus is on control algorithms. For that purpose we compare different control algorithms for a fixed control structure. The process to be considered is an industrial benchmark problem, which was treated in joint research with Bayer AG [21, 33]. The process and its open loop dynamic behavior is illustrated in Fig. 10.29. Components B and C are the reactants. They react in two consecutive equilibrium reactions to products A and E. The main product E is obtained in the bottoms of the column and the other product A in the distillate.

Temperature profiles after a stepwise increase of the heating rate are shown on the right side of Fig. 10.29. These profiles show distinct nonlinear wave characteristics as discussed in the previous section. Therefore the process is sensitive to disturbances and composition control is required. Again focus is on an inferential control scheme. Measured variables are the temperatures on trays 4 and 60, which are located within the upper and the lower ware front. Hence, they show good sensitivity to disturbances. Manipulated variables are the heating rate and the reflux ratio. For this process neither input nor output multiplicities occur.

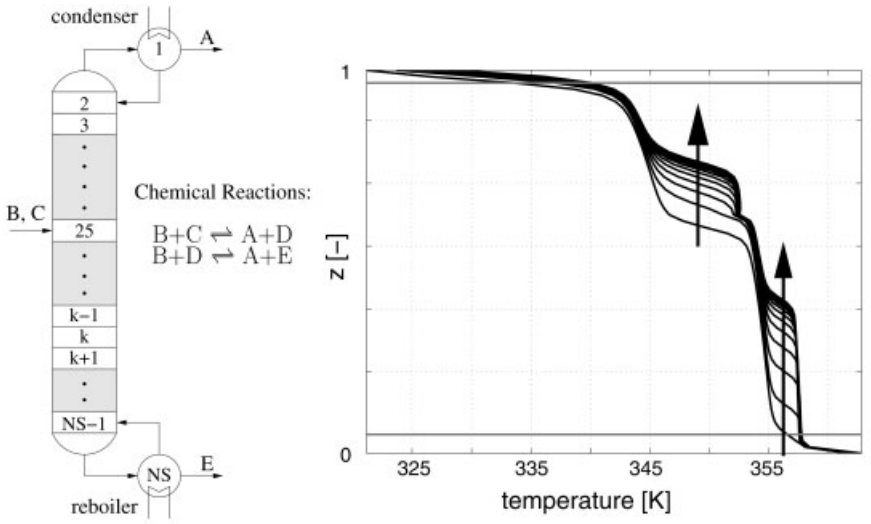

Fig. 10.29 Open loop temperature profiles of an industrial RD column after stepwise increasing the heating rate

Fig. 10.30 gives a comparison between open loop dynamics and closed loop dynamics for linear multi-input multi-output PI controllers and an advanced nonlinear controller. The nonlinear controller is based on asymptotic exact input/output linearization as proposed by Gilles and coworkers [29]. This is a model based controller, where the concentration profiles inside the column are reconstructed online from the two temperature measurements by means of a nonlinear state observer [21, 33].

Fig. 10.30 shows the time plots of the bottom key impurity for different disturbances. The concentration of this component is suitably scaled. From Fig. 10.30 we conclude that linear control is sufficient for stabilizing the desired steady state against disturbances. However, during the transient considerable impurities in the bottom products may rise for linear control. Therefore, Fig. 10.30 also illustrates the great potential of nonlinear control for advanced column operation including tight composition control, switching between different operating points and so on. Further, the model-based measurement technique provides full information about the composition profiles of the different components in the column. This information can also be valuable for open loop operation and supervision of RD columns.

For the implementation of advanced model-based controllers suitable models and suitable hardware is required including a computer for real-time simulation linked to the control system. In practice, this effort is only justified for a limited number of applications. For many applications standard PI controllers will suffice. Hence, finding a suitable control structure is often the dominating issue during control system design. Certainly, dynamics have to be considered for this and one should not only rely on steady state measures for comparing different control

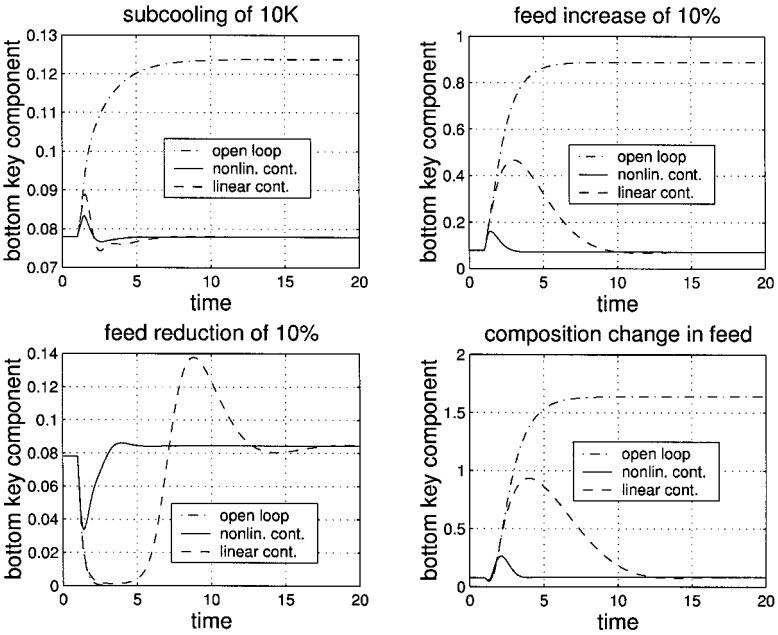

Fig. 10.30 Performance of linear control compared to nonlinear control for the industrial RD process in Fig. 10.29

structures. Further, it is often useful to have a look at the column profiles for proper sensor location. Non-uniqueness arising in inferential control can be avoided by including direct or indirect measures for conversion into the control scheme.

The optimal control structure always depends on the specific type of process considered. Further research is required to develop more general guidelines for control structure selection of RD processes depending on the dominating process characteristics.

10.9 Conclusions

In this chapter, an overview on the present knowledge of nonlinear dynamics and control of RD columns was given. First, focus was on open-loop dynamics. It was shown that these processes can show a distinct nonlinear behavior including multiple steady states, self-sustained oscillations, and nonlinear wave propagation. Different patterns of behavior were identified depending on the properties of the reaction system and the operating conditions.

In summary, the following general guidelines on the qualitative dynamic behavior of RD processes can be drawn from the present state of knowledge. Similar to

steady state design of RD columns [62, 106], we essentially have to distinguish two different regimes with regard to open-loop column dynamics. The first is the equilibrium regime, where the reactions are close to chemical equilibrium. The second, is the kinetic regime of the chemical reaction. The overall behavior between both regimes differs significantly.

In the equilibrium regime, the dynamic behavior of an RD column in transformed concentration variables is essentially the same like the dynamic behavior of a non-RD column. Hence it is not surprising that under these conditions we can observe all kinds of multiplicity, oscillations, and wave propagation phenomena like in non-RD. Any novel feature, such as reactive azeotropy, is introduced by the static transformation between physical and transformed concentrations. From this point of view, it seems that, at least qualitatively, we have a fairly good understanding of the concentration dynamics of RD processes in the equilibrium regime today. Open questions are related to a detailed understanding of oscillatory behavior in this regime.

In the kinetic regime, the dynamic behavior of RD processes is dominated by the chemical reaction. For closely boiling mixtures the behavior is similar to an isothermal reactor. Instead, if the boiling points of the individual components differ significantly, new phenomena are introduced by the interaction between separation and reaction kinetics, which can not be observed in a single phase reactor. A thorough understanding of spatiotemporal pattern formation in the kinetic regime is missing for both types of mixtures. This is therefore a challenging field for future research.

So far, emphasis was on simple reaction systems and simple column configurations. Further challenging tasks are related with the application of the RD technology to more complex reaction systems and/or more complex system configurations, like the coupled column system [102]. Safe and optimal operation of such systems will require more insight into their the dynamic behavior and additional patterns of behavior will be identified.

In the second part of this chapter, focus was on control of continuously operated RD processes. So far most control studies focus on processes that are operated close to chemical equilibrium. Emphasis was on the well-known esterification and etherification systems. The methods employed are similar to non-RD column control. It is worth noting that this is consistent with our conclusions on open-loop dynamics as drawn above. Additional problems may rise in indirect control schemes, where product compositions are inferred from temperature measurements. It was shown that these problems can be handled if in addition some direct or indirect measure of conversion is taken into account.

Control studies for kinetically controlled processes are missing to a large extent and further research is required to close this gap.

10.10
Acknowledgments

The authors thank all their students and partners from industries and academia who were involved in this research. Financial support from BMBF ('Bundesministerium für Bildung, Wissenschaft, Forschung und Technologie') under grants 03 D 0014 A7, 03 D 0013 B2, and 03 C 0268 A/B is gratefully acknowledged.

References

1 V. H. Agreda, L. R. Partin, and W. H. Heise. *Chem. Engng. Prog.*, **1990**, *40*, 40–46.
2 M. Al-Arfaj and W. L. Luyben. *Ind. Engng. Chem. Res.*, **2000**, *39*, 3298–3307.
3 R. Aris and N. R. Amundson. *Chem. Engng. Sci.*, **1958**, *7*, 121–155.
4 L. S. Balasubramhanya and F. J. Doyle III. *J. Proc. Control*, **2000**, *10*, 209–218.
5 R. Baur, A. P. Higler, R. Taylor, and R. Krishna. *Chem. Engng. J.*, **2000**, *76*, 33–47.
6 R. Baur, R. Taylor, and R. Krishna. *Chem. Engng. Sci.*, **2000**, *55*, 6139–6154.
7 R. Baur, R. Taylor, and R. Krishna. *Chem. Engng. Sci.*, **2001**, *56*, 1–18.
8 N. Bekiaris, G. A. Meski, C. M. Radu, and M. Morari. *Ind. Engng. Chem. Res.*, **1993**, *32*, 2023–2038.
9 B. Berdouzi, C.-H. Chan, and D. G. Retzloff. *Chem. Eng. Sci.*, **1989**, *44*, 436–442.
10 O. Bilous and N. R. Amundson. *AIChE J.*, **1955**, *1*, 513–521.
11 C. Bischof, B. Lang, W. Marquardt, and M. Mönnigmann, in *Proc. SCAN 2000, 9th GAMM-IMACS Int. Symp. Scientific Computing, Computer Arithmetic and Validated Numerics*, Sept. 19–22, Karlsruhe, Germany **2000**.
12 S. Blagov, B. Bessling, H. Schoenmakers, and H. Hasse. *Chem. Engng. Sci.*, **2000**, *55*, 5421–5436.
13 H. Bock, M. Jimoh, and G. Wozny. *Chem. Engng. Technol.*, **1997**, *20*, 182–191.
14 A. R. Ciric and D. Gu. *AIChE J.*, **1994**, *40*, 1479–1487.
15 A. R. Ciric and P. Miao. *Ind. Engng. Chem. Res.*, **1994**, *33*, 2738–2748.
16 T. E. Corrigan and J. H. Miller. *Ind. Engng. Chem. Process Des. Dev.*, **1968**, *7*, 383–384.
17 M. F. Doherty and J. D. Perkins. *Chem. Engng. Sci.*, **1982**, *37*, 381–392.
18 S. S. E. H. Elnashaie and S. S. Elshishini. *Modelling, Simulation and Optimization of Industrial Fixed Bed Catalytic Reactors*. Gordon and Breach, Philadelphia, **1993**.
19 S. S. E. H. Elnashaie and S. S. Elshishini. *Dynamic Modelling, Bifurcation and Dynamic Behavior Chaotic Behavior of Gas–Solid Catalytic Reactors*. Gordon and Breach, Philadelphia, **1996**.
20 G. Fernholz, S. Engell, L.-U. Kreul, and A. Gorak. *Comput. Chem. Engng.*, **2000**, *24*, 1569–1575.
21 G. Fernholz, M. Friedrich, S. Grüner, K. D. Mohl, A. Kienle, and E. D. Gilles, in *6th IFAC Symp. Dynamics and Control of Process Systems, DYCOPS 6*, (E. S. J. G. Stephanopoulos, J. H. Lee, eds) 137–142, **2001**.
22 V. Gehrke, PhD thesis, RWTH Aachen, in preparation.
23 V. Gehrke and W. Marquardt. *Comput. Chem. Engng.*, **1997**, *21* (Suppl), 1001–1006.
24 V. Gehrke, G. Pielen, and W. Marquardt, in *GVC-Fachausschuss Thermische Zerlegung von Gas- und Flüssigkeitsgemischen*, Wernigerode, 5–7 April **2000**.

25 V. Gehrke, C. Reder, and W. Marquardt. Project report LPT-pro-1998-02, Lehrstuhl für Prozesstechnik, RWTH-Aachen, **1998**.

26 E. D. Gilles, G. Lauschke, A. Kienle, and M. Storz. *A. Rev. Control*, **1996**, *20*, 9–22.

27 E. D. Gilles and B. Retzbach, in *Proc. 19th IEEE Conf. Decision Contr.*, Albuquerque, **1980**, 865–870.

28 E. D. Gilles, B. Retzbach, and F. Silberberger. *ACS Symposium Series*, **1980**, 481–492.

29 E. D. Gilles, M. Storz, and M. Friedrich. *Automatisierungstechnik*, **1994**, *42*, 135–148.

30 M. Golubitsky and D. G. Schaeffer. *Singularities and Groups in Bifurcation Theory, Vol. 1*, Springer, New York, **1985**.

31 J. C. Gonzalez and J. R. Fair. *Ind. Engng. Chem. Res.*, **1998**, *36*, 3833–3844.

32 J. C. Gonzalez, H. Subawalla, and J. R. Fair. *Ind. Engng. Chem. Res.*, **1998**, *36*, 3845–3853.

33 S. Grüner, K. D. Mohl, A. Kienle, E. D. Gilles, G. Fernholz, and M. Friedrich, in *6th IFAC Symp. Dynamics and Control of Process Systems, DYCOPS 6*, (E. S. J. G. Stephanopoulos, J. H. Lee, eds) 125–130, **2001**.

34 T. E. Güttinger and M. Morari. *Ind. Engng. Chem. Res.*, **1999**, *38*, 1633–1648.

35 T. E. Güttinger and M. Morari. *Ind. Engng. Chem. Res.*, **1999**, *38*, 1649–1665.

36 S. Hauan, T. Hertzberg, and K. M. Lien. *Comput. Chem. Engng.*, **1995**, *19* (Suppl), 327–332.

37 S. Hauan, S. M. Schrans, and K. M. Lien. *Ind. Engng. Chem. Res.*, **1997**, *36*, 3995–3998.

38 L. L. Hegedus, S. H. Oh, and K. Baron. *AIChE J.*, **1977**, *23*, 632–642.

39 A. P. Higler, R. Krishna, and R. Taylor. *Ind. Engng. Chem. Res.*, **2000**, *39*, 1596–1607.

40 A. P. Higler, R. Taylor, and R. Krishna. *Chem. Engng. Sci.*, **1999**, *54*, 1389–1395.

41 Y.-L. Hwang, G. K. Graham, G. E. Keller, J. Ting, and F. G. Helfferich. *AIChE J.*, **1996**, *42*, 2743–2760.

42 Y.-L. Hwang and F. G. Helfferich. *Chem. Engng. Sci.*, **1988**, *43*, 1099–1114.

43 Y.-L. Hwang and F. G. Helfferich. *Chem. Engng. Sci.*, **1989**, *44*, 1547–1568.

44 Y.-L. Hwang and F. G. Helfferich. *Chem. Engng. Sci.*, **1990**, *45*, 2907–2915.

45 R. Jacobs and R. Krishna. *Ind. Engng. Chem. Res.*, **1993**, *32*, 1706–1709.

46 E. W. Jacobsen, in *Proc. European Control Conference*, Groningen, **1993**, 661–666.

47 E. W. Jacobsen and S. Skogestad, in *Proc. American Control Conference*, Boston, **1991**.

48 E. W. Jacobsen and S. Skogestad. *AIChE J.*, **1991**, *37*, 499–511.

49 O. L. Karpilovsky, Y. A. Pisarenko, and L. A. Serafimov. *Distillation & Absorption '97, Trans. I. Chem E. Symp. Ser.*, **1997**, *142*, 685–694.

50 A. Kienle. *Nichtlineare Wellenphänomene und Stabilität stationärer Zustände in Destillationskolonnen*. VDI Fortschritt-Berichte Nr. 3/506. VDI-Verlag, Düsseldorf, **1997**.

51 A. Kienle. *Chem. Engng. Sci.*, **2000**, *55*, 1817–1828.

52 A. Kienle, in *Proc. 3rd Symp. Process Control: SPC-2000,* Ploiesti, Romania, **2000**, 72–78.

53 A. Kienle, G. Lauschke, V. Gehrke, and E. D. Gilles. *Chem. Engng. Sci.*, **1995**, *50*, 2361–2375.

54 A. Kienle and W. Marquardt. *Chem. Engng. Sci.*, **1991**, *46*, 1757–1769.

55 A. Kienle, W. Marquardt, and E. D. Gilles. *Comput. Chem. Engng.*, **1994**, *18* (Suppl.), 37–41.

56 A. Kienle, K. D. Mohl, and E. D. Gilles, in *Nichtlineare Dynamik bei chemischen Prozessen*, Dechema, **1995**, B2-1–B2-3.

57 A. Kienle, E. Stein, A. Rehm, and E. Kloppenburg, in *Proc. Eur. Control Conf.: ECC'99*, Karslruhe, **1999**, paper F1004-4.

58 A. Kumar and P. Daoutidis. *AIChE J.*, **1999**, *45*, 51–68.

59 L. Lang. PhD thesis, Universität Stuttgart, **1991**.

60 W. L. Luyben, B. D. Tyreus, and M. L. Luyben. *Plantwide Process Control*. McGraw Hill, New York, **1998**.

61 T. Magnussen, M. L. Michelsen, and A. Fredenslund. *Int. Chem. Engng. Symp. Ser.*, **1979**, *56*, 4.2/1–4.2/19.

62 M. F. Malone and M. F. Doherty. *Ind. Engng. Chem. Res.*, **2000**, *39*, 3953–3957.

63 M. Mangold, A. Kienle, K. D. Mohl, and E. D. Gilles. *Chem. Engng. Sci.*, **2000**, *55*, 441–454.

64 W. Marquardt. *Automatisierungstechnik*, **1987**, *35*, 156–162.

65 W. Marquardt. *Nichtlineare Wellenausbreitung, ein Weg zu reduzierten Modellen von Stofftrennprozessen*. VDI Fortschrittsberichte Nr. 8/161. VDI-Verlag, Düsseldorf, **1988**.

66 W. Marquardt. *Int. Chem. Engng.*, **1990**, *30*, 585–606.

67 W. Marquardt and M. Amrhein. *Comput. Chem. Engng.*, **1994**, *18* (Suppl.), 349–353.

68 T. Matsuura and M. Kato. *Chem. Engng. Sci.*, **1967**, *22*, 171–184.

69 J. C. Mecklenburgh. *Theory of Backmixing*. John Wiley and Sons, London, **1975**.

70 P. Miao and A. R. Ciric, in *Proc. AIChE Annual Meeting*, Miami Beach, **1995**.

71 K. D. Mohl, A. Kienle, and E. D. Gilles. *Chem. Engng. Technol.*, **1998**, *21*, 133–136.

72 K. D. Mohl, A. Kienle, E. D. Gilles, P. Rapmund, K. Sundmacher, and U. Hoffmann. *Comput. Chem. Engng.*, **1997**, *21* (Suppl.), 989–994.

73 K. D. Mohl, A. Kienle, E. D. Gilles, P. Rapmund, K. Sundmacher, and U. Hoffmann. *Chem. Engng. Sci.*, **1999**, *54*, 1029–1043.

74 K. D. Mohl, A. Kienle, K. Sundmacher, and E. D. Gilles. *Chem. Engng. Sci.*, **2001**, *56*, 5239–5254.

75 R. Monroy-Loperena and J. Alvarez-Ramirez. *Ind. Engng. Chem. Res.*, **2000**, *39*, 378–386.

76 D. Müller and W. Marquardt. *Ind. Engng. Chem. Res.*, **1997**, *36*, 5410–5418.

77 R. H. Nibbelke, J. H. J. B. Hoebink, and G. B. Marin. *Chem. Engng. Sci.*, **1998**, *37*, 2195–2210.

78 S. A. Nijhuis, F. P. J. M. Kerkhof, and A. N. S. Mak. *Ind. Engng. Chem. Res.*, **1993**, *32*, 2767–2774.

79 A. S. Parker, **1958**, US Patent 2 839 588.

80 E. Perez-Cisneros, M. Schenk, R. Gani, and P. A. Pilavachi. *Comput. Chem. Engng.*, **1996**, *20* (Suppl.), 267–272.

81 L. Perko. *Differential Equations and Dynamical Systems*, Springer, New York, **1991**.

82 F. B. Petlyuk and V. S. Avet'yan. *Theor. Found. Chem. Eng.*, **1971**, *5*, 457–463.

83 Y. A. Pisarenko, O. A. Epifanova, and L. A. Serafimov. *Theor. Found. Chem. Eng.*, **1988**, *22*, 281–286.

84 G. G. Podrebarac, F. T. Ng, and G. L. Rempel. *CHEMTECH*, **1997**, *May*, 37–45.

85 P. Rapmund, K. Sundmacher, and U. Hoffmann. *Chem. Engng. Technol.*, **1998**, *21*, 136–139.

86 L. F. Razon and R. A. Schmitz. *Chem. Engng. Sci.*, **1987**, *42*, 1005–1047.

87 C. Reder. Ph. D. thesis, RWTH Aachen, in preparation.

88 C. Reder, V. Gehrke, and W. Marquardt. *Comput. Chem. Engng.*, **1999**, *407–410*, 1817–1828.

89 B. Retzbach. *Mathematische Modelle von Destillationskolonnen zur Synthese von Regelungskonzepten*. VDI Fortschrittsberichte Nr. 8/126. VDI-Verlag, Düsseldorf, **1986**.

90 S. D. Roat, J. J. Downs, E. F. Vogel, and E. J. Doss, in *Chemical Process Control-CPC III*, (M. Morari and T. J. McAvoy, eds), Elsevier, New York, **1986**, 261–268

91 H. H. Rosenbrock. *Automatica*, **1962**, *1*, 31–53.

92 H. Schoenmakers. Personal communication, **2001**.

93 S. Schrans, S. de Wolf, and R. Baur. *Comput. Chem. Engng.*, **1996**, *20* (Suppl.), 1619–1624.

94 R. Seydel. *Practical Bifurcation and Stability Analysis: From Equilibrium to Chaos*, 2nd edn., Springer, New York, **1994**.

95 S. Skogestad. *Trans. IChemE.*, **1997**, *75A*, 539–562.

96 L. A. Smith, **1981**, US Patent No. 4,307,254.

97 M. G. Sneesby, M. O. Tad'e, R. Datta, and T. N. Smith. *Ind. Engng. Chem. Res.*, **1997**, *36*, 1855–1869.

98 M. G. Sneesby, M. O. Tad'e, and T. N. Smith. *Trans. IChemE.*, **1998**, *76A*, 525–531.

99 M. G. Sneesby, M. O. Tad'e, and T. N. Smith. *J. Proc. Control*, **1999**, *9*, 19–31.

100 M. G. Sneesby, M. O. Tad'e, and T. N. Smith. *Trans. IChemE.*, **2000**, *78A*, 283–292.

101 E. Sorensen and S. Skogestad. *J. Proc. Control*, **1994**, *4*, 205–217.

102 E. Stein, A. Kienle, and K. Sundmacher. *Chem. Engng.*, **2000**, *107*(13), 68–72.

103 K. Sundmacher, M. Gravekarstens, P. Rapmund, C. Thiel, and U. Hoffmann, in *Proc. 1st Eur. Congr. Chemical Engineering*, Vol. 2, Florence, 4–7 May **1997**, 215–221.

104 K. Sundmacher and U. Hoffmann. *Chem. Eng. J.*, **1995**, *57*, 219–228.

105 M. O. Tad'e and Y. C. Tian. *Sep. Purif. Technol.*, **2000**, *19*, 85–91.

106 R. Taylor and R. Krishna. *Chem. Engng. Sci.*, **2000**, *55*, 5183–5229.

107 J. Ting, F. G. Helfferich, Y.-L. Hwang, G. K. Graham, and G. E. Keller. *Ind. Engng. Chem. Res.*, **1999**, *38*, 3588–3605.

108 S. Ung and M. F. Doherty. *Chem. Engng. Sci.*, **1995**, *50*, 23–48.

109 C. van Heerden. *Chem. Engng. Sci.*, **1958**, *8*, 133–145.

110 R. M. Wajge and G. V. Reklaitis. *Chem. Engng. J.*, **1999**, *75*, 57–68.

Reactive Distillation. Edited by Kai Sundmacher, Achim Kienle

ISBNs: 3-527-30579-3 (Hardback); 3-527-60052-3 (Electronic)

Index